A SYSTEMATIC APPROACH FOR LINEAR PARAMETER VARYING MODELING AND CONTROL OF INTERNAL COMBUSTION ENGINES

By

Andrew Philip White

A DISSERTATION

Submitted to
Michigan State University
in partial fulfillment of the requirements
for the degree of

DOCTOR OF PHILOSOPHY

Mechanical Engineering

2012

ABSTRACT

A SYSTEMATIC APPROACH FOR LINEAR PARAMETER VARYING MODELING AND CONTROL OF INTERNAL COMBUSTION ENGINES

By

Andrew Philip White

In this dissertation, the modeling and control of time-varying automotive systems is addressed with the use of linear-parameter varying (LPV) control. In practice, many automotive systems with time-varying physical processes are operated with gain-scheduled controllers whose gains are manually calibrated through engine dynamometer and vehicle field tests for the best performance as functions of system operational conditions. However, this approach for gain scheduling is not only expensive and time consuming, but also does not guarantee the stability and performance of the closed-loop system for all time-varying parameters. LPV control techniques, on the other hand, can be used to design gain-scheduled controllers with guaranteed closed-loop stability and performance. The goal of this dissertation is to create a framework to design gain-scheduled controllers using LPV techniques, including, most importantly, the ability to select physically meaningful performance design constraints. As part of this effort, LPV control methods have been applied to the air-to-fuel ratio control of port-fuel-injection systems and the control of hydraulic and electric variable valve timing systems.

Gain scheduling controllers designed using the LPV method have traditionally included $\mathcal{H}_\infty$ performance constraints. This is largely due to the fact that $\mathcal{H}_\infty$ controllers can provide robust stability margins that $\mathcal{H}_2$ controllers cannot provide. However, since the $\mathcal{H}_\infty$ norm is defined as the root-mean-square gain, or ℓ_2 to ℓ_2 gain, from the exogenous input to the regulated output, controllers designed with only $\mathcal{H}_\infty$ performance constraints are not suitable

for use when hard constraints on responses or actuator signals must be met.

When hard constraints on responses or actuator signals must be met, a controller with a guaranteed ℓ_2 to ℓ_∞ gain is needed, which is a special type of $\mathcal{H}_2$ controller. When $\mathcal{H}_2$ performance is used to design a controller, normally a quadratic cost function that balances the output performance with the control input needed to achieve that performance is considered. However, unlike the conventional $\mathcal{H}_2$ performance criterion, the system ℓ_2 to ℓ_∞ gain provides a hard constraint (ℓ_∞) on the system output for a class of inputs with bounded ℓ_2 norm. Many practical control problems in automotive and aerospace systems impose hard constraints (or ℓ_∞ norm) on the system output. The existing mixed $\mathcal{H}_2/\mathcal{H}_\infty$ LPV control method cannot be used to solve this class of the control synthesis problems. To remedy this gap, this dissertation provides a control synthesis method which provides a guaranteed ℓ_2 to ℓ_∞ gain on the system output for LPV systems. The result is a gain-scheduled controller that can provide hard constraints on multiple system outputs. To demonstrate the effectiveness of this approach, both a numerical example and a simulation study with an electrical VVT system are presented.

This dissertation is dedicated to
my parents and my wife, Rebecca.

ACKNOWLEDGMENTS

I would like express my sincere gratitude to my co-advisors Professor Guoming Zhu and Professor Jonguen Choi for their support, advise, and guidance during my Ph.D. study at Michigan State University. During this time period, they have both shared their vast and diverse knowledge of control theory with me. I would especially like to thank Professor Guoming Zhu for providing me with the opportunity to apply my LPV controllers to practical control problems in the Engine Research Lab. I am also especially grateful for the guidance and support provided by Professor Jonguen Choi during the first two years of my graduate studies as a Masters student.

I would like to thank Professor Clark Radcliffe, Professor Ranjan Mukherjee, and Professor Hassan Khalil for serving on my Ph.D. committee. I have gained a wealth of knowledge from the lectures taught by these professors.

I would also like to thank Dr. Ryozo Nagamune, from the University of British Columbia, for his valuable valuable contributions on our collaborative research. His suggestions and comments on our paper "Gain-scheduling control of port-fuel-injection processes" during the revision process were immensely helpful.

The work that is performed in the Engine Research Lab is by nature a collaborative effort. Some of the research performed in this dissertation would not have been possible without the hard work put in by the people who set up the experiments in the lab. In particular I would like to thank Zhen Ren, Xiaojian Yang, Xuefei Chen, and Kevin Moran.

Last, but not least, I would like to thank my family and friends for their encouragement and support over the years.

TABLE OF CONTENTS

LIST OF TABLES

LIST OF FIGURES

Chapter 1

Introduction

1.1 Motivation

The goal of this research has been to establish a systematic procedure for the design of gain-scheduling controllers. In industry, gain-scheduled controllers are normally developed with long hours of ad-hoc tuning and calibration through engine dynamometer and vehicle field tests. While these controllers are often used successfully in many practical applications, the design process through which they are obtained is less than ideal. Not only is the process expensive and time consuming, but more importantly it does not guarantee the stability and performance of the closed-loop system for all possible time-varying parameters. Also, the performance of the closed-loop system with gain-scheduling controllers designed in this way is also dependent on the experience of person doing the calibration. In order to meet the challenges posed by the strict requirements facing many industries these days, a systematic process for designing gain-scheduled controllers with guaranteed performance and stability for all time-varying parameters is needed.

One promising promising solution is the advanced control theory known as linear-parameter varying (LPV) control [57, 44, 3, 2, 77, 81, 1, 23, 76, 10, 11, 12, 13]. LPV systems are time-varying systems whose time-varying components consist of measurable parameters that can vary over time. Over the years, many developments have been made in the area of LPV control theory. In the beginning, LPV control theory mainly consisted of heuris-

tic approaches that were carried over from classical gain-scheduling control, and as such these controllers provided no guaranteed stability, robustness, or performance. The authors of [57] provided analysis conditions for these heuristic approaches that could provided guaranteed stability with slowly varying parameters. Thankfully, more advanced methods based on the convex optimization of linear matrix inequalities (LMI) have been developed [44, 3, 2, 77, 81, 1, 23, 76, 10, 11, 12, 13].

Initially, the small gain theorem was applied to LPV plants with linear fractional transformational (LFT) dependence on the time-varying parameters [44, 3]. This approach allowed the parameter variations to be complex (i.e. have both real and imaginary parts). However, since the time-varying parameters in LPV systems rarely have imaginary parts, this was considered a major source of conservatism in gain-scheduling controller design using this method. Due to this, another method was developed that used a single or parameter-dependent quadratic Lyapunov function in the analysis and control design for LPV plants [2]. However, since this method allowed for arbitrarily fast parameter variation, it can produce conservative results with slowly varying parameters. To handle this problem, known bounds on the rate of parameter variation were incorporated into the analysis conditions by [77, 81, 1]. However, the method used by [77, 81, 1] formulates the control synthesis problem as semi-infinite convex optimization with parameter-dependent LMIs, which requires that the gridding of the parameter space to provide a finite convex optimization. A unified scheme was developed in [76] that joins both the small gain theorem and Lyapunov function approaches in an effort to provide a flexible approach for control engineers to trade-off between performance improvement, controller complexity, and design effort. However, to incorporate known bounds on the rate of parameter variation, the method developed in [76] still requires gridding of the parameter space, which increases the complexity of implement-

ing the controller in practice. An alternative method which does not require gridding of the parameter space was provided by [23, 10, 11, 12, 13] for affine-parameter dependent Lyapunov functions.

Although there has been a considerable amount of research on the design of gain-scheduling controllers via LPV control theory, there is still room for improvement. All of the LPV methods previously mentioned specify the performance of the LPV system as either $\mathcal{H}_\infty$ or $\mathcal{H}_2$ performance. The difficulty that arises with these methods is that real system performance is not easily related to the $\mathcal{H}_\infty$ and $\mathcal{H}_2$ performance criteria. Furthermore, the $\mathcal{H}_\infty$ and $\mathcal{H}_2$ performance criteria, as will be discussed in more detail in Chapter 3, cannot provide hard constraints on system outputs. As a result, engineers in industry could have a hard time utilizing the LPV methods in practical applications.

The open question is, how do we bridge the gap between practices used in industry and the advanced practices used in academia? The answer is to develop LPV controller synthesis methods that allow the use of physically meaningful design constraints. By considering the ℓ_2 to ℓ_∞ gain performance of the closed-loop system, physically meaningful performance design constraints, that can satisfy hard bounds, can be defined. This addition to the current LPV control theory is expected to be very useful engineers working on practical applications in industry.

1.2 Research Overview

1.2.1 Providing hard constraints for gain-scheduling controllers

This research considers the optimal control of polytopic, discrete-time linear parameter varying (LPV) systems with a guaranteed ℓ_2 to ℓ_∞ gain. Additionally, to guarantee robust

stability of the closed-loop system under parameter variations, $\mathcal{H}_\infty$ performance criterion is also considered as well. Controllers with a guaranteed ℓ_2 to ℓ_∞ gain and a guaranteed $\mathcal{H}_\infty$ performance (ℓ_2 to ℓ_2 gain) are mixed $\mathcal{H}_2/\mathcal{H}_\infty$ controllers. Normally, $\mathcal{H}_2$ controllers are obtained by considering a quadratic cost function that balances the output performance with the control input needed to achieve that performance. However, to obtain a controller with a guaranteed ℓ_2 to ℓ_∞ gain (closely related to the physical performance constraint), the cost function used in the $\mathcal{H}_2$ control synthesis minimizes the control input subject to maximal singular-value performance constraints on the output. This problem can be efficiently solved by a convex optimization with linear matrix inequality (LMI) constraints. The contribution of this research is the characterization of the control synthesis LMIs for both gain-scheduled state-feedback and dynamic output-feedback control used to obtain an LPV controller with a guaranteed ℓ_2 to ℓ_∞ gain and $\mathcal{H}_\infty$ performance. Numerical examples are presented to demonstrate the effectiveness of the proposed LPV methods.

1.2.2 Application of gain-scheduling control

The methods reviewed in Chapter 2 and developed in Chapter 3 have been applied to real control problems encountered in the control of internal combustion engines. Specifically, the methods from Chapter 2 are used to design the gain-scheduling controller for the air-to-fuel ratio control of port-fuel-injection processes presented in Chapter 4. The methods from Chapter 2 where also used to develop of the observer-based mixed $\mathcal{H}_2/\mathcal{H}_\infty$ output-feedback controller for the hydraulic variable valve timing actuator in Chapter 5. The guaranteed $\ell_2 - \ell_\infty$ gain controller synthesis techniques provided in Chapter 3 are applied to the control of the electric variable valve timing actuator in Chapter 6.

1.2.2.1 Air-to-fuel ratio control for port-fuel-injection processes

An event-based sampled discrete-time linear system representing a port-fuel-injection process based on wall-wetting dynamics is obtained and formulated as a linear parameter varying (LPV) system. The system parameters used in the engine fuel system model are engine speed, temperature, and load. These system parameters can be measured in real-time through physical or virtual sensors. A gain-scheduling controller for the obtained LPV system is then designed based on the numerically efficient convex optimization or linear matrix inequality (LMI) technique. To demonstrate the effectiveness of the proposed scheme, both simulation and hardware-in-the-loop (HIL) simulation results are presented. The HIL simulations not only show that the designed gain-scheduling controller is effective on a complex mixed mean-value and crank-based engine model [79], but it also demonstrates feasibility of implementing the designed gain-scheduling controller on actual hardware that could be used to control an engine.

1.2.2.2 Control of variable valve timing actuators

Two different variable valve timing actuators are considered in this dissertation. The first is the hydraulic cam phaser, which uses pressurized engine oil to phase the cam shaft. The second is an electric variable valve timing system that uses an electric motor connected to a planetary gear set to phase the cam shaft.

For the hydraulic cam phasing actuator, a family of linear models previously obtained from a series of closed-loop system identification tests [48, 52] is used to design a dynamic gain-scheduling controller. Using engine speed and oil pressure as the system parameters, the family of linear models was translated into a linear parameter varying (LPV) system. An observer-based gain-scheduling controller for the LPV system is then designed based on

the linear matrix inequality (LMI) technique. A discussion on weighting function selection for mixed $\mathcal{H}_2/\mathcal{H}_\infty$ controller synthesis is presented, with an emphasis placed on examining various frequency responses of the system. Test bench results show the effectiveness of the proposed scheme.

For the electric variable valve timing system, a discrete-time, linear parameter-varying (LPV) system representing the electric variable valve timing (VVT) system is developed with engine oil viscosity as the time-varying parameter. A gain-scheduled, dynamic, output-feedback controller is then designed such that the closed-loop system will have a guaranteed ℓ_2 to ℓ_∞ gain. This is done by first constructing a set of linear matrix inequality constraints and then performing a convex optimization to obtain the controller matrices which satisfy the constraints. Results from a simulation study demonstrate the effectiveness of the proposed scheme.

1.3 Organization

This dissertation is organized as follows: a review of existing LPV control synthesis techniques and the modeling required to utilize them is presented in Chapter 2. These techniques are extended in Chapter 3 such that hard constraints on system outputs can be obtained with the guaranteed ℓ_2 to ℓ_∞ gain control problem. In Chapter 4 a gain-scheduled air-to-fuel ratio controller for port-fuel-injection engines is developed using the wall-wetting parameters and engine speed as the time-varying parameters for the LPV control synthesis. Results for both a simulation study and a hardware-in-the loop simulation are presented. In Chapter 5, a family of LTI systems, representing a variable valve timing actuator, obtained through closed-loop system identification [48, 52] are converted into an LPV model. LPV control

synthesis is then applied to the LPV model to obtain a gain-scheduling controller for the variable valve timing actuator. The obtained controller is then validated on the variable valve timing actuator used for the system identification. In Chapter 6, a gain-scheduling controller with a guaranteed ℓ_2 to ℓ_∞ gain is designed to provide hard constraints on the system output of an electrical variable valve timing actuator. Chapter 7 concludes this dissertation by summarizing the results and providing directions for future research.

Chapter 2

Linear Parameter-Varying Modeling and Control Synthesis Methods

This chapter is split into the following two parts: modeling of LPV systems and control synthesis methods for LPV systems.

2.1 Modeling of LPV systems

Throughout this dissertation, the control synthesis methods used rely on the existence of an LPV model with a polytopic parameter dependence. Unfortunately, this is not the most intuitive form that an LPV model can take. Many physical systems have parameter variations that can be easily represented with LFTs. For this reason, we will demonstrate how to convert an LPV model with LFT parameter dependence into an LPV model with a polytopic parameter dependence.

Consider the following open-loop, discrete-time LPV system with LFT parameter depen-

dency:

$$\begin{bmatrix} x(k+1) \\ l(k) \\ z(k) \\ y(k) \end{bmatrix} = \begin{bmatrix} A & B_p & B_w & B_u \\ C_l & D_{lp} & D_{lw} & D_{lu} \\ C_z & D_{zp} & D_{zw} & D_{zu} \\ C_y & D_{yp} & D_{yw} & D_{yu} \end{bmatrix} \begin{bmatrix} x(k) \\ p(k) \\ w(k) \\ u(k) \end{bmatrix} \tag{2.1}$$
$$p(k) = \Theta(k) l(k)$$

where $x(k)$ is the state at time k, $w(k)$ is the exogenous input, and $u(k)$ is the control input. The vectors $z(k)$ and $y(k)$ are the performance output and the measurement for control. Also, $p(k)$ and $l(k)$ are the pseudo-input and pseudo-output connected by $\Theta(k)$. The time-varying parameter $\Theta(k)$ follows the structure

$$\Theta(k) \in \mathbf{\Theta} = \left\{ \mathrm{diag}(\theta_1 I_{n_1}, \theta_2 I_{n_2}, \cdots, \theta_N I_{n_N}) \right\}. \tag{2.2}$$

To emphasize the fact that there exists an LFT with respect to the time-varying parameter matrix $\Theta(k)$, the state-space matrices can be re-arranged into the following upper LFT:

$$\begin{bmatrix} l(k) \\ x(k+1) \\ z(k) \\ y(k) \end{bmatrix} = \underbrace{\left[\begin{array}{c|ccc} D_{lp} & C_l & D_{lw} & D_{lu} \\ \hline B_p & A & B_w & B_u \\ D_{zp} & C_z & D_{zw} & D_{zu} \\ D_{yp} & C_y & D_{yw} & D_{yu} \end{array}\right]}_{=:M} \begin{bmatrix} p(k) \\ x(k) \\ w(k) \\ u(k) \end{bmatrix} \tag{2.3}$$
$$p(k) = \Theta(k) l(k).$$

The time-varying matrix can be $\Theta(k)$ can be absorbed back into the state space matrices such that the state space matrices would be given by

$$\begin{bmatrix} x(k+1) \\ z(k) \\ y(k) \end{bmatrix} = \underbrace{\begin{bmatrix} A(\Theta(k)) & B_w(\Theta(k)) & B_u(\Theta(k)) \\ C_z(\Theta(k)) & D_{zw}(\Theta(k)) & D_{zu}(\Theta(k)) \\ C_y(\Theta(k)) & D_{yw}(\Theta(k)) & D_{yu}(\Theta(k)) \end{bmatrix}}_{=:H(\Theta)} \begin{bmatrix} x(k) \\ w(k) \\ u(k) \end{bmatrix} \tag{2.4}$$

where

$$\begin{aligned} H(\Theta) &:= \mathcal{F}_u(M, \Theta) \\ &= \begin{bmatrix} A & B_w & B_u \\ C_z & D_{zw} & D_{zu} \\ C_y & D_{yw} & D_{yu} \end{bmatrix} + \begin{bmatrix} B_p \\ D_{zp} \\ D_{yp} \end{bmatrix} \Theta(k) \left(I - D_{lp}\Theta(k)\right)^{-1} \begin{bmatrix} C_l & D_{lw} & D_{lu} \end{bmatrix}. \end{aligned} \tag{2.5}$$

It is clear from (2.5) that when the matrix D_{lp} is non-zero, then the system matrices are not affine functions, i.e., a linear combination of the time-varying parameters plus a constant translation. Since, as previously mentioned, all control synthesis methods covered in this book rely on an LPV model with a polytopic parameter dependence, the system matrices must be affine functions of the time-varying parameters. If the matrix D_{lp} is non-zero, then some approximation must be made. If the parameter variation is "small", then a first-order Taylor series approximation can be performed.

2.1.1 First-order Taylor series approximation of LPV systems

Using the first-order Taylor series expansion at $\Theta = \bar{\Theta}$, the LPV system can be approximated as

$$\hat{H}(\Theta(k)) = H(\bar{\Theta}) + \sum_{i=1}^{N} \left[\nabla H(\bar{\Theta})\right]_i (\theta_i(k) - \bar{\theta}_i) \tag{2.6}$$

where $\theta_i(k)$, for $i = 1, \ldots, N$ are the individual parameters in $\Theta(k)$, and $\left[\nabla H(\bar{\Theta})\right]_i$ is the partial derivative of the LFT system $H(\Theta)$ with respect to θ_i solved at $\bar{\Theta}$. The i^{th} partial derivative of the the upper LFT system $H(\Theta)$ is computed by [39]

$$[\nabla H(\Theta)]_i = M_{21}[I - \Theta M_{11}]^{-1} E_i [I - M_{11}\Theta]^{-1} M_{12}, \tag{2.7}$$

where

$$M_{11} = D_{lp}, \quad M_{12} = \begin{bmatrix} C_l & D_{lw} & D_{lu} \end{bmatrix}, \quad M_{21} = \begin{bmatrix} B_p \\ D_{zp} \\ D_{yp} \end{bmatrix}, \tag{2.8}$$

and the matrices E_i are defined such that

$$\Theta(k) = \sum_{i=1}^{N} \theta_i(k) E_i. \tag{2.9}$$

After performing this first-order Taylor series approximation, then the approximated system $\hat{H}(\Theta(k))$ will have affine parameter dependence with respect to $\Theta(k)$. As shown in the next section, a polytopic LPV model can be obtained from an LPV system with affine parameter dependence.

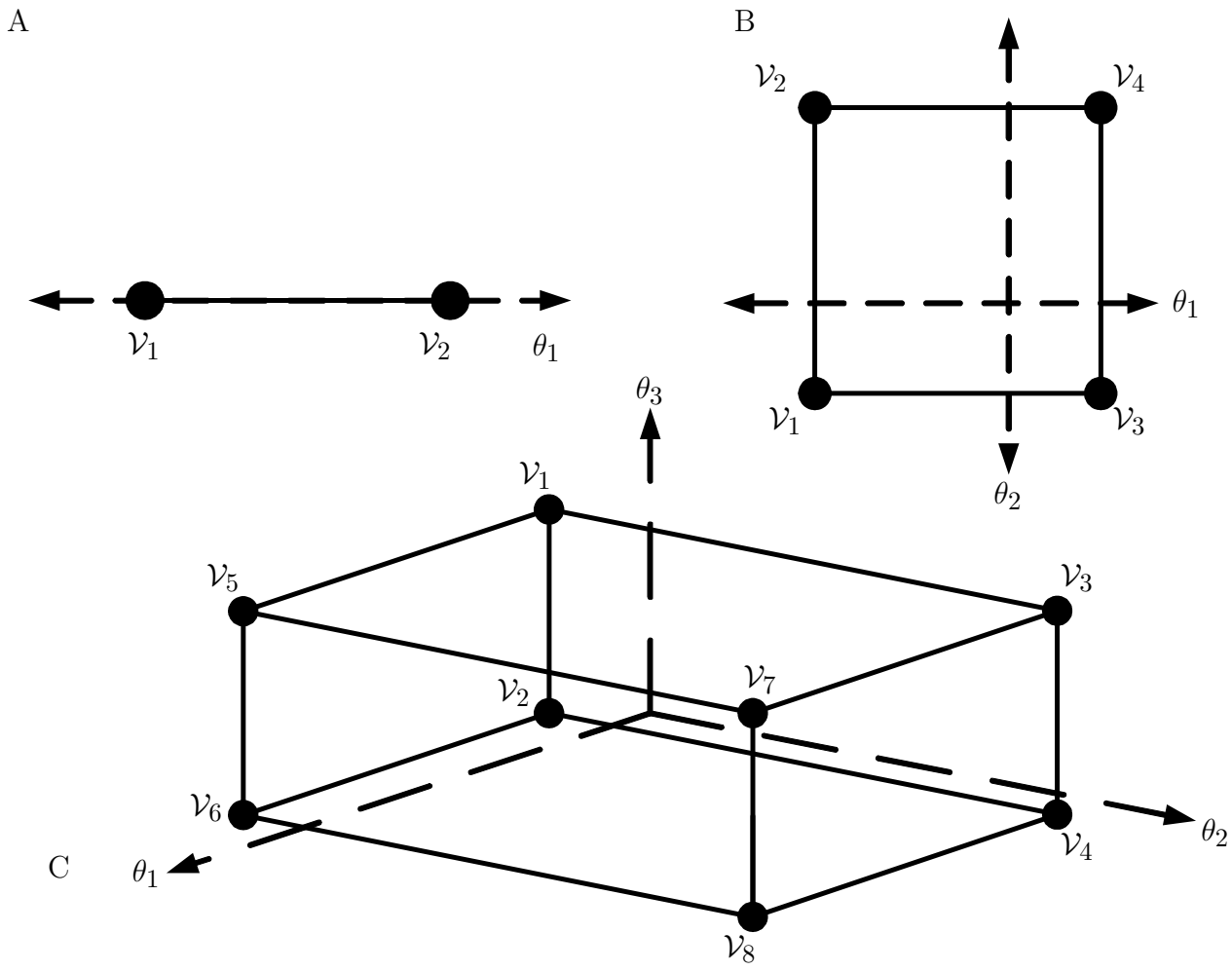

Figure 2.1: Examples of possible parameter space polytopes.

2.1.2 Polytopic linear time-varying system with Barycentric coordinates

The LPV system with affine parameter dependence can be represented by the following polytopic linear time-varying system

$$\begin{bmatrix} x(k+1) \\ z(k) \\ y(k) \end{bmatrix} = \underbrace{\begin{bmatrix} A(\lambda(k)) & B_w(\lambda(k)) & B_u(\lambda(k)) \\ C_z(\lambda(k)) & D_{zw}(\lambda(k)) & D_{zu}(\lambda(k)) \\ C_y(\lambda(k)) & D_{yw}(\lambda(k)) & D_{yu}(\lambda(k)) \end{bmatrix}}_{=:H(\lambda)} \begin{bmatrix} x(k) \\ w(k) \\ u(k) \end{bmatrix} \tag{2.10}$$

where the system matrices $A(\lambda(k))$, $B_w(\lambda(k))$, $B_u(\lambda(k))$, $C_z(\lambda(k))$, $C_y(\lambda(k))$, $D_{zw}(\lambda(k))$, $D_{zu}(\lambda(k))$, $D_{yw}(\lambda(k))$, and $D_{yu}(\lambda(k))$ belong to the polytope

$$\begin{aligned}\mathfrak{D} = \Bigg\{ & (A, B_w, B_u, C_z, C_y, D_{zw}, D_{zu}, D_{yw}, D_{yu})(\lambda_k) : \\ & (A, B_w, B_u, C_z, C_y, D_{zw}, D_{zu}, D_{yw}, D_{yu})(\lambda_k) \\ & = \sum_{i=1}^{N} \lambda_i(k)(A, B_w, B_u, C_z, C_y, D_{zw}, D_{zu}, D_{yw}, D_{yu})_i, \lambda_k \in \Lambda_N \Bigg\},\end{aligned} \tag{2.11}$$

with $(A, B_w, B_u, C_z, C_y, D_{zw}, D_{zu}, D_{yw}, D_{yu})_i$ the vertices of the polytope and $\lambda_k = \lambda(k) \in \mathbb{R}^N$ the vector of time-varying barycentric coordinates lying in the unit simplex

$$\Lambda_N = \left\{ \zeta \in \mathbb{R}^N : \sum_{i=1}^{N} \zeta_i = 1, \zeta_i \geq 0, i = 1, \cdots, N \right\}. \tag{2.12}$$

The vertices of the polytope $\mathfrak{D}$ are obtained by solving the system matrices of $\hat{H}(\Theta)$ at each of the vertices $\mathcal{V}_i$ for $i = 1, \ldots, N$. Then each of the state space matrices in $H(\lambda_k)$ are computed as the convex combination of the vertice systems of this polytope, such that, for example, the state matrix would be computed by

$$A(\lambda_k) = \sum_{i=1}^{N} \lambda_i(k) A_i. \tag{2.13}$$

Each of the other matrices in $H(\lambda_k)$ are computed in the same way. The convex combination coefficients $\{\lambda_i(\Theta)\}$ for a given Θ and set of vertices $\{\mathcal{V}_i\}$ are also known as the barycentric coordinates. The barycentric coordinate function is defined in [64] as

$$\lambda_i(\Theta) = \frac{\Upsilon_i(\Theta)}{\sum_i \Upsilon_i(\Theta)}, \tag{2.14}$$

where $\Upsilon_i(\Theta)$ is the weight function of vertex i for a point Θ inside of the convex polytope. The weight function is

$$\Upsilon_i(\Theta) = \frac{\text{vol}(\mathcal{V}_i)}{\Pi_{j \in ind(\mathcal{V}_i)}(n_j \cdot (\mathcal{V}_i - \Theta))}, \tag{2.15}$$

where $\text{vol}(\mathcal{V}_i)$ is the volume of the parallelepided span by the normals to the facets incident on vertex i, i.e., $\mathcal{V}_i$. $\{n_j\}$ is the collection of normal vectors to the facets incident on vertex i. The volume of a parallelepided can be found as

$$\text{vol}(\mathcal{V}_i) = |\det(n_{ind})| \,. \tag{2.16}$$

where n_{ind} is a matrix whose rows are the vectors n_j where $j \in ind(\mathcal{V}_i)$.

Since the polytopic LTV system have been defined, we will now focus our attention in the next section on the performance specifications for the polytopic LTV system.

2.2 Performance of discrete-time polytopic LPV systems

Consider the $\mathcal{H}_2$ or $\mathcal{H}_\infty$ weighted closed-loop discrete-time LPV system

$$H := \begin{cases} x(k+1) = \mathcal{A}(\lambda_k)x(k) + \mathcal{B}_w(\lambda_k)w(k), \quad x(0) = 0 \\ z(k) = \mathcal{C}_z(\lambda_k)x(k) + \mathcal{D}_w(\lambda_k)w(k) \end{cases} \tag{2.17}$$

where $x(k) \in \mathbb{R}^n$ is the state, $w(k) \in \mathbb{R}^r$ is the exogenous input, and $z(k) \in \mathbb{R}^p$ is the performance output. The system matrices $\mathcal{A}(\lambda_k)$, $\mathcal{B}_w(\lambda_k)$, $\mathcal{C}_z(\lambda_k)$, $\mathcal{D}_w(\lambda_k)$, belong to the polytope similar to $\mathfrak{D}$ in (2.11).

The $\mathcal{H}_\infty$ performance of the system (2.17) from $w(k)$ to $z(k)$ is defined by the quantity

$$\|H\|_\infty = \sup_{\|w(k)\|_2 \neq 0} \frac{\|z(k)\|_2}{\|w(k)\|_2} \tag{2.18}$$

with $w(k) \in \ell_2^r$ and $z(k) \in \ell_2^p$. By using the bounded real lemma, an upper bound for the $\mathcal{H}_\infty$ performance is characterized by the following lemma [12].

Lemma 1. *Consider the system H given by* (2.17)*. If there exist bounded matrices $G(\lambda_k)$ and $P(\lambda_k) = P(\lambda_k)^T > 0$ for all $\lambda_k \in \Lambda_N$ such that*

$$\begin{bmatrix} P(\lambda_{k+1}) & \mathcal{A}(\lambda_k)G(\lambda_k) & \mathcal{B}_w(\lambda_k) & 0 \\ G(\lambda_k)^T\mathcal{A}(\lambda_k)^T & G(\lambda_k) + G(\lambda_k)^T - P(\lambda_k) & 0 & G(\lambda_k)^T\mathcal{C}_z(\lambda_k)^T \\ \mathcal{B}_w(\lambda_k)^T & 0 & \eta I & \mathcal{D}_w(\lambda_k)^T \\ 0 & \mathcal{C}_z(\lambda_k)G(\lambda_k) & \mathcal{D}_w(\lambda_k) & \eta I \end{bmatrix} > 0 \tag{2.19}$$

then the system H is exponentially stable and

$$\|H\|_\infty \leq \inf_{P(\lambda_k), G(\lambda_k), \eta} \eta.$$

This lemma is an extension of a standard result provided by [18, 17].

The infinite horizon $\mathcal{H}_2$ performance of the system (2.17) from $w(k)$ to $z(k)$ is defined as

$$\|H\|_2^2 = \lim_{\mathrm{T}\to\infty} \sup \mathcal{E}\left\{ \frac{1}{\mathrm{T}} \sum_{k=0}^{\mathrm{T}} z(k)^T z(k) \right\} \tag{2.20}$$

where $w(k)$ is a zero-mean white noise Gaussian process with identity covariance, $\mathcal{E}$ denotes the expectation operator, and the positive integer T denotes the time horizon. An upper

bound for the $\mathcal{H}_2$ performance is characterized by the following lemma [12].

Lemma 2. *Consider the system H given by (2.17). If there exists bounded matrices $G(\lambda_k)$, $P(\lambda_k) = P(\lambda_k)^T > 0$, and $W(\lambda_k) = W(\lambda_k)^T$ for all $\lambda_k \in \Lambda_N$ such that*

$$\begin{bmatrix} P(\lambda_{k+1}) & \mathcal{A}(\lambda_k)G(\lambda_k) & \mathcal{B}_w(\lambda_k) \\ G(\lambda_k)^T\mathcal{A}(\lambda_k)^T & G(\lambda_k) + G(\lambda_k)^T - P(\lambda_k) & 0 \\ \mathcal{B}_w(\lambda_k)^T & 0 & I \end{bmatrix} > 0 \tag{2.21}$$

and

$$\begin{bmatrix} W(\lambda_k) - \mathcal{D}_w(\lambda_k)\mathcal{D}_w(\lambda_k)^T & \mathcal{C}_z(\lambda_k)G(\lambda_k) \\ G(\lambda_k)^T\mathcal{C}_z(\lambda_k)^T & G(\lambda_k) + G(\lambda_k)^T - P(\lambda_k) \end{bmatrix} > 0 \tag{2.22}$$

then the system H is exponentially stable and its $\mathcal{H}_2$ performance is bounded by ν given by

$$\nu^2 = \inf_{P(\lambda_k), G(\lambda_k), W(\lambda_k)} \sup_{\lambda_k \in \Lambda_N} \operatorname{trace}\{W(\lambda_k)\}$$

such that $\|H\|_2 \leq \nu$.

The proof for this lemma can be found in [12].

Note that the parameter dependent LMI conditions in Lemmas 1 and 2 must be evaluated for all λ_k in the unit simplex Λ_N. This leads to an infinite dimensional problem. By imposing an affine parameter-dependent structure on the Lyapunov matrix $P(\lambda_k)$, such that

$$P(\lambda_k) = \sum_{i=1}^{N} \lambda_i(k) P_i, \quad i = 1, \ldots, N, \tag{2.23}$$

a finite set of LMIs in terms of the vertices of the polytope $\mathfrak{D}$ can be obtained.

To reduce conservatism, the parameter variation rate

$$\Delta\lambda_i(k) = \lambda_i(k+1) - \lambda_i(k), \quad i = 1, \ldots, N \tag{2.24}$$

is assumed to be limited. Two limits have been considered in the literature. The first rate limit considered in the literature [40, 10, 11] is given by

$$-b\lambda_i(k) \leq \Delta\lambda_i(k) \leq b\left(1 - \lambda_i(k)\right), \quad i = 1, \ldots, N, \tag{2.25}$$

with $b \in [0, 1]$. With this parameter variation rate bound and the affine parameter-dependent structure in (2.23), the $\mathcal{H}_\infty$ performance criteria in Lemma 1 can be transformed into a finite number of LMIs, as shown in the next Lemma [10].

Lemma 3. *The system H* (2.17) *has an* $\mathcal{H}_\infty$ *performance bounded by* η *if there exist matrices* $G_i \in \mathbb{R}^{n\times n}$ *and symmetric matrices* $P_i \in \mathbb{R}^{n\times n}$ *such that*

$$\begin{bmatrix} (1-b)P_i + bP_\ell & \star & \star & \star \\ G_i^T\mathcal{A}_i^T & G_i + G_i^T - P_i & \star & \star \\ \mathcal{B}_{w,i}^T & 0 & \eta I & \star \\ 0 & \mathcal{C}_{z,i}G_i & \mathcal{D}_{w,i} & \eta I \end{bmatrix} > 0 \tag{2.26}$$

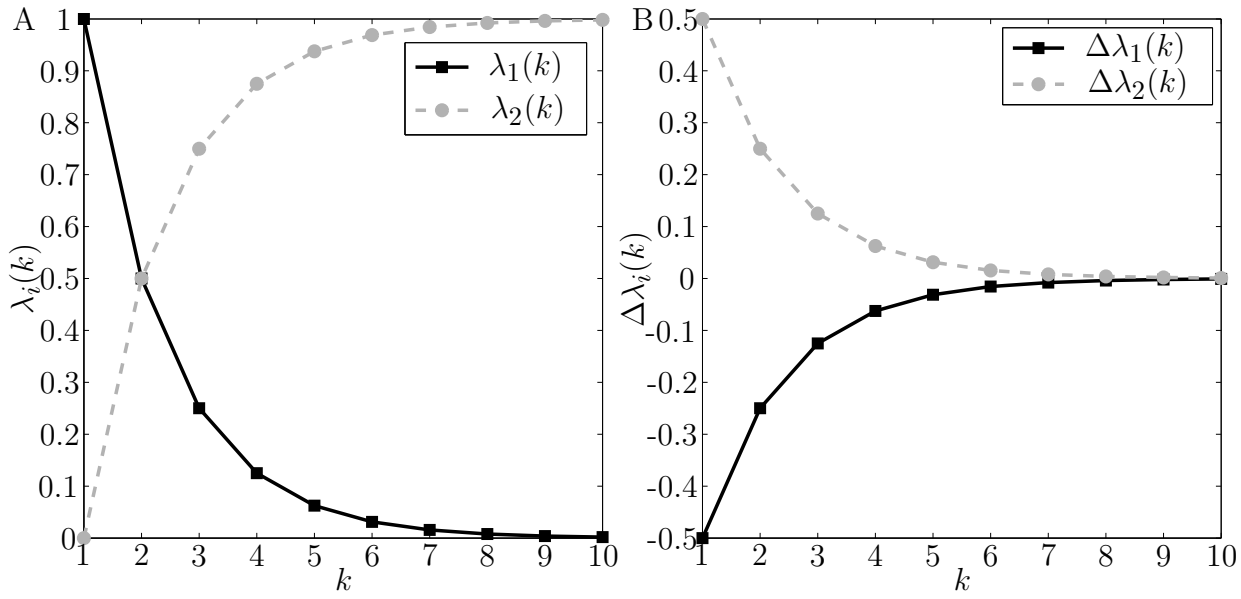

Figure 2.2: Fastest possible parameter transition between the extreme conditions with $N = 2$ and $b = 0.5$ when the rate limit given by (2.25) is in effect.

holds for $i = 1, \ldots, N$ *and* $\ell = 1, \ldots, N$ *and*

$$\begin{bmatrix} (1-b)P_i + (1-b)P_j + 2bP_\ell & \star & \star & \star \\ G_j^T\mathcal{A}_i^T + G_i^T\mathcal{A}_j^T & G_i + G_i^T + G_j + G_j^T - P_i - P_j & \star & \\ \mathcal{B}_{w,i}^T + \mathcal{B}_{w,j}^T & 0 & 2\eta I & \star \\ 0 & \mathcal{C}_{z,i}G_j + \mathcal{C}_{z,j}G_i & \mathcal{D}_{w,i} + \mathcal{D}_{w,j} & 2\eta I \end{bmatrix} > 0 \tag{2.27}$$

holds for $\ell = 1, \ldots, N$, $i = 1, \ldots, N-1$, *and* $j = i+1, \ldots, N$.

A proof for this lemma can be found in [10].

While the rate limit (2.25) can be useful, it is, however, not very realistic. To see this, one only needs to consider the example parameter variation with $N = 2$ and $b = 0.5$ as displayed in Fig. 2.2. In this example, the time-varying parameter starts at one extreme and moves the other extreme as quickly as the parameter variation rate limit (2.25) allows. It is clear that the maximum parameter variation rate is dependent on the current value of the

parameters with the rate limit given by (2.25).

A more realistic parameter variation limit that is not dependent on the current value of the time-varying parameter is considered in [41, 12]. This limit is given by

$$-b \leq \Delta\lambda_i(k) \leq b, \quad i = 1, \ldots, N, \tag{2.28}$$

with $b \in [0, 1]$. When using this parameter variation rate, the uncertainty domain, where the vector $(\lambda(k), \Delta\lambda(k))^T \in \mathbb{R}^{2N}$ takes values, is modeled by the compact set

$$\begin{aligned}\Gamma_b = \Bigg\{ & \delta \in \mathbb{R}^{2N} : \delta \in \text{co}\{g^1, \ldots, g^M\}, g^j = \begin{pmatrix} f^j \\ h^j \end{pmatrix}, \quad f^j \in \mathbb{R}^N, \quad h^j \in \mathbb{R}^N, \\ & \sum_{i=1}^{N} f_i^j = 1 \text{ with } f_i^j \geq 0, i = 1, \ldots, N, \sum_{i=1}^{N} h_i^j = 0, \quad j = 1, \ldots, M \Bigg\}\end{aligned} \tag{2.29}$$

defined as the convex combination of the vectors g^j, for $j = 1, \ldots, M$, given a priori. This definition of Γ_b ensures that $\lambda(k) \in \Lambda_N$ and that

$$\sum_{i=1}^{N} \Delta\lambda_i(k) = 0 \tag{2.30}$$

holds for all $k \geq 0$. For a given bound b, the columns of Γ_b can be generated as the columns of a matrix `V` as follows [12] (in MATLAB code)

```
V = zeros(2*N,N^2+(N-1)^2+(N-1));
for i = 1:1:N
    V(i,(i-1)*N+1) = 1;
    ind = 1;
    for j = 1:1:N
```

```
        if j ISNOT i
            V(i,(i-1)*N+ind+1) = 1;
            V(N+i,(i-1)*N+ind+1) = -b;
            V(N+j,(i-1)*N+ind+1) = b;

            V(i,N^2+(i-1)*(N-1)+ind) = b;
            V(j,N^2+(i-1)*(N-1)+ind) = 1-b;
            V(N+i,N^2+(i-1)*(N-1)+ind) = -b;
            V(N+j,N^2+(i-1)*(N-1)+ind) = b;

            ind = ind + 1;
        end
    end
end
f = V(1:N,:);
h = V(N+1:2*N,:);
```

With the uncertainty set Γ_b, each $\lambda_i(k)$ and $\Delta\lambda_i(k)$ for $i = 1, 2, \ldots, N$ are given by

$$\lambda_i(k) = \sum_{j=1}^{M} f_i^j \gamma_j(k) \quad \text{and} \quad \Delta\lambda_i(k) = \sum_{j=1}^{M} h_i^j \gamma_j(k) \tag{2.31}$$

such that the affine representation of $P(\lambda_k)$ is given by

$$\begin{aligned} P(\lambda_k) &= \sum_{i=1}^{N} \lambda_i(k) P_i = \sum_{i=1}^{N} \left(\sum_{j=1}^{M} f_i^j \gamma_j(k) \right) P_i \\ &= \sum_{j=1}^{M} \gamma_j(k) \left(\sum_{i=1}^{N} f_i^j P_i \right) = \sum_{j=1}^{M} \gamma_j(k) \tilde{P}_j = \tilde{P}(\gamma(k)) \end{aligned} \tag{2.32}$$

with $\tilde{P}_j = \sum_{i=1}^{N} f_i^j P_i$ as shown in [12]. Using the same structure for λ_k, the system matrices in H (2.17) are also converted to the new representation in terms of $\gamma(k) \in \Lambda_M$, such that

$$\mathcal{A}(\lambda_k) = \tilde{\mathcal{A}}(\gamma(k)) = \sum_{j=1}^{M} \gamma_j(k) \tilde{\mathcal{A}}_j \tag{2.33}$$

with $\tilde{\mathcal{A}}_j = \sum_{i=1}^{N} f_i^j \mathcal{A}_i$. All other matrices in H are converted the same way. It is also shown in [12], that by combining (2.31) with the fact that $\lambda_{k+1} = \lambda_k + \Delta\lambda_k$,

$$\begin{aligned} P(\lambda_{k+1}) &= \sum_{i=1}^{N} (\lambda_i(k) + \Delta\lambda_i(k)) P_i = \sum_{i=1}^{N} \left(\sum_{j=1}^{M} \left(f_i^j + h_i^j \right) \gamma_j(k) \right) P_i \\ &= \sum_{j=1}^{M} \gamma_j(k) \left(\sum_{i=1}^{N} \left(f_i^j + h_i^j \right) P_i \right) = \sum_{j=1}^{M} \gamma_j(k) \hat{P}_j = \hat{P}(\gamma(k)) \end{aligned} \tag{2.34}$$

with $\hat{P}_j = \sum_{i=1}^{N} \left(f_i^j + h_i^j \right) P_i$. The authors of [12] note that due to these representations of $P(\lambda_k)$ and $P(\lambda_{k+1})$, the LMIs of Lemma 1 and Lemma 2 can be rewritten with a dependency on $\gamma(k)$. They also note that a convenient parameterization of the slack variable $G(\lambda_k)$ is given by

$$G(\lambda_k) = G(\gamma(k)) = \sum_{j=1}^{M} \gamma_j(k) G_j, \quad \gamma(k) \in \Lambda_M. \tag{2.35}$$

Using these parameterizations, the next two lemmas present a finite-dimensional set of LMIs

that guarantee the LMI conditions of Lemmas 1 and 2 [12].

Lemma 4. *Consider the system H, given by* (2.17). *Assume that the vectors f^j and h^j of Γ_b are given. If there exist, for $j = 1, \ldots, M$, matrices $G_j \in \mathbb{R}^{n\times n}$ and, for $i = 1, \ldots, N$, symmetric positive-definite matrices $P_i \in \mathbb{R}^{n\times n}$ such that*

$$\begin{bmatrix} \sum_{i=1}^{N} \left(f_i^j + h_i^j\right) P_i & \star & \star & \star \\ G_j^T \tilde{\mathcal{A}}_j^T & G_j + G_j^T - \sum_{i=1}^{N} f_i^j P_i & \star & \star \\ \tilde{\mathcal{B}}_{w,j}^T & 0 & \eta I & \star \\ 0 & \tilde{\mathcal{C}}_{z,j} G_j & \tilde{\mathcal{D}}_{w,j} & \eta I \end{bmatrix} > 0 \tag{2.36}$$

for $j = 1, \ldots, M$ and

$$\begin{bmatrix} \sum_{i=1}^{N} \left(f_i^j + f_i^\ell + h_i^j + h_i^\ell\right) P_i & \star & \star & \star \\ G_j^T \tilde{\mathcal{A}}_\ell^T + G_\ell^T \tilde{\mathcal{A}}_j^T & \Theta_{22,j\ell} & \star & \star \\ \tilde{\mathcal{B}}_{w,j}^T + \tilde{\mathcal{B}}_{w,\ell}^T & 0 & 2\eta I & \star \\ 0 & \tilde{\mathcal{C}}_{z,j} G_\ell + \tilde{\mathcal{C}}_{z,\ell} G_j & \tilde{\mathcal{D}}_{w,j} + \tilde{\mathcal{D}}_{w,\ell} & 2\eta I \end{bmatrix} > 0 \tag{2.37}$$

with

$$\Theta_{22,j\ell} = G_j + G_j^T + G_\ell + G_\ell^T - \sum_{i=1}^{N} \left(f_i^j + f_i^\ell\right) P_i$$

for $j = 1, \ldots, M-1$ and $\ell = j+1, \ldots, M$, then the system H is exponentially stable and

$$\|H\|_\infty \leq \min_{P_i, G_j, \eta} \eta.$$

The proof for this lemma can be found in [12].

Lemma 5. *Consider the system H, given by* (2.17). *Assume that the vectors f^j and h^j of*

Γ_b *are given. If there exist, for* $j = 1, \ldots, M$, *matrices* $G_j \in \mathbb{R}^{n\times n}$ *and, for* $i = 1, \ldots, N$, *symmetric positive-definite matrices* $P_i \in \mathbb{R}^{n\times n}$ *and* $W_i \in \mathbb{R}^{p\times p}$ *such that*

$$\begin{bmatrix} \sum_{i=1}^{N} \left(f_i^j + h_i^j\right) P_i & \star & \star \\ G_j^T \tilde{\mathcal{A}}_j^T & G_j + G_j^T - \sum_{i=1}^{N} f_i^j P_i & \star \\ \tilde{\mathcal{B}}_{w,j}^T & 0 & I \end{bmatrix} > 0 \tag{2.38}$$

for $j = 1, \ldots, M$,

$$\begin{bmatrix} \sum_{i=1}^{N} \left(f_i^j + f_i^\ell + h_i^j + h_i^\ell\right) P_i & \star & \star \\ G_j^T \tilde{\mathcal{A}}_\ell^T + G_\ell^T \tilde{\mathcal{A}}_j^T & \widehat{GP}_{j\ell} & \star \\ \tilde{\mathcal{B}}_{w,j}^T + \tilde{\mathcal{B}}_{w,\ell}^T & 0 & 2I \end{bmatrix} > 0 \tag{2.39}$$

where

$$\widehat{GP}_{j\ell} = G_j + G_j^T + G_\ell + G_\ell^T - \sum_{i=1}^{N} \left(f_i^j + f_i^\ell\right) P_i$$

for $j = 1, \ldots, M-1$, *and* $\ell = j+1, \ldots, M$,

$$\begin{bmatrix} \sum_{i=1}^{N} f_i^j W_i - \tilde{\mathcal{D}}_{w,j} \tilde{\mathcal{D}}_{w,j}^T & \star \\ G_j^T \tilde{\mathcal{C}}_{z,j}^T & G_j + G_j^T - \sum_{i=1}^{N} f_i^j P_i \end{bmatrix} > 0 \tag{2.40}$$

for $j = 1, \ldots, M$,

$$\begin{bmatrix} \sum_{i=1}^{N} \left(f_i^j + f_i^\ell\right) W_i - \tilde{\mathcal{D}}_{w,j} \tilde{\mathcal{D}}_{w,\ell}^T + \tilde{\mathcal{D}}_{w,\ell} \tilde{\mathcal{D}}_{w,j}^T & \star \\ G_j^T \tilde{\mathcal{C}}_{z,\ell}^T + G_\ell^T \tilde{\mathcal{C}}_{z,j}^T & \widehat{GP}_{j\ell} \end{bmatrix} > 0 \tag{2.41}$$

for $j = 1, \ldots, M-1$, *and* $\ell = j+1, \ldots, M$, *then the system* H *is exponentially stable and*

its $\mathcal{H}_2$ performance is bound by ν given by

$$\nu^2 = \min_{P_i, G_j, W_i} \max_i \operatorname{trace}\{W_i\}.$$

The proof for this lemma can be found in [12].

2.3 Control Synthesis Methods for LPV systems

2.3.1 Static Output Feedback Control Synthesis

In this section, the gain-scheduled static output feedback controller synthesis results from [10] and [12] are reviewed.

Consider the following $\mathcal{H}_\infty$ and $\mathcal{H}_2$ weighted, discrete-time polytopic time-varying systems H^∞ and H^2:

$$H^\infty := \begin{cases} x(k+1) = A(\lambda_k)x(k) + B_{\infty w}(\lambda_k)w_\infty(k) + B_u(\lambda_k)u(k) \\ z_\infty(k) = C_{\infty z}(\lambda_k)x(k) + D_{\infty w}(\lambda_k)w_\infty(k) + D_{\infty u}(\lambda_k)u(k) \\ y(k) = C_y x(k), \quad C_y = \begin{bmatrix} I_q, & 0 \end{bmatrix} \end{cases} \tag{2.42}$$

$$H^2 := \begin{cases} x(k+1) = A(\lambda_k)x(k) + B_{2w}(\lambda_k)w_2(k) + B_u(\lambda_k)u(k) \\ z_2(k) = C_{2z}(\lambda_k)x(k) + D_{2w}(\lambda_k)w_2(k) + D_{2u}(\lambda_k)u(k) \\ y(k) = C_y x(k), \quad C_y = \begin{bmatrix} I_q, & 0 \end{bmatrix} \end{cases} \tag{2.43}$$

where $x(k) \in \mathbb{R}^n$ is the state, $w_\infty(k) \in \mathbb{R}^{r\infty}$ and $w_2(k) \in \mathbb{R}^{r2}$ are the $\mathcal{H}_\infty$ and $\mathcal{H}_2$ exogenous inputs, $z_\infty(k) \in \mathbb{R}^{p\infty}$ and $z_2(k) \in \mathbb{R}^{p2}$ are the $\mathcal{H}_\infty$ and $\mathcal{H}_2$ performance outputs, and $y \in \mathbb{R}^q$ is the measurement for control. The system matrices of H^∞ and H^2 belong to a polytope

similar to the one given in (2.11).

2.3.2 $\mathcal{H}_\infty$ Control Synthesis

In [10], gain-scheduled static output feedback synthesis LMIs that stabilize the system H^∞ with a guaranteed $\mathcal{H}_\infty$ performance bound are presented. The rate of variation of the parameters (2.24) is assumed to be limited by (2.25).

Extending the analysis result presented in Lemma 3, the authors of [10] characterize a finite set of LMI conditions for the synthesis of a gain scheduled $\mathcal{H}_\infty$ static output feedback controller for the system (2.42).

Lemma 6. *Consider the system H^∞, given by (2.42). If there exist matrices $G_{i,1} \in \mathbb{R}^{q\times q}$, $G_{i,2} \in \mathbb{R}^{n-q,q}$, $G_{i,3} \in \mathbb{R}^{n-q\times n-q}$, $Z_i \in \mathbb{R}^{m\times q}$, and symmetric matrices $P_i \in \mathbb{R}^{n\times n}$ such that*

$$\begin{bmatrix} (1-b)P_i + bP_\ell & \star & \star & \star \\ G_i^T A_i^T + Z_i^T B_{u,i}^T & G_i + G_i^T - P_i & \star & \star \\ B_{\infty w,i}^T & 0 & \eta I & \star \\ 0 & C_{\infty z,i}G_i + D_{\infty u,i}Z_i & D_{\infty w,i} & \eta I \end{bmatrix} > 0 \tag{2.44}$$

hold for $i = 1,\ldots,N$ and $\ell = 1,\ldots,N$ and

$$\begin{bmatrix} (1-b)P_i + (1-b)P_j + 2bP_\ell & \star & \star & \star \\ \Theta_{21,ij} & \widehat{GP}_{ij} & \star & \star \\ B_{\infty w,i}^T + B_{\infty w,j}^T & 0 & 2\eta I & \star \\ 0 & \Theta_{42,ij} & D_{\infty w,i} + D_{\infty w,j} & 2\eta I \end{bmatrix} > 0 \tag{2.45}$$

where

$$\widehat{GP}_{ij} = G_i + G_i^T + G_j + G_j^T - P_i - P_j$$

with

$$\Theta_{21,ij} = G_j^T A_i^T + G_i^T A_j^T + Z_j^T B_{u,i}^T + Z_i^T B_{u,j}^T$$

$$\Theta_{42,ij} = C_{\infty z,i} G_j + C_{\infty z,j} G_i + D_{\infty u,i} Z_j + D_{\infty u,j} Z_i$$

hold for $\ell = 1, \ldots, N$, $i = 1, \ldots, N-1$, *and* $j = i+1, \ldots, N$, *with*

$$G_i = \begin{bmatrix} G_{i,1} & 0 \\ G_{i,2} & G_{i,3} \end{bmatrix} \quad \textit{and} \quad Z_i = \begin{bmatrix} Z_{i,1} & 0 \end{bmatrix},$$

then the parameter-dependent static output feedback gain

$$K(\lambda_k) = \hat{Z}(\lambda_k)\hat{G}(\lambda_k)^{-1}, \tag{2.46}$$

with

$$\hat{Z}(\lambda(k)) = \sum_{i=1}^{N} \lambda_i(k) Z_{i,1} \quad \textit{and} \quad \hat{G}(\lambda(k)) = \sum_{i=1}^{N} \lambda_i(k) G_{i,1}$$

stabilizes the system (2.42) *with a guaranteed* $\mathcal{H}_\infty$ *performance bounded by* η *for all* $\lambda \in \Lambda_N$ *and* $\Delta\lambda$ *that satisfies* (2.25).

A proof for this lemma can be found in [10].

2.3.3 Mixed $\mathcal{H}_2/\mathcal{H}_\infty$ Control Synthesis

In [12], gain-scheduled static output feedback synthesis LMIs that stabilize the systems H^∞ and H^2 with guaranteed $\mathcal{H}_\infty$ and $\mathcal{H}_2$ performance bounds are presented. As in [10], the rate

of variation of the parameters (2.24) is assumed to be limited by an a priori known bound b, given by (2.28).

The authors of [12] extend the analysis results of Lemmas 4 and 5 to characterize a finite set of LMI conditions for the synthesis of a gain scheduled mixed $\mathcal{H}_2/\mathcal{H}_\infty$ static output feedback controller for the systems H^2 (2.43) and H^∞ (2.42).

Lemma 7. *Consider the systems H^∞ and H^2, given by* (2.42) *and* (2.43). *Assume that the vectors f^j and h^j of Γ_b are given. Additionally, assume that a prescribed $\mathcal{H}_\infty$ performance bound η is given. If there exist, for $i = 1, \ldots, N$, matrices $G_{i,1} \in \mathbb{R}^{n\times n}$, $Z_{i,1} \in \mathbb{R}^{m\times q}$ and symmetric positive-definite matrices $P_{\infty,i} \in \mathbb{R}^{n\times n}$, $P_{2,i} \in \mathbb{R}^{n\times n}$, and $W_i \in \mathbb{R}^{p\times p}$, and, for $j = 1, \ldots, M$, matrices $G_{\infty j,2} \in \mathbb{R}^{(n-q)\times q}$, $G_{2j,2} \in \mathbb{R}^{(n-q)\times q}$, $G_{\infty j,3} \in \mathbb{R}^{(n-q)\times(n-q)}$, and $G_{2j,3} \in \mathbb{R}^{(n-q)\times(n-q)}$ such that*

$$\begin{bmatrix} \sum_{i=1}^{N}\left(f_i^j + h_i^j\right)P_{\infty,i} & \star & \star & \star \\ G_{\infty,j}^T\tilde{A}_j^T + Z_j^T\tilde{B}_{u,j}^T & G_{\infty,j} + G_{\infty,j} - \sum_{i=1}^{N} f_i^j P_{\infty,i} & \star & \star \\ \tilde{B}_{\infty w,j}^T & 0 & \eta I & \star \\ 0 & \tilde{C}_{\infty z,j}G_{\infty,j} + \tilde{D}_{\infty u,j}Z_j & \tilde{D}_{\infty w,j} & \eta I \end{bmatrix} = \Theta_j > 0 \quad (2.47)$$

for $j = 1, \ldots, M$ and

$$\begin{bmatrix} \sum_{i=1}^{N}\left(f_i^j + f_i^\ell + h_i^j + h_i^\ell\right)P_{\infty,i} & \star & \star & \star \\ \Theta_{21,j\ell} & \Theta_{22,j\ell} & \star & \star \\ \tilde{B}_{\infty w,j}^T + \tilde{B}_{\infty w,\ell}^T & 0 & 2\eta I & \star \\ 0 & \Theta_{42,j\ell} & \tilde{D}_{\infty w,j} + \tilde{D}_{\infty w,\ell} & 2\eta I \end{bmatrix} = \Theta_{jl} > 0 \quad (2.48)$$

with

$$\Theta_{21,j\ell} = G_{\infty,j}^T \tilde{A}_\ell^T + G_{\infty,\ell}^T \tilde{A}_j^T + Z_j^T \tilde{B}_{u,\ell}^T + Z_\ell^T \tilde{B}_{u,j}^T$$

$$\Theta_{22,j\ell} = G_{\infty,j} + G_{\infty,j}^T + G_{\infty,\ell} + G_{\infty,\ell}^T - \sum_{i=1}^{N} \left(f_i^j + h_i^j \right) P_{\infty,i}$$

$$\Theta_{42,j\ell} = \tilde{C}_{\infty z,j} G_{\infty,\ell} + \tilde{C}_{\infty z,\ell} G_{\infty,j} + \tilde{D}_{u,j} Z_\ell + \tilde{D}_{u,\ell} Z_j$$

for $j = 1, \ldots, M-1$ *and* $\ell = j+1, \ldots, M$, *and*

$$\begin{bmatrix} \sum_{i=1}^{N} \left(f_i^j + h_i^j \right) P_{2,i} & \star & \star \\ G_{2,j}^T \tilde{A}_j^T + Z_j^T \tilde{B}_{u,j}^T & G_{2,j} + G_{2,j}^T - \sum_{i=1}^{N} f_i^j P_{2,i} & \star \\ \tilde{B}_{w2,j}^T & 0 & I \end{bmatrix} = \Phi_j > 0 \tag{2.49}$$

for $j = 1, \ldots, M$, *and*

$$\begin{bmatrix} \sum_{i=1}^{N} \left(f_i^j + f_i^\ell + h_i^j + h_i^\ell \right) P_{2,i} & \star & \star \\ \Phi_{21,j\ell} & \Phi_{22,j\ell} & \star \\ \tilde{B}_{w2,j}^T + \tilde{B}_{w2,\ell}^T & 0 & 2I \end{bmatrix} = \Phi_{j\ell} > 0 \tag{2.50}$$

with

$$\Phi_{21,j\ell} = G_{2,j}^T \tilde{A}_\ell^T + G_{2,\ell}^T \tilde{A}_j^T + Z_j^T \tilde{B}_{u,\ell}^T + Z_\ell^T \tilde{B}_{u,j}^T$$

$$\Phi_{22,j\ell} = G_{2,j} + G_{2,j}^T + G_{2,\ell} + G_{2,\ell}^T - \sum_{i=1}^{N} \left(f_i^j + f_i^\ell \right) P_{2,i}$$

for $j = 1, \ldots, M-1$ *and* $\ell = j+1, \ldots, M$, *and*

$$\begin{bmatrix} \sum_{i=1}^{N} f_i^j W_i - \tilde{D}_{2w,j}\tilde{D}_{2w,j}^T & \star \\ G_{2,j}^T \tilde{C}_{2z,j}^T + Z_j^T \tilde{D}_{2u,j}^T & G_{2,j} + G_{2,j}^T - \sum_{i=1}^{N} f_i^j P_{2,i} \end{bmatrix} = \Psi_j > 0 \tag{2.51}$$

for $j = 1, \ldots, M$, *and*

$$\begin{bmatrix} \sum_{i=1}^{N} \left(f_i^j + f_i^\ell\right) W_i - \tilde{D}_{2w,j}\tilde{D}_{2w,\ell}^T + \tilde{D}_{2w,\ell}\tilde{D}_{2w,j}^T & \star \\ G_{2,j}^T \tilde{C}_{2z,\ell}^T + G_{2,\ell}^T \tilde{C}_{2z,j}^T + Z_j^T \tilde{D}_{2u,\ell}^T + Z_\ell^T \tilde{D}_{2u,j}^T & \Psi_{22,j\ell} \end{bmatrix} = \Psi_{j\ell} > 0 \tag{2.52}$$

with

$$\Psi_{22,j\ell} = G_{2,j} + G_{2,j}^T + G_{2,\ell} + G_{2,\ell}^T - \sum_{i=1}^{N} \left(f_i^j + f_i^\ell\right) P_{2,i}$$

for $j = 1, \ldots, M-1$ *and* $\ell = j+1, \ldots, M$ *where*

$$\begin{aligned} G_{\infty j} &= \begin{bmatrix} \sum_{i=1}^{N} f_i^j G_{i,1} & 0 \\ G_{\infty j,2} & G_{\infty j,3} \end{bmatrix}, \quad G_{2j} = \begin{bmatrix} \sum_{i=1}^{N} f_i^j G_{i,1} & 0 \\ G_{2j,2} & G_{2j,3} \end{bmatrix}, \quad \textit{and} \\ Z_j &= \begin{bmatrix} \sum_{i=1}^{N} f_i^j Z_{i,1} & 0 \end{bmatrix}, \end{aligned} \tag{2.53}$$

then the parameter-dependent static output feedback gain

$$K(\lambda_k) = \hat{Z}(\lambda_k)\hat{G}(\lambda_k)^{-1} \tag{2.54}$$

with

$$\hat{Z}(\lambda_k) = \sum_{i=1}^{N} \lambda_i(k) Z_{i,1} \quad \textit{and} \quad \hat{G}(\lambda_k) = \sum_{i=1}^{N} \lambda_i(k) G_{i,1} \tag{2.55}$$

stabilizes the system H^∞ *with a guaranteed* $\mathcal{H}_\infty$ *performance bounded by* η *and the system*

H^2 with a guaranteed $\mathcal{H}_2$ performance bounded by ν given by

$$\nu^2 = \min_{P_{\infty,i},P_{2,i},G_{i,1},G_{\infty j,2},G_{2j,2},G_{\infty j,3},G_{2j,3},Z_{i,1},W_i} \max_i \operatorname{trace}\{W_i\}. \tag{2.56}$$

The proof for Lemma 7 is provided by [12].

Chapter 3

Guaranteed $\ell_2 - \ell_\infty$ gain control of LPV systems

3.1 Introduction

The design of multi-objective, mixed $\mathcal{H}_2/\mathcal{H}_\infty$ controllers has been a topic of interest for sometime [9, 54, 32, 30, 15, 56, 35, 17, 12]. The goal of using both $\mathcal{H}_2$ and $\mathcal{H}_\infty$ performance criteria is to design a controller which can meet multiple performance objectives. In [9] and [54] mixed $\mathcal{H}_2/\mathcal{H}_\infty$ control was introduced by minimizing the $\mathcal{H}_2$ norm of a closed-loop transfer function subject to an $\mathcal{H}_\infty$ norm constraint of another closed-loop transfer function. In [32], mixed $\mathcal{H}_2/\mathcal{H}_\infty$ state-feedback and output-feedback controllers were designed for continuous-time systems by using a convex optimization approach to solve the coupled nonlinear matrix Riccati equations and in [30] a similar approach is used for discrete-time systems. The state-feedback $\mathcal{H}_2/\mathcal{H}_\infty$ design with regional pole placement was addressed by [15] using the linear matrix inequality (LMI) approach. In [56] and [35], the LMI approach for multi-objective control synthesis for output-feedback controllers is presented. In [18], an extra instrumental variable was added to the LMI stability conditions to build a parameter dependent Lyapunov function capable of proving the stability of uncertain linear-time-invariant (LTI) systems. The new extended LMI conditions in [18] were used in [17] to develop $\mathcal{H}_2$ and $\mathcal{H}_\infty$ LMI conditions for linear state-feedback and output-feedback controllers

for uncertain LTI systems. The extended LMI conditions provided by [17] were utilized in [11] and [10] to develop linear parameter varying (LPV) static output feedback controllers that meet $\mathcal{H}_2$ [11] and $\mathcal{H}_\infty$ [10] performance bounds for linear time-varying (LTV) systems with polytopic uncertainty. The results presented in [11] and [10] were extended in [12] to cover the synthesis of multi-objective $\mathcal{H}_2/\mathcal{H}_\infty$ gain-scheduled output feedback controllers.

Gain scheduling controllers designed using the LPV method have traditionally included $\mathcal{H}_\infty$ performance constraints. This is largely due to the fact that $\mathcal{H}_\infty$ controllers can provide robust stability margins that $\mathcal{H}_2$ controllers cannot provide [83]. However, since the $\mathcal{H}_\infty$ norm is defined as the root-mean-square gain, or ℓ_2 to ℓ_2 gain, from the exogenous input to the regulated output, controllers designed with only $\mathcal{H}_\infty$ performance constraints are not suitable for use when hard constraints on responses or actuator signals must be met.

When hard constraints on responses or actuator signals must be met, a controller with a guaranteed ℓ_2 to ℓ_∞ gain is needed, which is a special type of $\mathcal{H}_2$ controller [87]. A controller with a guaranteed ℓ_2 to ℓ_∞ gain provides strict bounds on the regulated output while minimizing the control input as much as possible. This problem was solved for LTI systems in [87], where it is referred to as the output covariance constraint (OCC) problem. The OCC problem defined in [87] is to find a controller for a given system to minimize the weighted control input cost subject to a set of output constraints. The OCC problem has two interesting interpretations: stochastic and deterministic. The stochastic interpretation is obtained by first assuming that the $\mathcal{H}_2$ exogenous inputs are uncorrelated zero-mean white noises with a given intensity. Then the OCC problem minimizes the weighted control input covariance subject to the output covariance constraints, such that the constraints are interpreted as constraints on the variance of the performance variables. The deterministic interpretation is obtained by assuming that the $\mathcal{H}_2$ exogenous inputs are unknown but belong

to a bounded ℓ_2 energy set. Then the OCC problem minimizes the weighted control input while ensuring that the maximum singular values, or ℓ_∞ response, of the regulated outputs are less than the corresponding output constraints. In other words, the OCC problem is the problem of minimizing the weighted sum of worst-case peak values on the control signal subject to the constraints on the worst-case peak values of the performance variables. This interpretation is important in applications where hard constraints on responses or actuator signals cannot be ignored, such as space telescope pointing [86], machine tool control, and system identification of biological systems. For both interpretations, a solution to the OCC control problem results in a controller with a guaranteed ℓ_2 to ℓ_∞ gain.

The main contributions of this chapter are the guaranteed $\ell_2 - \ell_\infty$ gain controller synthesis LMIs for gain-scheduled state-feedback and dynamic output-feedback control for discrete-time polytopic LPV systems in Section 3.3. When these LMIs are satisfied, the optimal state-feedback or dynamic output-feedback LPV controller obtained guarantees that for a finite disturbance energy, hard constraints on the regulated output are met. The guaranteed ℓ_2 to ℓ_∞ gain is achieved by modifying $\mathcal{H}_2$ control synthesis LMIs covered in Chapter 2 to minimize the weighted control input cost while ensuring the output covariances meet the performance constraints.

The chapter is organized as follows. Section 3.2 formally introduces the $\ell_2 - \ell_\infty$ gain performance criteria. The mixed $\ell_2 - \ell_\infty/\mathcal{H}_\infty$ control problem is formulated in Section 3.3 to obtain gain-scheduled state-feedback and dynamic output-feedback controllers that have a guaranteed ℓ_2 to ℓ_∞ gain. In Section 3.4, a numerical example is presented to illustrate the performance of the algorithm. Some concluding remarks for this work are provided in Section 3.5.

3.2 $\ell_2 - \ell_\infty$ Performance of Discrete-time Systems

Consider again the discrete-time, closed-loop, LPV system H in (2.17), which for convenience is reproduced here

$$H := \begin{cases} x(k+1) = \mathcal{A}(\lambda_k)x(k) + \mathcal{B}_w(\lambda_k)w(k), \quad x(0) = 0 \\ \qquad z(k) = \mathcal{C}_z(\lambda_k)x(k) + \mathcal{D}_w(\lambda_k)w(k). \end{cases}$$

As in Chapter 2, the system matrices $\mathcal{A}(\lambda_k)$, $\mathcal{B}_w(\lambda_k)$, $\mathcal{C}_z(\lambda_k)$, $\mathcal{D}_w(\lambda_k)$, also belong to a polytope similar to $\mathfrak{D}$ in (2.11).

To define the $\ell_2 - \ell_\infty$ performance criteria for the system H, first the following assumptions are made:

1. The system output $z(k)$ is partitioned into $z(k) = [z_p(k)^T,\ z_u(k)^T]^T$,
2. and the feed-through matrix $\mathcal{D}(\lambda_k) = 0$,

such that the system output $z(k)$ is given by

$$z(k) := \begin{bmatrix} z_p(k) \\ z_u(k) \end{bmatrix} = \begin{bmatrix} \mathcal{C}_p(\lambda_k) \\ \mathcal{C}_u(\lambda_k) \end{bmatrix} x(k), \tag{3.1}$$

where the vector $z_p(k)$ contains all the variables whose dynamic responses are of interest and the vector $z_u(k)$ contains the weighted control variables to be minimized. The impulse response of the variables in $z_p(k)$ is given by

$$h(k) = \mathcal{C}_p(\lambda_k) \left(\prod_{\ell=0}^{k-1} \mathcal{A}(\lambda_\ell) \right) \mathcal{B}_w(\lambda_k), \text{ with } \prod_{\ell=k}^{k-1} \mathcal{A}(\lambda_\ell) = I,$$

for $k \geq 0$. If we define the ℓ_∞ and ℓ_2 norms

$$\|z_p\|_\infty^2 = \sup_{k\geq 0} z_p^T(k) z_p(k), \quad \|w\|_2^2 = \sum_{\ell=0}^{\infty} w^T(\ell) w(\ell), \tag{3.2}$$

then from [74, 85] it can be shown that

$$\|z_p\|_\infty^2 \leq \overline{\sigma}\left(\sum_{k=0}^{\infty} h(k) h^T(k)\right) \|w\|_2^2, \tag{3.3}$$

where $\overline{\sigma}(\cdot)$ denotes the maximum singular value. In [12] it is demonstrated that

$$\sum_{k=0}^{\infty} h(k) h^T(k) = \mathcal{C}_p(\lambda_k) \bar{\mathcal{P}}(\lambda_k) \mathcal{C}_p^T(\lambda_k) \tag{3.4}$$

where $\bar{\mathcal{P}}(\lambda_k)$ is the closed-loop controllability Gramian from the disturbance input $w(k)$ satisfying

$$\bar{\mathcal{P}}(\lambda_{k+1}) = \mathcal{A}(\lambda_k) \bar{\mathcal{P}}(\lambda_k) \mathcal{A}(\lambda_k)^T + \mathcal{B}(\lambda_k) \mathcal{B}(\lambda_k)^T, \tag{3.5}$$

such that

$$\|z_p\|_\infty^2 \leq \overline{\sigma}\left(\mathcal{C}_p(\lambda_k) \bar{\mathcal{P}}(\lambda_k) \mathcal{C}_p^T(\lambda_k)\right) \|w\|_2^2. \tag{3.6}$$

Suppose that some a priori information about the constraints on the performance of z_p is known such that an output covariance bound $\overline{Z}_p$ can be constructed. It is the purpose of this chapter to design an LPV state-feedback or dynamic, output feedback controller with

$$\|z_p\|_\infty^2 \leq \overline{\sigma}\left(\overline{Z}_p\right) \|w\|_2^2, \tag{3.7}$$

such that the guaranteed $\ell_2 - \ell_\infty$ gain is given by

$$\sup_{w \in \ell_2, \|w\|_2^2 \neq 0} \frac{\|z_p\|_\infty^2}{\|w\|_2^2} \leq \overline{\sigma}\left(\overline{Z}_p\right), \tag{3.8}$$

where

$$Z_p(\lambda_k) = \mathcal{C}_p(\lambda_k)\bar{\mathcal{P}}(\lambda_k)\mathcal{C}_p(\lambda_k)^T \leq \overline{Z}_p. \tag{3.9}$$

This problem, which we call the guaranteed $\ell_2 - \ell_\infty$ gain problem, is defined as follows: find a static state feedback or full-order dynamic output feedback controller to minimize the control energy

$$Z_u(\lambda_k) = \text{trace}\left\{\mathcal{C}_u(\lambda_k)\bar{\mathcal{P}}(\lambda_k)\mathcal{C}_u(\lambda_k)^T\right\}, \tag{3.10}$$

of the closed-loop system H, subject to the hard constraint $\overline{Z}_p$.

Theorem 8. *Consider the system H, given by* (2.17) *with the performance output given by* (3.1). *Given the output covariance* $\overline{Z}_p$, *if there exist parameter-dependent matrices* $\mathcal{G}(\lambda_k)$, $\mathcal{P}(\lambda_k) = \mathcal{P}(\lambda_k)^T > 0$, *and* $\mathcal{W}(\lambda_k) = \mathcal{W}(\lambda_k)^T > 0$, *for all* $\lambda_k \in \Lambda_N$, *such that*

$$\begin{bmatrix} \mathcal{P}(\lambda_{k+1}) & \mathcal{A}(\lambda_k)\mathcal{G}(\lambda_k) & \mathcal{B}(\lambda_k) \\ \mathcal{G}(\lambda_k)^T\mathcal{A}(\lambda_k)^T & \mathcal{G}(\lambda_k) + \mathcal{G}(\lambda_k)^T - \mathcal{P}(\lambda_k) & 0 \\ \mathcal{B}(\lambda_k)^T & 0 & I \end{bmatrix} > 0, \tag{3.11}$$

$$\begin{bmatrix} \mathcal{W}(\lambda_k) & \mathcal{C}_u(\lambda_k)\mathcal{G}(\lambda_k) \\ \mathcal{G}(\lambda_k)^T\mathcal{C}_u(\lambda_k)^T & \mathcal{G}(\lambda_k) + \mathcal{G}(\lambda_k)^T - \mathcal{P}(\lambda_k) \end{bmatrix} > 0, \tag{3.12}$$

$$\overline{Z}_p - \mathcal{C}_p(\lambda_k)\mathcal{P}(\lambda_k)\mathcal{C}_p(\lambda_k)^T \geq 0, \tag{3.13}$$

then the closed-loop system (2.17) *is exponentially stable with a guaranteed* ℓ_2 *to* ℓ_∞ *perfor-*

mance given by

$$\sup_{w\in\ell_2,\|w\|_2^2\neq 0} \frac{\|z_p\|_\infty^2}{\|w\|_2^2} \leq \overline{\sigma}\left(\overline{Z}_p\right), \tag{3.14}$$

and a control energy bounded by

$$\begin{aligned} \overline{Z}_u &= \inf_{\mathcal{P}(\lambda_k),\mathcal{G}(\lambda_k),\mathcal{W}(\lambda_k)} \sup_{\lambda_k\in\Lambda_N} \operatorname{trace}\left\{\mathcal{W}(\lambda_k)\right\}, \\ &\geq \operatorname{trace}\left\{\mathcal{C}_u(\lambda_k)\mathcal{P}(\lambda_k)\mathcal{C}_u(\lambda_k)^T\right\} \geq Z_u(\lambda_k). \end{aligned} \tag{3.15}$$

Proof. The closed-loop system H is stabilized with the control energy bounded by (3.15) as a result of applying Lemma 2. However, the guaranteed $\ell_2 - \ell_\infty$ gain performance (3.14) is a result of the LMI (3.13). Since (3.11) implies that

$$\mathcal{P}(\lambda_{k+1}) > \mathcal{A}(\lambda_k)\mathcal{P}(\lambda_k)\mathcal{A}(\lambda_k)^T + \mathcal{B}(\lambda_k)\mathcal{B}(\lambda_k)^T, \tag{3.16}$$

there exist matrices $M(\lambda_k) = M(\lambda_k)^T > 0$ such that

$$\mathcal{P}(\lambda_{k+1}) = \mathcal{A}(\lambda_k)\mathcal{P}(\lambda_k)\mathcal{A}(\lambda_k)^T + \mathcal{B}(\lambda_k)\mathcal{B}(\lambda_k)^T + M(\lambda_k). \tag{3.17}$$

Consequently, $\mathcal{P}(\lambda_k) > \bar{\mathcal{P}}(\lambda_k)$ for all $k \geq 0$, which shows that

$$\overline{Z}_p \geq \mathcal{C}_p(\lambda_k)\mathcal{P}(\lambda_k)\mathcal{C}_p(\lambda_k)^T \geq \mathcal{C}_p(\lambda_k)\bar{\mathcal{P}}(\lambda_k)\mathcal{C}_p(\lambda_k)^T = Z_p(k). \tag{3.18}$$

Thus, it follows that the guaranteed $\ell_2 - \ell_\infty$ gain (3.14) is satisfied.

□

Since LMI conditions have been characterized for the $\ell_2 - \ell_\infty$ gain performance of a

polytopic LPV system, attention will now be focused on using this LMI conditions to develop LMIs for the controller synthesis of gain-scheduled state feedback and dynamic, output feedback controllers.

3.3 Controller Synthesis for mixed $\ell_2 - \ell_\infty/\mathcal{H}_\infty$ Control Problem

This section considers the design of minimum energy gain-scheduled controllers that provide a guaranteed $\ell_2 - \ell_\infty$ gain for the closed-loop system, while also satisfying some other $\mathcal{H}_\infty$ performance criteria for robustness. Thus, in this section we consider the following discrete-time polytopic time-varying systems: the system H^h with the $\ell_2 - \ell_\infty$ gain, which provides hard constraints that must be satisfied, given by

$$H^h := \begin{cases} x_p(k+1) = A(\lambda_k)x_p(k) + B_h(\lambda_k)w_h(k) + B_u(\lambda_k)u(k) \\ z_p(k) = C_p(\lambda_k)x_p(k) \\ z_u(k) = D_{hu}(\lambda_k)u(k) \\ y(k) = C_y(\lambda_k)x_p(k) + D_{yh}(\lambda_k)w_h(k) \end{cases} \tag{3.19}$$

and the $\mathcal{H}_\infty$ weighted system H^∞ given by

$$H^\infty := \begin{cases} x_p(k+1) = A(\lambda_k)x_p(k) + B_\infty(\lambda_k)w_\infty(k) + B_u(\lambda_k)u(k) \\ z_\infty(k) = C_\infty(\lambda_k)x_p(k) + D_\infty(\lambda_k)w_\infty(k) + D_{\infty u}(\lambda_k)u(k) \\ y(k) = C_y(\lambda_k)x_p(k) + D_{y\infty}(\lambda_k)w_\infty(k) \end{cases} \tag{3.20}$$

where $x_p(k) \in \mathbb{R}^n$ is the state, $w_h(k) \in \mathbb{R}^{rh}$ and $w_\infty \in \mathbb{R}^{r\infty}$ are the exogenous inputs, and $u(k) \in \mathbb{R}^m$ is the control input. The outputs $z_u(k) \in \mathbb{R}^{ph}$ and $z_\infty(k) \in \mathbb{R}^{p\infty}$ are the weighted system performance outputs for the mixed control synthesis, while the output $z_p(k) \in \mathbb{R}^c$ contains all variables whose dynamic responses have hard constraints that must be met. The output vector $y(k) \in \mathbb{R}^q$ is the measurement to be used for control. The goal is to provide a finite-dimensional set of LMIs for the synthesis of both gain-scheduled state feedback controllers of the form

$$u(k) = K(\lambda_k)x(k) \tag{3.21}$$

and gain-scheduled, strictly proper, output feedback controllers of the form

$$\begin{aligned} x_c(k+1) &= A_c(\lambda_k)x_c(k) + B_c(\lambda_k)y(k) \\ u(k) &= C_c(\lambda_k)x_c(k) \end{aligned} \tag{3.22}$$

such that the closed-loop systems given by

$$H_{cl}^h := \begin{cases} x(k+1) = \mathcal{A}(\lambda_k)x(k) + \mathcal{B}_h(\lambda_k)w_h(k), \\ \quad z_p(k) = \mathcal{C}_p(\lambda_k)x(k), \\ \quad z_u(k) = \mathcal{C}_u(\lambda_k)x(k), \end{cases} \tag{3.23}$$

and

$$H_{cl}^\infty := \begin{cases} x(k+1) = \mathcal{A}(\lambda_k)x(k) + \mathcal{B}_\infty(\lambda_k)w_\infty(k), \\ \quad z_\infty = \mathcal{C}_\infty(\lambda_k)x(k) + \mathcal{D}_\infty(\lambda_k)w_\infty(k), \end{cases} \tag{3.24}$$

are exponentially stable and satisfy hard constraints on desired performance outputs for all possible trajectories of the parameter $\lambda_k \in \Lambda_N$, while minimizing the control energy and satisfying a robustness criteria defined as an $\mathcal{H}_\infty$ performance bound.

3.3.1 Gain-Scheduled State Feedback Control Synthesis

In this section, it is assumed that the state vector, $x_p(k)$, is available for feedback without corruption from the exogenous inputs $w_h(k)$ or $w_\infty(k)$. This is a standard assumption, and as in [17] can be enforced on the measurement equation in (3.19) and (3.20) by assigning to the matrices $C_y(\lambda_k)$, $D_{yh}(\lambda_k)$, and $D_{y\infty}(\lambda_k)$ the values $C_y(\lambda_k) = I$, $D_{yh}(\lambda_k) = 0$, and $D_{y\infty}(\lambda_k) = 0$. The feedback structure provided by the gain-scheduled state-feedback controller (3.21), produces the closed-loop systems H_{cl}^h and H_{cl}^∞ in (3.23) and (3.24), where $x(k) = x_p(k)$ and the closed-loop system matrices given by

$$\begin{aligned}
&\mathcal{A}(\lambda_k) = A(\lambda_k) + B_u(\lambda_k)K(\lambda_k), \quad \mathcal{B}_h(\lambda_k) = B_h(\lambda_k), \quad \mathcal{B}_\infty(\lambda_k) = B_\infty(\lambda_k), \\
&\mathcal{C}_p(\lambda_k) = C_p(\lambda_k), \quad \mathcal{C}_u(\lambda_k) = D_{hu}(\lambda_k)K(\lambda_k), \\
&\mathcal{C}_\infty(\lambda_k) = C_\infty(\lambda_k) + D_{\infty u}(\lambda_k)K(\lambda_k), \quad \mathcal{D}_\infty(\lambda_k) = D_\infty(\lambda_k).
\end{aligned} \tag{3.25}$$

When substituting these closed-loop matrices into the first LMI of Theorem 8, the following bilinear matrix inequality results:

$$\begin{bmatrix} P_h(\lambda_k) & (A(\lambda_k) + B_u(\lambda_k)K(\lambda_k))\,G(\lambda_k) & B_h(\lambda_k) \\ \star & G(\lambda_k) + G(\lambda_k)^T - P_h(\lambda_k) & 0 \\ \star & \star & I \end{bmatrix} > 0. \tag{3.26}$$

Multiplying the instrumental variable into the parenthesis gives

$$\begin{bmatrix} P_h(\lambda_k) & A(\lambda_k)G(\lambda_k) + B_u(\lambda_k)K(\lambda_k)G(\lambda_k) & B_h(\lambda_k) \\ \star & G(\lambda_k) + G(\lambda_k)^T - P_h(\lambda_k) & 0 \\ \star & \star & I \end{bmatrix} > 0, \tag{3.27}$$

which clearly shows a multiplication between the state-feedback controller $K(\lambda_k)$ and the instrumental variable $G(\lambda_k)$. However, by letting $L(\lambda_k) = K(\lambda_k)G(\lambda_k)$, the following LMI is recovered:

$$\begin{bmatrix} P_h(\lambda_k) & A(\lambda_k)G(\lambda_k) + B_u(\lambda_k)L(\lambda_k) & B_h(\lambda_k) \\ \star & G(\lambda_k) + G(\lambda_k)^T - P_h(\lambda_k) & 0 \\ \star & \star & I \end{bmatrix} > 0. \tag{3.28}$$

The same substitution can be made in the second LMI of Theorem 8 to produce the following LMI:

$$\begin{bmatrix} W(\lambda_k) & D_{hu}(\lambda_k)L(\lambda_k) \\ \star & G(\lambda_k) + G(\lambda_k)^T - P_h(\lambda_k) \end{bmatrix} > 0. \tag{3.29}$$

The parameter-dependent, full-state feedback controller is solved for by performing a convex optimization over a set of linear matrix inequalities. The LMIs in this section are an extension of the work presented in [12], which is covered in Chapter 2. Using the parameterizations (2.32), (2.33), and (2.34) from Chapter 2, the finite-dimensional LMIs in the following theorem can be solved to obtain a full-state feedback controller (3.21) such that the closed-loop systems for H^h and H^∞ have a guaranteed $\ell_2 - \ell_\infty$ and $\mathcal{H}_\infty$ gain, respectively.

In the following theorem, the LMI conditions from Lemma 7 are adapted to solve the mixed controller synthesis problem posed in this section for the gain-scheduled state-feedback control problem.

Theorem 9. *Consider the system H^h, given by* (3.19)*. Assume that the vectors f^j and h^j of Γ_b are given. Given $\overline{Z}_p$, if there exists, for $i = 1, 2, \ldots, N$, matrices, $G_i \in \mathbb{R}^{n\times n}$ and $Z_i \in \mathbb{R}^{m\times n}$, and symmetric positive-definite matrices $P_{h,i} \in \mathbb{R}^{n\times n}$ and $W_i \in \mathbb{R}^{p_h\times p_h}$ such*

that

$$\begin{bmatrix} \hat{P}_{h,j} & \star & \star \\ \tilde{G}_j^T \tilde{A}_j^T + \tilde{Z}_j^T \tilde{B}_{u,j}^T & \tilde{G}_j + \tilde{G}_j^T - \tilde{P}_{h,j} & \star \\ \tilde{B}_{h,j}^T & 0 & I \end{bmatrix} = \Phi_j > 0 \tag{3.30}$$

for $j = 1, 2, \ldots, M$, *and*

$$\begin{bmatrix} \hat{P}_{h,j} + \hat{P}_{h,\ell} & \star & \star \\ \Phi_{21,j\ell} & \Phi_{22,j\ell} & \star \\ \tilde{B}_{h,j}^T + \tilde{B}_{h,\ell}^T & 0 & 2I \end{bmatrix} = \Phi_{j\ell} > 0 \tag{3.31}$$

with

$$\Phi_{21,j\ell} = \tilde{G}_j^T \tilde{A}_\ell^T + \tilde{G}_\ell^T \tilde{A}_j^T + \tilde{Z}_j^T \tilde{B}_{u,\ell}^T + \tilde{Z}_\ell^T \tilde{B}_{u,j}^T$$

$$\Phi_{22,j\ell} = \tilde{G}_j + \tilde{G}_j^T + \tilde{G}_\ell + \tilde{G}_\ell^T - \tilde{P}_{h,j} - \tilde{P}_{h,\ell}$$

for $j = 1, \ldots, M-1$ *and* $\ell = j+1, \ldots, M$, *and*

$$\begin{bmatrix} \tilde{W}_j & \star \\ \tilde{Z}_j^T \tilde{D}_{hu,j}^T & \tilde{G}_j + \tilde{G}_j^T - \tilde{P}_{h,j} \end{bmatrix} = \Psi_j > 0 \tag{3.32}$$

for $j = 1, 2, \ldots, M$ *and*

$$\begin{bmatrix} \tilde{W}_j + \tilde{W}_\ell & \star \\ \tilde{Z}_j^T \tilde{D}_{hu,\ell}^T + \tilde{Z}_\ell^T \tilde{D}_{hu,j}^T & \Psi_{22,j\ell} \end{bmatrix} = \Psi_{j\ell} > 0 \tag{3.33}$$

with

$$\Psi_{22,j\ell} = \tilde{G}_j + \tilde{G}_j^T + \tilde{G}_\ell + \tilde{G}_\ell^T - \tilde{P}_{h,j} - \tilde{P}_{h,\ell}$$

for $j = 1, \ldots, M-1$ *and* $\ell = j+1, \ldots, M$ *and*

$$\overline{Z}_p - C_{p,i} P_{h,i} C_{p,i}^T \geq 0, \quad i = 1, 2, \ldots, N, \tag{3.34}$$

with

$$\hat{P}_{h,j} = \sum_{i=1}^{N} \left(f_i^j + h_i^j \right) P_{h,i}, \quad \tilde{P}_{h,j} = \sum_{i=1}^{N} f_i^j P_{h,i},$$
$$\tilde{G}_j = \sum_{i=1}^{N} f_i^j G_i, \ \tilde{Z}_j = \sum_{i=1}^{N} f_i^j Z_i, \ \textit{and} \quad \tilde{W}_j = \sum_{i=1}^{N} f_i^j W_i.$$

then the parameter-dependent full state feedback gain

$$K(\lambda) = \hat{Z}(\lambda) \hat{G}(\lambda)^{-1} \tag{3.35}$$

with

$$\hat{Z}(\lambda) = \sum_{i=1}^{N} \lambda_i Z_i \quad \textit{and} \quad \hat{G}(\lambda) = \sum_{i=1}^{N} \lambda_i G_i \tag{3.36}$$

stabilizes the the system H^h *with a guaranteed (weighted) control energy bounded by* $\overline{Z}_u$ *given by*

$$\begin{aligned} \overline{Z}_u &= \min_{P_{\infty,i}, P_{\sigma,i}, G_i, Z_i, W_i} \max_i \operatorname{trace}\{W_i\} \\ &\geq \operatorname{trace}\{R K(\lambda) P_h(\lambda) K(\lambda)^T\} = Z_u(\lambda_k) \end{aligned} \tag{3.37}$$

while also ensuring that the hard constraint $\overline{Z}_p$ *is satisfied. Additionally, consider the system*

H^∞, *given by* (3.20). *If there exist, for* $i = 1, 2, \ldots, N$, *symmetric positive-definite matrices* $P_{\infty,i} \in \mathbb{R}^{n\times n}$ *such that*

$$\begin{bmatrix} \hat{P}_{\infty,j} & \star & \star & \star \\ \tilde{G}_j^T \tilde{A}_j^T + \tilde{Z}_j^T \tilde{B}_{u,j}^T & \tilde{G}_j + \tilde{G}_j^T - \tilde{P}_{\infty,j} & \star & \star \\ \tilde{B}_{\infty,j}^T & 0 & \eta I & \star \\ 0 & \tilde{C}_{\infty,j}\tilde{G}_j + \tilde{D}_{\infty u,j}\tilde{Z}_j & \tilde{D}_{\infty,j} & \eta I \end{bmatrix} = \Theta_j > 0 \tag{3.38}$$

for $j = 1, 2, \ldots, M$ *and*

$$\begin{bmatrix} \hat{P}_{\infty,j} + \hat{P}_{\infty,\ell} & \star & \star & \star \\ \Theta_{21,j\ell} & \Theta_{22,j\ell} & \star & \star \\ \tilde{B}_{\infty,j}^T + \tilde{B}_{\infty,\ell}^T & 0 & 2\eta I & \star \\ 0 & \Theta_{42,j\ell} & \tilde{D}_{\infty,j} + \tilde{D}_{\infty,\ell} & 2\eta I \end{bmatrix} = \Theta_{j\ell} > 0 \tag{3.39}$$

with

$$\Theta_{21,j\ell} = \tilde{G}_j^T \tilde{A}_\ell^T + \tilde{G}_\ell^T \tilde{A}_j^T + \tilde{Z}_j^T \tilde{B}_{u,\ell}^T + \tilde{Z}_\ell^T \tilde{B}_{u,j}^T$$

$$\Theta_{22,j\ell} = \tilde{G}_j + \tilde{G}_j^T + \tilde{G}_\ell + \tilde{G}_\ell^T - \tilde{P}_{\infty,j} - \tilde{P}_{\infty,\ell}$$

$$\Theta_{42,j\ell} = \tilde{C}_{\infty,j}\tilde{G}_\ell + \tilde{C}_{\infty,\ell}\tilde{G}_j + \tilde{D}_{\infty u,j}\tilde{Z}_\ell + \tilde{D}_{\infty u,\ell}\tilde{Z}_j$$

for $j = 1, 2, \ldots, M-1$ *and* $\ell = j+1, \ldots, M$, *where*

$$\hat{P}_{\infty,j} = \sum_{i=1}^{N} \left(f_i^j + h_i^j \right) P_{\infty,i}, \quad \tilde{P}_{\infty,j} = \sum_{i=1}^{N} f_i^j P_{\infty,i},$$

then the parameter-dependent full-state feedback gain $K(\lambda)$ given by (3.35) *also stabilizes the system H^∞ with a guaranteed $\mathcal{H}_\infty$ performance bounded by η.*

Proof. The following properties are a consequence of applying Lemma 7:

- The system H^∞ is stabilized with a guaranteed $\mathcal{H}_\infty$ performance bounded by η when the LMIs (3.38) and (3.39) are satisfied.
- The system H^h is stabilized with a guaranteed (weighted) control energy bounded by $\overline{Z}_u$ (3.37) when the LMIs (3.30),(3.31),(3.32), and (3.33) are satisfied.

However, the fact the output constraint (3.7) is satisfied for $i = 1, 2, \ldots, N$ follows from the LMI constraint (3.34)

$$\overline{Z}_p - C_{p,i} P_{h,i} C_{p,i}^T \geq 0, \quad i = 1, 2, \ldots, N.$$

Since the LMIs (3.30),(3.31),(3.32), and (3.33) are all required to be positive-definite, from [12] it can be shown that

$$P_h(\lambda_k) = \sum_{i=1}^{N} \lambda_i(k) P_{h,i} > \bar{\mathcal{P}}(\lambda_k), \quad \forall k \geq 0,$$

where $\bar{\mathcal{P}}(\lambda_k)$ is the controllability Gramian satisfying (3.5). Thus, it is also true that

$$\overline{Z}_p - C_p(\lambda_k) \bar{P}(\lambda_k) C_p(\lambda_k)^T \geq 0$$

such that

$$Z_p(\lambda_k) = C_p(\lambda_k) \bar{\mathcal{P}}(\lambda_k) C_p(\lambda_k)^T \leq \overline{Z}_p.$$

□

3.3.2 Output Feedback LMIs

The feedback structure provided by the gain-scheduled dynamic output-feedback controller (3.22), produces the closed-loop systems H_{cl}^{h} and H_{cl}^{∞} in (3.23) and (3.24) where $x(k) = [x_p^T(k) \quad x_c^T(k)]^T$ with the closed-loop system matrices given by

$$
\begin{aligned}
\mathcal{A}(\lambda_k) &= \begin{bmatrix} A(\lambda_k) & B_u(\lambda_k)C_c(\lambda_k) \\ B_c(\lambda_k)C_y(\lambda_k) & A_c(\lambda_k) \end{bmatrix}, \\
\mathcal{B}_h(\lambda_k) &= \begin{bmatrix} B_h(\lambda_k) \\ B_c(\lambda_k)D_{yh}(\lambda_k) \end{bmatrix}, \quad \mathcal{B}_\infty(\lambda_k) = \begin{bmatrix} B_\infty(\lambda_k) \\ B_c(\lambda_k)D_{y\infty}(\lambda_k) \end{bmatrix}, \\
\mathcal{C}_p(\lambda_k) &= \begin{bmatrix} C_p(\lambda_k) & 0 \end{bmatrix}, \quad \mathcal{C}_u(\lambda_k) = \begin{bmatrix} 0 & D_{hu}(\lambda_k)C_c(\lambda_k) \end{bmatrix}, \\
\mathcal{C}_\infty(\lambda_k) &= \begin{bmatrix} C_\infty(\lambda_k) & D_{\infty u}(\lambda_k)C_c(\lambda_k) \end{bmatrix}, \quad \mathcal{D}_\infty(\lambda_k) = D_\infty(\lambda_k).
\end{aligned}
\tag{3.40}
$$

For the full-state feedback problem, the parameter-dependent, strictly proper output feedback controller is also solved for by performing a convex optimization over a set of linear matrix inequalities. The LMIs in this section are an extension of the work presented in [13]. It is clear that when substituting the closed-loop matrices (3.40) into the matrix inequalities of the performance conditions in Lemma 1 and Theorem 8 nonlinear matrix inequalities result, due to the multiplication between the unknown controller matrices and the slack variable $\mathcal{G}(\lambda_k)$. To obtain set of LMI conditions, the authors in [13] first chose the slack variable $\mathcal{G}(\lambda_k)$ to be independent of the scheduling parameter λ_k, such that $\mathcal{G}(\lambda_k) = \mathcal{G}$. Then the slack variable $\mathcal{G}$, its inverse $\mathcal{G}^{-1}$, the Lyapunov matrix $\mathcal{P}(\lambda_k)$, and the controller

matrices $\mathcal{K}(\lambda_k)$ are partitioned as

$$\mathcal{G} := \begin{bmatrix} X & Z_1 \\ U & Z_2 \end{bmatrix}, \quad \mathcal{G}^{-1} := \begin{bmatrix} Y^T & Z_3 \\ V^T & Z_4 \end{bmatrix},$$
$$\mathcal{P}(\lambda_k) := \begin{bmatrix} P(\lambda_k) & P_2(\lambda_k) \\ P_2(\lambda_k)^T & P_3(\lambda_k) \end{bmatrix}, \quad \mathcal{K}(\lambda_k) := \begin{bmatrix} A_c(\lambda_k) & B_c(\lambda_k) \\ C_c(\lambda_k) & 0 \end{bmatrix}.$$

From the definition of $\mathcal{G}$ and $\mathcal{G}^{-1}$, it is clear that the following relationship must hold:

$$\mathcal{G}\mathcal{G}^{-1} = \begin{bmatrix} X & Z_1 \\ U & Z_2 \end{bmatrix} \begin{bmatrix} Y^T & Z_3 \\ V^T & Z_4 \end{bmatrix} = \begin{bmatrix} XY^T + Z_1V^T & XZ_3 + Z_1Z_4 \\ UY^T + Z_2V^T & UZ_3 + Z_2Z_4 \end{bmatrix} = \begin{bmatrix} I & 0 \\ 0 & I \end{bmatrix},$$

such that $XY^T + Z_1V^T = I$ and $UY^T + Z_2V^T = 0$. Now, as done in [56, 35, 17, 13], the parameter-independent transformation matrix

$$\mathcal{T} := \begin{bmatrix} I & Y^T \\ 0 & V^T \end{bmatrix} \tag{3.41}$$

is introduced and the following nonlinear parameter-dependent change of variables is defined:

$$\begin{aligned} \begin{bmatrix} Q(\lambda_k) & F(\lambda_k) \\ L(\lambda_k) & 0 \end{bmatrix} := \begin{bmatrix} V & YB_u(\lambda_k) \\ 0 & I \end{bmatrix} \mathcal{K}(\lambda_k) \begin{bmatrix} U & 0 \\ C_y(\lambda_k)X & I \end{bmatrix} \\ + \begin{bmatrix} Y \\ 0 \end{bmatrix} A(\lambda_k) \begin{bmatrix} X & 0 \end{bmatrix}, \end{aligned} \tag{3.42}$$

$$\begin{bmatrix} P(\lambda_k) & J(\lambda_k) \\ J(\lambda_k)^T & H(\lambda_k) \end{bmatrix} := \mathcal{T}^T \mathcal{P} \mathcal{T}, \tag{3.43}$$

$$S := YX + VU. \tag{3.44}$$

The nonlinear matrix inequalities that result from substituting the closed-loop matrices into the matrix inequalities in Theorem 8 can be transformed into the following LMIs:

$$\begin{bmatrix} P(\lambda_k) & J(\lambda_k) & A(\lambda_k)X + B_u(\lambda_k)L(\lambda_k) & A(\lambda_k) & B_w(\lambda_k) \\ \star & H(\lambda_k) & Q(\lambda_k) & YA(\lambda_k) + F(\lambda_k)C_y(\lambda_k) & YB_w(\lambda_k) \\ \star & \star & X + X^T - P(\lambda_k) & I + S^T - J(\lambda_k) & 0 \\ \star & \star & \star & Y + Y^T - H(\lambda_k) & 0 \\ \star & \star & \star & \star & I \end{bmatrix} > 0 \tag{3.45}$$

$$\begin{bmatrix} W(\lambda_k) & D_{zu}(\lambda_k)L(\lambda_k) & 0 \\ \star & X + X^T - P(\lambda_k) & I + S^T - J(\lambda_k) \\ \star & \star & Y + Y^T - H(\lambda_k) \end{bmatrix} > 0 \tag{3.46}$$

$$\overline{Z}_p - C_p(\lambda_k)P(\lambda_k)C_p(\lambda_k)^T > 0 \tag{3.47}$$

by using the congruence transformations $T_1 = \text{diag}(\mathcal{T}, \mathcal{T}, I)$ and $T_2 = \text{diag}(I, \mathcal{T})$ on the first and second nonlinear matrix inequalities, respectively. While the matrix inequalities in (3.45), (3.46), and (3.47) are now LMIs, they are still infinite dimensional and must be evaluated for all values of time-varying barycentric coordinates λ_k. To obtain a finite-dimensional set of LMIs, the parameter dependent structure imposed on the Lyapunov matrix in (2.23) is imposed on the Lyapunov matrix here as well. In the following, the same parameterizations used for the state-feedback case are utilized for the gain-scheduled dynamic output-feedback

control problem.

Theorem 10. *Consider the system H^h, given by* (3.19). *Assume that the vectors f^j and h^j of Γ_b are given. Given $\overline{Z}_p$, if there exists matrices $X \in \mathbb{R}^{n\times n}$, $Y \in \mathbb{R}^{n\times n}$, and for $i = 1, 2, \ldots, N$, matrices, $J_{h,i} \in \mathbb{R}^{n\times n}$, $L_i \in \mathbb{R}^{m\times n}$, and $F_i \in \mathbb{R}^{n\times q}$, and symmetric positive-definite matrices $P_{h,i} \in \mathbb{R}^{n\times n}$, $H_{h,i} \in \mathbb{R}^{n\times n}$, and $W_i \in \mathbb{R}^{p_h\times p_h}$ such that*

$$\begin{bmatrix} \hat{P}_{h,j} & \hat{J}_{h,j} & \tilde{A}_j X + \tilde{B}_{u,j}\tilde{L}_j & \tilde{A}_j & \tilde{B}_{h,j} \\ \star & \hat{H}_{h,j} & \tilde{Q}_j & Y\tilde{A}_j + \tilde{F}_j\tilde{C}_{y,j} & Y\tilde{B}_{h,j} + \tilde{F}_j\tilde{D}_{yh,j} \\ \star & \star & X + X^T - \tilde{P}_{h,j} & I + S^T - \tilde{J}_{h,j} & 0 \\ \star & \star & \star & Y + Y^T - \tilde{H}_{h,j} & 0 \\ \star & \star & \star & \star & I \end{bmatrix} = \Psi_j > 0 \quad (3.48)$$

for $j = 1, \ldots, M$, and

$$\begin{bmatrix} \hat{P}_j + \hat{P}_\ell & \hat{J}_j + \hat{J}_\ell & \Psi_{13,j\ell} & \tilde{A}_j + \tilde{A}_\ell & \tilde{B}_{h,j} + \tilde{B}_{h,\ell} \\ \star & \hat{H}_j + \hat{H}_\ell & \tilde{Q}_j + \tilde{Q}_\ell & \Psi_{24,j\ell} & \Psi_{25,j\ell} \\ \star & \star & \Psi_{33,j\ell} & 2I + 2S^T - \tilde{J}_j - \tilde{J}_\ell & 0 \\ \star & \star & \star & 2Y + 2Y^T - \tilde{H}_j - \tilde{H}_\ell & 0 \\ \star & \star & \star & \star & 2I \end{bmatrix} = \Psi_{j\ell} > 0 \quad (3.49)$$

with

$$\Psi_{13,j\ell} = \tilde{A}_j X + \tilde{A}_\ell X + \tilde{B}_{u,j}\tilde{L}_\ell + \tilde{B}_{u,\ell}\tilde{L}_j$$

$$\Psi_{24,j\ell} = Y\tilde{A}_j + Y\tilde{A}_\ell + \tilde{F}_j\tilde{C}_{y,\ell} + \tilde{F}_\ell\tilde{C}_{y,j}$$

$$\Psi_{25,j\ell} = Y\tilde{B}_{h,j} + Y\tilde{B}_{h,\ell} + \tilde{F}_j\tilde{D}_{yh,\ell} + \tilde{F}_\ell\tilde{D}_{yh,j}$$

$$\Psi_{33,j\ell} = 2X + 2X^T - \tilde{P}_j - \tilde{P}_\ell$$

for $j = 1, \ldots, M-1$ *and* $\ell = j+1, \ldots, M$, *and*

$$\begin{bmatrix} \tilde{W}_j & \tilde{D}_{hu,j}\tilde{L}_j & 0 \\ \star & X + X^T - \tilde{P}_j & I + S^T - \tilde{J}_j \\ \star & \star & Y + Y^T - \tilde{H}_j \end{bmatrix} = \Phi_j > 0 \tag{3.50}$$

for $j = 1, \ldots, M$, *and*

$$\begin{bmatrix} \tilde{W}_j + \tilde{W}_\ell & \tilde{D}_{hu,j}\tilde{L}_\ell + \tilde{D}_{hu,\ell}\tilde{L}_j & 0 \\ \star & 2X + 2X^T - \tilde{P}_j - \tilde{P}_\ell & 2I + 2S^T - \tilde{J}_j - \tilde{J}_\ell \\ \star & \star & 2Y + 2Y^T - \tilde{H}_j - \tilde{H}_\ell \end{bmatrix} = \Phi_{j\ell} > 0 \tag{3.51}$$

for $j = 1, \ldots, M-1$ *and* $\ell = j+1, \ldots, M$, *and*

$$\overline{Z}_p - C_{p,i}P_{\sigma,i}C_{p,i}^T \geq 0, \quad i = 1, 2, \ldots, N, \tag{3.52}$$

where

$$
\begin{aligned}
\hat{P}_{h,j} &= \sum_{i=1}^{N}(f_i^j + h_i^j)P_{h,i}, \quad \hat{J}_{h,j} = \sum_{i=1}^{N}(f_i^j + h_i^j)J_{h,i}, \quad \hat{H}_{h,j} = \sum_{i=1}^{N}(f_i^j + h_i^j)H_{h,i}, \\
\tilde{P}_{h,j} &= \sum_{i=1}^{N} f_i^j P_{h,i}, \quad \tilde{J}_{h,j} = \sum_{i=1}^{N} f_i^j J_{h,i}, \quad \tilde{H}_{h,j} = \sum_{i=1}^{N} f_i^j H_{h,i}, \\
\tilde{Q}_j &= \sum_{i=1}^{N} f_i^j Q_i, \quad \tilde{L}_j = \sum_{i=1}^{N} f_i^j L_i, \quad \tilde{F}_j = \sum_{i=1}^{N} f_i^j F_i, \\
\tilde{A}_j &= \sum_{i=1}^{N} f_i^j A_i, \quad \tilde{B}_{u,j} = \sum_{i=1}^{N} f_i^j B_{u,i}, \quad \tilde{B}_{w,j} = \sum_{i=1}^{N} f_i^j B_{w,i}, \\
\tilde{C}_{z,j} &= \sum_{i=1}^{N} f_i^j C_{z,i}, \quad \tilde{D}_{zu,j} = \sum_{i=1}^{N} f_i^j D_{zu,i}, \quad \tilde{D}_{zw,j} = \sum_{i=1}^{N} f_i^j D_{zw,i}, \\
\tilde{C}_{y,j} &= \sum_{i=1}^{N} f_i^j C_{y,i}, \quad \tilde{D}_{yw,j} = \sum_{i=1}^{N} f_i^j D_{yw,i},
\end{aligned}
\tag{3.53}
$$

then the parameter-dependent, strictly proper output feedback controller

$$
\begin{aligned}
x_c(k+1) &= A_c(\lambda_k)x_c(k) + B_c(\lambda_k)y(k) \\
u(k) &= C_c(\lambda_k)x_c(k)
\end{aligned}
$$

with

$$
\begin{aligned}
A_c(\lambda_k) &= V^{-1}\left(Q(\lambda_k) - YA(\lambda_k)X - YB_u(\lambda_k)L(\lambda_k) - F(\lambda_k)C_y(\lambda_k)X\right)U^{-1} \\
B_c(\lambda_k) &= V^{-1}F(\lambda_k) \\
C_c(\lambda_k) &= L(\lambda_k)U^{-1}
\end{aligned}
\tag{3.54}
$$

stabilizes the system H^h with a guaranteed (weighted) control energy bounded by $\overline{Z}_u$ while also ensuring that the hard constraint $\overline{Z}_p$ is satisfied. Additionally, consider the system H^∞, given by (3.20)*. If there exist, for $i = 1, 2, \ldots, N$, matrices $J_{\infty,i} \in \mathbb{R}^{n\times n}$ and symmetric*

positive-definite matrices $P_{\infty,i} \in \mathbb{R}^{n\times n}$ *and* $H_{\infty,i} \in \mathbb{R}^{n\times n}$ *such that*

$$\begin{bmatrix} \hat{P}_{\infty,j} & \hat{J}_{\infty,j} & \tilde{A}_j X + \tilde{B}_{u,j}\tilde{L}_j & \tilde{A}_j & \tilde{B}_{\infty,j} & 0 \\ \star & \hat{H}_{\infty,j} & \tilde{Q}_j & Y\tilde{A}_j + \tilde{F}_j\tilde{C}_{y,j} & \Theta_{25,j} & 0 \\ \star & \star & X + X^T - \tilde{P}_{\infty,j} & I + S^T - \tilde{J}_{\infty,j} & 0 & \Theta_{36,j} \\ \star & \star & \star & Y + Y^T - \tilde{H}_{\infty,j} & 0 & \tilde{C}_{\infty,j}^T \\ \star & \star & \star & \star & \eta I & \tilde{D}_{\infty,j}^T \\ \star & \star & \star & \star & \star & \eta I \end{bmatrix} = \Theta_j > 0 \qquad (3.55)$$

with

$$\Theta_{25,j} = Y\tilde{B}_{\infty,j} + \tilde{F}_j\tilde{D}_{y\infty,j}$$

$$\Theta_{36,j} = X^T\tilde{C}_{\infty,j}^T + \tilde{L}_j^T\tilde{D}_{\infty u,j}^T$$

for $j = 1, \ldots, M$

$$\begin{bmatrix} \hat{P}_{\infty,j} + \hat{P}_{\infty,\ell} & \hat{J}_{\infty,j} + \hat{J}_{\infty,\ell} & \Theta_{13,j\ell} & \tilde{A}_j + \tilde{A}_\ell & \Theta_{15,j\ell} & 0 \\ \star & \hat{H}_{\infty,j} + \hat{H}_{\infty,\ell} & \tilde{Q}_j + \tilde{Q}_\ell & \Theta_{24,j\ell} & \Theta_{25,j\ell} & 0 \\ \star & \star & \Theta_{33,j\ell} & \Theta_{34,j\ell} & 0 & \Theta_{36,j\ell} \\ \star & \star & \star & \Theta_{44,j\ell} & 0 & \Theta_{46,j\ell} \\ \star & \star & \star & \star & 2\eta I & \Theta_{56,j\ell} \\ \star & \star & \star & \star & \star & 2\eta I \end{bmatrix} = \Theta_{j\ell} > 0 \qquad (3.56)$$

with

$$\Theta_{13,j\ell} = \tilde{A}_j X + \tilde{A}_\ell X + \tilde{B}_{u,j}\tilde{L}_\ell + \tilde{B}_{u,\ell}\tilde{L}_j$$

$$\Theta_{15,j\ell} = \tilde{B}_{\infty,j} + \tilde{B}_{\infty,\ell}$$

$$\Theta_{24,j\ell} = Y\tilde{A}_j + Y\tilde{A}_\ell + \tilde{F}_j\tilde{C}_{y,\ell} + \tilde{F}_\ell\tilde{C}_{y,j}$$

$$\Theta_{25,j\ell} = Y\tilde{B}_{\infty,j} + Y\tilde{B}_{\infty,\ell} + \tilde{F}_j\tilde{D}_{y\infty,\ell} + \tilde{F}_\ell\tilde{D}_{y\infty,j}$$

$$\Theta_{33,j\ell} = 2X + 2X^T - \tilde{P}_{\infty,j} - \tilde{P}_{\infty,\ell}$$

$$\Theta_{34,j\ell} = 2I + 2S^T - \tilde{J}_{\infty,j} - \tilde{J}_{\infty,\ell}$$

$$\Theta_{36,j\ell} = X^T\tilde{C}^T_{\infty,j} + X^T\tilde{C}^T_{\infty,\ell} + \tilde{L}^T_j\tilde{D}^T_{\infty u,\ell} + \tilde{L}^T_\ell\tilde{D}^T_{\infty u,j}$$

$$\Theta_{44,j\ell} = 2Y + 2Y^T - \tilde{H}_{\infty,j} - \tilde{H}_{\infty,\ell}$$

$$\Theta_{46,j\ell} = \tilde{C}^T_{\infty,j} + \tilde{C}^T_{\infty,\ell}$$

$$\Theta_{56,j\ell} = \tilde{D}^T_{\infty,j} + \tilde{D}^T_{\infty,\ell}$$

for $j = 1, \ldots, M-1$ *and* $\ell = j+1, \ldots, M$, *and*

$$\begin{aligned}
\tilde{P}_{\infty,j} &= \sum_{i=1}^{N} f_i^j P_{\infty,i}, \quad \hat{P}_{\infty,j} = \sum_{i=1}^{N}(f_i^j + h_i^j)P_{\infty,i}, \\
\tilde{J}_{\infty,j} &= \sum_{i=1}^{N} f_i^j J_{\infty,i}, \quad \hat{J}_{\infty,j} = \sum_{i=1}^{N}(f_i^j + h_i^j)J_{\infty,i}, \\
\tilde{H}_{\infty,j} &= \sum_{i=1}^{N} f_i^j H_{\infty,i}, \quad \hat{H}_{\infty,j} = \sum_{i=1}^{N}(f_i^j + h_i^j)H_{\infty,i},
\end{aligned} \tag{3.57}$$

then the parameter-dependent, strictly proper output feedback controller also stabilizes the system H^∞ *with a guaranteed* $\mathcal{H}_\infty$ *performance bounded by* η.

The proof of Theorem 10 is similar to the proof for Theorem 9 and is omitted.

3.4 Numerical Example

Consider the discrete-time LPV system (originally used in [19], and later used in [4] and [17])

$$
\begin{aligned}
x_p(k+1) &= \underbrace{\begin{bmatrix} 2+\delta_1 & 0 & 1 \\ 1 & 0.5 & 0 \\ 0 & 1 & -0.5 \end{bmatrix}}_{A(\delta_1(k))} x_p(k) + \underbrace{\begin{bmatrix} 1+\delta_2 \\ 0 \\ 0 \end{bmatrix}}_{Bu(\delta_2(k))} u(k) + \underbrace{\begin{bmatrix} 0 \\ 1 \\ 0 \end{bmatrix}}_{B_h} w_p(k) \\
z_p(k) &= \underbrace{\begin{bmatrix} 1 & 0 & 0 \\ 0 & 1 & 0 \\ 0 & 0 & 1 \end{bmatrix}}_{C_p} x_p(k) \\
z_u(k) &= u(k)
\end{aligned}
\tag{3.58}
$$

where δ_i, $i = 1, 2$ are the time-varying parameters. In this section, two design examples with different performance constraints will be considered for both state-feedback and dynamic output-feedback control.

3.4.1 State Feedback Control

For the state-feedback controller design, the time-varying parameters were assumed to have the following parameter variation bounds:

$$
\delta_1 \in [-1,\, 1], \quad \text{and} \quad \delta_2 \in [-0.5,\, 0.5]. \tag{3.59}
$$

The discrete-time LPV system (3.58) is converted to the discrete-time polytopic LPV system (3.19) by solving $A(\delta_1)$ and $B_u(\delta_2)$ at the vertices of the parameter space polytope of δ_1 and δ_2. The exogenous ℓ_2 disturbance w_p is a scalar and the performance variable z_p has three components.

In the following, we consider two different ℓ_2 to ℓ_∞ gain designs. The designs differ in the grouping of the performance variables inside of z_p used to define the constraints (3.9). The constraints for each design are given as follows:

$$\textbf{Design 1:} \quad Z_p \leq 1.85 \times I_3, \tag{3.60}$$

$$\textbf{Design 2:} \quad Z_{p,1} \leq 1.85, \quad Z_{p,2} \leq 1.85 \times I_2, \tag{3.61}$$

where for design 1, Z_p denotes the (3×3) output covariance matrix corresponding to the all performance outputs in z_p grouped together. In design 2, $Z_{p,1}$ denotes the (1×1) output variance corresponding to the first performance output of z_p and $Z_{p,2}$ denotes the (2×2) output covariance matrix corresponding to the second and third performance outputs grouped together.

For each design, to enhance the robustness of the closed-loop system with the controller $K(\lambda_k)$ with respect to uncertainty in the measurements of the time-varying parameters δ_1 and δ_2, the closed-loop $\mathcal{H}_\infty$ norms of the transfer functions of some appropriately defined extra inputs and outputs that 'pull out' [19, 17] the uncertain parameters are bounded.

Specifically, the following H^∞ system is defined:

$$H^\infty = \begin{cases} x(k+1) = A(\delta_1(k))x(k) + B_u(\delta_2(k))u(k) + \begin{bmatrix} 1 \\ 0 \\ 0 \end{bmatrix} w_{\infty,1}(k) + \begin{bmatrix} 1 \\ 0 \\ 0 \end{bmatrix} w_{\infty,2}(k) \\ z_{\infty,1}(k) = \begin{bmatrix} 1 & 0 & 0 \end{bmatrix} x(k) \\ z_{\infty,2}(k) = u(k) \end{cases} \tag{3.62}$$

so that the robustness requirement is given by

$$\|H_{z_{\infty,i} w_{\infty,i}}(\lambda)\|_\infty < \eta = 100, \quad i = 1, 2, \tag{3.63}$$

where η defines the robustness level. Note that the notation used here, specifically $w_{\infty,1}(k)$ and $w_{\infty,2}(k)$ with the same input matrix, was selected to match what is found in the literature [19, 17].

For each of the ℓ_2-ℓ_∞ designs (3.60)-(3.61), the LMIs in Theorem 9 are programmed into MATLAB using the LMI parser YALMIP [34] and solved with SeDuMi [59] to minimize the cost function (3.37). As shown in Fig. 3.1 and Fig. 3.3A, each design is feasible and the achieved covariance bound is tight with the design bound in at least one dimension. The constraint in design 1 ensures that the covariance bound ellipsoid of Z_p remains inside of the sphere displayed in Fig. 3.1A. Side views of the covariance bound Z_p are displayed in Fig. 3.1B, Fig. 3.1C, and Fig. 3.1D. As displayed in Fig. 3.1C, the output covariance Z_p is tight with the bound in the $z_{p,2}$-$z_{p,3}$ plane.

For design 2, the constraints ensure that the variance of the first output of z_p will be

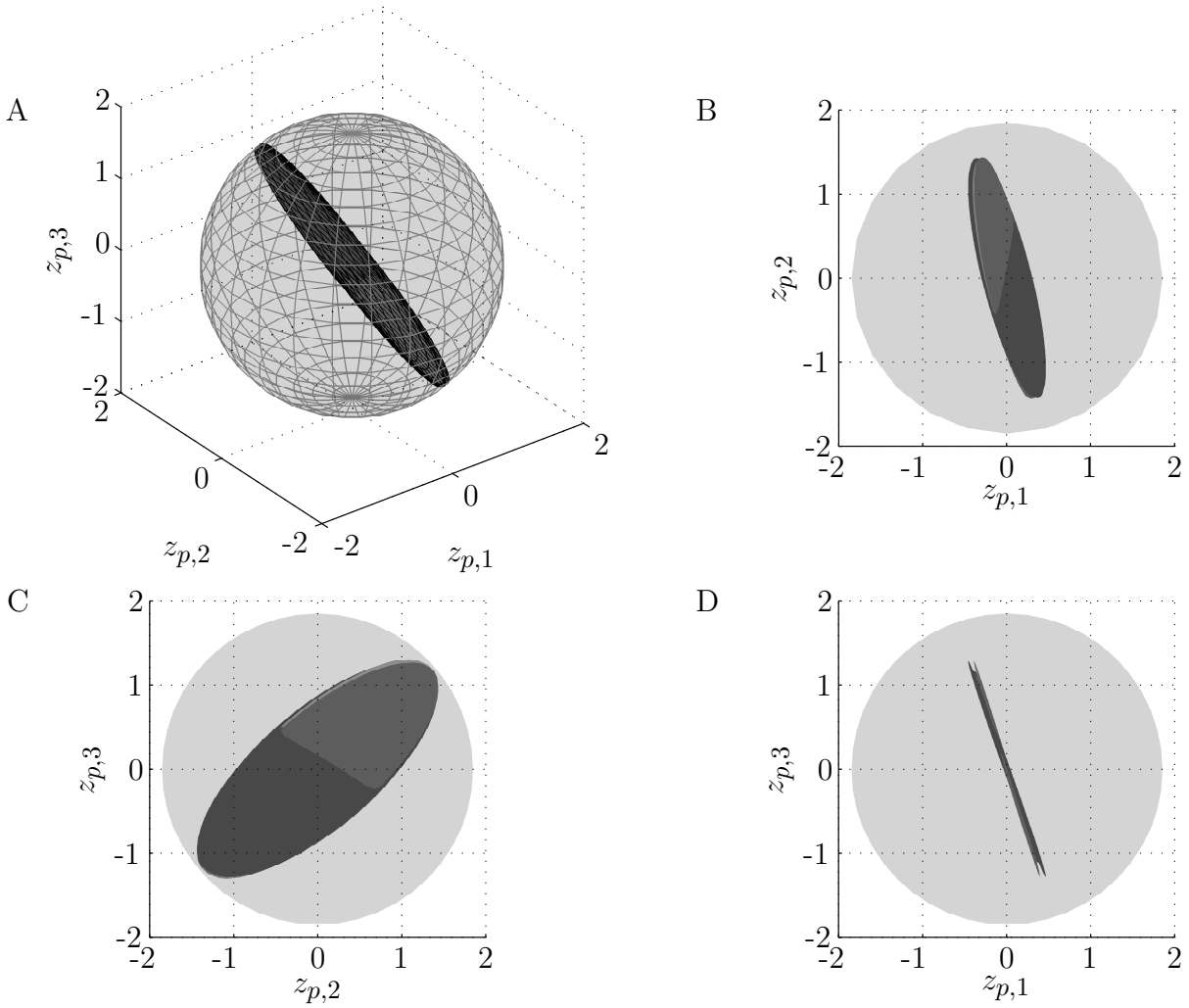

Figure 3.1: **Design 1:** The covariance bound Z_p achieved compared to the constraint (3.60).

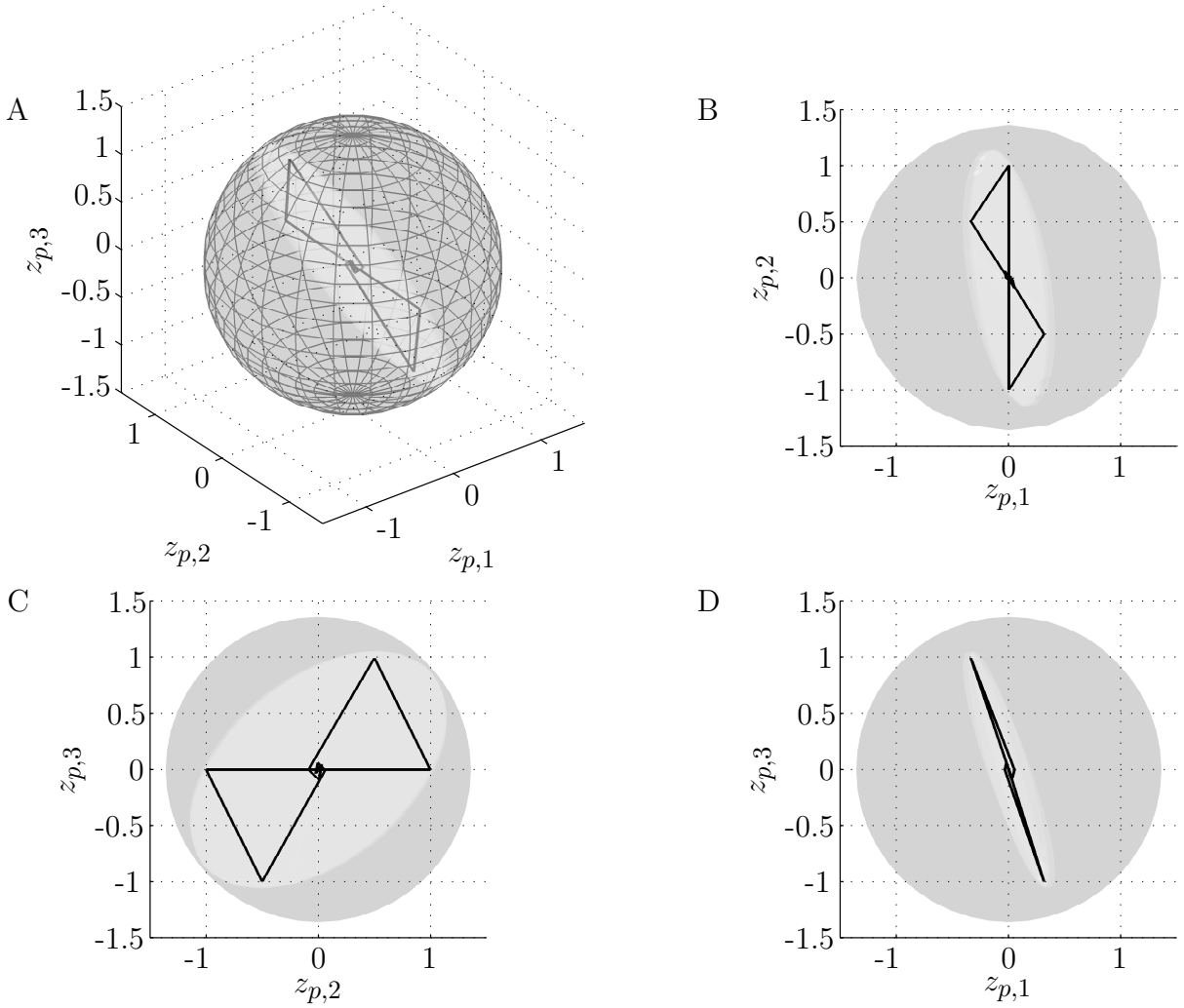

Figure 3.2: **Design 1:** The output response of $z_{p,1}$, $z_{p,2}$, and $z_{p,3}$ plotted against each other for design 1 simulated with a positive (I_1) and negative (I_2) impulse function and compared with the ℓ_∞ norm bound.

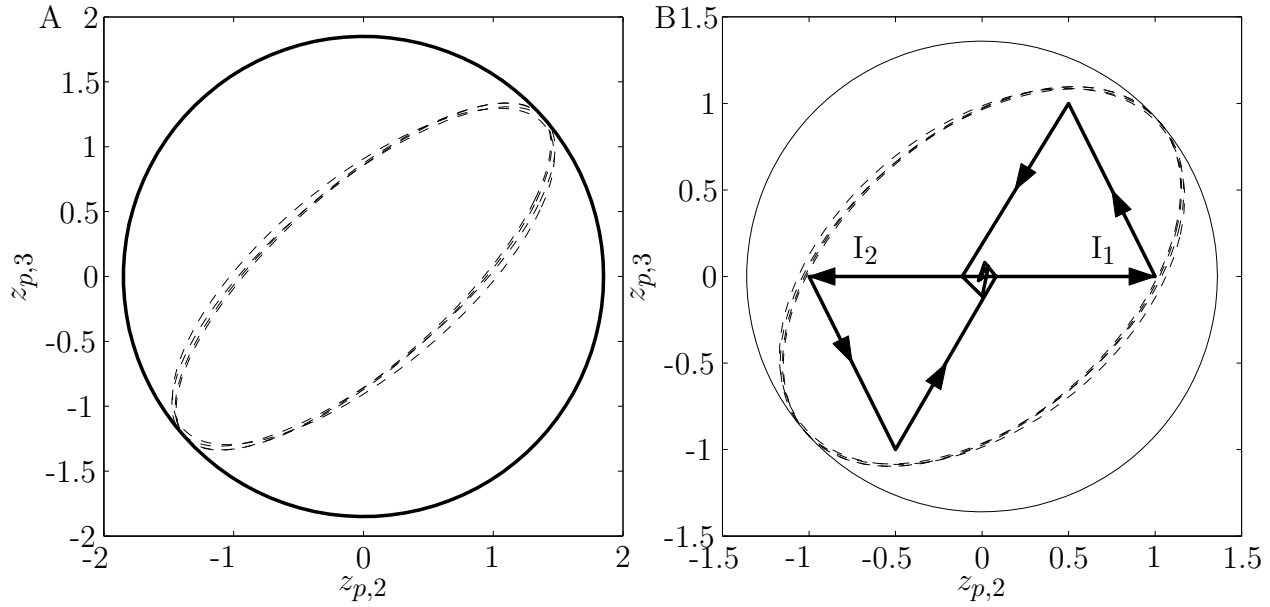

Figure 3.3: **Design 2:** A. The covariance bound $Z_{p,2}$ achieved compared to the second constraint in (3.61). B. The output response of $z_{p,2}$ plotted against $z_{p,3}$ for design 2 simulated with a positive and negative impulse function and compared with the ℓ_∞ norm bound.

below 1.85 and the covariance bound of second and third outputs of z_p will remain inside of the circle in Fig. 3.3A. The dashed ellipses in Fig. 3.3A are the obtained output covariances at each of the vertices for $i = 1, \ldots, 4$, and as shown they are tight with the bound.

To test the performance of each design, we simulate each of the controllers with a positive impulse (I_1) followed by a negative impulse (I_2) as displayed in Fig. 3.4A. To see the effect of the time-varying parameters, the parameters δ_1 and δ_2 are varied as displayed in Fig. 3.4B. The values used to compute the controller at each time step k are the noisy measurements displayed with a gray dashed line. The response to the ℓ_2 disturbance $w_p(k)$ for design 1 is displayed in Fig. 3.2. The response in Fig. 3.2 is plotted inside of the ℓ_∞ norm constraint (the square root of the covariance bound) sphere and the achieved ℓ_∞ norm bound ellipsoid. In Fig. 3.3B, the response of design 2 is plotted inside of the ℓ_∞ norm constraint circle and the achieved ℓ_∞ norm bound ellipse. The path of the response, with respect to each of the impulses (I_1) and (I_2), is also displayed in Fig. 3.3B. As shown in Fig. 3.2 and Fig. 3.3B, the

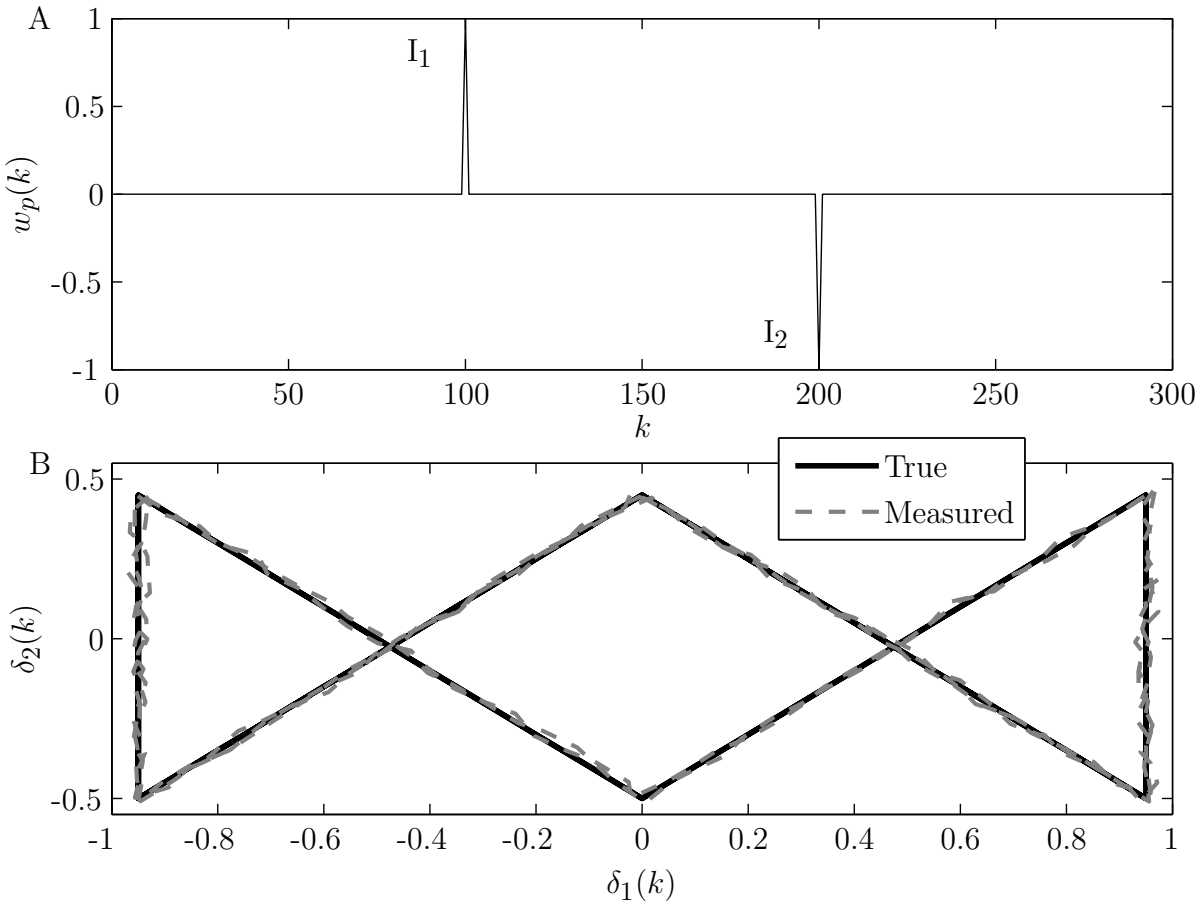

Figure 3.4: The ℓ_2 disturbance (A) and the parameter variation (B) used to simulate each controller design.

response for each design stays inside of the ℓ_∞ bound.

3.4.2 Dynamic Output-Feedback Control

For the dynamic output-feedback controller design, the measurement equation in [19, 4, 17] is given as

$$y(k) = \begin{bmatrix} 0 & 1+\delta_3(k) & 0 \end{bmatrix} x(k), \tag{3.64}$$

where δ_3 is an additional time-varying parameter. As one might guess, this is much more restrictive than the state feedback case. The good news is that the system is still observable (assuming $\delta_3 \neq -1$). However, the bad news is that in order to obtain a feasible controller with the LMIs provided by Theorem 10, some modifications need to be made to the problem. The modified discrete-time LPV is given by

$$\begin{aligned}
x_p(k+1) &= \underbrace{\begin{bmatrix} 2+\delta(k) & 0 & 1 \\ 1 & 0.5 & 0 \\ 0 & 1 & -0.5 \end{bmatrix}}_{A(\delta(k))} x_p(k) + \underbrace{\begin{bmatrix} 1+\delta(k) \\ 0 \\ 0 \end{bmatrix}}_{B_u(\delta(k))} u(k) + \underbrace{\begin{bmatrix} 0 \\ 0.1 \\ 0 \end{bmatrix}}_{B_h} w_p(k) \\
z_p(k) &= \underbrace{\begin{bmatrix} 1 & 0 & 0 \\ 0 & 1 & 0 \\ 0 & 0 & 1 \end{bmatrix}}_{C_p} x_p(k) \\
z_u(k) &= u(k) \\
y(k) &= \underbrace{\begin{bmatrix} 0 & 1+\delta(k) & 0 \end{bmatrix}}_{C_y(\delta(k))} x(k) + 0.01v(k)
\end{aligned} \tag{3.65}$$

Notice that in the modified system, each of the time-varying parameters δ_i, $i = 1, 2, 3$ have been set equal to each other such that $\delta = \delta_1 = \delta_2 = \delta_3$, which was originally done by the authors in [4]. Also, as in [4], the time-varying parameter δ is assumed to have the following parameter variation bound:

$$\delta \in [-0.2, \quad 0.2]. \tag{3.66}$$

As for the state-feedback design case, the discrete-time LPV system (3.65) is converted to the discrete-time polytopic LPV system (3.19) by solving $A(\delta)$, $B_u(\delta)$, and $C_y(\delta)$ at the vertices of the parameter space polytope of δ. For the dynamic output-feedback design, the exogenous ℓ_2 disturbance is given by the process disturbance $w_p(k)$ and the measurement disturbance $v(k)$, such that $w(k) = [w_p(k),\ v(k)]^T$. The performance variable z_p, again has three components.

As we did for the state-feedback control example, we also consider two different ℓ_2 to ℓ_∞ gain designs for the dynamic output-feedback control example. As before, the designs differ in the grouping of the performance variables inside of z_p used to define the constraints (3.9). The constraints for each design are given as follows:

$$\textbf{Design 1:} \quad Z_p \leq 5 \times I_3, \tag{3.67}$$

$$\textbf{Design 2:} \quad Z_{p,1} \leq 5, \quad Z_{p,2} \leq 5 \times I_2, \tag{3.68}$$

where for design 1, Z_p denotes the (3×3) output covariance matrix corresponding to the all performance outputs in z_p grouped together. In design 2, $Z_{p,1}$ denotes the (1×1) output variance corresponding to the first performance output of z_p and $Z_{p,2}$ denotes the (2×2) output covariance matrix corresponding to the second and third performance outputs

grouped together.

The robustness of the closed-loop system with the dynamic output-feedback controller with respect to uncertainty in the measurements of the time-varying parameter δ, the closed-loop $\mathcal{H}_\infty$ norms of the transfer functions of some appropriately defined extra inputs and outputs that 'pull out' [19, 17] the uncertain parameters are bounded. The system H^∞ used for the dynamic output-feedback design is the same as given in (3.62), with the following additions:

$$\begin{aligned} y(k) &= C_y(\delta(k))x(k) + w_{\infty,3}(k) \\ z_{\infty,3}(k) &= \begin{bmatrix} 0 & 1 & 0 \end{bmatrix} x(k) \end{aligned} \tag{3.69}$$

such that the robustness requirement is now given by

$$\|H_{z_{\infty,i}w_{\infty,i}}(\lambda)\|_\infty < \eta = 100, \quad i = 1, 2, 3, \tag{3.70}$$

where η defines the robustness level.

For each of the ℓ_2-ℓ_∞ designs (3.67)-(3.68), the LMIs in Theorem 10 are programmed into MATLAB and solved with LMI Lab [22] to minimize the control energy Z_u. As shown in Fig. 3.5 and Fig. 3.7A, each design is feasible and the achieved covariance bound is tight with the design bound in at least one dimension. The constraint in design 1 ensures that the covariance bound ellipsoid of Z_p remains inside of the sphere displayed in Fig. 3.1A. Side views of the covariance bound Z_p are displayed in Fig. 3.5B, Fig. 3.5C, and Fig. 3.5D. As displayed in Fig. 3.5C, the output covariance Z_p is tight with the bound in the $z_{p,2}$-$z_{p,3}$ plane.

For design 2, the constraints ensure that the variance of the first output of z_p will be

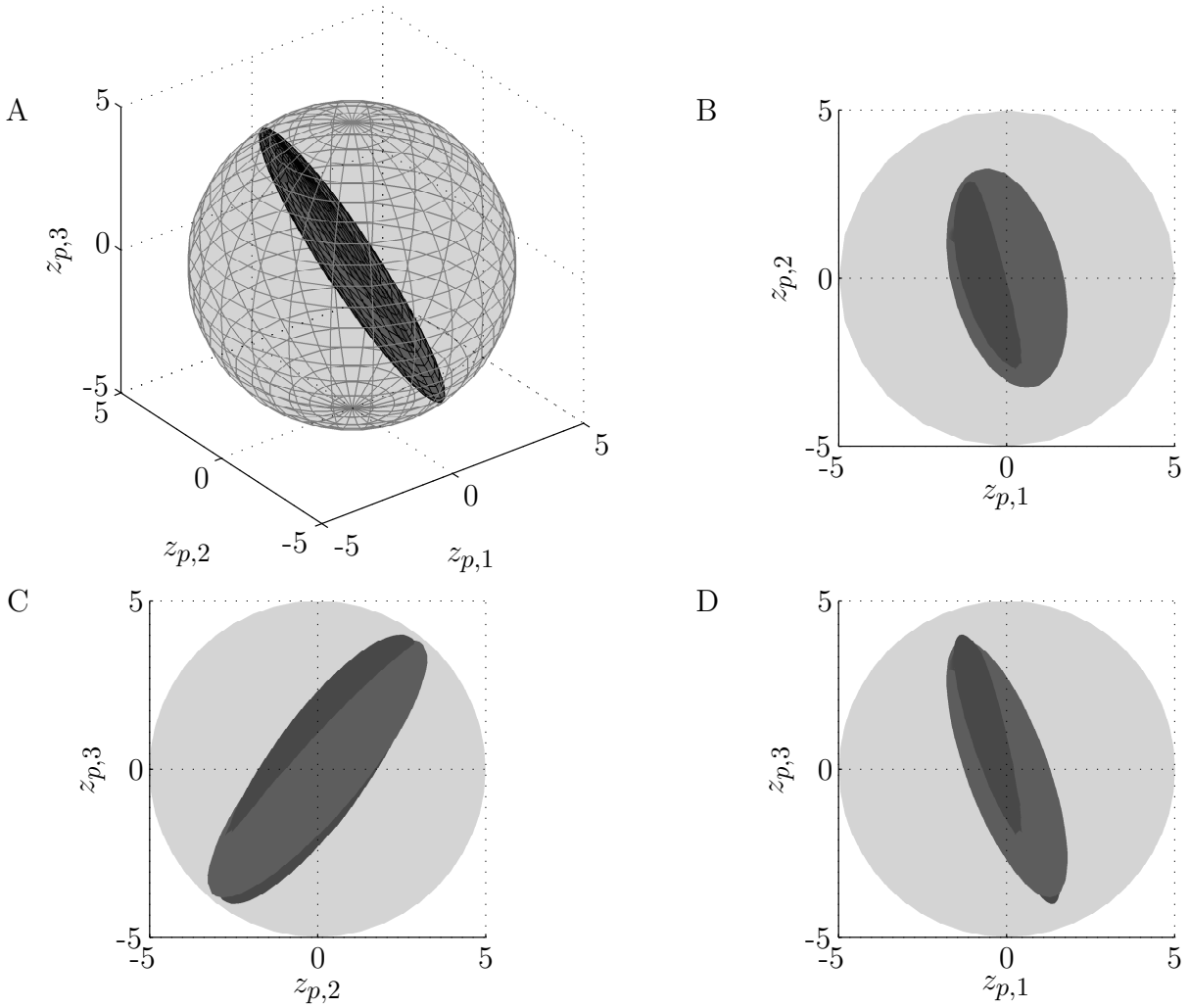

Figure 3.5: **Design 1:** The covariance bound Z_p achieved compared to the constraint (3.60).

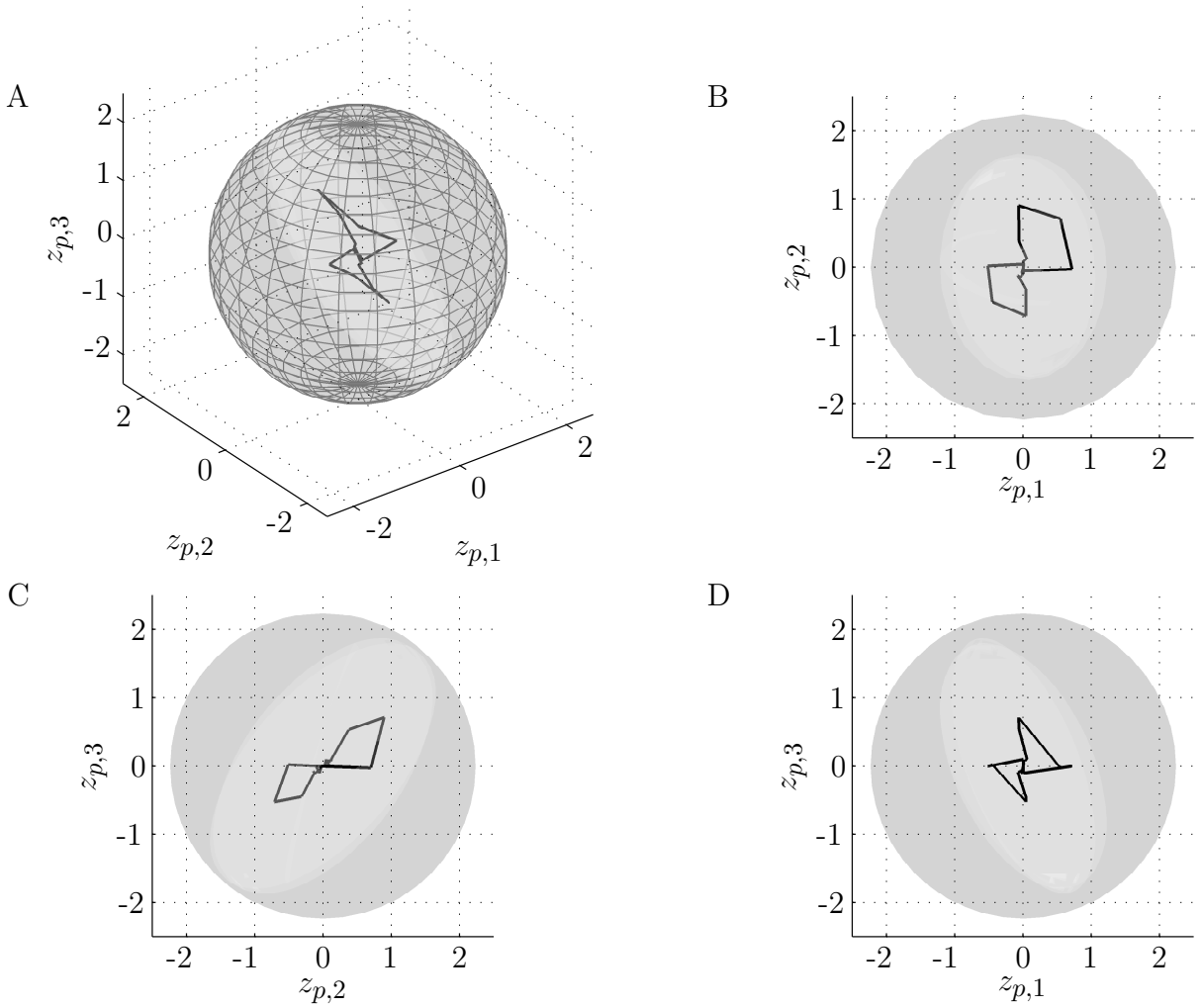

Figure 3.6: **Design 1:** The output response of $z_{p,1}$, $z_{p,2}$, and $z_{p,3}$ plotted against each other for design 1 simulated with a positive (I_1) and negative (I_2) impulse function and compared with the ℓ_∞ norm bound.

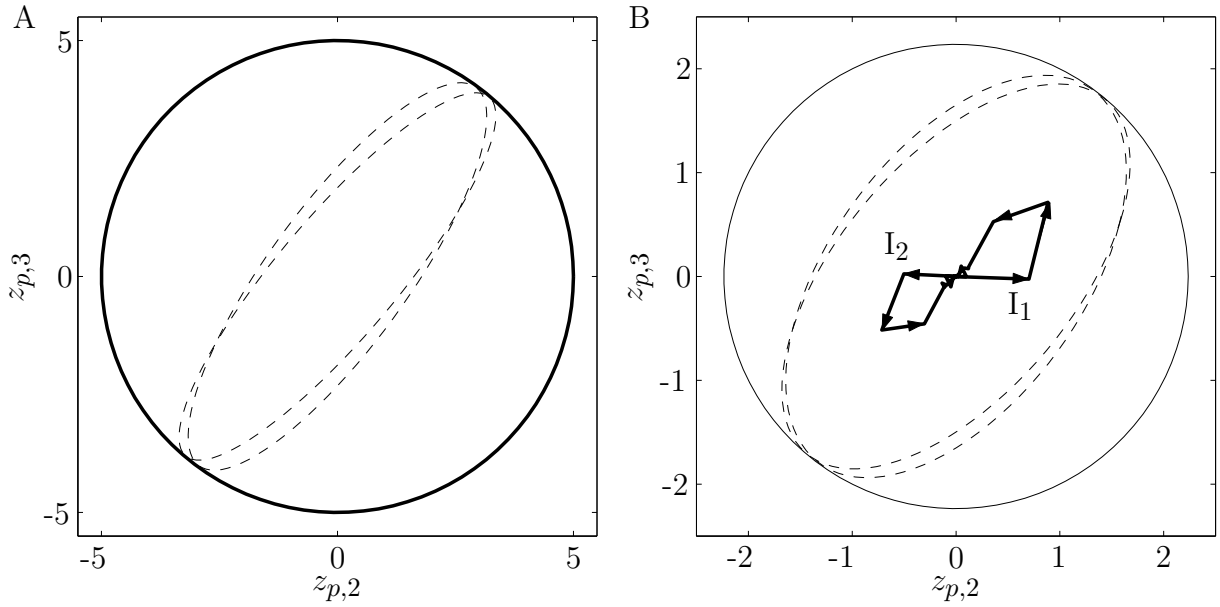

Figure 3.7: **Design 2:** A. The covariance bound $Z_{p,2}$ achieved compared to the second constraint in (3.61). B. The output response of $z_{p,2}$ plotted against $z_{p,3}$ for design 2 simulated with a positive and negative impulse function and compared with the ℓ_∞ norm bound.

below 5 and the covariance bound of second and third outputs of z_p will remain inside of the circle in Fig. 3.7A. The dashed ellipses in Fig. 3.7A are the obtained output covariances at each of the vertices for $i = 1, 2$, and as shown they are tight with the bound.

To test the performance of each design, we again simulate each of the controllers with a positive impulse (I_1) followed by a negative impulse (I_2) as displayed in Fig. 3.8A. To see the effect of the time-varying parameter, the parameter δ was varied as displayed in Fig. 3.8B. As before, the values used to compute the controller at each time step k are the noisy measurements displayed with a gray dashed line. The response to the ℓ_2 disturbance $w_p(k)$ for design 1 is displayed in Fig. 3.6. The response in Fig. 3.6 is plotted inside of the ℓ_∞ norm constraint (the square root of the covariance bound) sphere and the achieved ℓ_∞ norm bound ellipsoid. In Fig. 3.7B, the response of design 2 is plotted inside of the ℓ_∞ norm constraint circle and the achieved ℓ_∞ norm bound ellipse. The path of the response, with respect to each of the impulses (I_1) and (I_2), is also displayed in Fig. 3.7B. As shown

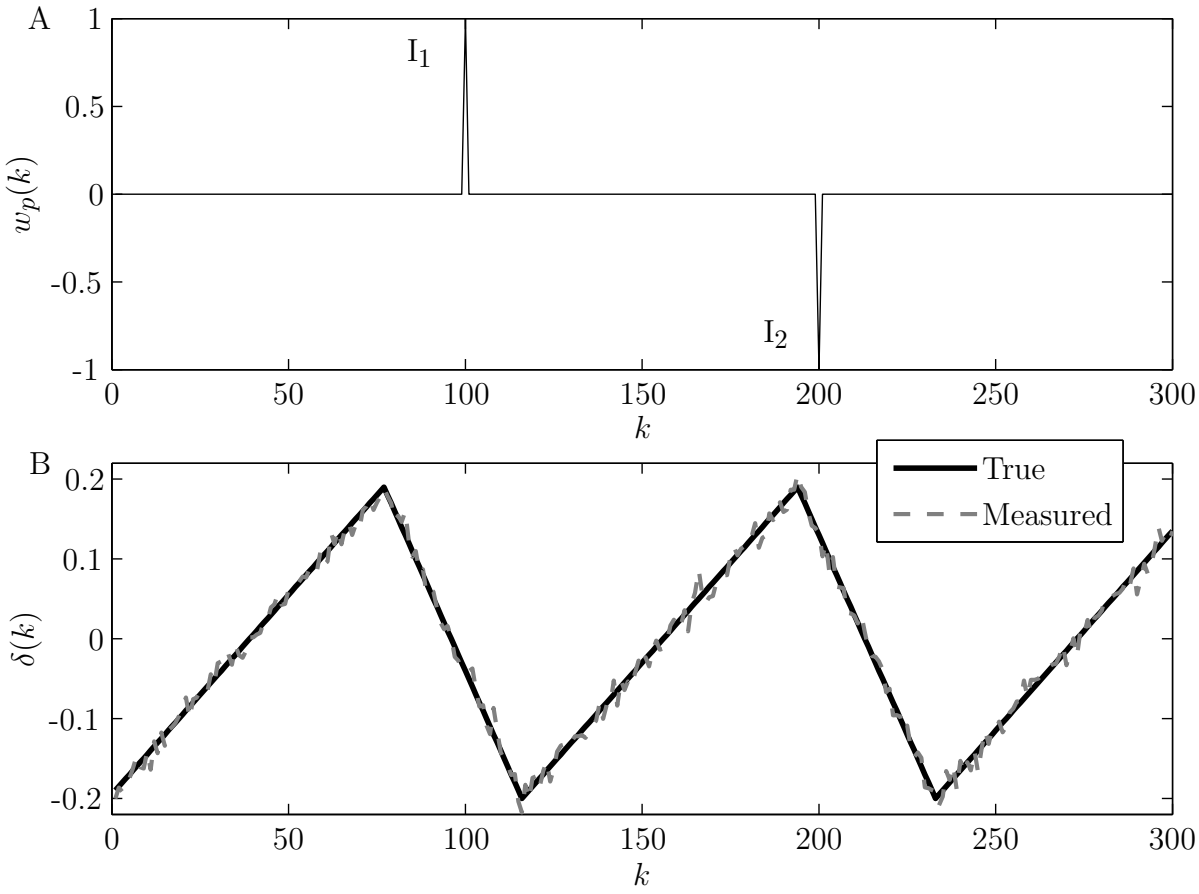

Figure 3.8: The ℓ_2 disturbance (A) and the parameter variation (B) used to simulate each controller design.

in Fig. 3.6 and Fig. 3.7B, the response for each design stays inside of the ℓ_∞ bound. It is interesting to note that the response to the positive impulse (I_1) is larger than the response to the negative impulse (I_2). This is caused by the different time-varying parameter $\delta(k)$ values at the time of each impulse, as is displayed in Fig. 3.8.

3.5 Conclusions

In this chapter, discussion motivating the necessity of the $\ell_2 - \ell_\infty$ gain performance criteria was provided. Then, the $\ell_2 - \ell_\infty$ gain performance criteria was introduced to allow for the specification of hard constraints when designing gain-scheduling controllers. Controller synthesis LMIs are provided for the synthesis of state-feedback and dynamic output-feedback controllers with guaranteed $\ell_2 - \ell_\infty$ gain and $\mathcal{H}_\infty$ performance. To demonstrate the effectiveness of the controller synthesis LMIs provided in this chapter, gain-scheduled state-feedback and dynamic output-feedback controllers are designed for a numerical example.

Chapter 4

Gain-Scheduling Control of Port-Fuel-Injection Processes

4.1 Introduction

Increasing concerns about global climate change and ever-increasing demands on fossil fuel capacity call for reduced emissions and improved fuel economy. Port-fuel-injection (PFI) fuel systems are widely used in vehicles today; however, direct-injection (DI) fuel systems have also been introduced to markets globally. To improve the full load performance of DI engines at high speed, Toyota introduced an engine with a stoichiometric DI system with a DI injector and an intake port injector for each cylinder (see [29]). The use of gasoline PFI and ethanol DI dual-fuel system to substantially increase gasoline engine efficiency is described by [28]. This shows that with the introduction of DI fuel systems for the internal combustion engine, PFI fuel systems will remain part of the engine fuel system for improved engine performance, which is the main motivation for revisiting the air-to-fuel (A/F) ratio control problem for a PFI fuel system.

There have been several fuel control strategies developed for internal combustion engines to improve the efficiency and exhaust emissions. A key development in the evolution was the introduction of a closed-loop fuel injection control algorithm [53], followed by the linear quadratic control method [14], and an optimal control and Kalman filtering design [47].

Specific applications of A/F ratio control based on observer measurements in the intake manifold were developed by [8]. Another approach was based on measurements of exhaust gas A/F ratio measured by the oxygen sensor and on the throttle position [42]. [16] also developed a nonlinear sliding mode control of A/F ratio based upon the oxygen sensor feedback. Continuing research efforts of A/F ratio control include adaptive approaches [62, 80], observer-based controllers [46], H_∞ controllers [36], model predictive controllers [38], sliding mode controllers [43], and linear parameter-varying controllers [25, 82, 88]. Conventional A/F ratio control for automobiles uses both closed-loop feedback and feedforward control to have good steady state and fast transient responses.

For a spark-ignited engine equipped with a port-fuel-injection system, the wall-wetting dynamics are commonly used to model the fuel injection process; and the wall-wetting effects are compensated on the basis of simple time-invariant linear models that are tuned and calibrated through engine dynamometer and vehicle tests. These models are quite effective for an engine operated at steady state or slow transition conditions but they are difficult to use at fast transient and other special operational conditions, for instance, during engine cold start. One of the approaches to model the wall-wetting dynamics during engine cold start is to describe it using a family of linear models to approximate the system dynamics at a given engine coolant temperature, speed and load conditions, that is, to translate the fuel system model into a linear parameter varying (LPV) system.

As stated earlier, the use of LPV modeling to control the A/F ratio of a port-fuel-injection system has been reported by [25, 82, 88]. In [88], a continuous-time, LPV model is developed considering only engine speed as a time-varying parameter. Due to the simplicity of the model used, the issue of engine cold start is not addressed. Furthermore, the control synthesis method used in [88] relies on gridding the parameter space at a finite number of

grid points. In [82], a large variable time delay is present in the A/F ratio control loop for a lean burn spark ignition engine. LPV control methods are used to compensate for the variable time delay. In [25], a discrete-time, LPV model is developed with manifold absolute pressure, exhaust value closing, and inlet value opening as the time-varying parameters. However, only manifold absolute pressure is used as a scheduling parameter in the gain-scheduling control that is synthesized. Also, [25] does not address the issue of engine cold start. Additionally, all LPV control synthesis methods used by [25] are based in continuous time, relying on Tustin's (bilinear) transformation to convert the discrete-time system to a continuous-time system, thus fixing the engine speed and sampling rate of the discrete-time system. In contrast to all of these efforts, in this chapter an event-based, gain-scheduling controller for an event-based, discrete-time LPV system with wall-wetting parameters and engine speed as time-varying parameters is designed. To cope with practical situations, the discrete-time LPV control synthesis method in Lemma 6 is used to develop the event-based, gain-scheduling controller. An affine LPV model including the feedforward control dynamics is obtained. Gain-Scheduling controllers have been synthesized to guarantee the robust stability and performance of the affine LPV model.

The contribution of this chapter is as follows. First, an event-based, discrete-time LPV model for the wall-wetting and oxygen sensor dynamics with wall-wetting parameters and engine speed as scheduling variables is developed. Then an event-based, gain-scheduling controller for the derived LPV model is designed. To cope with practical situations, the discrete-time LPV control synthesis method given by [10] is used to develop the event-based, gain-scheduling controller.

The control structures used in this study are proportional-integral (PI) and proportional-integral-derivative (PID). PI controllers are widely used in industry since they are well un-

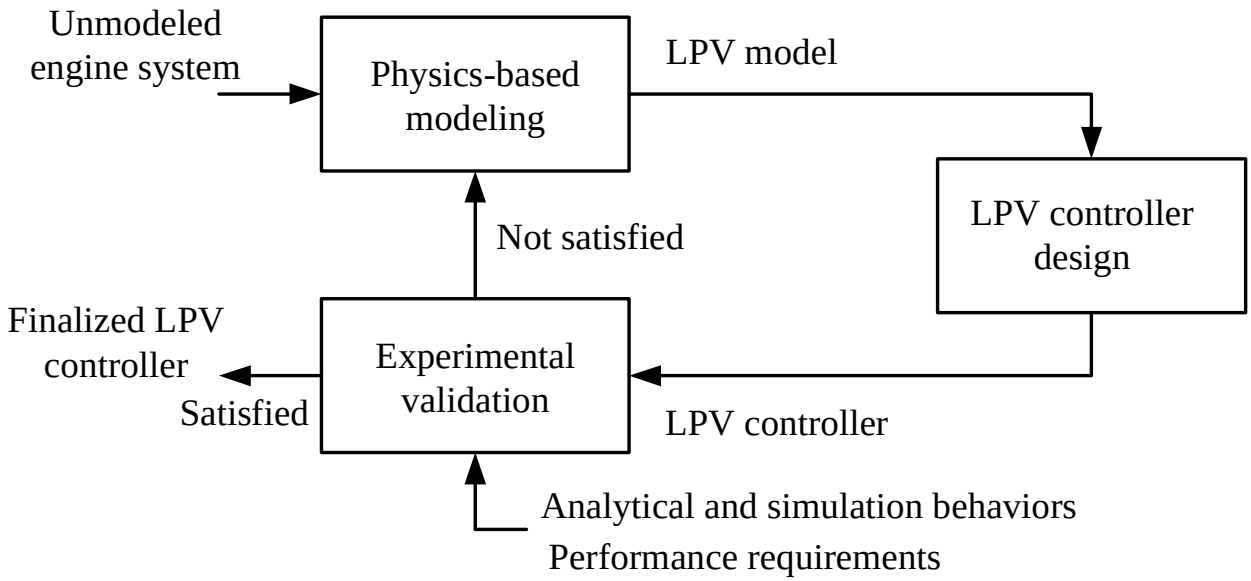

Figure 4.1: Flowchart of the design and validation process of an LPV controller.

derstood by field control engineers. The PI gains are often calibrated in field tests for the best performance as functions of system operational conditions. However, the system stability and performance are not guaranteed for all time-varying parameters. Therefore, LPV techniques proposed in this chapter are applied to design gain-scheduling PI controllers for guaranteed stability and performance for all time-varying parameters. Furthermore, the addition of derivative control to a PI controller adds an extra layer of complexity. The design of a PID controller at a single operating point can be a difficult iterative procedure, which would make calibrating PID gains as functions of system operational conditions very time consuming. However, designing a gain-scheduling PID controller using LPV techniques provided in this chapter is as simple as adding a derivative channel to the control input. The ability to design either a gain-scheduling PI or PID controller with guaranteed stability and performance in one shot without requiring hours of calibration is expected to be well received by industrial control engineers.

The process of designing an LPV controller for any automotive application is depicted

in Fig. 4.1. Due to the complexity of internal combustion engines, designing controllers for specific engine systems using an entire engine model is extremely difficult if even possible. Therefore, to design a controller for a specific engine subsystem, first a physics-based simplified model is developed to represent the engine subsystem. After the varying parameters are identified, the physics-based model can be transformed into an LPV model. LPV controller design can then be carried out on the LPV model to develop an LPV controller. Once the LPV controller is obtained it must be tested on the original engine to ensure that it meets all stability and performance requirements. A cost effective way of validating developed LPV controllers is to implement them in a rapid prototyping real-time control systems and validate them through hardware-in-the-loop (HIL) simulations.

In this work, we first develop a physics-based model for the port-fuel-injection process based on the wall-wetting dynamics and formulate it as an LPV system. The system parameters used in the engine fuel system model are engine speed, temperature, and load. These system parameters can be obtained in real-time through physical or virtual sensors. A gain-scheduling controller is then obtained for the derived LPV system based on the numerically efficient convex optimization (or LMI) techniques. To validate the gain-scheduling PI and PID controllers, HIL simulations were performed using a mixed mean-value and crank-based engine model [79].

This chapter is organized as follows. The models and the modeling techniques used are given in Section 6.2. The design of the gain-scheduling controller in Section 4.3 is covered by first introducing the control strategy in Section 4.3.1. Then the feed-forward compensated generalized plant is developed in Section 4.3.2 and its first-order Taylor series expansion is computed in Section 4.3.3. Next the measurement for control is elaborated in Section 4.3.4. The gain-scheduling synthesis problem is stated in Section 4.3.5. In Section 4.3.6, the aug-

mented LPV plant obtained in Section 4.3.4 is converted into a polytopic time-varying system, which is an LPV system with a polytopic dependency on a scheduling parameter that takes values in the unit-simplex, so that the gain-scheduling controller synthesis technique reviewed in Section 2.3.2 given by [10] can be performed. For comparison, a linear time-invariant feedback $\mathcal{H}_\infty$ controller is designed in Section 4.4 using the nominal parameters. Simulation results from three separate engine operating conditions are presented in Section 4.5. Next, an HIL simulation set up is introduced in Section 4.6 and components of the mixed mean-value and crank-based engine model [79] are reviewed. In Section 4.7 the results from the HIL simulations are presented. The concluding remarks are given in the final section.

4.2 Event-based discrete-time system modeling

In this section, the dynamics of the plant (Fig. 4.2) will be carefully explained and modeled to develop a control oriented linear parameter varying (LPV) model. The plant given in Fig. 4.2 shows the port-fuel-injection process for a single cylinder engine. However, the methods used in this chapter can be extended to a multiple cylinder engine by using the individual cylinder fuel-gas ratio estimation method developed by [60].

4.2.1 Sampling period of the event-based discrete-time system

The discrete-time linear system is obtained by event-based sampling of the port-fuel-injection process; hence the sampling time of this discrete-time system is the period of an engine cycle,

$$t_s = \frac{1}{N_e}\frac{\text{min.}}{\text{rev.}}\left(\frac{60\text{ sec.}}{1\text{ min.}}\right)\left(\frac{2\text{ rev.}}{1\text{ cycle}}\right) = \frac{120}{N_e}\frac{\text{sec.}}{\text{cycle}}, \tag{4.1}$$

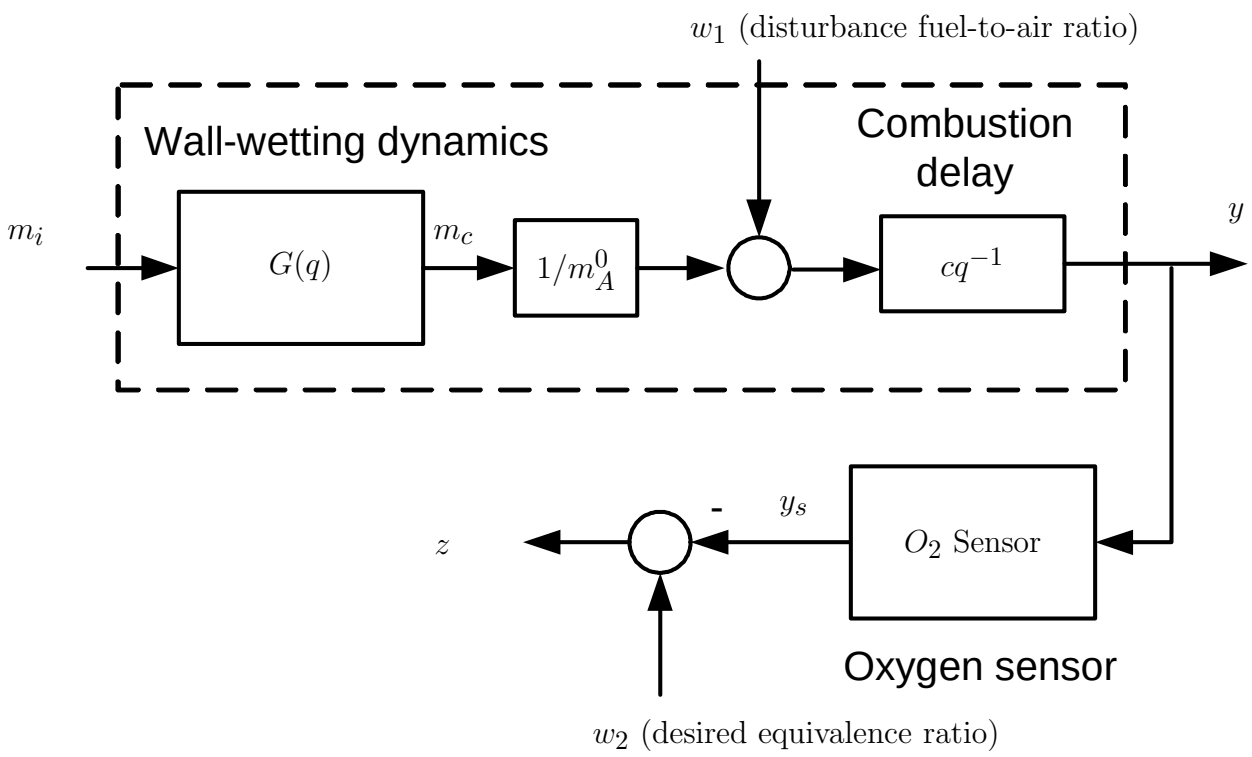

Figure 4.2: The block diagram of the port-fuel-injection process and sensor dynamics.

where N_e represents the engine speed in revolutions per minute (rpm) (see general engine modeling techniques in [7]).

4.2.2 Dynamics of the port-fuel-injection process

The wall-wetting dynamics can be described as follows:

$$\begin{aligned} m_w(k) &= (1-\alpha_k)m_w(k-1) + (1-\beta_k)m_i(k), \\ m_c(k) &= \alpha_k m_w(k-1) + \beta_k m_i(k), \end{aligned} \tag{4.2}$$

where $k \in \mathbb{Z}_{\geq 0}$, and m_w, m_c, and m_i denote the amount of fuel, on the wall, in the cylinder, and injected, respectively. The coefficients $\alpha \in [0,\, 1]$, and $\beta \in [0,\, 1]$, are the ratios of the fuel delivered from the wall to the cylinder, and of the fuel entering the cylinder from injection,

respectively. For notational simplicity, α_k and β_k will be used to denote the wall-wetting parameters at time k, such that $\alpha_k = \alpha(k)$ and $\beta_k = \beta(k)$. These values can be estimated online through an available set of engine sensors, which allows application of gain-scheduling control to the plant. Using the discrete-time dynamics in (4.2), the transfer function $G(q)$ from m_i to m_c is

$$G(q) := \frac{m_c(k)}{m_i(k)} = \frac{\beta_k + (\alpha_k - \beta_k)q^{-1}}{1 - (1 - \alpha_k)q^{-1}}, \tag{4.3}$$

where q is the *forward shift operator* that satisfies $qu(k) = u(k+1)$. The dotted box in the block diagram in Fig. 4.2 illustrates the fuel-injection process. The output of $G(q)$ is the input to the gain block of $1/m_A^0$, which is the nominal value of the inverse of the mass of air trapped in the cylinder m_A. The signal w_1 represents the deviation

$$\left(\frac{m_c}{m_A} - \frac{m_c}{m_A^0} \right),$$

which will be treated as a disturbance. Another constant gain factor $c = 14.6$ in Fig. 4.2 is the value for the air-to-fuel-ratio at stoichiometric. After the combustion delay block the equivalence ratio y is generated. The diagram of the transfer function from the amount of fuel injected m_i and the disturbance w_1 to the equivalence ratio y (inverse of normalized air-to-fuel ratio) is shown in the dotted box in Fig. 4.2.

4.2.3 Dynamics of the oxygen sensor

To measure y, a full range oxygen sensor is placed in the exhaust manifold at some distance downstream from the exhaust valve. Notice that the continuous-time dynamics and

delays will change in the event-based, discrete-time system according to the speed of the engine (or the sampling time). Therefore, the objective of this section is to obtain oxygen sensor dynamics in the form of the finite dimensional, event-based, discrete-time LPV system. Finite dimensionality is required for the applicability of most LPV controller design techniques and the controller design method which will be presented in Section 4.3. To this end, in general, one can approximate the continuous-time system with a delay by a finite dimensional event-based, discrete-time LPV system in any standard method. To illustrate this procedure, we demonstrate how we approximate the oxygen sensor dynamics by Taylor series approximation in which the approximation error can be minimized by increasing the order of the Taylor series approximation.

The dynamics of the oxygen sensor are modeled as a first-order sensor delay coupled with the transport delay of the exhaust gas mixture. The transport delay, $T_D = \dfrac{d}{N_e}$, of the exhaust gas mixture is both a function of the oxygen sensor placement, which determines the constant d, and the engine speed, N_e. The combined transfer function in the continuous time domain is

$$y_s(s) = \frac{\exp\left(-T_D s\right)}{T_{O_2} s + 1} y(s), \tag{4.4}$$

where y_s is the equivalence ratio measured by the sensor and T_{O_2} is the time constant of the oxygen sensor. Since the delay

$$T_D \in \left[\frac{d}{\overline{N_e}}, \frac{d}{\underline{N_e}} \right]$$

is small, Equation (4.4) can be approximated by the second-order system

$$y_s(s) = \frac{1}{T_D s + 1} \frac{1}{T_{O_2} s + 1} y(s),$$

which has the state-space representation

$$\begin{aligned} \dot{x}_{O_2} &= \underbrace{\begin{bmatrix} -\frac{1}{T_D} & \frac{1}{T_D} \\ 0 & -\frac{1}{T_{O_2}} \end{bmatrix}}_{=:A_{O_2}} x_{O_2} + \underbrace{\begin{bmatrix} 0 \\ \frac{1}{T_{O_2}} \end{bmatrix}}_{=:B_{O_2}} y, \\ y_s &= \underbrace{\begin{bmatrix} 1 & 0 \end{bmatrix}}_{=:C_{O_2}} x_{O_2}. \end{aligned} \tag{4.5}$$

Using t_s as the sampling rate, the corresponding discrete system of Eq. (4.5) is

$$\begin{aligned} x_{O_2}(k+1) &= A_{O_2 d} x_{O_2}(k) + B_{O_2 d} y(k), \\ y_s(k) &= C_{O_2 d} x_{O_2}(k), \end{aligned} \tag{4.6}$$

where, due to the invertibility of the matrix A_{O_2} in (4.5),

$$\begin{aligned} A_{O_2 d} &= \exp(A_{O_2} t_s), \\ B_{O_2 d} &= \left(\int_0^{t_s} \exp(A_{O_2} \tau) d\tau \right) B_{O_2} = A_{O_2}^{-1} (A_{O_2 d} - I) B_{O_2}, \\ C_{O_2 d} &= C_{O_2}. \end{aligned}$$

Since both T_D and t_s are functions of engine speed, N_e, naturally $A_{O_2 d}$ and $B_{O_2 d}$ are as well. To capture this parameter variation, the matrices $A_{O_2 d}$ and $B_{O_2 d}$ are now computed

for a given transport delay of $T_D = \dfrac{80}{N_e}$. To solve for $A_{O_2 d}$, first A_{O_2} is multiplied by t_s

$$\begin{aligned} A_{O_2}\, t_s &= \begin{bmatrix} -\dfrac{N_e}{80} & \dfrac{N_e}{80} \\ 0 & -\dfrac{1}{T_{O_2}} \end{bmatrix} \dfrac{120}{N_e} \\ &= \begin{bmatrix} -\dfrac{3}{2} & \dfrac{3}{2} \\ 0 & -\dfrac{120}{T_{O_2} N_e} \end{bmatrix}. \end{aligned} \tag{4.7}$$

Next, the matrix exponent of $A_{O_2}\, t_s$ is computed, which gives

$$A_{O_2 d} = \begin{bmatrix} \exp\left(-\dfrac{3}{2}\right) & p_1(N_e) \\ 0 & p_2(N_e) \end{bmatrix}, \tag{4.8}$$

where

$$p_1(N_e) = \frac{-\dfrac{3}{2}\left(\exp\left(-\dfrac{3}{2}\right) - \exp\left(-\dfrac{120}{T_{O_2} N_e}\right)\right)}{-\dfrac{120}{T_{O_2} N_e} + \dfrac{3}{2}}, \tag{4.9a}$$

$$p_2(N_e) = \exp\left(-\frac{120}{T_{O_2} N_e}\right). \tag{4.9b}$$

To represent the parameter variation in $A_{O_2 d}$, a fourth-order Taylor series approximation of $p_1(N_e)$ and $p_2(N_e)$ is used. To ensure that the coefficients of the Taylor series approximations of $p_1(N_e)$ and $p_2(N_e)$ are numerically stable with respect to the condition number [61],

$\frac{1}{N_e} \in [\frac{1}{\overline{\overline{N_e}}}, \frac{1}{\underline{\underline{N_e}}}]$ is normalized to γ in the following way:

$$\gamma = \frac{\frac{1}{N_e} - \frac{1}{N_{e,0}}}{\frac{1}{N_e} + \frac{1}{N_{e,0}}} \quad \text{where} \quad \frac{1}{N_{e,0}} = \frac{\frac{1}{\overline{\overline{N_e}}} + \frac{1}{\underline{\underline{N_e}}}}{2}. \tag{4.10}$$

Solving equation (4.10) for $\frac{1}{N_e}$, and substituting into equations (4.9a) and (4.9b), $p_1(\gamma)$ and $p_2(\gamma)$ are found to be

$$p_1(\gamma) = \frac{-\frac{3}{2}\left(\exp\left(-\frac{3}{2}\right) - \exp\left(-\frac{120}{T_{O_2} N_{e,0}}\left(\frac{1+\gamma}{1-\gamma}\right)\right)\right)}{-\frac{120}{T_{O_2} N_{e,0}}\left(\frac{1+\gamma}{1-\gamma}\right) + \frac{3}{2}}, \tag{4.11a}$$

$$p_2(\gamma) = \exp\left(-\frac{120}{T_{O_2} N_{e,0}}\left(\frac{1+\gamma}{1-\gamma}\right)\right). \tag{4.11b}$$

Finally, the forth-order Taylor series approximation of $A_{O_2 d}$ is represented with the following lower LFT:

$$A_{O_2 d} = \mathcal{F}_\ell(M_{A_{O_2 d}}, \gamma I_4) \tag{4.12}$$

where

$$M_{A_{O_2 d}} = \left[\begin{array}{cc:cccc} \exp\left(-\frac{3}{2}\right) & a_0 & a_1 & a_2 & a_3 & a_4 \\ 0 & b_0 & b_1 & b_2 & b_3 & b_4 \\ \hdashline 0 & 1 & 0 & 0 & 0 & 0 \\ 0 & 0 & 1 & 0 & 0 & 0 \\ 0 & 0 & 0 & 1 & 0 & 0 \\ 0 & 0 & 0 & 0 & 1 & 0 \end{array}\right] \tag{4.13}$$

and

$$a_1 = \frac{1}{1!}\frac{d^1 p_1(0)}{d\gamma^1}, \quad a_2 = \frac{1}{2!}\frac{d^2 p_1(0)}{d\gamma^2}, \quad a_3 = \frac{1}{3!}\frac{d^3 p_1(0)}{d\gamma^3}, \quad a_4 = \frac{1}{4!}\frac{d^4 p_1(0)}{d\gamma^4},$$
$$b_1 = \frac{1}{1!}\frac{d^1 p_2(0)}{d\gamma^1}, \quad b_2 = \frac{1}{2!}\frac{d^2 p_2(0)}{d\gamma^2}, \quad b_3 = \frac{1}{3!}\frac{d^3 p_2(0)}{d\gamma^3}, \quad b_4 = \frac{1}{4!}\frac{d^4 p_2(0)}{d\gamma^4}.$$

Now focusing attention on B_d, recall that $B_{O_2 d} = A_{O_2}^{-1}(A_{O_2 d} - I)B_{O_2}$ (see (4.6)). Since $A_{O_2 d}$ is already found, $A_{O_2}^{-1}$ is now computed. The inverse of A_{O_2} is given by

$$A_{O_2}^{-1} = T_D T_{O_2} \begin{bmatrix} -\frac{1}{T_{O_2}} & -\frac{1}{T_D} \\ 0 & -\frac{1}{T_D} \end{bmatrix} = \begin{bmatrix} -T_D & -T_{O_2} \\ 0 & -T_{O_2} \end{bmatrix} = \begin{bmatrix} -\frac{80}{N_e} & -T_{O_2} \\ 0 & -T_{O_2} \end{bmatrix}. \tag{4.14}$$

Thus, $A_{O_2}^{-1}$ can be represented with the following lower LFT:

$$A_{O_2}^{-1} = \mathcal{F}_\ell \left(M_{A_{O_2}^{-1}}, \frac{1}{N_e} \right), \tag{4.15}$$

where

$$M_{A_{O_2}^{-1}} = \left[\begin{array}{cc:c} 0 & -T_{O_2} & -80 \\ 0 & -T_{O_2} & 0 \\ \hdashline 1 & 0 & 0 \end{array}\right]. \tag{4.16}$$

To normalize $\frac{1}{N_e}$ to γ, the following upper LFT is used:

$$\frac{1}{N_e} = \mathcal{F}_u(M_\gamma, \gamma), \quad \text{where} \quad M_\gamma = \left[\begin{array}{c:c} \frac{1}{\frac{2}{N_{e,0}}} & \frac{1}{\frac{1}{N_{e,0}}} \end{array}\right]. \tag{4.17}$$

The approximated state-space matrices $\hat{A}_{O_2 d}$ and $\hat{B}_{O_2 d}$ are represented in Fig. 4.3 by their respective dotted boxes. The approximated state matrix $\hat{A}_{O_2 d}$ block is formed by the

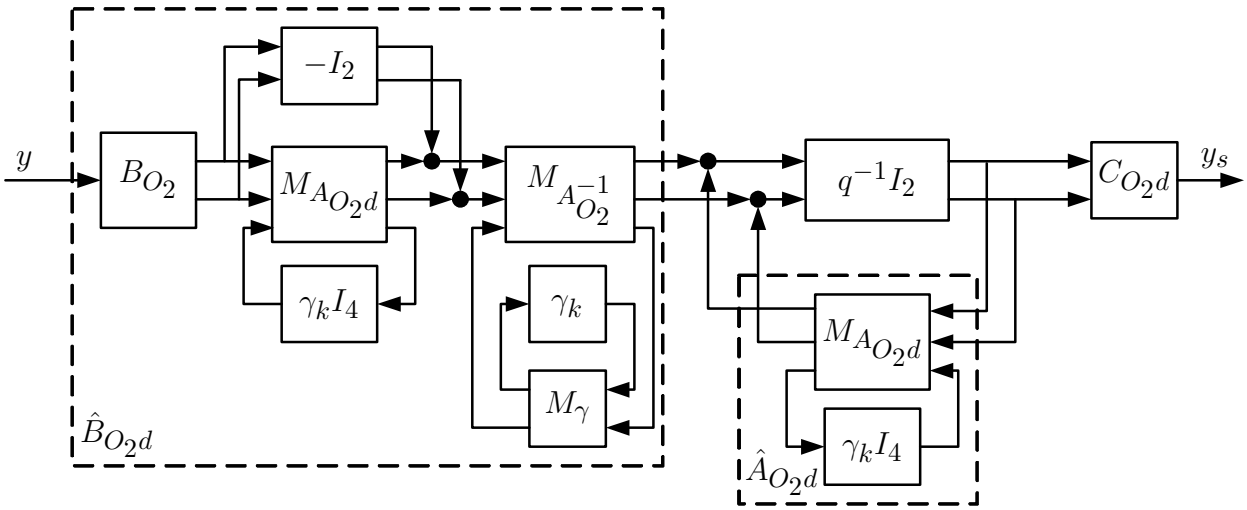

Figure 4.3: Block diagram of the combined dynamics of the exhaust gas and sensor delays.

lower LFT $M_{A_{O_2d}}$ connected to the time-varying parameter matrix $\gamma_k I_4$. The approximated input matrix $\hat{B}_{O_2d}$ block is formed by the matrix multiplications of B_{O_2d} in Eq. (4.6). The $\hat{A}_{O_2d}$, $\hat{B}_{O_2d}$, and C_{O_2d} blocks are then connected in the standard state-space interconnection [58]. After performing the interconnection displayed in Fig. 4.3, the fourth-order approximated system used for controller design is given by

$$\begin{aligned} \hat{x}_{O_2}(k+1) &= \hat{A}_{O_2d}(\gamma_k)\hat{x}_{O_2}(k) + \hat{B}_{O_2d}(\gamma_k)y(k), \\ \hat{y}_s(k) &= C_{O_2d}\hat{x}_{O_2}(k), \end{aligned} \tag{4.18}$$

where

$$\hat{A}_{O_2d}(\gamma_k) = \begin{bmatrix} \exp(-\dfrac{120}{d}) & a(\gamma_k) \\ 0 & b(\gamma_k) \end{bmatrix},$$

$$\hat{B}_{O_2d}(\gamma_k) = \begin{bmatrix} \dfrac{d\,(\gamma_k+1)}{v_0\,(\gamma_k-1)}\left(\dfrac{a(\gamma_k)}{T_{O_2}}\right) - b(\gamma_k) + 1 \\ 1 - b(\gamma_k) \end{bmatrix}.$$

The approximated state matrix $\hat{A}_{O_2d}(\gamma_k)$ follows directly from (4.8). The approximated

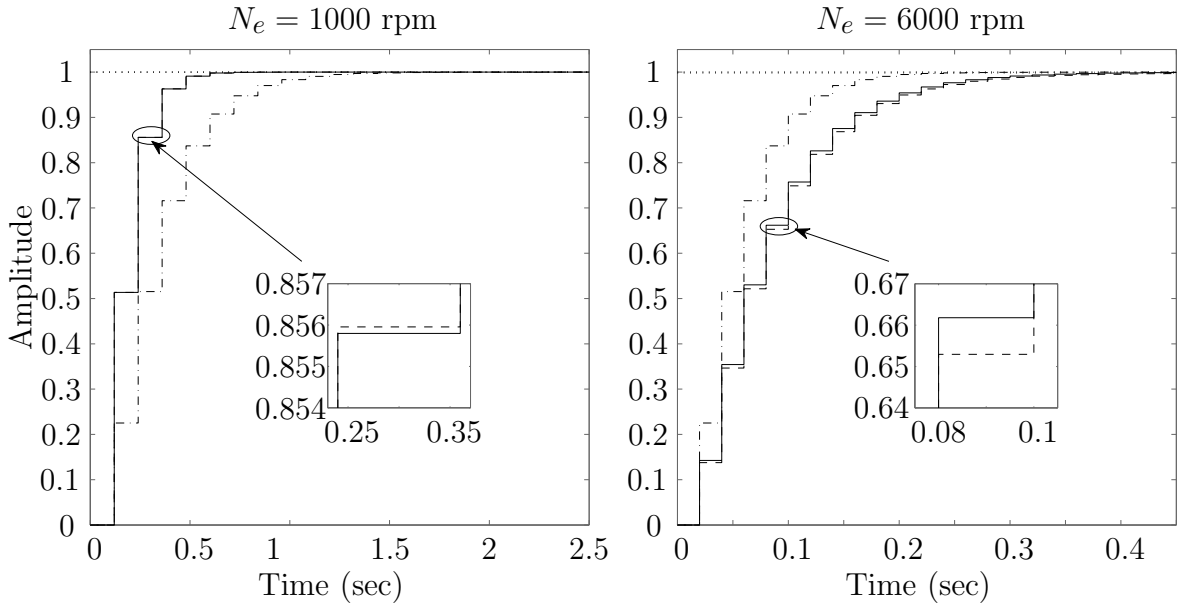

Figure 4.4: Comparison of the response to a unit step function for the 4^{th} order Taylor series approximation model in Eq. 4.18 (dashed line) and a model Eq. 4.6 with the engine speed fixed at 3500 rpm (dash-dot line) to the exact discretized oxygen sensor delay model in Eq. 4.6 (solid line) at 1000 rpm and 6000 rpm.

input matrix $\hat{B}_{O_2d}(\gamma_k)$ follows from the matrix operations performed to compute B_{O_2d} in (4.6). The following polynomial functions $a(\gamma_k)$ and $b(\gamma_k)$:

$$a(\gamma_k) = 0.3972 - 0.4891\gamma_k - 0.0984\gamma_k^2 + 0.0608\gamma_k^3 + 0.0975\gamma_k^4,$$

$$b(\gamma_k) = 0.3114 - 0.7266\gamma_k + 0.1211\gamma_k^2 + 0.3095\gamma_k^3 + 0.2231\gamma_k^4,$$

were found when selecting an oxygen sensor time constant of $T_{O_2} = 0.06$ seconds and a transport delay of $T_D = \dfrac{80}{N_e}$, by setting $d = 80$, indicating that the transport delay is about 54 ms at an engine speed of 1500 rpm. This was determined empirically through engine calibration tests.

To demonstrate the effectiveness of the proposed model for the event-based sampling of the oxygen sensor delay, a comparison is made between the proposed 4^{th} order Taylor series approximation model and a fixed model computed at the nominal engine speed (3500 rpm).

In Fig. 4.4, the step response of the 4^{th} order Taylor series approximation model (dashed line) is compared to the exact discretized model (solid line) at engine speeds of 1000 rpm and 6000 rpm. The fixed model computed at the nominal engine speed (dash-dot line) is also compared to the exact model in Fig. 4.4. It is clear that the fixed model computed at the nominal engine speed either responds too slowly when the engine speed is less than the nominal speed or too quickly when the engine speed is greater than the nominal speed. However, the approximated model's response very closely follows the exact model's response as shown in Fig. 4.4.

4.2.4 An LPV system

In summary, by combining the wall-wetting dynamics in (4.2) and the oxygen sensor delay and dynamics in (4.18) as shown in Fig. 4.2, we obtain the following LPV system for the event-based discrete-time port-fuel-injection and oxygen sensor dynamics:

$$\begin{aligned}
\begin{bmatrix} x_{ww}(k+1) \\ x_{comb}(k+1) \\ \hat{x}_{O_2}(k+1) \end{bmatrix} &= \begin{bmatrix} 1-\alpha_k & 0 & 0 \\ \dfrac{c\alpha_k}{m_A^0} & 0 & 0 \\ 0 & \hat{B}_{O_2d}(\gamma_k) & \hat{A}_{O_2d}(\gamma_k) \end{bmatrix} \begin{bmatrix} x_{ww}(k) \\ x_{comb}(k) \\ \hat{x}_{O_2}(k) \end{bmatrix} \\
&\quad + \begin{bmatrix} 1-\beta_k \\ \dfrac{c\beta_k}{m_A^0} \\ 0 \end{bmatrix} m_i(k) + \begin{bmatrix} 0 \\ c \\ 0 \end{bmatrix} w_1(k), \qquad (4.19) \\
z(k) &= \begin{bmatrix} 0 & 0 & -C_{O_2d} \end{bmatrix} \begin{bmatrix} x_{ww}(k) \\ x_{comb}(k) \\ \hat{x}_{O_2}(k) \end{bmatrix} + w_2(k),
\end{aligned}$$

where $x_{ww}(k) = m_w(k-1)$ and $x_{comb}(k)$ are the wall-wetting state and the combustion state for the system in the dotted box in Fig. 4.2.

Table 4.1: Modeling parameters.

Parameter	Value used in Study
T_{O_2} is a constant	0.06
T_D is a function of engine speed, N_e	$\frac{80}{N_e}$

Table 4.2: Measurable time varying parameters (scheduling parameters).

$\alpha(\text{cylinder head temperature}(t), \text{manifold absolute pressure}(t)) \in [0.081, 0.1]$
$\beta(\text{cylinder head temperature}(t), \text{manifold absolute pressure}(t)) \in [0.28, 0.89]$
$\gamma(N_e(t)) = \frac{\frac{1}{N_e(t)} - \frac{1}{N_{e,0}}}{\frac{1}{N_e(t)} + \frac{1}{N_{e,0}}} \in [-0.55556, 0.26316]$

As can be seen from (Eqs. 4.5, 4.6, 4.18, and 4.19), to apply the model of the LPV system, one needs to identify T_D and T_{O_2} (which are shown in Table 4.1) and measurable time varying parameters such as α, β, and γ (which are shown in Table 6.1), which will be used for scheduling the gain of the controller. In particular, the identified bounds of scheduling variables ($[\underline{\alpha}, \overline{\alpha}]$, $[\underline{\beta}, \overline{\beta}]$ and $[\underline{\gamma}, \overline{\gamma}]$) as shown in Table 6.1 will be used in synthesizing the gain-scheduling controller. From now on, a compact notation Θ will denote an appropriate gain-scheduling matrix that contains the scheduling variables. The specific structure of Θ will be presented in Eq. (4.24) of Section 4.3.2. In addition, the LPV system in Eq. (4.19) is denoted by $P(\Theta)$. In the following section, we illustrate how to design the LPV gain-scheduling controller as a function of Θ for the LPV model developed in this section.

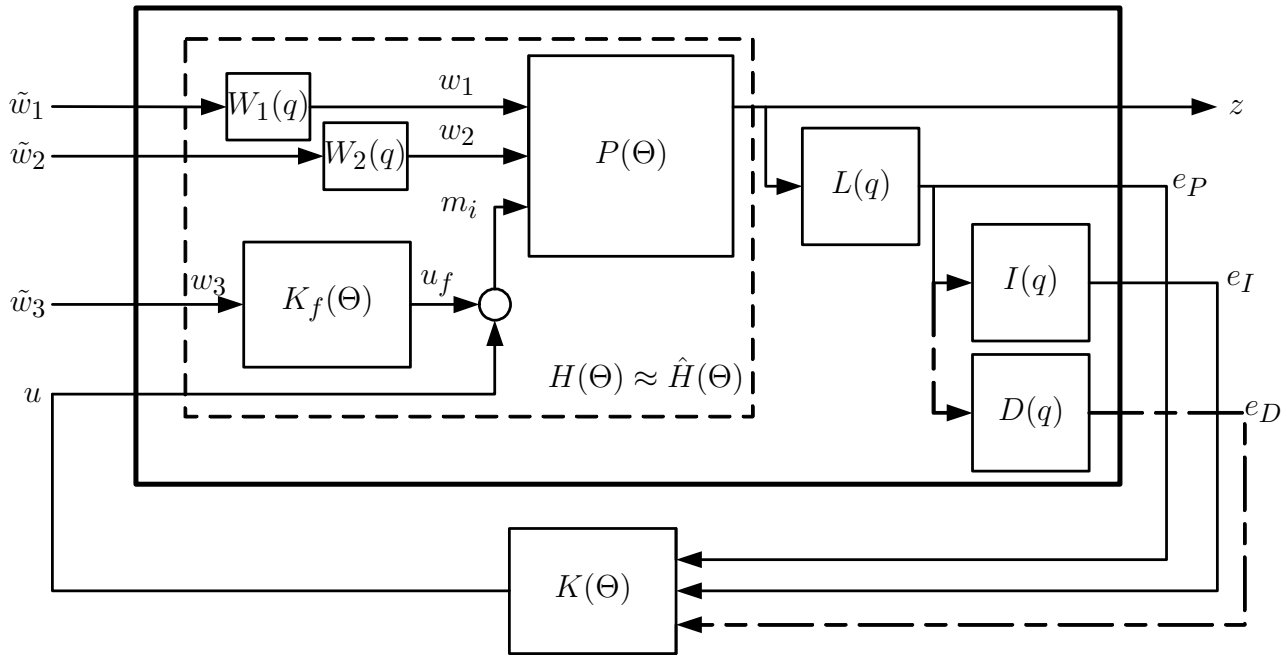

Figure 4.5: The proposed control strategy for the fuel injection process (without the weighting functions $W_1(q)$ and $W_2(q)$). Weighting functions $W_1(q)$ and $W_2(q)$ are only used for controller synthesis. A first-order Taylor series expansion is applied to the to the systems inside the dashed box and the LPV control strategy is applied to the all of the systems inside of the bold box.

4.3 LPV gain-scheduling controller design

4.3.1 Control Strategy

The objective of the control system is to regulate the equivalence ratio y to a reference input w_2 using feed-forward and feedback control against the disturbance signal w_1 (See Fig. 4.2) and the time-varying wall-wetting dynamics. In particular, we want to guarantee the stability of the closed-loop system and also minimize the effect of the disturbances for any conceivable wall-wetting dynamics variations. The proposed control architecture is illustrated in Fig. 6.2. This scheme has five possible components, that is a feedback controller $K(\Theta)$, a feed-forward controller $K_f(\Theta)$, a filter $L(q)$, an integrator $I(q)$, and possibly a differentiator $D(q)$ (if a PID controller is desired).

The feedback controller $K(\Theta)$ will be designed for the generalized plant (solid box of Fig. 6.2), after selecting $K_f(\Theta)$, $L(q)$, $I(q)$, possibly $D(q)$, and weighting functions $W_1(q)$ and $W_2(q)$. Next, we will explain how to select these functions. After the selection, we will derive the generalized plant in Section 4.3.4 and we will synthesize $K(\Theta)$ for the derived generalized plant in Section 4.3.5.

The feed-forward controller $K_f(\Theta)$ is designed using the inverse of $cG(q)$

$$K_f(\Theta) = \frac{G^{-1}(q)}{c} = \frac{1}{c}\left(\frac{1-(1-\alpha_k)q^{-1}}{\beta_k + (\alpha_k - \beta_k)q^{-1}}\right).$$

The selection of the inverse of the plant as a feed-forward controller is a standard technique [58]. The input to the feed-forward controller is the mass of the air m_A, which can be measured online, multiplied by the equivalence ratio set point w_2. This is denoted by w_3, such that $w_3 = w_2 m_A$. $L(q)$ is designed as a low-pass filter such that the error output $z(k)$ is filtered with it

$$L(q) = \frac{0.9999}{q - 0.0001405}.$$

The reason to filter the error output is that the control synthesis technique given by [10] requires that the output matrix be independent of the time-varying parameters and the measurement for control must not be corrupted by the unweighted exogenous input, $\tilde{w}(k)$ of the generalized plant. The low-pass filtering for this purpose is a standard procedure [2]. The low-pass filter $L(q)$ was obtained from the discretization of the following first-order continuous transfer function:

$$L^c(s) = \frac{2\pi f_c}{s + 2\pi f_c}$$

with a sample period of $\frac{120}{N_{e,0}}$. The cut-off frequency f_c of $L^c(s)$ was selected to be 20 Hz,

which is high enough to obtain low error between the intended output of the continuous-time filter $L^c(q)$ and the observed output of the discrete-time filter $L(q)$ at different engine speeds, since the sampling rate is engine speed dependent. The filtered output is also integrated using the integrator

$$I(q) = \frac{1}{q-1}$$

to obtain zero steady-state error. To enhance the response of the closed-loop system when large changes in w_1 are present, then derivative action [5]

$$D(q) := \frac{e_D(k)}{e_P(k)} = \frac{F(q-1)}{(F+1)q-1}$$

is introduced, where F is chosen to set the location of the pole of the derivative filter. Notice that $I(q)$ and $D(q)$ are not functions of the sampling rate, t_s. This is due to the requirement that, as previously stated, that the output matrix $\hat{C}_2$ be independent of the time-varying parameters. For this reason, $I(q)$ is really just a numerical summation and $D(q)$ is a filtered, numerical differencer.

To use ℓ_2 gain or $\mathcal{H}_\infty$ norm [84] for the performance criterion for shaping the frequency response of the closed-loop system, weighing functions (which can be considered design parameters) are also introduced in Fig. 6.2. The weighting functions are selected in the continuous-time domain as

$$W_1^c(s) = \frac{100}{50s+1},$$
$$W_2^c(s) = \left(\frac{20}{50s+1}\right)^2.$$

The bandwidth (or cut-off frequency) of each weighting function is very small and the DC

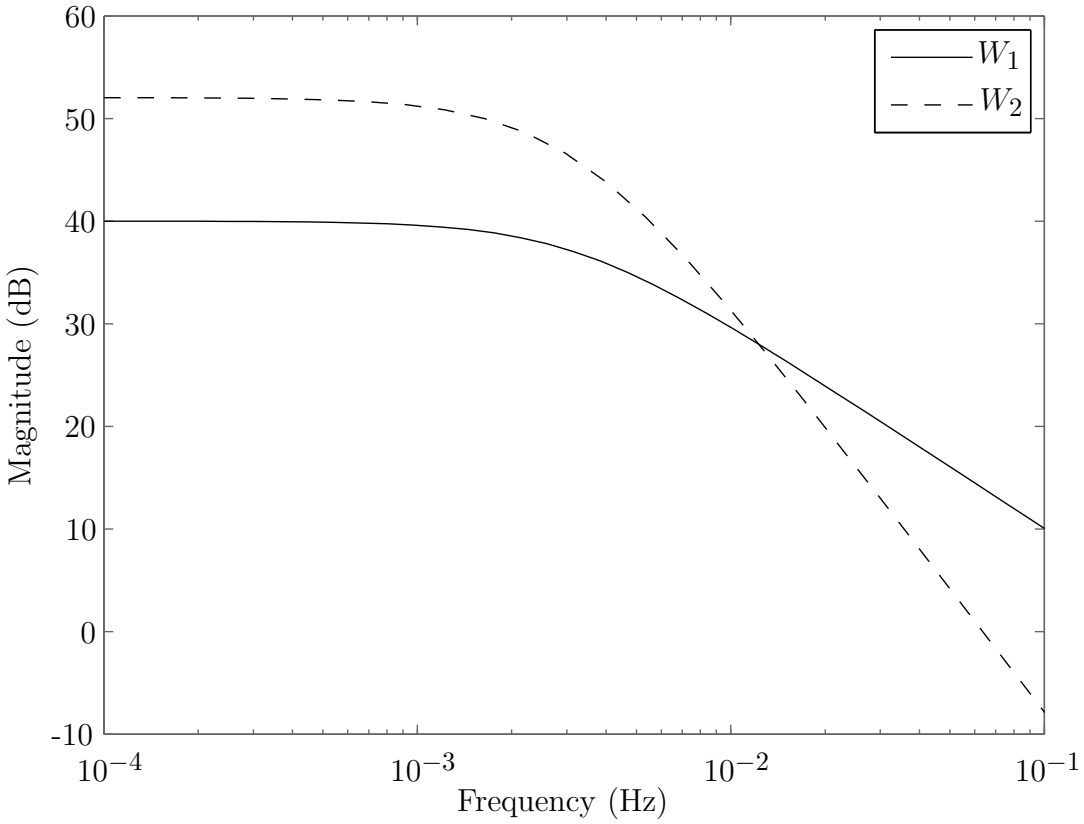

Figure 4.6: Magnitude plot of the weighting functions W_1 and W_2.

gain is large, as shown in Fig. 4.6. The weighting functions are selected to model the frequency content of their respective input. For the fuel-to-air ratio disturbance w_1, the weighting function $W_1^c(s)$ is selected as a simple first-order low-pass filter to place an emphasis on low frequency disturbances, such as a step throttle change. The weighting function $W_2^c(s)$ is chosen to be a second-order low-pass filter with a high DC gain (4 times larger than that of $W_1^c(s)$) to provide more weight on the low frequency signals since w_2 is the step input of the desired equivalence ratio. To incorporate the weighting functions $W_1^c(s)$ and $W_2^c(s)$ into the discrete time system, they were discretized at a sample period of $\frac{120}{N_{e,0}}$ to obtain the

following discrete-time weighting functions:

$$W_1(q) = \frac{0.1411}{q - 0.9986},$$
$$W_2(q) = \frac{0.0003982q + 0.0003979}{q^2 - 1.997178q + 0.997180}.$$

The input to each of the weighting functions are the unweighted exogenous inputs which are denoted by $\tilde{w}_1$, $\tilde{w}_2$, and $\tilde{w}_3$. Since there is no weighting function for w_3, in this case $\tilde{w}_3 = w_3$; which means that it is weighted equally at all frequencies. Notice that the weighting functions are chosen by the expected system inputs and their relative (frequency) importance, and they are only used for controller synthesis [84, 58].

4.3.2 Feed-forward compensated generalized plant

The feed-forward compensated generalized plant is denoted by $H(\Theta)$. As depicted in the dashed box of Fig. 6.2, the feed-forward compensated generalized plant consists of the feed-forward controller $K_f(\Theta)$, the plant $P(\Theta)$, and the weighting functions $W_1(q)$ and $W_2(q)$. The components of the feed-forward controller $K_f(\Theta)$ and the plant $P(\Theta)$ are illustrated in Fig. 4.7. The feed-forward controller $K_f(\Theta)$ components are encased inside of the dashed box in Fig. 4.7 and the plant $P(\Theta)$ components are outside of the dashed box.

In the feed-forward control compensated generalized plant $H(\Theta)$, the time-varying parameters α_k and β_k are equivalently transformed to a constant nominal value plus a time-varying fluctuation. For instance, the parameter variation of $\alpha_k \in [\underline{\alpha}, \overline{\alpha}]$ with $\alpha_0 = \dfrac{\underline{\alpha} + \overline{\alpha}}{2}$ is represented by

$$\alpha_\delta(k) = \alpha_k - \alpha_0 \in [\underline{\alpha} - \alpha_0, \overline{\alpha} - \alpha_0],$$

so that the parameter range of $\alpha_\delta(k)$ is centered around zero. Hence, α_k is replaced by

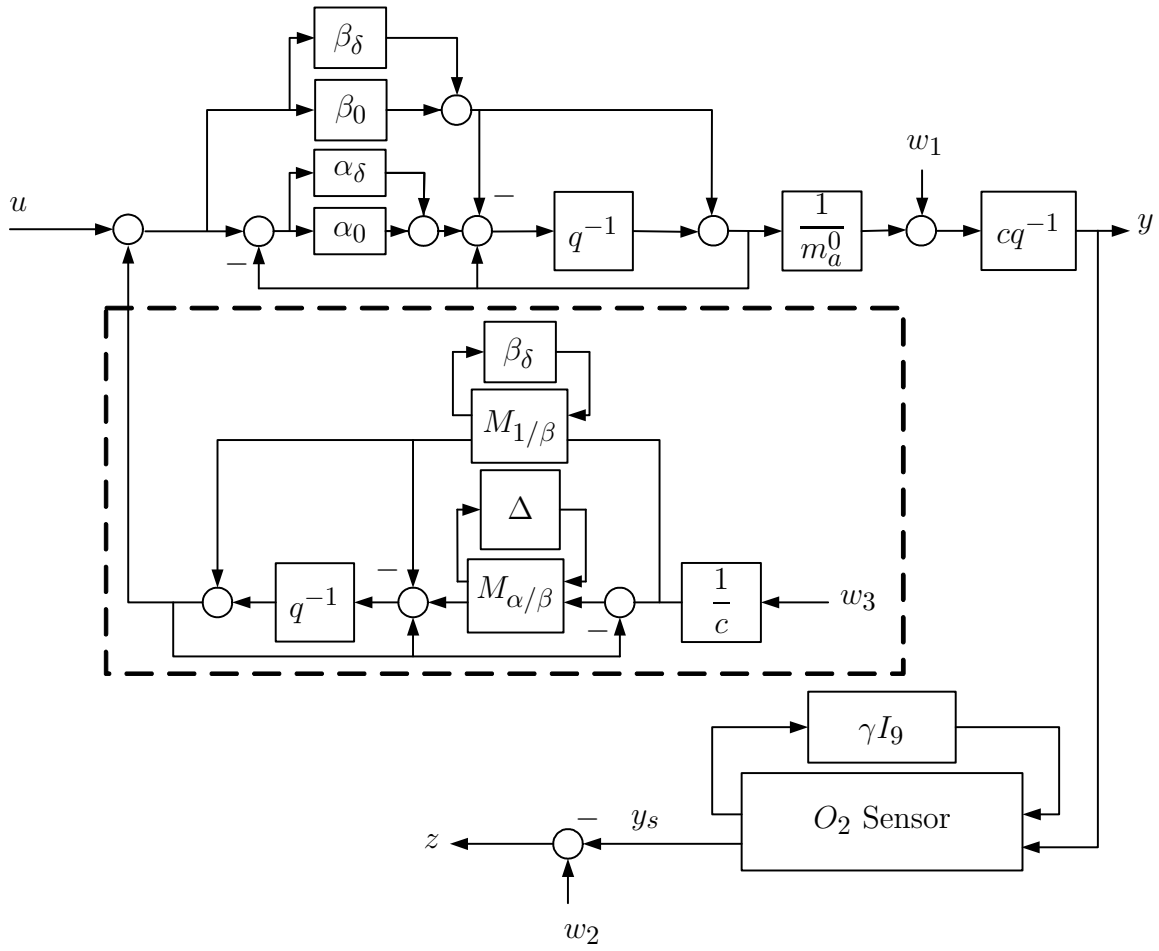

Figure 4.7: The feed-forward control compensated generalized plant with the time-varying parameters included.

$\alpha_0 + \alpha_\delta(k)$. The same is done for $\beta_k \in [\underline{\beta}, \overline{\beta}]$ as well. The parameter variation of v is represented by γ as shown in Eq. (4.10). The upper LFTs (see Appendix A) inside the dotted box in Fig. 4.7, $M_{1/\beta}$ and $M_{\alpha/\beta}$ are used to isolate the time-varying parameters $\beta_\delta(k)$ and $\alpha_\delta(k)$ [84]. β_δ is isolated from $\frac{1}{\beta_k}$ by

$$\frac{1}{\beta_k} = \frac{1}{\beta_0 + \beta_\delta(k)} = \mathcal{F}_u\left(M_{1/\beta}, \beta_\delta(k)\right), \tag{4.20}$$

where

$$M_{1/\beta} = \left[\begin{array}{c:c} -\frac{1}{\beta_0} & -\frac{1}{\beta_0} \\ \hdashline \frac{1}{\beta_0} & \frac{1}{\beta_0} \end{array}\right]. \tag{4.21}$$

Both $\beta_\delta(k)$ and $\alpha_\delta(k)$ are isolated from $\dfrac{\alpha_k}{\beta_k}$ by

$$\frac{\alpha_k}{\beta_k} = \frac{\alpha_0 + \alpha_\delta(k)}{\beta_0 + \beta_\delta(k)} = \mathcal{F}_u\left(M_{\alpha/\beta}, \Delta(k)\right), \tag{4.22}$$

where

$$M_{\alpha/\beta} = \left[\begin{array}{cc:c} -\frac{1}{\beta_0} & -\frac{1}{\beta_0} & -\frac{\alpha_0}{\beta_0} \\ 0 & 0 & 1 \\ \hdashline \frac{1}{\beta_0} & \frac{1}{\beta_0} & \frac{\alpha_0}{\beta_0} \end{array}\right], \quad \text{and} \quad \Delta(k) = \left[\begin{array}{cc} \beta_\delta(k) & 0 \\ 0 & \alpha_\delta(k) \end{array}\right].$$

With the parameter variation represented in this way, the system is written as a discrete-time LPV system with LFT parameter dependency,

$$\begin{aligned} \left[\begin{array}{c} x(k+1) \\ l(k) \\ z(k) \end{array}\right] &= \left[\begin{array}{cccc} A & B_0 & B_1 & B_2 \\ C_0 & D_{00} & D_{01} & D_{02} \\ C_1 & D_{10} & D_{11} & D_{12} \end{array}\right] \left[\begin{array}{c} x(k) \\ p(k) \\ \tilde{w}(k) \\ u(k) \end{array}\right], \\ p(k) &= \Theta(k) l(k), \end{aligned} \tag{4.23}$$

where $x(k) \in \mathbb{R}^n$ is the state at time k, $\tilde{w}(k) \in \mathbb{R}^r$ is the unweighted exogenous input, $z(k) \in \mathbb{R}^p$ is the error output, $p(k), l(k) \in \mathbb{R}^{n_p}$ are the pseudo-input and pseudo-output connected by $\Theta(k)$, and $u(k) \in \mathbb{R}^m$ is the control input. The state-space matrices for the LPV system in (4.23) are provided in Appendix B.

The time-varying parameter Θ in Eq. (4.23) follows the structure

$$\Theta \in \mathbf{\Theta} = \{\text{diag}(\beta_\delta I_3, \alpha_\delta I_2, \gamma I_9) : |\alpha_\delta| \leq \delta_1, |\beta_\delta| \leq \delta_2, |\gamma| \leq 1\}, \tag{4.24}$$

where $\delta_1 = \dfrac{\overline{\alpha} - \underline{\alpha}}{2}$ and $\delta_2 = \dfrac{\overline{\beta} - \underline{\beta}}{2}$.

4.3.3 First-order Taylor series expansion of the LPV system

By inspection of the LPV system in Eq. (4.23), D_{00} was found to be a non-zero matrix. Hence, the system matrices are not affine functions, i.e., a linear combination of the time-varying parameters plus a constant translation. It is noted at this juncture that LPV control techniques exist which do handle rational parameter variation, namely the method developed by [75]. However, for discrete-time systems, no controller formula covering all parameter variation is given by [75]. Instead, for each set of parameters a controller must be solved for using the method given by [21]. Since a different controller is needed for each set of parameters, gridding over the parameter space [1] is necessary, which increases the complexity of implementing the controller in practice. In contrast, the method developed by [10] does not require any gridding over the parameter space. Also, as shown in Eq. (4.24) and Table 6.1 each of the parameters are less than 1 at all times. Therefore, neglecting the higher-order parameter variation is a justifiable approximation. Hence, to utilize the control synthesis technique given by [10], we calculate the first-order Taylor series approximation of the system matrices to obtain affine functions in Θ. To find the Taylor series expansion, first the LFT

(4.23) is re-arranged to the following representation:

$$\begin{bmatrix} l(k) \\ x(k+1) \\ z(k) \end{bmatrix} = \underbrace{\left[\begin{array}{c|ccc} D_{00} & C_0 & D_{01} & D_{02} \\ \hline B_0 & A & B_1 & B_2 \\ D_{10} & C_1 & D_{11} & D_{12} \end{array}\right]}_{=:M} \begin{bmatrix} p(k) \\ x(k) \\ \tilde{w}(k) \\ u(k) \end{bmatrix}, \tag{4.25}$$

$$p(k) = \Theta(k) l(k).$$

Notice that Eq. (4.25) is an upper LFT, i.e.,

$$\begin{aligned} H(\Theta) &:= \mathcal{F}_u(M, \Theta) \\ &= \begin{bmatrix} A & B_1 & B_2 \\ C_1 & D_{11} & D_{12} \end{bmatrix} + \begin{bmatrix} B_0 \\ D_{10} \end{bmatrix} \Theta \left(I - D_{00}\Theta\right)^{-1} \begin{bmatrix} C_0 & D_{01} & D_{02} \end{bmatrix}. \end{aligned} \tag{4.26}$$

Using the Taylor series expansion at $\Theta = 0$, the system can be approximated as

$$\begin{aligned} \hat{H}(\Theta) &= H(0) + \alpha_\delta \left[\nabla_{\alpha_\delta} H(0)\right] + \beta_\delta \left[\nabla_{\beta_\delta} H(0)\right] + \gamma \left[\nabla_\gamma H(0)\right], \\ &=: \begin{bmatrix} \hat{A}(\alpha_\delta, \beta_\delta, \gamma) & \hat{B}_1(\alpha_\delta, \beta_\delta, \gamma) & \hat{B}_2(\alpha_\delta, \beta_\delta, \gamma) \\ \hat{C}_1(\alpha_\delta, \beta_\delta, \gamma) & \hat{D}_{11}(\alpha_\delta, \beta_\delta, \gamma) & \hat{D}_{12}(\alpha_\delta, \beta_\delta, \gamma) \end{bmatrix}, \end{aligned} \tag{4.27}$$

where the relationship between α_δ, β_δ, and γ, and Θ can be found in Eq. (4.24) and $[\nabla_a H(0)]$ is the partial derivative of the LFT system $H(\Theta)$ in Eq. (4.26) with respect to a, which can be calculated as shown by [39]. The state-space representation after performing the Taylor series expansion is given by

$$\begin{bmatrix} x(k+1) \\ z(k) \end{bmatrix} = \begin{bmatrix} \hat{A}(\alpha_\delta, \beta_\delta, \gamma) & \hat{B}_1(\alpha_\delta, \beta_\delta, \gamma) & \hat{B}_2(\alpha_\delta, \beta_\delta, \gamma) \\ \hat{C}_1(\alpha_\delta, \beta_\delta, \gamma) & \hat{D}_{11}(\alpha_\delta, \beta_\delta, \gamma) & \hat{D}_{12}(\alpha_\delta, \beta_\delta, \gamma) \end{bmatrix} \begin{bmatrix} x(k) \\ \tilde{w}(k) \\ u(k) \end{bmatrix}. \tag{4.28}$$

4.3.4 An augmented LPV system for synthesis

To create an appropriate measurement for gain-scheduling control, the LPV system $\hat{H}(\Theta)$ must be augmented with the low-pass filter $L(q)$, the integrator $I(q)$, and the numerical differencer $D(q)$ (when designing a gain-scheduled PID controller).

4.3.4.1 PI Control

After augmenting the affine LPV system with the low pass filter and the integrator the augmented state space representation is given by

$$\begin{bmatrix} x_{AUG}(k+1) \\ z(k) \\ e(k) \end{bmatrix} = \begin{bmatrix} \tilde{A}(\alpha_\delta, \beta_\delta, \gamma) & \tilde{B}_1(\alpha_\delta, \beta_\delta, \gamma) & \tilde{B}_2(\alpha_\delta, \beta_\delta, \gamma) \\ \tilde{C}_1(\alpha_\delta, \beta_\delta, \gamma) & \tilde{D}_{11}(\alpha_\delta, \beta_\delta, \gamma) & \tilde{D}_{12}(\alpha_\delta, \beta_\delta, \gamma) \\ \tilde{C}_2 & 0 & 0 \end{bmatrix} \begin{bmatrix} x_{AUG}(k) \\ \tilde{w}(k) \\ u(k) \end{bmatrix} \tag{4.29}$$

where the augmented states are given by $x_{AUG}(k) = \begin{bmatrix} x(k)^\mathsf{T} \; x_L(k) \; x_I(k) \end{bmatrix}^\mathsf{T} \in \mathbb{R}^{n_{AUG}}$ with $n_{AUG} = n+2$, and the measurement for control is given by $e(k) = [e_P(k) \; e_I(k)]^\mathsf{T} \in \mathbb{R}^q$ with

$q = 2$. The state-space matrices are given by

$$\tilde{A}(\alpha_\delta, \beta_\delta, \gamma) = \begin{bmatrix} \hat{A}(\alpha_\delta, \beta_\delta, \gamma) & 0 & 0 \\ B_L \hat{C}_1(\alpha_\delta, \beta_\delta, \gamma) & A_L & 0 \\ 0 & C_L & 1 \end{bmatrix},$$

$$\tilde{B}_1(\alpha_\delta, \beta_\delta, \gamma) = \begin{bmatrix} \hat{B}_1(\alpha_\delta, \beta_\delta, \gamma) \\ B_L \hat{D}_{11}(\alpha_\delta, \beta_\delta, \gamma) \\ 0 \end{bmatrix},$$

$$\tilde{B}_2(\alpha_\delta, \beta_\delta, \gamma) = \begin{bmatrix} \hat{B}_2(\alpha_\delta, \beta_\delta, \gamma) \\ B_L \hat{D}_{12}(\alpha_\delta, \beta_\delta, \gamma) \\ 0 \end{bmatrix},$$

$$\tilde{C}_1(\alpha_\delta, \beta_\delta, \gamma) = \begin{bmatrix} \hat{C}_1(\alpha_\delta, \beta_\delta, \gamma) & 0 & 0 \end{bmatrix},$$

$$\tilde{C}_2 = \begin{bmatrix} 0 & C_L & 0 \\ 0 & 0 & 1 \end{bmatrix},$$

and $\tilde{D}_{11}(\alpha_\delta, \beta_\delta, \gamma) = \hat{D}_{11}(\alpha_\delta, \beta_\delta, \gamma)$, $\tilde{D}_{12}(\alpha_\delta, \beta_\delta, \gamma) = \hat{D}_{12}(\alpha_\delta, \beta_\delta, \gamma)$. The matrices ($A_L$, B_L, C_L) represent the state-space matrices of the low-pass filter $L(q)$.

4.3.4.2 PID Control

When designing a gain-scheduling PID controller, the augmented the affine LPV system with the low pass filter, the integrator, and the numerical differencer, the augmented state space representation is given by

$$\begin{bmatrix} x_{AUG}(k+1) \\ z(k) \\ e(k) \end{bmatrix} = \begin{bmatrix} \tilde{A}(\alpha_\delta, \beta_\delta, \gamma) & \tilde{B}_1(\alpha_\delta, \beta_\delta, \gamma) & \tilde{B}_2(\alpha_\delta, \beta_\delta, \gamma) \\ \tilde{C}_1(\alpha_\delta, \beta_\delta, \gamma) & \tilde{D}_{11}(\alpha_\delta, \beta_\delta, \gamma) & \tilde{D}_{12}(\alpha_\delta, \beta_\delta, \gamma) \\ \tilde{C}_2 & 0 & 0 \end{bmatrix} \begin{bmatrix} x_{AUG}(k) \\ \tilde{w}(k) \\ u(k) \end{bmatrix} \tag{4.30}$$

where the augmented states are given by $x_{AUG}(k) = \begin{bmatrix} x(k)^\mathsf{T} & x_L(k) & x_I(k) & x_D(k) \end{bmatrix}^\mathsf{T} \in \mathbb{R}^{n_{AUG}}$ with $n_{AUG} = n+3$, and the measurement for control is given by $e(k) = [e_P(k)\ e_I(k)\ e_D(k)]^\mathsf{T} \in$

$\mathbb{R}^q$ with $q = 3$. The state-space matrices are given by

$$\tilde{A}(\alpha_\delta, \beta_\delta, \gamma) = \begin{bmatrix} \hat{A}(\alpha_\delta, \beta_\delta, \gamma) & 0 & 0 & 0 \\ B_L\hat{C}_1(\alpha_\delta, \beta_\delta, \gamma) & A_L & 0 & 0 \\ 0 & C_L & 1 & 0 \\ 0 & B_D C_L & 0 & A_D \end{bmatrix},$$

$$\tilde{B}_1(\alpha_\delta, \beta_\delta, \gamma) = \begin{bmatrix} \hat{B}_1(\alpha_\delta, \beta_\delta, \gamma) \\ B_L\hat{D}_{11}(\alpha_\delta, \beta_\delta, \gamma) \\ 0 \\ 0 \end{bmatrix},$$

$$\tilde{B}_2(\alpha_\delta, \beta_\delta, \gamma) = \begin{bmatrix} \hat{B}_2(\alpha_\delta, \beta_\delta, \gamma) \\ B_L\hat{D}_{12}(\alpha_\delta, \beta_\delta, \gamma) \\ 0 \\ 0 \end{bmatrix},$$

$$\tilde{C}_1(\alpha_\delta, \beta_\delta, \gamma) = \begin{bmatrix} \hat{C}_1(\alpha_\delta, \beta_\delta, \gamma) & 0 & 0 & 0 \end{bmatrix},$$

$$\tilde{C}_2 = \begin{bmatrix} 0 & C_L & 0 & 0 \\ 0 & 0 & 1 & 0 \\ 0 & D_D C_L & 0 & C_D \end{bmatrix},$$

and $\tilde{D}_{11}(\alpha_\delta, \beta_\delta, \gamma) = \hat{D}_{11}(\alpha_\delta, \beta_\delta, \gamma)$, $\tilde{D}_{12}(\alpha_\delta, \beta_\delta, \gamma) = \hat{D}_{12}(\alpha_\delta, \beta_\delta, \gamma)$. The matrices ($A_L$, B_L, C_L) represent the state-space matrices of the low-pass filter $L(q)$ and the the matrices (A_D, B_D, C_D, D_D) represent the state-space matrices of the filtered, numerical differencer $D(q)$.

4.3.5 A gain-scheduling control synthesis problem

Having augmented all components for the controller synthesis, we need to synthesize the $\mathcal{H}_\infty$ gain-scheduling controller $K(\Theta)$. The ℓ_2 gain of the LPV system in Eq. (4.29) with a

gain-scheduling feedback controller is defined as

$$\max_{\Theta\in\mathsf{\Theta},\|\tilde{w}\|_{\ell_2}\neq 0} \frac{\|z\|_{\ell_2}}{\|\tilde{w}\|_{\ell_2}}. \tag{4.31}$$

Now we formally state the gain-scheduling control design problem.

Problem : The goal is to design a static gain-scheduling control $u(k) = K(\Theta)e(k)$ that stabilizes the closed-loop system and minimizes the worst-case ℓ_2 gain ($\mathcal{H}_\infty$ norm) of the closed-loop LPV system in Eq. (4.31) for any trajectories of $\Theta(k) \in \mathsf{\Theta}$.

The gain-scheduling method provided by [10] guarantees an $\mathcal{H}_\infty$ cost such that for an exogenous input $\tilde{w}$, the performance output z satisfies

$$\|z\|_{\ell_2} < \eta \, \|\tilde{w}\|_{\ell_2},$$

for any trajectories of $\Theta(k) \in \mathsf{\Theta}$. This method was derived for discrete-time polytopic time-varying systems. Therefore, in the next section, we will transform the augmented, affine system into a polytopic time-varying system to synthesize the controller.

4.3.6 Controller synthesis for polytopic linear time-varying system

The augmented state-space representation ($\tilde{A}(\alpha_\delta, \beta_\delta, \gamma)$, $\tilde{B}_1(\alpha_\delta, \beta_\delta, \gamma)$, ...) in either (4.29) or (4.30) can be converted into a discrete-time polytopic time-varying system ($\bar{A}[\lambda(k)]$, $\bar{B}_1[\lambda(k)]$, ...) by using the state-space matrices at vertices $\{\mathcal{V}_i\}$ of the parameter space polytope displayed in Fig. 4.8. Any system inside of the convex parameter set is represented by a convex combination of the vertex systems as weighted by the vector $\lambda(k)$ of barycentric

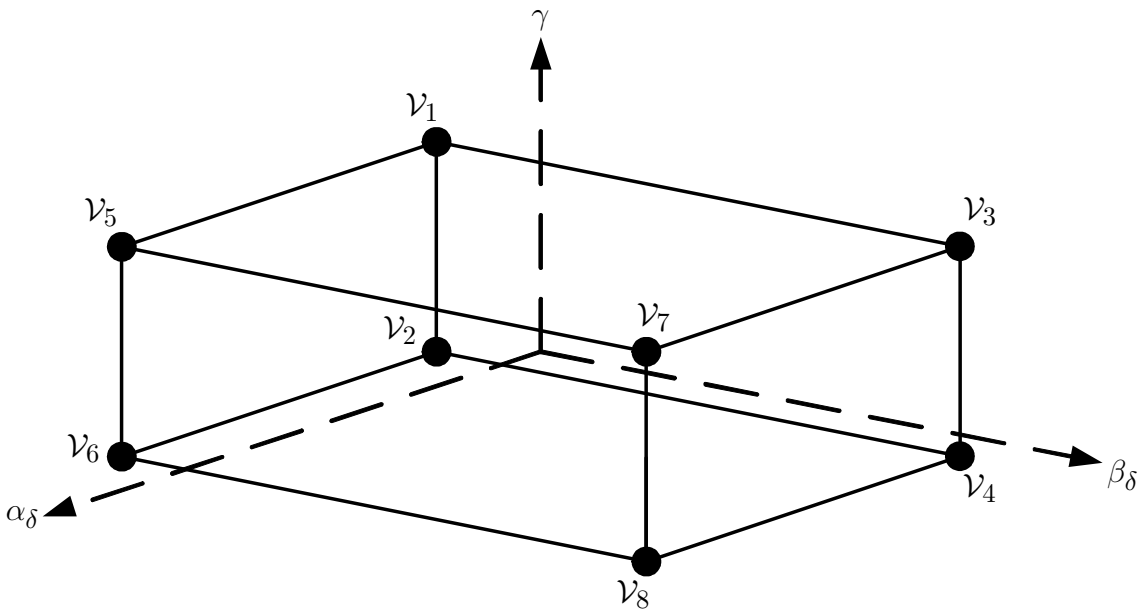

Figure 4.8: Parameter space polytope.

coordinates. Barycentric coordinates are used to specify the location of a point as the center of mass, or barycenter, of masses placed at the vertices of a simplex. [64] provides a formula, which is covered in Appendix 2.1.2, for computing the barycentric coordinates for any convex polytope. The discrete-time polytopic linear time-varying system is given by

$$\begin{aligned}\begin{bmatrix} x(k+1) \\ z(k) \\ e(k) \end{bmatrix} &= \begin{bmatrix} \bar{A}[\lambda(k)] & \bar{B}_1[\lambda(k)] & \bar{B}_2[\lambda(k)] \\ \bar{C}_1[\lambda(k)] & \bar{D}_{11}[\lambda(k)] & \bar{D}_{12}[\lambda(k)] \\ \bar{C}_2 & 0 & 0 \end{bmatrix} \begin{bmatrix} x(k) \\ w(k) \\ u(k) \end{bmatrix}, \\ e(k) &= \begin{bmatrix} e_P(k) & e_I(k) \end{bmatrix}^{\mathsf{T}},\end{aligned} \tag{4.32}$$

where, for all $k \in \mathbb{Z}_{\geq 0}$, $\lambda(k)$ is the vector of time-varying barycentric coordinates that belong to the unit simplex (2.12). A way to compute the barycentric coordinate vector $\lambda(k)$ for a given $\alpha_\delta(k)$, $\beta_\delta(k)$, and $\gamma(k)$ is provided in Appendix 2.1.2. For all $k \in \mathbb{Z}_{\geq 0}$, the rate of variation of the weights

$$\Delta\lambda_i(k) = \lambda_i(k+1) - \lambda_i(k), \quad i = 1, \cdots, N$$

is limited by the calculated bound b such that

$$-b\lambda_i(k) \leq \Delta\lambda_i(k) \leq b(1-\lambda_i(k)), \quad i = 1, \cdots, N \tag{4.33}$$

where $b \in [0, 1]$.

The system matrices $\bar{A}[\lambda(k)] \in \mathbb{R}^{n\times n}$, $\bar{B}_1[\lambda(k)] \in \mathbb{R}^{n\times r}$, $\bar{B}_2[\lambda(k)] \in \mathbb{R}^{n\times m}$, $\bar{C}_1[\lambda(k)] \in \mathbb{R}^{p\times n}$, $\bar{D}_{11}[\lambda(k)] \in \mathbb{R}^{p\times r}$, $\bar{D}_{12}[\lambda(k)] \in \mathbb{R}^{p\times m}$ belong to the polytope

$$\begin{aligned}\mathcal{D} = \{&(\bar{A}, \bar{B}_1, \bar{B}_2, \bar{C}_1, \bar{D}_{11}, \bar{D}_{12})(\lambda(k)) : \\ &(\bar{A}, \bar{B}_1, \bar{B}_2, \bar{C}_1, \bar{D}_{11}, \bar{D}_{12})(\lambda(k)) \\ &= \sum_{i=1}^{N} \lambda_i(k)(\bar{A}, \bar{B}_1, \bar{B}_2, \bar{C}_1, \bar{D}_{11}, \bar{D}_{12})_i, \lambda(k) \in \Lambda_N\}.\end{aligned}$$

The system matrices at any time k are the weighted summation of vertex system matrices $\{\mathcal{V}_i\}$ weighted by their barycentric coordinates $\lambda_i(k)$, i.e.

$$\bar{A}(k) = \sum_{i=1}^{N} \lambda_i(k)\bar{A}(\mathcal{V}_i), \quad i = 1, \cdots, N.$$

The same computation holds for $\bar{B}_1$, $\bar{B}_2$, $\bar{C}_1$, $\bar{D}_{11}$, and $\bar{D}_{12}$ as well.

Lemma 6 provides a finite set of LMIs that can be used to design the gain-scheduling controller. Due to Lemma 6, if there exists matrices $G_{i,1} \in \mathbb{R}^{q\times q}$, $G_{i,2} \in \mathbb{R}^{(n_{AUG}-q)\times q}$, $G_{i,3} \in \mathbb{R}^{(n_{AUG}-q)\times(n_{AUG}-q)}$, $Z_{i,1} \in \mathbb{R}^{m\times q}$ and symmetric matrices $P_i \in \mathbb{R}^{n_{AUG}\times n_{AUG}}$ such that the LMI conditions in Eq. (2.44) and Eq. (2.45) are satisfied, the gain-scheduling static feedback control is then obtained as shown in (2.46). The LMI's in Eqs. (2.44) and (2.45) are solved by programming them into MATLAB using the LMI lab solver [22], which is included in the Robust Control toolbox. The matrices $G_{i,1}$, $G_{i,2}$, $G_{i,3}$, $Z_{i,1}$, P_i, and the

$\mathcal{H}_\infty$ cost η are programmed in MATLAB as free matrix variables for the LMI optimization to choose. During the solution process, the the $\mathcal{H}_\infty$ cost η is minimized until the optimal solution is obtained.

4.4 Design of LTI Feedback Controller

The open-loop state-space plant used for designing this controller is the same as the one in Fig. 4.7, but has the low-pass filter $L(q)$ and the integrator $I(q)$ added without performing any Taylor series expansion. Using the nominal parameters, the closed-loop state-space representation is

$$\begin{aligned} x(k+1) &= A_{CL}(K)x(k) + B_1 w(k), \\ z(k) &= C_{CL}(K)x(k) + D_{11}w(k), \end{aligned} \tag{4.34}$$

where

$$A_{CL}(K) = A + B_2 K C_2 \quad \text{and} \quad C_{CL}(K) = C_1 + D_{12} K C_2.$$

Denoting the transfer function from w to z by H_{wz}, the inequality $\|H_{wz}\|_\infty^2 < \mu$ holds if, and only if, there exists a symmetric matrix P such that

$$\begin{bmatrix} P & A_{CL}(K)P & B_1 & 0 \\ PA_{CL}^T(K) & P & 0 & PC_{CL}^T(K) \\ B_1^T & 0 & I & D_{11}^T \\ 0 & C_{CL}(K)P & D_{11} & \mu I \end{bmatrix} \succ 0 \tag{4.35}$$

is feasible [17]. The optimal feedback controller K for the closed-loop system (4.34) is formulated as the optimization of the bilinear matrix inequality (BMI)

$$\min_{\mu,P,K} \ \mu \quad \text{subject to (4.35)} \tag{4.36}$$

where $P = P^T \in \mathbb{R}^{n\times n}$ and $K \in \mathbb{R}^{1\times 2}$ for a PI controller or $K \in \mathbb{R}^{1\times 3}$ for a PID controller. The BMI (4.36) was solved using the PENBMI software [33] as a MATLAB function in conjunction with the YALMIP [34] programming interface to find the fixed $\mathcal{H}_\infty$ PI controller $K_{PI} = [1.8260 \quad 0.3205]$ and the PID controller $K_{PID} = [1.4871 \quad 0.5009 \quad 0.8942]$.

4.5 Simulation Results

To validate the effectiveness of the proposed gain-scheduling controller, simulations are shown using the original plant in Eq. (4.23) for the following cases: engine cold start, load change, and engine speed change.

The necessity of a gain-scheduled controller is demonstrated by comparing its performance with that of a fixed gain $\mathcal{H}_\infty$ controller for the nominal parameters. The fixed gain $\mathcal{H}_\infty$ control synthesis procedure is reviewed in Appendix 4.4.

In each simulation, the time varying parameters α and β are corrupted by low-pass filtered white noise of up to 10% their nominal values to represent the slowly drifting offset that might occur in practical situations. To see transient responses, the initial conditions of the plant for Case 1 were chosen such that a little extra fuel is injected at first, giving a slightly higher equivalence ratio than 1. The initial conditions in Cases 2 and 3 were set such that the plant would start with an equivalence ratio of 1. For the following simulation

cases, the extracted profiles of time varying parameters from engine dynamometer tests were used.

4.5.1 Case 1: Engine Cold Start

We simulate an engine operation when it was started at freezing temperatures ($0°C$) and heated to its normal operation temperature of approximately $100°C$ within about 2 minutes at an engine speed of 1500 rpm. The purpose of this simulation is to emulate the cold start of an internal combustion engine when the engine is operated at high idle speed during the warm-up. Note that during the engine warm-up process the fuel vapor is much less at low temperature than that at high temperature. Therefore, this leads to quite different wall wetting dynamics. The wall wetting dynamics coefficients α and β defined in Eq. (4.3) were obtained from actual engine test data and they are functions of engine cylinder head temperature, speed and load. Since speed and load are fixed in this simulation, both α and β are functions of engine temperature and their values are shown in Fig. 4.9E. Notice that the transient response at 25 seconds in Fig. 4.9 is due to the change in the wall-wetting parameters as shown in Fig. 4.9E. When the engine has been warming up for about 90 seconds, the closed-loop system with the fixed $\mathcal{H}_\infty$ controller becomes unstable, while the LPV controller remains stable. Thus, in Fig. 4.9A, one can readily see the LPV controller's advantage of guaranteed stability as the parameters vary with time.

4.5.2 Case 2: Load Change

In this case we simulate an engine dynamometer experiment for an engine operated at a temperature of $80°C$ with an engine speed of 1500 rpm. After the engine is stably operated

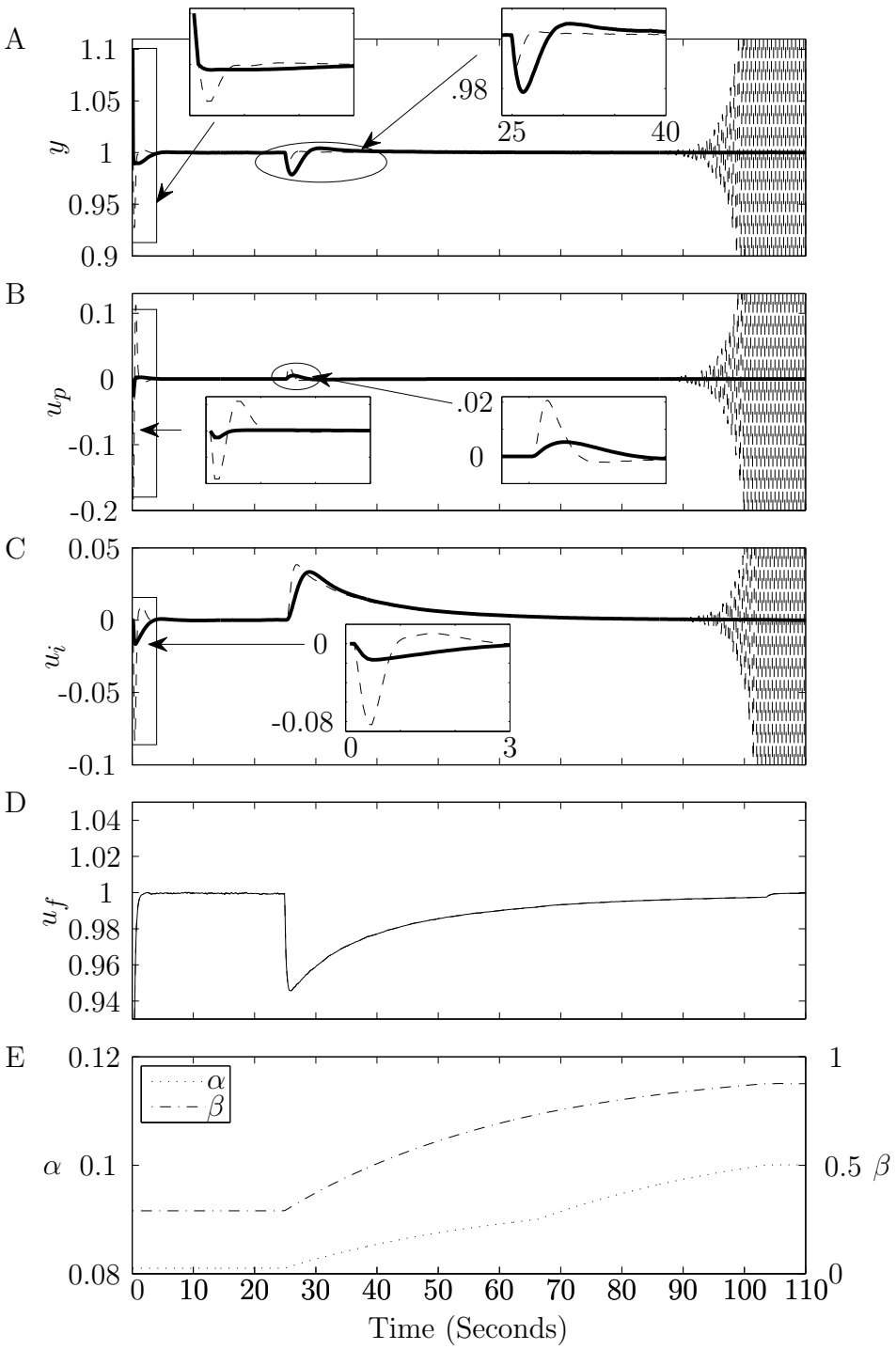

Figure 4.9: Case 1 Engine Cold Start: In plots A, B, C, and D the equivalence ratio $y(k)$, proportional control $u_p(k)$, integral control $u_i(k)$, and the feed-forward control are compared for the gain-scheduling feedback controller (solid line) and the fixed $\mathcal{H}_\infty$ controller (dashed line). The time varying parameters α (dotted line, left axis) and β (dash-dot line, right axis) are displayed in plot E.

at this condition with a 32% throttle, the load is increased by a step throttle position from 32% to 46%. Note that in the dynamometer test, the engine speed was maintained by dynamometer by increasing the load torque. This is similar to the driving condition that a step throttle is applied to maintain the vehicle speed when the vehicle is driven up a hill. Note that the step increment of throttle position produces a slight change in the wall-wetting parameter β as shown in Fig. 4.10E. But in Fig. 4.10, one can find the benefit of guaranteed performance of the gain-scheduling controller over the time-varying parameters. Note that the step throttle occurred at the 30^{th} second results in a momentary spike in the equivalence ratio due to the step air mass flow; but it is quickly pulled back into its target level by the gain-scheduled controller, while the fixed $\mathcal{H}_\infty$ controller takes much longer time with a lot of oscillations and uses more control effort.

4.5.3 Case 3: Engine Speed Change

In this simulation, an engine was operated in a dynamometer with its cylinder head temperature at $80°C$. To demonstrate the capability for the gain-scheduling controller to handle fast engine speed variations, smoothed step commands were applied to the engine dynamometer to manipulate the engine speeds shown in Fig. 4.11F. The resulting engine wall-wetting dynamic parameters, shown in Fig. 4.11E, were used in the simulation. In Fig. 4.11A, one can see that both controllers, gain-scheduling and fixed $\mathcal{H}_\infty$, regulate the engine equivalence ratio to its target value of one within 5% error except at 25^{th} second when the engine speed was increased abruptly from 1000 rpm to 4500 rpm. In this case, the engine equivalence ratio response converges to its target value smoothly for the gain-scheduling controller but with a lot of oscillations for the fixed $\mathcal{H}_\infty$ controller. This situation is similar to a transmission gear shifting where a rapid engine speed change may occur. Again, one can see the advantage of

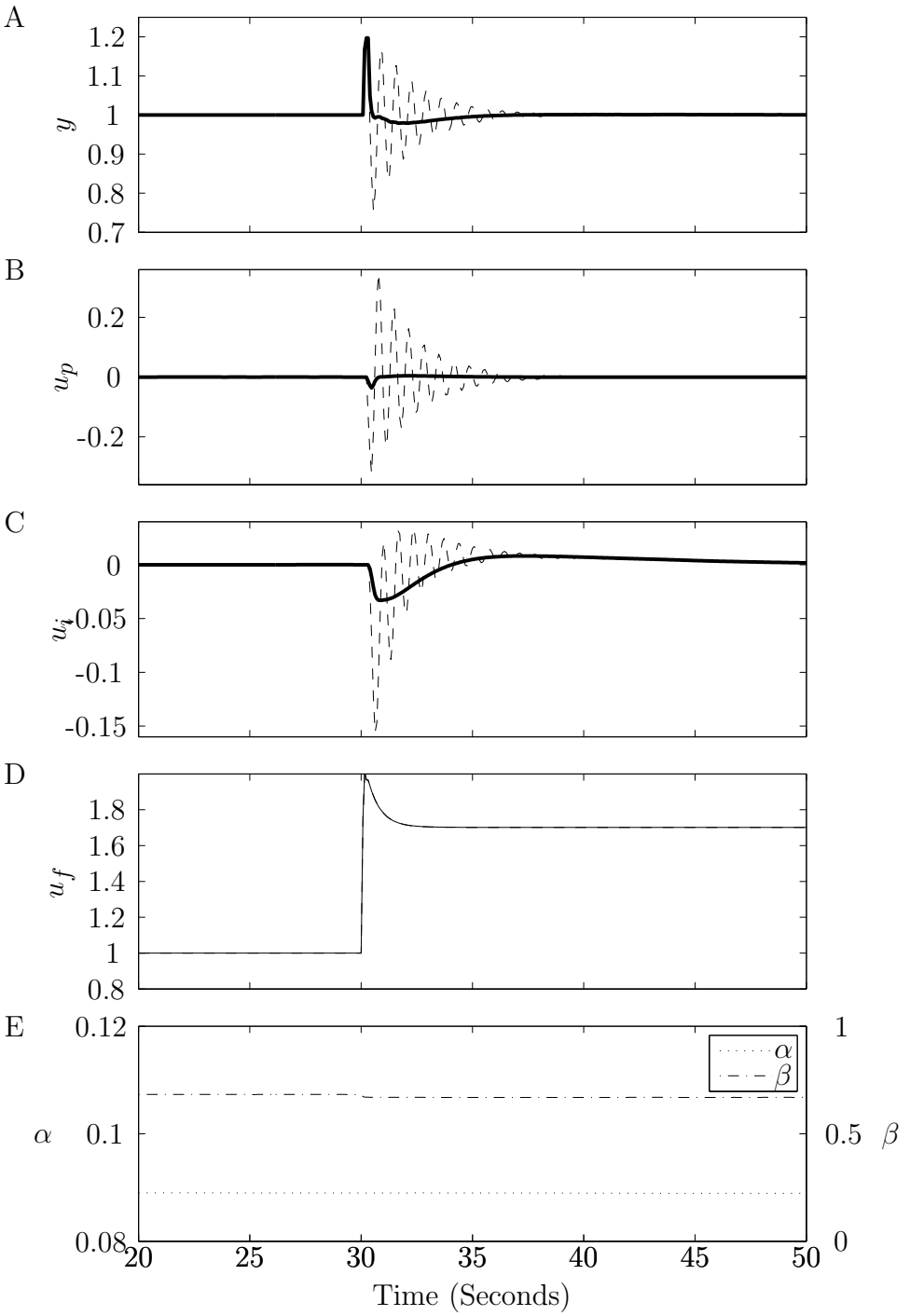

Figure 4.10: Case 2 Load Change: In plots A, B, C, and D the equivalence ratio $y(k)$, proportional control $u_p(k)$, integral control $u_i(k)$, and the feed-forward control are compared for the gain-scheduling feedback controller (solid line) and the fixed $\mathcal{H}_\infty$ controller (dashed line). The time varying parameters α (dotted line, left axis) and β (dash-dot line, right axis) are displayed in plot E.

guaranteed performance over the time-varying parameters as the gain-scheduled controller regulates the equivalence ratio back into safe limits quicker and with less overshoot than the fixed $\mathcal{H}_\infty$ controller.

4.6 HIL Simulation

The engine model used for the HIL simulation is a control oriented four cylinder dual fuel mean-value engine model developed at Michigan State University [79], which satisfies the requirements of validating an engine controller. The term "mean-value" indicates that the developed engine model neglects the reciprocating behavior of the engine, assuming all processes and effects are spread out over the engine cycle. For the HIL simulation, this model describes the input-output behavior of the physical engine systems with reasonable simulation accuracy using relatively low computational throughput. Ref. [26] provides a good overview of engine modeling, and most of dynamic equations used in our modeling work are from this reference book. This engine model also includes all engine transient dynamics. Figure 4.12 shows the overall mean-valve engine model architecture, along with main subsystem models, such as air-to-fuel ratio, manifold air pressure (MAP), brake mean effective pressure (BMEP), engine torque, exhaust temperature, etc.

4.6.1 Mean Value Engine Models

The subsystems that are described mathematically by their averaged dynamic behaviors are given below.

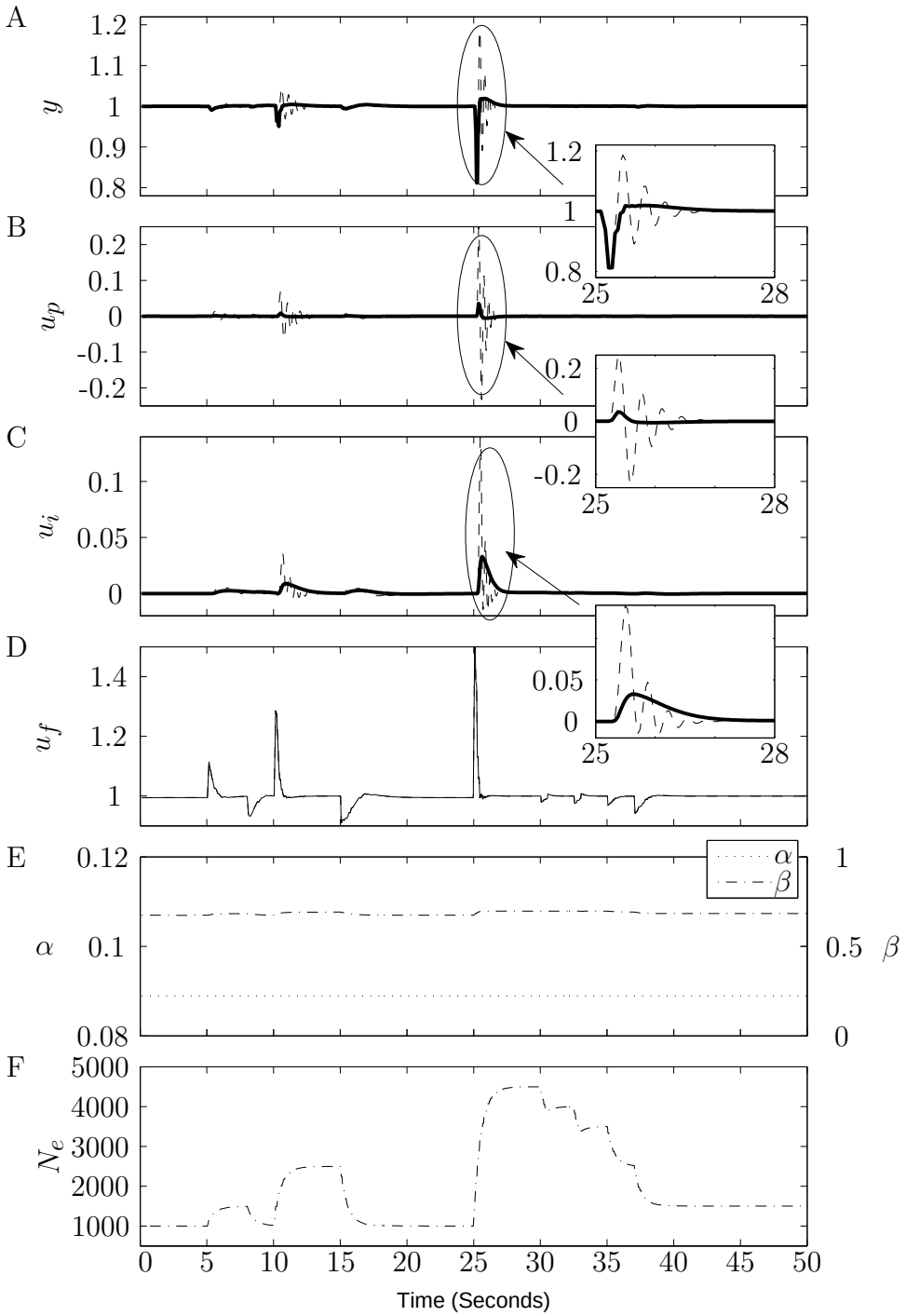

Figure 4.11: Case 3 Engine Speed Change: In plots A, B, C, and D the equivalence ratio $y(k)$, proportional control $u_p(k)$, integral control $u_i(k)$, and the feed-forward control are compared for the gain-scheduling feedback controller (solid line) and the fixed $\mathcal{H}_\infty$ controller (dashed line). The wall-wetting parameters α (dotted line, left axis) and β (dash-dot line, right axis) are displayed in plot E. The engine speed v is displayed in plot F.

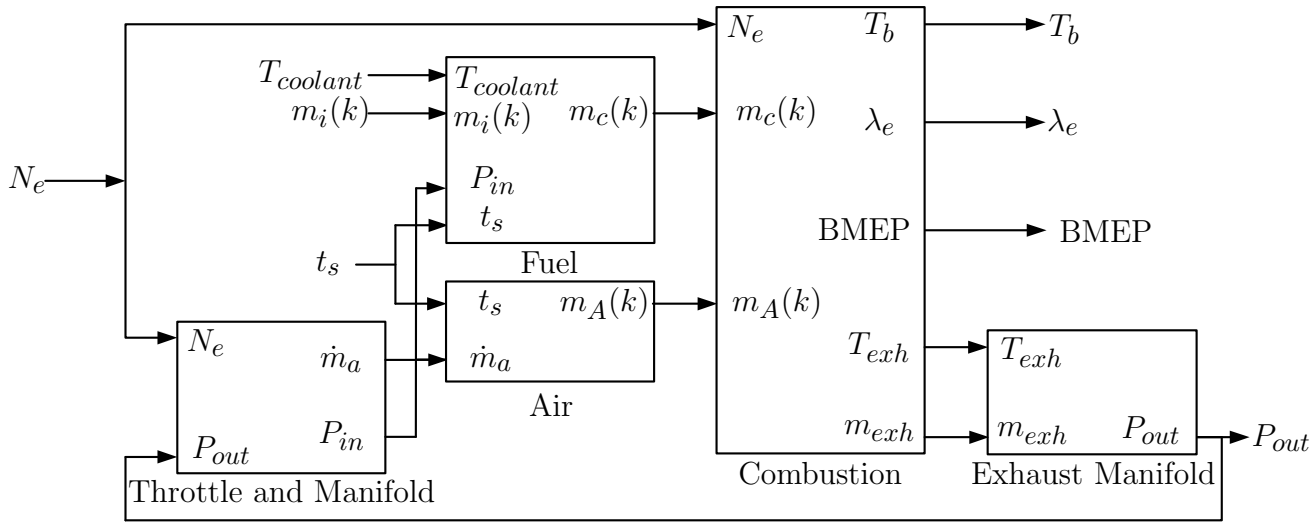

Figure 4.12: Mean Value Engine Model.

4.6.1.1 Valve Model

The valve model is used to compute the mass flow rate of air across the valve. The model used for the intake throttle and the EGR valve follow the governing equations

$$m_v = C_d(\theta)A(\theta)\frac{P_u}{\sqrt{RT_u}}\Psi\left(\frac{P_d}{P_u}\right), \tag{4.37}$$

and

$$\Psi\left(\frac{P_d}{P_u}\right) = \begin{cases} \sqrt{2\frac{P_d}{P_u}\left(1-\frac{P_d}{P_u}\right)} & \text{if } \frac{1}{2} < \frac{P_d}{P_u} < 1, \\ \frac{1}{\sqrt{2}} & \text{if } \frac{P_d}{P_u} < \frac{1}{2}, \end{cases} \tag{4.38}$$

where C_d is the valve discharge coefficient; θ is the valve opening angle; R is the gas constant; A is the valve open area; P_u and T_u are the pressure and temperature upstream from the valve; and m_v is the mass flow rate across the valve. The governing equations (4.37)-(4.38) follow the assumption that the spacial effects of the connecting pipes before and after the valve are neglected and that the thermodynamic characteristics of the connecting pipes are isentropic expansion.

4.6.1.2 Manifold Filling Dynamic Model

The manifold pressure of the intake and the exhaust is computed as a function of time by the governing equation

$$P_m(t) = P_m(0) + \int_0^t \frac{RT_m}{V_m}(m_{in} - m_{out})dt \tag{4.39}$$

where P_m is the manifold pressure; T_m is the manifold temperature; V_m is the manifold volume; m_{in} and m_{out} are the inlet and outlet air mass flow rates; and R is the universal gas constant. The assumptions made by the governing equation (4.39) are that the receiving behavior is an adiabatic process; the thermodynamic states are uniform over the manifold volume; and the manifold temperature is averaged over one engine cycle.

4.6.1.3 Engine Respiration Model

The mass flow rate of the air across of the engine cylinders, m_e, is computed by the engine respiration model

$$\dot{m}_e = \frac{P_{in}}{RT_{in}} \frac{V_d N_e}{30} \kappa \left(\frac{P_{out}}{P_{in}}, v \right) \tag{4.40}$$

where κ is a two degree of freedom look-up table; P_{in} and T_{in} are the mean pressure and temperature at the intake manifold; P_{out} is the mean pressure at the exhaust manifold; V_d is the engine displacement.

4.6.1.4 Crankshaft Dynamic Model

The crankshaft dynamic model, based on Newton's theory assuming a rigid crankshaft, is derived as

$$\dot{N}_e = \frac{60}{2\pi}\frac{T_b - T_l}{J_e} \tag{4.41}$$

where J_e is the rotational inertia of the engine crankshaft; and T_b and T_l are the engine brake and load torques. The desired engine speed is maintained by an engine dynamometer model that generates the engine load torque, T_l, using a feedback PID controller.

4.6.2 Event Based Engine Models

The mathematical models used to simulate the cycle-to-cycle varying variables of engine subsystems are given below. Each variable in this sections is updated based on the engine cycle (k) and is independent of time, t.

4.6.2.1 Event Based Wall-Wetting Dynamics

When port-fuel-injection is used to deliver fuel to the engine cylinders, some of the fuel injected after each injector pulse enters the cylinders. However, the remaining fuel sticks to the walls of the intake port and on the back of the intake valve. The total fuel entering the engine cylinders then consists of fuel injected from the current injection pulse and fuel vapor from the fuel mass stored on the walls from previous injection pulses. Knowledge of this process is necessary to control the metering of fuel for precise air-to-fuel ratio control. The event based wall-wetting dynamics used in the engine for HIL simulation are the same as those in Eq. (4.2).

4.6.2.2 Event Based Engine Air-to-fuel Ratio

The gas exchange behavior of the engine introduces dynamics into the air-fuel ratio calculation. Since the engine uses exhaust gas recirculation, a substantial amount of the burned gas remains in the cylinder. The gas fraction carries the air-to-fuel ratio of the previous engine cycle into the current cycle. Due to this behavior, the air-fuel ratio is modeled cycle-to-cycle as

$$\lambda_e(k) = \frac{\tilde{\lambda}_e(k) M_{fresh}(k) + \lambda_e(k-1) M_{burnt}(k)}{M_{fresh}(k) + M_{burnt}(k)}, \tag{4.42}$$

where $\tilde{\lambda}_e$ is the normalized air-to-fuel ratio defined as

$$\tilde{\lambda}_e(k) = \frac{m_A(k)}{m_c(k)} \frac{1}{c}. \tag{4.43}$$

λ_e is the normalized air-to-fuel ratio of the gas mixture inside the engine cylinder after the intake valve is closed. M_{fresh} is the mass of the fresh gas mixture charge in the cylinder, which is the summation of the fresh air mass m_A and the fresh fuel mass m_c, and M_{burnt} is the burned gas remaining in the engine cylinder after the exhaust valve closes, which includes burned gas due to both internal and external EGR (exhaust gas recirculation). Note that these dynamics are quite different from the LPV design model described in Fig. 4.2.

4.6.2.3 Event Based Engine Brake Torque

Every combustion event, the engine brake torque calculation is triggered using the following equation:

$$T_b(k) = \frac{m_c(k) H_l n}{4\pi} \eta_e(N_e, \chi, \theta_{st}, x_{EGR}) \tag{4.44}$$

where n is the number of engine cylinders; H_l is the lower heat value of the fuel; η_e is the engine efficiency, which is a function of engine speed, normalized air-to-fuel ratio, spark timing θ_{st}, and the exhaust-gas-recirculation rate x_{EGR}.

4.6.3 Set-up and Implementation

The mean value engine model was implemented into an Opal-RT HIL system using MATLAB/Simulink. The engine model was updated at a sample period of 1 millisecond. Similarly, the LPV controller, along with feedforward controller, was implemented as an event-based discrete controller in Simulink into a Mototron Engine Control Module (ECU) sampled every 5 milliseconds as a function call, see HIL simulation scheme shown in Figure 4.13. The Opal-RT HIL simulator communicates with the Mototron ECU controller through the high speed controller-area network (CAN), where signals were sent and received with minimal delay.

The Opal-RT simulation step size of 1 millisecond was chosen in order to emulate a real-world continuous time engine. Similarly, the Mototron sample rate of 5 milliseconds for the controller updating is used in many production engine control systems. The CAN communication between Opal-RT and Mototron has a time delay between the time when signals are sent from Mototron and the time when they are received by Opal-RT, and vice versa. This delay was less than 1 millisecond for our setup since only a few variables were communicated between the HIL simulator and Mototron controller, see the timing scheme in Figure 4.14. The event based function call was implemented as follows. At each sample time, the controller checks if the event based sample condition is met; and if so, the function call will be made to execute the event based control strategy (see Figure 4.14). Since the sample period of the event-based LPV controller is a function of engine speed and it can

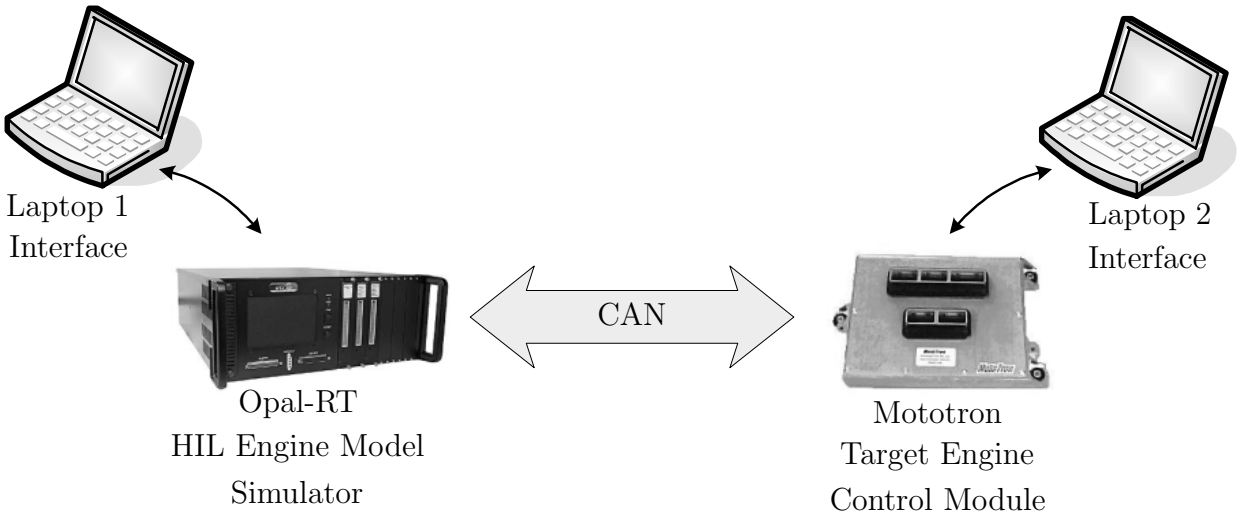

Figure 4.13: HIL engine model and controller setup.

executed with a 5ms sample period, the LPV controller can not be updated exactly at each fuel injection event. This leads to some sample time error between ideal event based sampling and actual function call implementation.

4.7 HIL Simulation Results

In Fig. 4.15-4.18, the responses for the gain-scheduling PI and PID controllers are given by, respectively, the solid gray and black lines. The gray dashed line shows the response of the fixed gain $\mathcal{H}_\infty$ PID controller. In each of the HIL simulations, white Gaussian noise was added to each of the measured signals to represent measurement noise. The standard deviation of the noise added to each signal was set such that the value of the noise would not be larger than the following percentages of the measured signals: air flow $m_A \sim 3\%$, equivalence ratio $y_s \sim 2\%$, coolant temperature $\sim 5\%$, intake pressure $\sim 5\%$, and engine speed $N_e \sim 1\%$. Even though the cycle-to-cycle combustion variations typically present in internal combustion engines are correlated to engine speed, load and temperatures, the

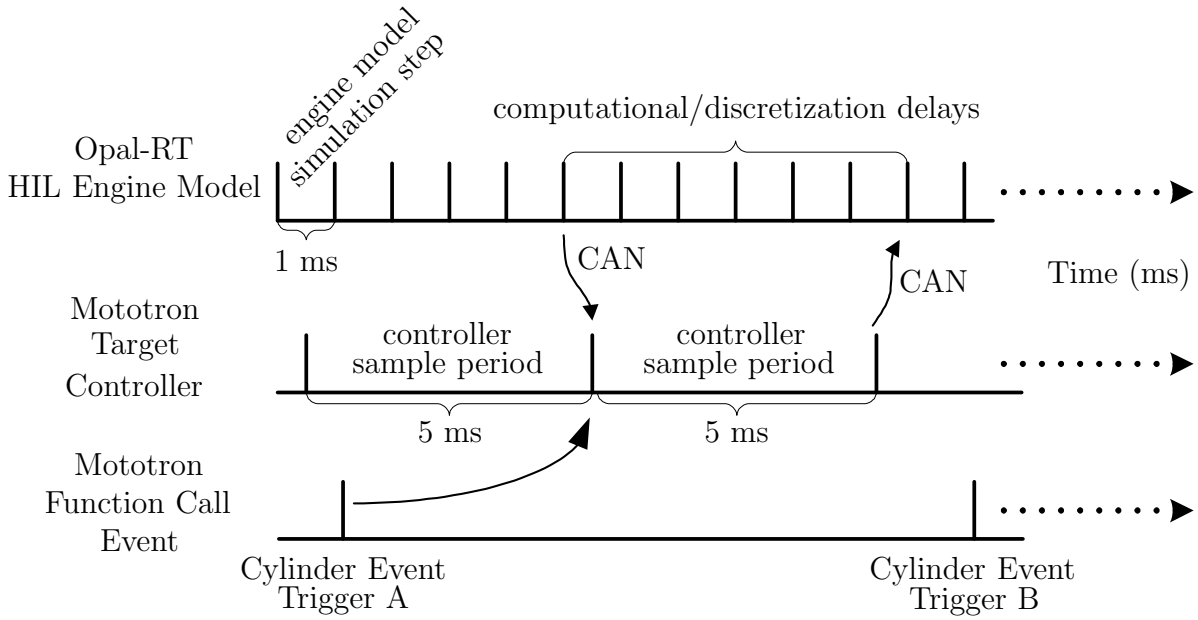

Figure 4.14: HIL timing scheme.

sensor measurement noise, due to cycle-to-cycle combustion variations and sensor noise, was simplified as a Gaussian white noise due to its simplicity and broad bandwidth. Also, in each of the HIL simulations, the fuel injected is saturated, as a function of the mass air flow, to $\pm 25\%$ of the fueling that keeps equivalence ratio at one.

4.7.1 Case 1: Engine Cold Start

We simulate an engine cold start process from freezing temperatures ($0°C$) to its normal operation temperature of approximately $100°C$ within about 2 minutes at an engine speed of 1500 rpm. The purpose of this simulation is to emulate the cold start of an internal combustion engine when the engine is operated at high idle speed during the warm-up. Note that during the engine warm-up process the fuel vapor is much less at low temperature than that at high temperature. Therefore, this leads to quite different wall-wetting dynamics.

The wall-wetting dynamics coefficients α and β defined in Eq. (4.3) were obtained from actual engine test data and they are functions of engine coolant temperature, speed and load. Since speed and load were fixed in this simulation, both α and β were functions of engine temperature and their values are shown in Fig. 4.16C. The responses of the gain scheduling PI and PID controllers during this simulation, given in Fig. 4.16, are nearly identical. However, at between 100 and 110 seconds, the fixed gain $\mathcal{H}_\infty$ PID controller becomes saturated causing the measured equivalence ratio to oscillate between 0.8 and 1.2, while both LPV controllers continue to regulate the equivalence ratio to the desired value of 1. Also, in Fig. 4.16B, the mass of the fuel injected when using the fixed gain $\mathcal{H}_\infty$ PID controller has noticeable perturbations due to the noise added to the measured equivalence ratio. However, the gain scheduling PI and PID controllers have no noticeable perturbations which demonstrates that not only do they remain stable over the entire operating range of the engine, but they are also robust to the added measurement noise.

For comparison purposes, a simulation was carried out using the control model described in Section 6.2 for the engine cold start problem with the response displayed in Fig. 4.15. In this simulation, no measurement noise is added to the measured signals. Also, a saturation level is not imposed on the feedback control input.

4.7.2 Case 2: Load Change

In this case we simulate an engine dynamometer experiment for an engine operated at a temperature of $80°C$ with an engine speed of 1500 rpm. After the engine is stably operated at this condition with a 32% throttle, the load is increased by a step throttle position from 32% to 46%. Note that in the dynamometer test, the engine speed was maintained by dynamometer through torque regulation. This is similar to the driving condition that a step

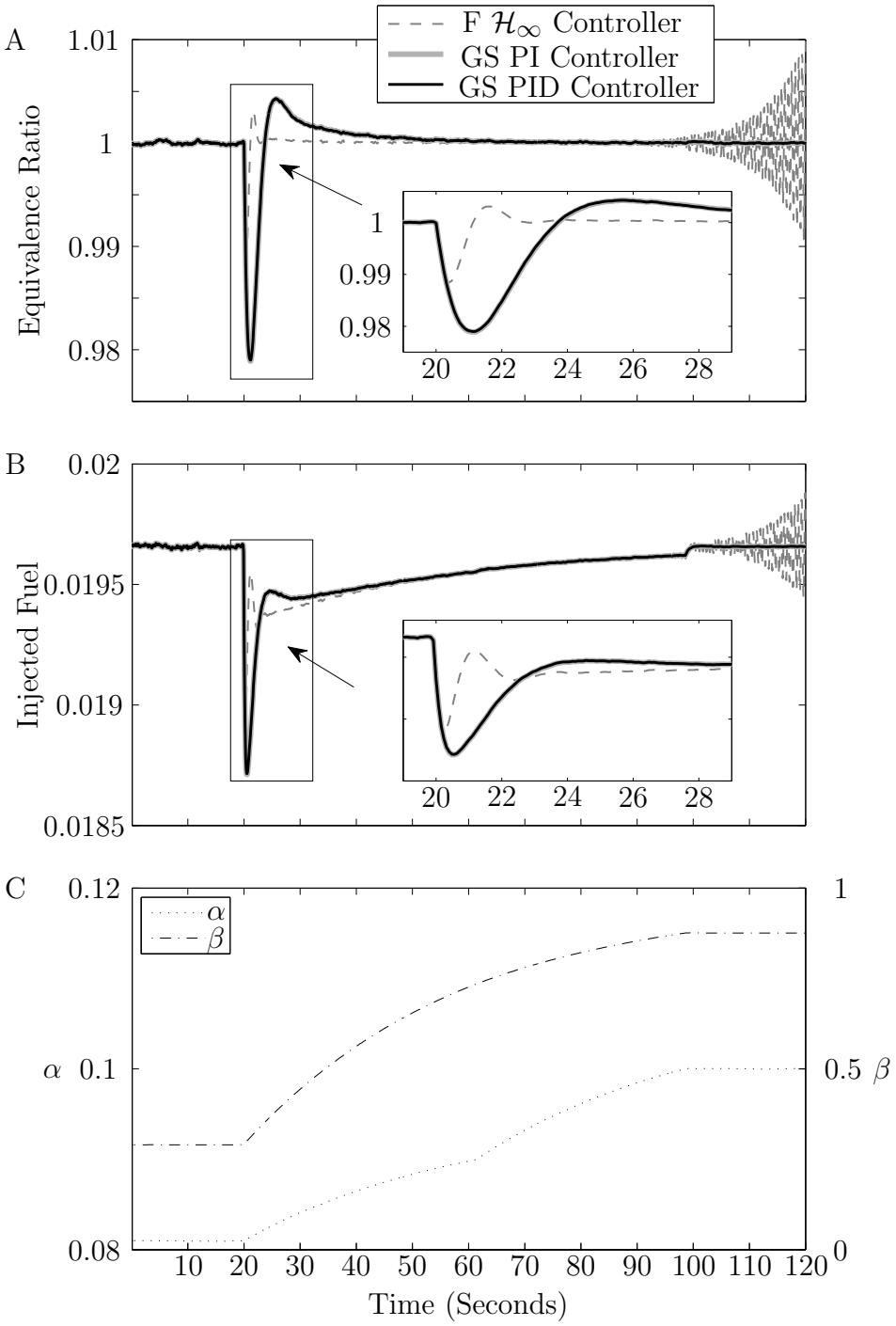

Figure 4.15: Case 1: Engine Cold Start using simple model.

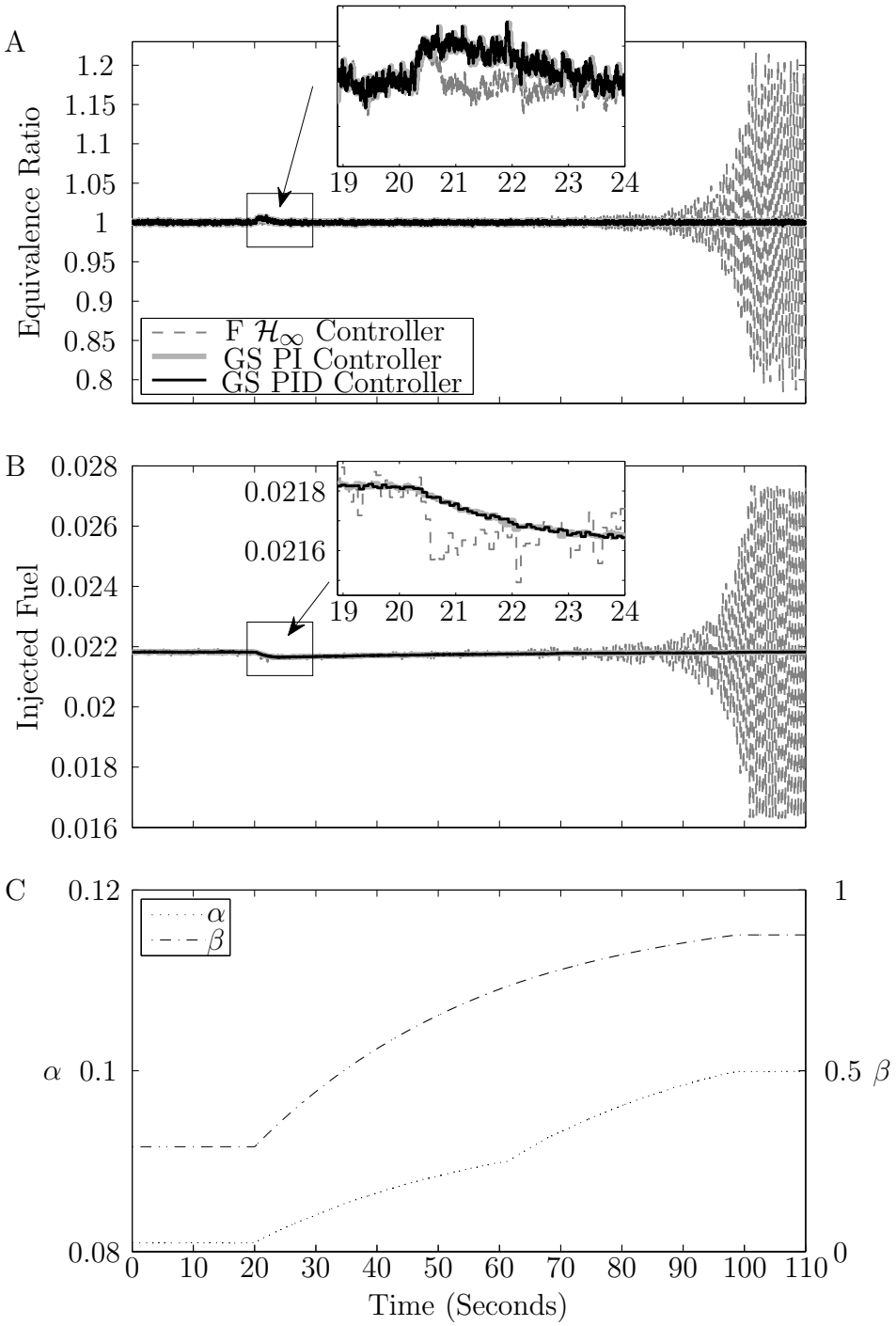

Figure 4.16: Case 1: Engine Cold Start using HIL.

throttle is applied to maintain the vehicle speed when the vehicle is driven up a hill. Note that the step increment of throttle position produces a slight change in the wall-wetting parameter β as shown in Fig. 4.17C. The responses of each controller is given in Fig. 4.17A. Notice that the throttle step occurring at the 30^{th} second results in a drop in the equivalence ratio due to the step air mass flow. In the detail of Fig. 4.17A, we see that with the gain-scheduling PID controller the equivalence ratio only drops to approximately 0.85, while the gain-scheduling PI and fixed gain $\mathcal{H}_\infty$ controller both drop to nearly 0.8. Also, notice that the equivalence ratio with fixed gain $\mathcal{H}_\infty$ PID controller overshot to over 1.1 with over fueling as seen in the detail of Fig. 4.17B.

4.7.3 Case 3: Engine Speed Change

In this simulation, an engine was operated on a dynamometer with its coolant temperature at $80°C$. To demonstrate the capability for the gain scheduling controller to handle engine speed variations, a smoothed step command from 1500 rpm to 2500 rpm was applied to the engine dynamometer to manipulate the engine speed as shown in Fig. 4.18D. The resulting engine wall-wetting dynamics parameters, shown in Fig. 4.18C, were used in the simulation. Notice in Fig. 4.18A that the gain-scheduling PID controller regulates the equivalence ratio of the engine to the target value of 1 within 5% error, while the measured equivalence ratio of the engine with the gain-scheduling PI controller and the fixed gain $\mathcal{H}_\infty$ PID controller go above 1.05. Also, the equivalence ratio with the fixed gain $\mathcal{H}_\infty$ PID controller drops to below 0.95, while both gain-scheduling controllers only lower the equivalence ratio to about 0.96. The equivalence ratio with the fixed gain $\mathcal{H}_\infty$ PID controller also has many oscillations and uses more control effort as shown in the detail of Fig. 4.18B, which hurts engine transient fuel economy.

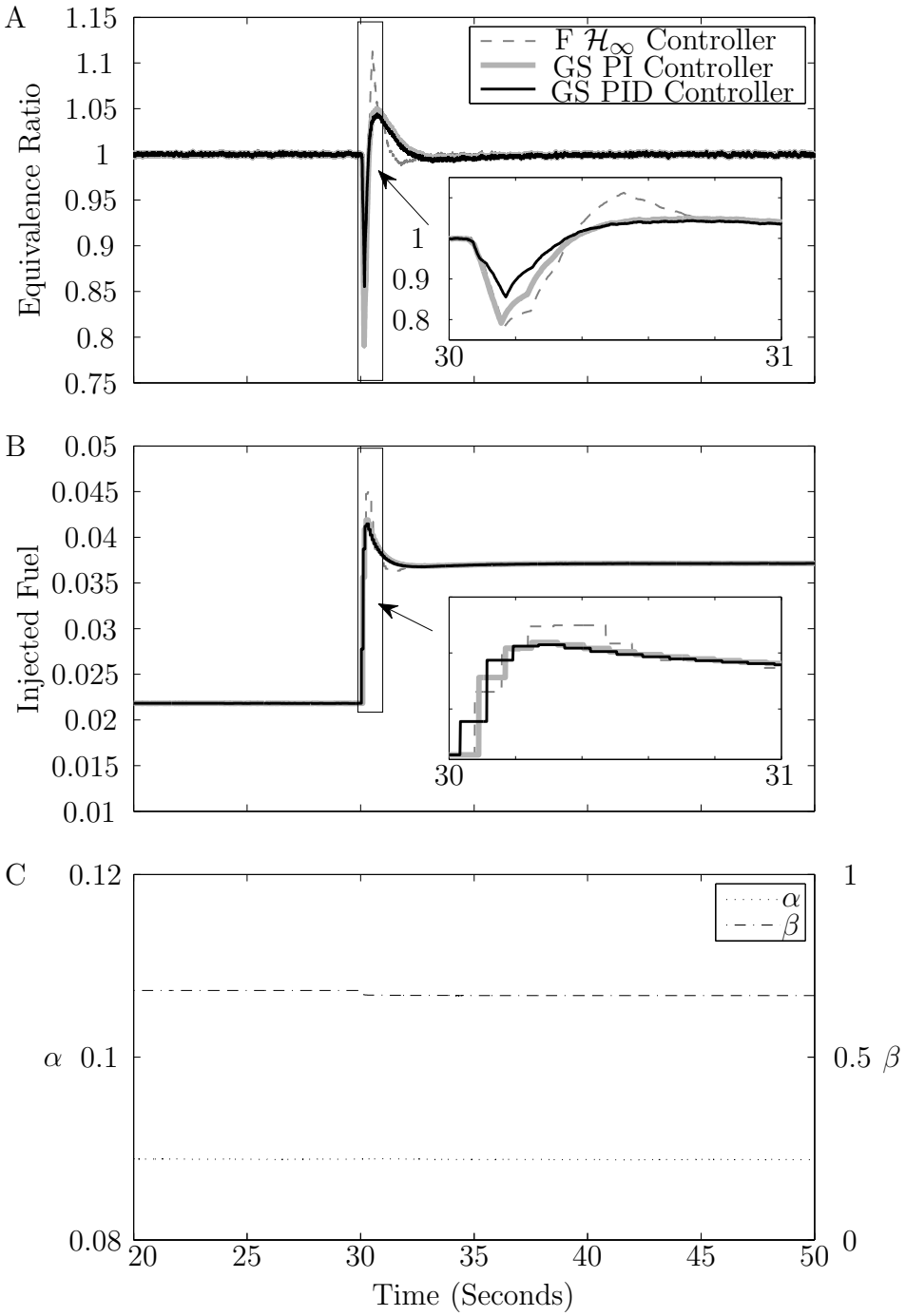

Figure 4.17: Case 2: Engine Load Change using HIL.

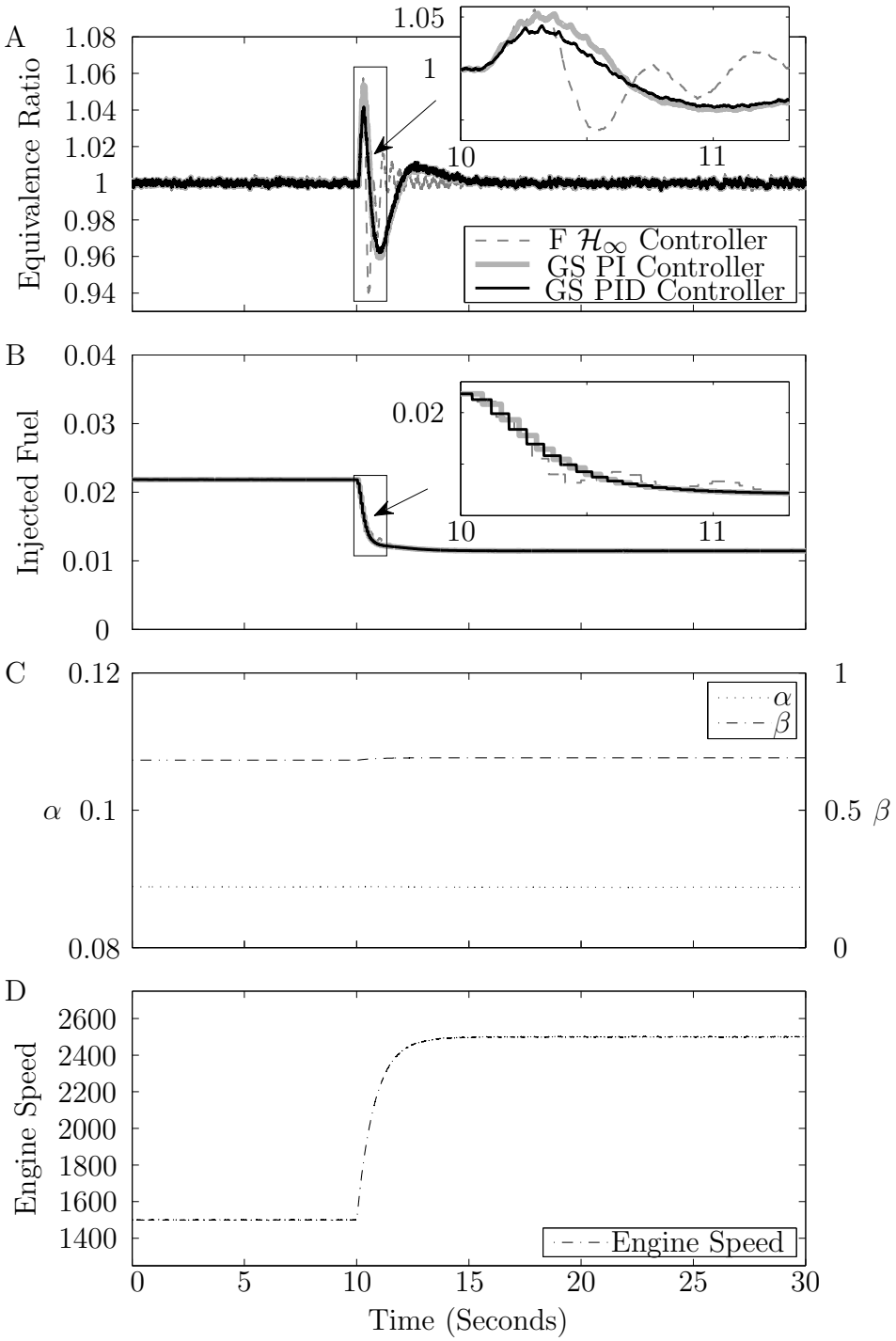

Figure 4.18: Case 3: Engine Speed Change using HIL.

4.7.4 Case 4: Combined Load and Engine Speed Change

In this simulation, an engine was operated on a dynamometer with its coolant temperature at $80^{\circ}C$. To demonstrate the capability for the gain scheduling controller to handle load changes combined with engine speed variations, the load is increased by a step throttle position from 32% to 46% and then combined with an engine speed variation generated by a smoothed step command from 1500 rpm to 2000 rpm as shown in Fig. 4.19D. The resulting engine wall-wetting dynamics parameters are shown in Fig. 4.19C. Notice in Fig. 4.19A both of the gain-scheduling controllers drop the measured equivalence ratio to approximately 0.85, while the fixed gain $\mathcal{H}_\infty$ PID controller drops the measured equivalence ratio below 0.85. Also, the fixed gain $\mathcal{H}_\infty$ PID controller overshoots to nearly 1.15 with over fueling as seen in the detail of Fig. 4.17B.

4.8 Conclusion

In this chapter, a systematic process for developing gain-scheduling PI and PID controllers for discrete-time LPV systems is presented. First, a control oriented LPV model is developed by using the dynamics of a port-fuel-injection process. Then the LPV model obtained is investigated and found to contain parameter variation that is not affine. Due to limitations in current LPV control schemes for discrete-time systems discussed in Section 4.3.3, a first-order Taylor series approximation is performed on the LPV system $H(\Theta)$ in (4.26) to obtain an approximated LPV system $\hat{H}(\Theta)$ in (4.27) with only affine parameter variation. The measurement for control is generated by augmenting the approximated LPV system with a low-pass filter and an integrator. The augmented, approximated LPV system is then converted to a polytopic LPV system so that the synthesis method given by [10] can be uti-

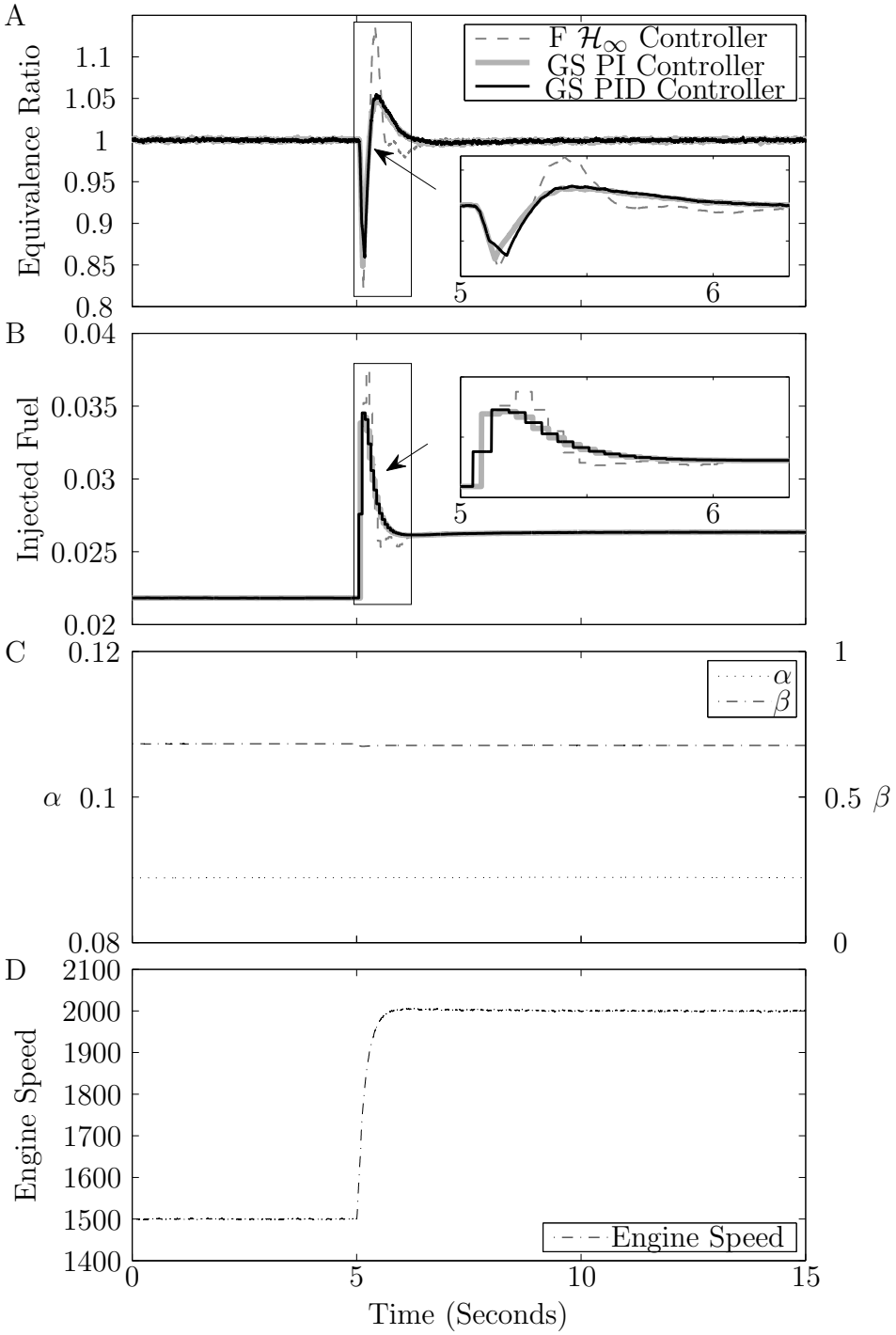

Figure 4.19: Case 4: Combined Load and Engine Speed Change using HIL.

lized. To validate the gain-scheduling controller found with the finally obtained LPV system $\hat{H}(\Theta)$, simulations are performed using the original LPV system $H(\Theta)$. From the simulation results, it is clear that although the approximated LPV system $\hat{H}(\Theta)$ is used to design the gain-scheduling controller it still performs very well when applied to the original LPV system $H(\Theta)$. Furthermore, not only do the HIL simulation results reaffirm the success of the simulation results, they also demonstrate the feasibility of implementing of the proposed LPV scheme on a hardware controller that could be used as an engine control module.

To the authors' knowledge, this is the first work to develop an air-to-fuel ratio gain-scheduling controller for the port-fuel-injection process using the wall-wetting parameters α and β, and the engine speed N_e as scheduling variables. Future investigation that would further this research effort includes developing a systematic framework for the off-line estimation of the wall-wetting parameters α and β over all operating conditions for a given intake manifold.

Chapter 5

Mixed $\mathcal{H}_2/\mathcal{H}_\infty$ Observer-Based LPV Control of a Hydraulic Engine Cam Phasing Actuator

5.1 Introduction

The intake and exhaust valve timing of an internal combustion (IC) engine greatly influence the fuel economy, emissions, and performance of an IC engine. Conventional valvetrain systems can only optimize the intake and exhaust valve timing for one given operational condition. That is, the optimized valve timing can either improve fuel economy and reduce emissions at low engine speeds or maximize engine power and torque outputs at high engine speeds. However, with the development of continuously variable valve timing (VVT) systems [37], the intake and exhaust valve timing can be modified as a function of engine speed and load to obtain both improved fuel economy and reduced emissions at low engine speeds and increased power and torque at high engine speeds.

To adjust the intake and exhaust timing, the most common cam phasing system is the hydraulic van type cam phaser [20]. The control of hydraulic cam phasing systems has been discussed in [24] and [52]. In [24], a significant nonlinearity in the hydraulic cam phasing

system is noted and a nonlinear controller is designed to compensate for it. In [52], an $\mathcal{H}_2$ controller is designed using the output covariance constraint (OCC) control design approach [87]. In this chapter, a gain-scheduling controller is developed using linear parameter varying (LPV) control design.

In recent years, the use of LPV modeling and control in automotive applications has received a great deal of attention. LPV modeling and control techniques have been applied to both diesel engines [65, 55] and gasoline spark-ignition engines [88, 82, 66, 69]. In [65], LPV control techniques are applied to the air path of turbocharged diesel engines to control the transient exhaust gas fraction pumped into the cylinders to reduce nitrous oxide emissions. In [55], an LPV identification technique is applied to a nonlinear turbocharged diesel engine to obtain an LPV model suitable for control synthesis. In [88], a continuous-time LPV model is developed considering only engine speed as a time-varying parameter. In [82], a large variable time delay is present in the air-fuel ratio control loop for a lean burn spark ignition engine. LPV control methods are used to compensate for the variable time delay. In [66] and [69], event-based gain-scheduling proportional-integral (PI) and proportional-integral-derivative (PID) controllers are developed using the wall-wetting parameters and engine speed as time-varying parameters. In this chapter, the techniques used in [66] and [69] to obtain the static PI and PID gain-scheduling controllers are augmented to develop an observer-based dynamic LPV controller using the dynamics of the plant.

To obtain the model of the VVT system, closed-loop system identification was used in [48] and [52]. A main reason for selecting closed-loop system identification in [48] and [52] was due to high open-loop gains that makes it difficult to maintain the cam phaser operated at a fixed location for system identification. During the system identification process, it was found that the system gain of the VVT actuator is a function of engine speed, load, oil

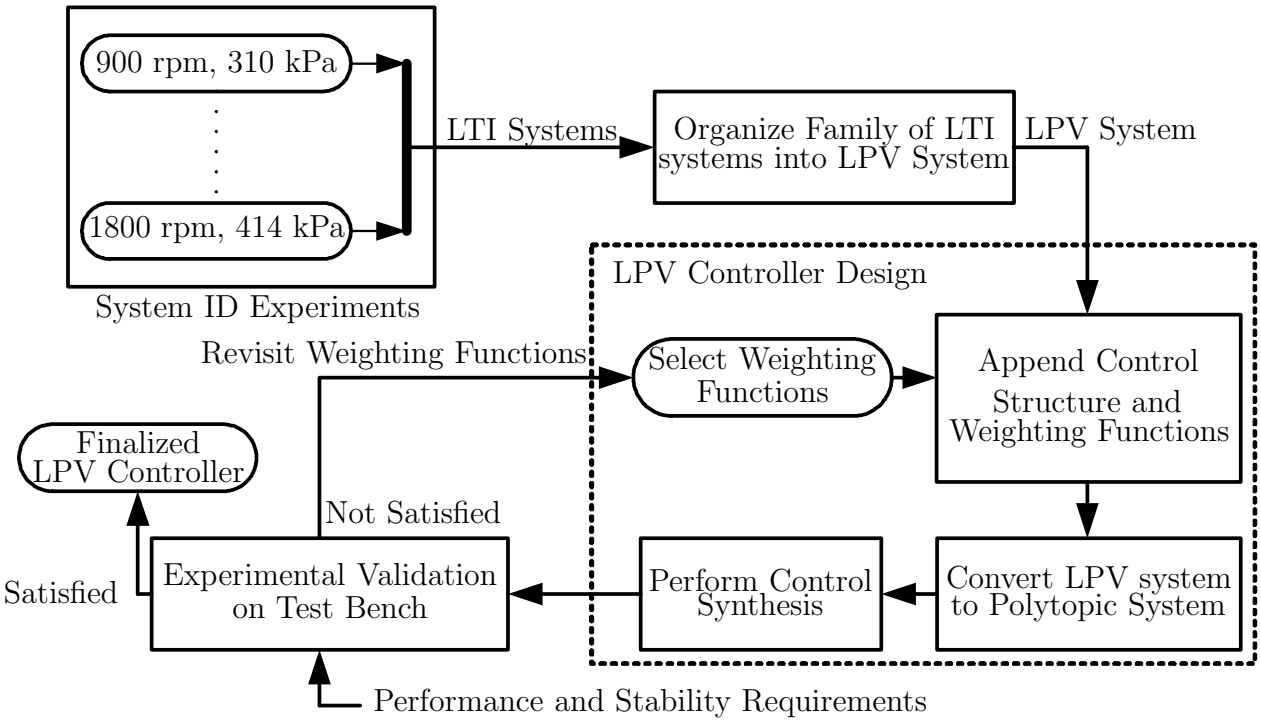

Figure 5.1: Flowchart of the design and validation process of an LPV controller.

pressure, and temperature. Therefore, it seems only natural to exploit the knowledge of how the system gain of the VVT actuator varies with the time varying parameters. To do this, the VVT system can be described as a family of linear models to approximate the system dynamics for a given engine speed, load, oil pressure, and temperature. Thus formulating an LPV model for the VVT system.

The purpose of this chapter is to develop a dynamic gain-scheduling controller with guaranteed stability and performance over all time-varying parameters. To do this, the process depicted in Fig. 5.1 was followed. First, a family of linear-time-invariant (LTI) models was obtained. Using engine speed and the oil pressure as system parameters, a family of linear models of the VVT system were obtained by performing multiple system identifications while maintaining engine speed and oil pressure at specified levels. With the family of linear models, the LPV model of the VVT system was formulated. To design

the dynamic gain-scheduling controller, a standard control structure of observer-based state feedback with integral control was employed. This control structure, along with $\mathcal{H}_2$ and $\mathcal{H}_\infty$ performance weighting functions, were then appended onto the LPV model of the VVT system to obtain the LPV system of the generalized plant. Then the LPV system of the generalized plant was converted to a polytopic system, which is an LPV system with a polytopic dependency on a scheduling parameter that takes values in the unit-simplex, so that the mixed $\mathcal{H}_2/\mathcal{H}_\infty$ discrete-time LPV control synthesis method given by [12] could be applied to obtain the gain-scheduled state feedback and observer gains. Once a potential controller was obtained, its performance was experimentally validated on the test bench used to obtain the family of LTI systems. If the performance and stability requirements of the VVT system are not satisfied when testing the LPV controller, the selected $\mathcal{H}_2$ and $\mathcal{H}_\infty$ performance weighting functions are modified and the control synthesis procedure is performed again. This loop is performed until stability and satisfactory performance are obtained on the test bench.

As stated previously, a multi-objective, mixed $\mathcal{H}_2/\mathcal{H}_\infty$ control design is performed in this chapter. The goal of using both $\mathcal{H}_2$ and $\mathcal{H}_\infty$ performance criteria is to design a controller which can meet multiple performance objectives. In this chapter, a loose $\mathcal{H}_\infty$ performance bound is used to guarantee stability of the closed-loop system under parameter variations. Meanwhile, a tight $\mathcal{H}_2$ performance bound is used to make the LPV controller robust to input disturbances. The selection of $\mathcal{H}_2$ and $\mathcal{H}_\infty$ performance weighting functions is an important design problem. The selection of $\mathcal{H}_\infty$ performance weighting functions can be done as described in [83] and [58]. However, the selection of $\mathcal{H}_2$ performance weighting functions is not covered in such detail. In [87], a systematic way is provided for iteratively tuning the output $\mathcal{H}_2$ weighting functions for robust control of LTI systems. Unfortunately,

no such iterative procedure exist yet for LPV systems.

The chapter is organized as follows. The family of linear models obtained from the series of bench identification tests are introduced in Section 5.2 and the LPV system is formulated. In Section 6.3, the LPV gain-scheduling controller design method is provided. The bench test set-up is discussed in Section 5.4.1. In Section 5.4.2, the obtained LPV gain-scheduling controller is operated on the test bench and compared to the baseline PI and OCC controllers used in [48]. Concluding remarks are given in the final section.

5.2 LPV System Modeling

To obtain a family of linear models, the closed-loop system identification outlined in [48] was performed at a series of fixed engine speeds N_e and oil pressures p. The open-loop transfer functions of the identified family of linear VVT systems sampled at 5 ms are given by

$$\begin{aligned} G(N_e, p = 310\,\text{kPa}\,(45\text{ psi})) &= \frac{\Psi(N_e, p)\,(0.0859q - 0.0609)}{q^2 - 1.9547q + 0.9553}, \\ G(N_e, p = 414\,\text{kPa}\,(60\text{ psi})) &= \frac{\Psi(N_e, p)\,(0.0615q - 0.0364)}{q^2 - 1.9547q + 0.9553} \end{aligned} \tag{5.1}$$

where $\Psi(N_e, p)$ is the gain at a specific engine speed N_e and oil pressure p as given in Table 5.1 and q is the *forward shift operator* that satisfies $qu(k) = u(k+1)$.

By inspection of the identified transfer functions in (5.1), the LPV model for the VVT system is given by

$$G(\alpha_k, \beta_k) = \frac{\alpha_k q + \beta_k}{q^2 - 1.9547q + 0.9553} \tag{5.2}$$

where α_k and β_k are used as the time-varying parameters. For notational simplicity, α_k and β_k will be used to denote the parameters at time k, such that $\alpha_k = \alpha(k)$ and $\beta_k = \beta(k)$.

Table 5.1: Identified Gain $\Psi(N_e, p)$

Pressure, p	Engine Speed, N_e (rpm)	Gain $\Psi(N_e, p)$
310 kPa (45 psi)	900	0.70
	1500	0.72
	1800	0.68
414 kPa (60 psi)	900	0.95
	1500	0.98
	1800	0.93

Table 5.2: Time-varying parameters (scheduling parameters).

$\alpha(N_e(t), p(t)) \in [0.0571, 0.0618]$
$\beta(N_e(t), p(t)) \in [-0.0438, -0.0339]$

The values of α_k and β_k are found for a specific value of engine speed N_e and oil pressure p by multiplying the appropriate Ψ value found in Table 5.1 with the appropriate transfer function in 5.1. The range of values that α_k and β_k can take are given in Table 6.1.

Using the transfer function in (5.2), a state-space representation of the VVT system is found to be

$$\begin{aligned} x_G(k+1) &= \underbrace{\begin{bmatrix} 0 & -0.9553 \\ 1 & 1.9547 \end{bmatrix}}_{A_G} x_G(k) + \underbrace{\begin{bmatrix} \beta_k \\ \alpha_k \end{bmatrix}}_{B_G} u_G(k), \\ y(k) &= \underbrace{\begin{bmatrix} 0 & 1 \end{bmatrix}}_{C_G} x_G(k). \end{aligned} \tag{5.3}$$

For convenience, the compact notation $\Theta = [\alpha_k, \beta_k]$ will be used to denote the scheduling variables for the remainder of the chapter.

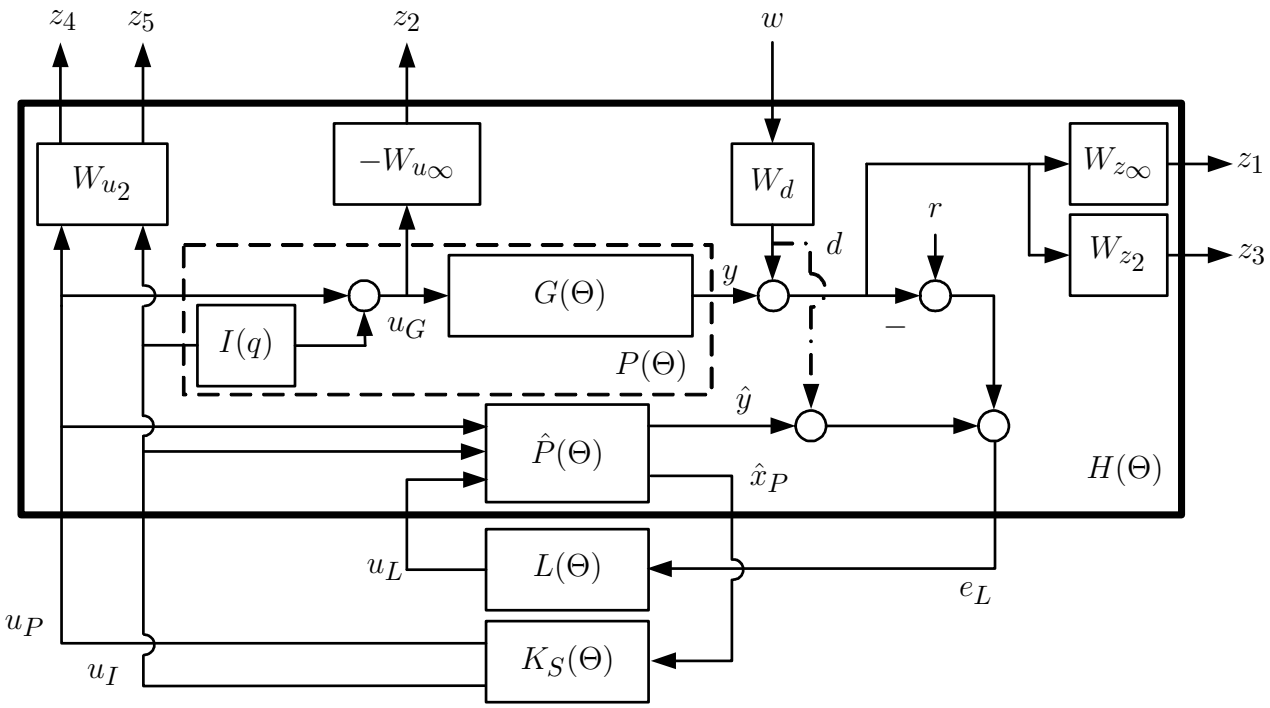

Figure 5.2: Proposed control architecture for the VVT system

5.3 LPV Gain Scheduling Controller Design

5.3.1 Control Strategy

The objective of the control system is to regulate the cam phase y to a reference phase r using feedback control against the disturbance signal d and the time-varying parameters α_k and β_k. In particular, we want to guarantee the stability of the closed-loop system and also minimize the effect of the disturbances for any conceivable engine speed and oil pressure variations. The proposed control architecture is illustrated in Fig. 6.2. This scheme has four components, that is a state observer $\hat{P}(\Theta)$, observer gains $L(\Theta)$, a state feedback controller $K_S(\Theta)$, and an integrator $I(q)$.

The multi-input, single-output LPV plant $P(\Theta)$, depicted inside of the dotted box in Fig. 6.2, is obtained by augmenting the VVT system $G(\Theta)$ with the forward Euler method,

discrete-time integrator $I(q) = t_s/(q-1)$, where t_s is the sample period of the discrete-time system in seconds. The integrator $I(q)$ introduces integral action into the system to ensure that the steady-state error between the measured cam phase y and the reference phase r can be eliminated. By allowing the input to the VVT plant $G(\Theta)$ to be equal to

$$u_G(k) = u_P(k) + \frac{t_s}{q-1}u_I(k),$$

as displayed in the dotted box of Fig. 6.2, one possible state-space representation of $P(\Theta)$ is found to be

$$\begin{aligned} x_P(k+1) &= \underbrace{\begin{bmatrix} 0 & -0.9553 & \sqrt{t_s}\beta_k \\ 1 & 1.9547 & \sqrt{t_s}\alpha_k \\ 0 & 0 & 1 \end{bmatrix}}_{A_P(\Theta)} x_P(k) + \underbrace{\begin{bmatrix} \beta_k & 0 \\ \alpha_k & 0 \\ 0 & \sqrt{t_s} \end{bmatrix}}_{B_P(\Theta)} \underbrace{\begin{bmatrix} u_P(k) \\ u_I(k) \end{bmatrix}}_{u_S(k)}, \\ y(k) &= \underbrace{\begin{bmatrix} 0 & 1 & 0 \end{bmatrix}}_{C_P} x_P(k). \end{aligned} \tag{5.4}$$

In (5.4), it is clear that the state matrix $A_P(\Theta)$ and the input matrix $B_P(\Theta)$ are both affected by the time-varying parameters α_k and β_k.

The state observer $\hat{P}(\Theta)$ is used to obtain the estimated states $\hat{x}_P$ of the plant. The observer $\hat{P}(\Theta)$ has the standard state-space representation

$$\begin{aligned} \hat{x}_P(k+1) &= A_P(\Theta)\hat{x}_P(k) + B_P(\Theta)u_S(k) + L(\Theta)e_L(k), \\ \hat{y}(k) &= C_P\hat{x}_P(k), \end{aligned}$$

where the error input to the plant observer is given by $e_L(k) = r(k) - (y(k) + d(k)) +$

$(\hat{y}(k)+d(k))$, which simplifies to $e_L(k) = r(k) - y(k) + \hat{y}(k)$. Since we are solving the S/KS mixed-sensitivity $\mathcal{H}_\infty$ optimization using the regulation form, during control synthesis we let the set point r equal zero as shown in [58], thus further simplifying the observer input error to $e_L(k) = -y(k) + \hat{y}(k)$. This satisfies the condition in [12] that the measurement for control is not corrupted by the exogenous input $w(k)$. Notice in Fig. 6.2 that the output disturbance $d(k)$ is connected to the estimated plant output $\hat{y}(k)$ by dash-dot lines. This is to signify that the exogenous input $d(k)$ is only available to the observer during control synthesis. However, during implementation since the output disturbance $d(k)$ cannot be measured it is not available to the observer.

To use mixed $\mathcal{H}_2/\mathcal{H}_\infty$ norms as the performance criteria for shaping the frequency response of the closed-loop system, weighting matrices (which can be considered control design parameters) are introduced in Fig. 6.2. Oftentimes, the weighting matrices are chosen as frequency dependent functions; however, for this problem static weighting matrices sufficed. The weighting matrix W_d was selected to model the signal d using the signal based approach discussed in [58]. The $\mathcal{H}_\infty$ performance weighting functions W_{z_∞} and W_{u_∞} were selected to limit the maximum magnitude of the sensitivity function $|S(j\omega)|$ and the controller multiplied by the sensitivity function $|KS(j\omega)|$ as discussed in [83]. In this study, the $\mathcal{H}_\infty$ performance weighting functions were selected primarily for LPV stability. However, the $\mathcal{H}_2$ performance weighting functions were selected for LPV performance. The weighting matrices W_{z_2} and W_{u_2} were selected using an iterative trial-and-error process. In the iterative process, W_{z_2} and W_{u_2} started out with values of unity. The control synthesis procedure outlined in Algorithm 1 was then carried out and the sensitivity function was computed and examined. The values used in the weighting function W_{u_2} were then increased and the control synthesis was carried out again and the sensitivity function was examined again. This procedure

was executed until desirable characteristics were displayed in the frequency response of the controller, the sensitivity function, and the controller multiplied by the sensitivity function. The resulting weighting matrices are as follows:

$$W_d = 0.01, \quad W_r = 1, \quad W_{u_\infty} = 10,$$
$$W_{u_2} = \begin{bmatrix} 15 & 0 \\ 0 & 15 \end{bmatrix}, \quad W_{z_\infty} = 1, \quad \text{and} \quad W_{z_2} = 1.$$

These weighting matrices where tuned to obtain the frequency responses plotted with the bold lines in Fig. 5.3. For comparison, a full-order dynamic output covariance constraint (OCC) controller (dashed lines) [52] was used. This controller is known to work well on the VVT cam phaser test bench at the fixed operational condition of 1500 rpm and 414 kPa (60 psi) oil pressure, so it was deemed an appropriate starting point.

In Fig. 5.3, the frequency responses of the LPV controller and the OCC controller are displayed at the corner points of the parameter space polytope (i.e. $[\underline{\alpha}, \underline{\beta}]$, $[\underline{\alpha}, \overline{\beta}]$, $[\overline{\alpha}, \underline{\beta}]$, $[\overline{\alpha}, \overline{\beta}]$, where $\underline{\alpha} = \alpha_{\min}$ and $\overline{\alpha} = \alpha_{\max}$). In Fig. 5.3A, the frequency response of each controller is displayed. At low frequencies, each controller has high gain due to the integral action built into each controller. In Fig. 5.3B, the sensitivity function of each controller is displayed. In a typical feedback system, the sensitivity function is linked to the tracking error performance [83]. At low frequencies, each controller's sensitivity function is small, which minimizes tracking error and maximizes disturbance rejection. Fig. 5.3C displays the frequency response of the controller multiplied by the sensitivity function for each controller. This plot shows that over the frequency range of 1Hz-20Hz the mixed $\mathcal{H}_2/\mathcal{H}_\infty$ dynamic LPV controller has lower control effort than the full-order dynamic OCC controller. Since

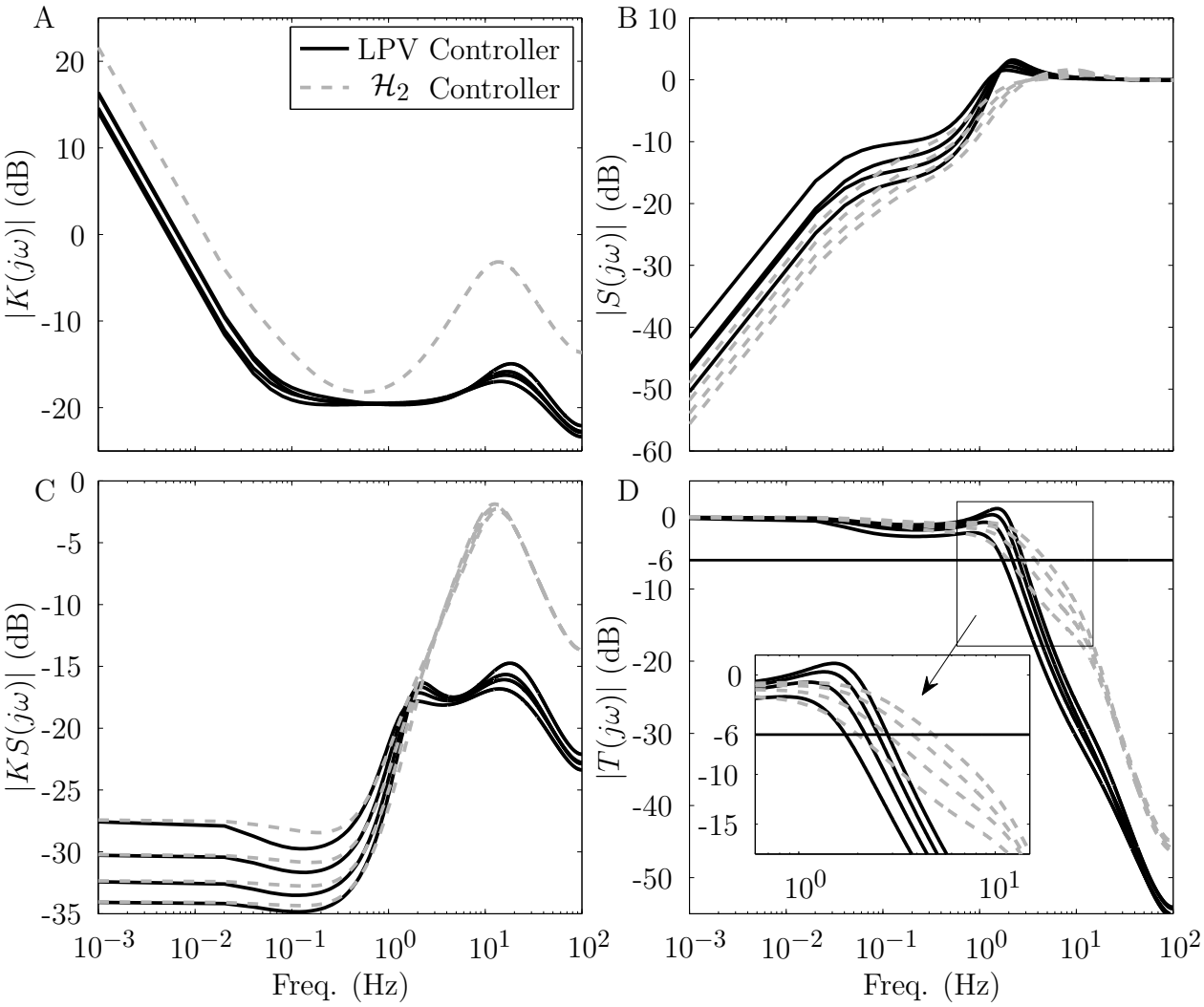

Figure 5.3: Frequency response comparison of the mixed $\mathcal{H}_2/\mathcal{H}_\infty$ dynamic LPV controller with an OCC ($\mathcal{H}_2$) controller [52] at the corner points of the parameter space polytope.

this is the frequency range over which the output disturbance $d(k)$ is generally active, it means that the mixed $\mathcal{H}_2/\mathcal{H}_\infty$ dynamic LPV controller should be robust to the disturbance $d(k)$. The frequency response of the closed-loop transfer functions with the mixed $\mathcal{H}_2/\mathcal{H}_\infty$ dynamic LPV controller and the OCC controller are displayed in Fig. 5.3D. The benefit of the mixed $\mathcal{H}_2/\mathcal{H}_\infty$ dynamic LPV controller can be seen in the close-up view in Fig. 5.3D. At -6 dB, the closed-loop bandwidth with the OCC controller varies between approximately 2 to 4.8 Hz. However, the closed-loop bandwidth with the LPV controller only varies between

approximately 1.8 to 2.9 Hz, which is a reduction in span of about 60%.

As displayed in Fig. 6.2, the state feedback gains $K_S(\Theta)$ and the observer gains $L(\Theta)$ are placed outside of the solid, bold box. This designates that the control synthesis in Algorithm 1 is performed on only the items inside of the box. By isolating the static gains $K_S(\Theta)$ and $L(\Theta)$, the design of the observer-based dynamic controller is transformed into the design of a single static controller $K(\Theta)$ by using the following structure:

$$\underbrace{\begin{bmatrix} u_S(k) \\ u_L(k) \end{bmatrix}}_{u(k)} = \underbrace{\begin{bmatrix} K_S(\Theta) & 0 \\ 0 & L(\Theta) \end{bmatrix}}_{K(\Theta)} \underbrace{\begin{bmatrix} \hat{x}_P(k) \\ e_L(k) \end{bmatrix}}_{e(k)} \tag{5.5}$$

where $\hat{x}_p \in \mathbb{R}^3$, $e_L \in \mathbb{R}$, $u_S \in \mathbb{R}^2$, and $u_L \in \mathbb{R}^3$.

5.3.2 Generalized Plant

As shown in Fig. 6.2, the state feedback controller $K_S(\Theta)$ and observer gains $L(\Theta)$ are designed for the generalized LPV plant $H(\Theta)$. The generalized LPV plant $H(\Theta)$ is composed by the multi-input, single-output LPV plant $P(\Theta)$ and its corresponding state observer $\hat{P}(\Theta)$, along with the static weighting matrices W_d, W_{u_∞}, W_{u_2}, W_{z_∞} and W_{z_2}. The state-space realization of the generalized plant $H(\Theta)$ is found by combining the state-space realizations

of $P(\Theta)$ and $\hat{P}(\Theta)$ and performing the connections in Fig. 6.2 to obtain

$$\underbrace{\begin{bmatrix} x_P(k+1) \\ \hat{x}_P(k+1) \end{bmatrix}}_{x(k+1)} = \underbrace{\begin{bmatrix} A_P(\Theta) & 0 \\ 0 & A_P(\Theta) \end{bmatrix}}_{\hat{A}(\Theta)} \underbrace{\begin{bmatrix} x_P(k) \\ \hat{x}_P(k) \end{bmatrix}}_{x(k)} + \underbrace{\begin{bmatrix} B_P(\Theta) & 0 \\ B_P(\Theta) & I \end{bmatrix}}_{\hat{B}(\Theta)} \underbrace{\begin{bmatrix} u_S(k) \\ u_L(k) \end{bmatrix}}_{u(k)} \tag{5.6}$$

$$z(k) = C_z x(k) + D_w w(k) + D_u u(k)$$

$$e(k) = C_e x(k)$$

where $x(k) \in \mathbb{R}^n$ is the state at time k, $w(k) \in \mathbb{R}^r$ is the unweighted exogenous input, $u(k) \in \mathbb{R}^m$ is the control input, $z(k) \in \mathbb{R}^p$ is the performance output, and $e(k) \in \mathbb{R}^q$ is the measurement for control. The state matrix $A_P(\Theta)$ and the input matrix $B_P(\Theta)$ are both given in (5.4) and the other state-space matrices are given by

$$C_z = \begin{bmatrix} 0 & 1 & 0 & 0 & 0 & 0 \\ 0 & 0 & -10\sqrt{t_s} & 0 & 0 & 0 \\ 0 & 1 & 0 & 0 & 0 & 0 \\ 0 & 0 & 0 & 0 & 0 & 0 \\ 0 & 0 & 0 & 0 & 0 & 0 \end{bmatrix}, \quad D_w = \begin{bmatrix} 1 \\ 0 \\ 1 \\ 0 \\ 0 \end{bmatrix},$$

$$D_u = \begin{bmatrix} 0 & 0 & 0 & 0 & 0 \\ -10 & 0 & 0 & 0 & 0 \\ 0 & 0 & 0 & 0 & 0 \\ 15 & 0 & 0 & 0 & 0 \\ 0 & 15 & 0 & 0 & 0 \end{bmatrix}, \quad C_e = \begin{bmatrix} 0 & 0 & 0 & 1 & 0 & 0 \\ 0 & 0 & 0 & 0 & 1 & 0 \\ 0 & 0 & 0 & 0 & 0 & 1 \\ 0 & -1 & 0 & 0 & 1 & 0 \end{bmatrix}.$$

5.3.3 A gain-scheduling control synthesis problem

Now that the state-space representation of the generalized plant $H(\Theta)$ has been obtained, the mixed $\mathcal{H}_2/\mathcal{H}_\infty$ gain-scheduling controller $K(\Theta)$ must be synthesized. The $\mathcal{H}_\infty$-norm from $w(k)$ to $\mathcal{Z}_\infty = [z_1,\, z_2]^\mathsf{T}$ of the LPV system $H(\Theta)$ in (5.6) with the gain-scheduling controller is defined as

$$\|H(\Theta)\|_\infty = \sup_{\Theta\in\mathsf{\Theta},\|w\|_{\ell_2}\neq 0} \frac{\|\mathcal{Z}_\infty\|_{\ell_2}}{\|w\|_{\ell_2}}. \tag{5.7}$$

The $\mathcal{H}_2$-norm from $w(k)$ to $\mathcal{Z}_2 = [z_3(k),\, z_4(k),\, z_5(k)]^\mathsf{T}$ of the LPV system $H(\Theta)$ with the gain-scheduling controller is defined as

$$\|H(\Theta)\|_2^2 = \lim_{T\to\infty} \sup \mathcal{E}\left\{\frac{1}{T}\sum_{k=0}^{T} \mathcal{Z}_2\mathcal{Z}_2^\mathsf{T}\right\}, \tag{5.8}$$

where $\mathcal{E}$ denotes the expectation operator and the positive integer T denotes the time horizon. Now we formally state the gain-scheduling control design problem.

Problem : The goal is to design a static gain-scheduling control $u(k) = K(\Theta)e(k)$ that stabilizes the closed-loop system and minimizes the worst-case $\mathcal{H}_\infty$ and $\mathcal{H}_2$ norms of the closed-loop LPV system in (5.7) and (5.8) for any trajectories of $\Theta(k) \in \mathsf{\Theta}$.

The gain-scheduling method provided by [12] was derived for discrete-time polytopic time-varying systems. Therefore, in the next section, the state-space representation of $H(\Theta)$ in (5.6) will be transformed into a polytopic time-varying system so that the controller $K(\Theta)$ can be synthesized.

5.3.4 Polytopic linear time-varying system

The state-space representation of the generalized plant $H(\Theta)$ in (5.6) can be converted into a discrete-time polytopic time-varying system by solving the state matrix $\hat{A}(\Theta)$ and the input matrix $\hat{B}(\Theta)$ at the vertices of the parameter space polytope, e.g. the state matrix at vertice $\mathcal{V}_2$ is given by $A_2 = \hat{A}(\Theta = [\underline{\alpha}, \overline{\beta}])$. Any Θ inside of the convex parameter set is represented by a convex combination of the vertex systems as weighted by the vector $\lambda(k)$ of barycentric coordinates. Barycentric coordinates are used to specify the location of a point as the center of mass, or barycenter, of masses placed at the vertices of a simplex. A formula for computing the barycentric coordinates for any convex polytope is provided by [64]. The discrete-time polytopic time-varying system is given by

$$\begin{aligned} x(k+1) &= A(\lambda(k))x(k) + B_u(\lambda(k))u(k) \\ z(k) &= C_z x(k) + D_w w(k) + D_u u(k) \\ e(k) &= C_e x(k) \end{aligned} \tag{5.9}$$

where the state matrix $A(\lambda(k)) \in \mathbb{R}^{n\times n}$ and the input matrix $B(\lambda(k)) \in \mathbb{R}^{n\times m}$ belong to the polytope

$$\mathcal{D} = \left\{ (A, B_u)(\lambda(k)) : (A, B_u)(\lambda(k)) = \sum_{i=1}^{4} \lambda_i(k)(A, B_u)_i, \lambda(k) \in \Lambda \right\}, \tag{5.10}$$

and the other state-space matrices are the same as in (5.6). The state matrix $A(\lambda(k))$ and the input matrix $B_u(\lambda(k))$ are the weighted summation of the vertex matrices as weighted

by the vector $\lambda(k)$ of barycentric coordinates, i.e.

$$A(\lambda(k)) = \sum_{i=1}^{4} \lambda_i(k) A_i \quad \text{and} \quad B_u(\lambda(k)) = \sum_{i=1}^{4} \lambda_i(k) B_i$$

where A_i and B_i are the vertices of the polytope and $\lambda(k) \in \mathbb{R}^4$ is the barycentric coordinate vector which exists in the unit simplex

$$\Lambda = \left\{ \zeta \in \mathbb{R}^4 : \sum_{i=1}^{4} \zeta_i = 1, \zeta_i \geq 0, i = 1, \cdots, 4 \right\}. \tag{5.11}$$

For all $k \in \mathbb{Z}_{\geq 0}$, the rate of variation of the barycentric coordinates $\Delta\lambda_i(k) = \lambda_i(k+1) - \lambda_i(k)$, is limited such that $-b \leq \Delta\lambda_i(k) \leq b$, with $b \in [0, 1]$, which should be selected with the application in mind. If a worst-case set of parameter variation is known, then this bound can be calculated.

A finite set of LMIs in [12] can be used to design the $\mathcal{H}_2/\mathcal{H}_\infty$ gain-scheduling controller $K(\Theta)$ in (5.5). Due to Theorems 8 and 9 of [12], if there exists for $i = 1, \ldots, 4$, matrices $G_{i,K_s} \in \mathbb{R}^{3\times 3}$, $G_{i,L} \in \mathbb{R}^{(q-3)\times(q-3)}$, $Z_{i,K_s} \in \mathbb{R}^{(m-3)\times 3}$, and $Z_{i,L} \in \mathbb{R}^{3\times 1}$ assembled as

$$G_{i,1} = \begin{bmatrix} G_{i,K_s} & 0 \\ 0 & G_{i,L} \end{bmatrix} \quad \text{and} \quad Z_{i,1} = \begin{bmatrix} Z_{i,K_s} & 0 \\ 0 & Z_{i,L} \end{bmatrix}, \tag{5.12}$$

along with the other matrix variables defined in Theorems 8 and 9 of [12] satisfying the $\mathcal{H}_\infty$ LMIs and the $\mathcal{H}_2$ LMIs in [12], then the $\mathcal{H}_2/\mathcal{H}_\infty$ controller $K(\lambda(k))$ is given by

$$K(\lambda(k)) = \hat{Z}(\lambda(k))\hat{G}(\lambda(k))^{-1}, \tag{5.13}$$

with

$$\hat{Z}(\lambda(k)) = \sum_{i=1}^{4} \lambda_i(k) Z_{i,1} \quad \text{and} \quad \hat{G}(\lambda(k)) = \sum_{i=1}^{4} \lambda_i(k) G_{i,1}.$$

This control is proved to stabilize affine parameter-dependent systems such as (5.9) with a guaranteed $\mathcal{H}_2$ and $\mathcal{H}_\infty$ performance for all $\lambda \in \Lambda$ and $|\Delta\lambda| \leq b$. In this work, to ensure that all possible parameter variations would be covered, we selected $b = 0.4$. The LMI conditions of Theorems 8 and 9 of [12] are solved by programming them into MATLAB using the LMI parser YALMIP [34] and solved using SeDuMi [59]. During the solution process, the goal is to calculate the gain-scheduled feedback controller $K(\lambda(k))$ that minimizes the bound ν on the $\mathcal{H}_2$ performance from $w(k)$ to $[z_3,\ z_4,\ z_5]^\mathsf{T}$ under a prescribed bound η on the $\mathcal{H}_\infty$ norm from $w(k)$ to $[z_1,\ z_2]^\mathsf{T}$. The procedure for performing the mixed $\mathcal{H}_2/\mathcal{H}_\infty$ control synthesis is outlined in Algorithm 1.

Note that the minimum feasible $\mathcal{H}_\infty$ bound η_L can be solved for by using an iterative algorithm [58], such as the bisection algorithm.

The resulting LPV controller solved at an engine speed and oil pressure of $N_e = 1500$rpm and $p = 414$kPa (60 psi) (for comparison with the $\mathcal{H}_2$ output covariance controller) is found to be

$$K_{LPV}(q) = \frac{0.109255247q^3 - 0.302866405q^2 + 0.278279285q - 0.0846677044}{q^4 - 3.132121334q^3 + 3.625898107q^2 - 1.853079890q + 0.359303117}. \quad (5.14)$$

As stated previously, the robust $\mathcal{H}_2$ controller designed in [52] using the OCC control design algorithm presented in [87] is used for comparison with the LPV controller. The robust $\mathcal{H}_2$ OCC controller designed in [52] is given by

$$K_{OCC}(q) = \frac{0.3158302q^3 - 0.9301618q^2 + 0.9129406q - 0.2986088}{q^4 - 3.4051293q^3 + 4.3533113q^2 - 2.4909563q + 0.5427743}. \quad (5.15)$$

Algorithm 1 Mixed $\mathcal{H}_2/\mathcal{H}_\infty$ Gain-Scheduling Synthesis

Require: Polytopic LPV system in (5.9), rate of variation bound $b \in [0, 1]$, $\mathcal{H}_2$ and $\mathcal{H}_\infty$ input and output channels of (5.9), and a range of prescribed $\mathcal{H}_\infty$ bounds $\eta \in [\eta_L, \eta_U]$, where it is assumed that η_L is the minimum feasible $\mathcal{H}_\infty$ bound.

Ensure: The gain-scheduling controller matrices $G_{i,1}$ and $Z_{i,1}$ needed to compute $K(\lambda(k))$ in (5.13).

1: Determine selection matrices L_j and M_j for each performance specification j as in Section 5.3 of [12].
2: Compute H_j using selection matrices L_j and M_j for each performance specification j, for $j = 1, 2$.
3: Compute the vectors f^j and h^j using rate of variation bound b as shown in Appendix 11.3 of [12].
4: Using equation (28) of [12], convert the polytopic LPV system in (5.9) to the form used in the LMIs of Theorems 8 and 9 of [12].
5: **for** $\eta = \eta_L{:}\eta_U$ **do**
6: Initialize the matrix variables introduced in Theorems 8 and 9 of [12] as free matrix variables into MATLAB using the YALMIP interface [34].
7: Using G_{i,K_s}, $G_{i,L}$, Z_{i,K_s}, and $Z_{i,L}$, generate $G_{i,1}$ and $Z_{i,1}$ as shown in (5.12).
8: Using the YALMIP interface [34], program the $\mathcal{H}_\infty$ LMIs in Theorem 8 of [12] using prescribed bound η and the $\mathcal{H}_2$ LMIs in Theorem 9 of [12] into MATLAB.
9: Using an LMI solver, like SeDuMi [59], solve the system of LMIs with the objective of minimizing $\sum_{i=1}^{4} Tr\{W_i\}$, where W_i is a positive-definite $\mathcal{H}_2$ free matrix variable introduced in Theorem 9 of [12], thus minimizing the $\mathcal{H}_2$ norm.
10: **end for**
11: Select the solution that minimizes the $\mathcal{H}_2$ norm the most, yet still has an acceptable bound η on the $\mathcal{H}_\infty$ norm.

Figure 5.4: VVT phase actuator test bench

5.4 VVT System Test Bench

5.4.1 Bench Test Set-up

The closed-loop system identification outlined in Ref. [52] and the control design testing were conducted on the VVT test bench displayed in Fig. 5.4. A Ford 5.4L V8 engine head was modified and mounted on the test bench. The cylinder head has a single cam shaft with a VVT actuator for one exhaust and two intake valves. These valves introduce a cyclic torque disturbance to the cam shaft. The cam shaft is driven by an electrical motor (simulating the crankshaft) through a timing belt, see Fig. 5.5.

An encoder is installed on the motor shaft, which generates the crank angle signal with one degree resolution, along with a so-called gate signal (one pulse per revolution). A plate with five magnets adhered is mounted at the other side of the extended cam shaft. As displayed in Fig. 5.5, one magnet is placed on the edge of the plate and is used to synchronize

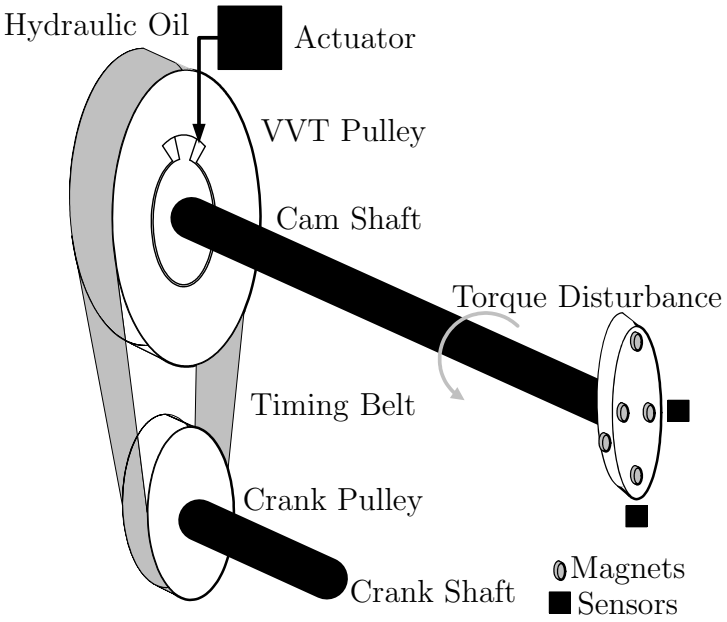

Figure 5.5: VVT phase actuator test bench diagram

the top dead center position of the combustion phase. The other four magnets on the face of the plate are used to determine the cam phase four times per engine cycle. The two squares in Fig. 5.5 represent hall-effect cam position sensors. As the cam shaft rotates, the magnets on the plate face pass the hall-effect cam position sensor used to to determine cam phase and the magnet on the edge of the plate passes the hall-effect cam position sensor used to determine top dead center position. Within an engine cycle, the cam position sensor generates four cam position pulses, which are sampled by an Opal-RT real-time controller. By comparing these pulse locations with respect to the encoder gate signal, the Opal-RT controller calculates the cam phase with one crank degree resolution.

The cam phase actuator system consists of a solenoid driver circuit, a solenoid actuator, and a hydraulic cam actuator. The solenoid actuator is controlled by a pulse-width modulation (PWM) signal, whose duty cycle is linearly proportional to the DC voltage command. An electrical oil pump was used to supply pressurized engine oil to be used for lubrication and as hydraulic actuating fluid for the cam phase actuator. The cam actuator command

voltage signal is generated by the Opal-RT prototype controller and sent to the solenoid driver. The PWM duty cycle is linearly proportional to input voltage with a maximum duty cycle 99% corresponding to 5 V and a minimal duty cycle of 1% corresponding to 0 V. The solenoid actuator controls the hydraulic fluid (engine oil) flow and changes the cam phase. The cam position sensor signal is sampled by the Open-RT prototype controller and the corresponding cam phase is calculated within the Opal-RT real-time controller.

A PI controller was tuned for the VVT system on the test bench for comparison purpose with the LPV and OCC controllers. The PI gains tuning process was completed at different engine speeds and oil pressures. The following tuned PI controller achieves good balance between response time and over-shoot oscillations at different conditions:

$$K_{PI}(q) = \frac{0.2q - 0.1995}{q - 1}. \tag{5.16}$$

5.4.2 Bench Test Results

The mixed $\mathcal{H}_2/\mathcal{H}_\infty$ observer-based dynamic LPV controller was tested on the VVT cam phaser bench at engine speeds of 900, 1200, 1500, and 1800 rpm for both engine oil pressures of 310 (45) and 414 kPa (60 psi). The step response of each controller is displayed in Fig. 5.6 for the cam advance (-20° to 0°) and the cam retard (0° to -20°) at an engine speed of 900 rpm and an oil pressure of 310 kPa (45 psi). In Fig. 5.6B, the control effort of both the LPV and $\mathcal{H}_2$ controllers is visibly lower than the PI controller. Also noticeable in Fig. 5.6B is that the control effort corrections produced by the LPV controller are smaller than those produced by the $\mathcal{H}_2$ controller. This was anticipated from frequency response plot of each controller in Fig. 5.3A. Since the LPV controller has lower gain than the $\mathcal{H}_2$ controller, it

is less sensitive to the change in error signal (which has the resolution of one crank degree in the experiment), which makes the LPV controller more robust to disturbances in the cam phase when compared to the $\mathcal{H}_2$ controller. This is even more noticeable during cam retard in Figs. 5.6C and 5.6D. The performance of the LPV controller in comparison with the $\mathcal{H}_2$ and PI controllers can also be shown by computing the control variance once the cam phase has reached steady state. During cam advance with an engine speed of 900 rpm and oil pressure of 310 kPa (45 psi), the control variances of the LPV, $\mathcal{H}_2$, and PI controllers were found to be 0.0048 V^2, 0.0265 V^2 and 0.0079 V^2, respectively. During cam retard at the same engine conditions, the control variances of the LPV, $\mathcal{H}_2$, and PI controllers were found to be 0.0063 V^2, 0.0281 V^2 and 0.0068 V^2, respectively. Similar values for the control variance for each controller were found at all other engine conditions tested as well. The control variances of the LPV controller under all engine conditions tested were found to be approximately anywhere from 6% to 33% of the control variance of the $\mathcal{H}_2$ controller.

In Fig. 5.7, the mean of the measured overshoot from ten test runs at each engine condition is plotted for each controller. It is easy to see from Fig. 5.7A and Fig. 5.7B, that in all cases both the $\mathcal{H}_2$ controller and LPV controller obtain lower overshoot than the PI controller, with the $\mathcal{H}_2$ controller displaying the lowest overshoot in most cases. However, during the cam retard situation displayed in Fig. 5.7B, the overshoot of the LPV controller is much closer to that of the $\mathcal{H}_2$ controller and is even smaller than the $\mathcal{H}_2$ controller at an engine speed of 1800 rpm. The difference in performance between cam advance and cam retard is attributed to the fact that the dynamics are slightly different. During cam advance, the actuating torque generated by the oil pressure overcomes the cam load torque causing the cam phase to advance. However, during cam retard, the oil trapped inside the actuator bleeds back to the oil reserve when the cam phase is pushed back by the cam load shaft.

This difference in dynamics between the cam advance and cam retard, as shown in Fig. 5.7A and Fig. 5.7B, generally results in lower overshoot and faster settling and rising times for the cam retard performance compared to the cam advance performance. Also, while the overshoot performance of all of the controllers in Fig. 5.7A and Fig. 5.7B is above 15%, none of the controllers include feedforward control. With feedforward control the overshoot would be significantly reduced.

In Figs. 5.8A and 5.8B the mean of the measured 5% settling time from ten test runs is displayed. It is observed that for nearly all cases the LPV controller settles quicker than the $\mathcal{H}_2$ controller, with one exception of when the engine is operated with an oil pressure of 310 kPa (45 psi) and at an engine speed of 1800 rpm. For the cam advance, the PI controller almost uniformly has the quickest settling time. However, as observed in Fig. 5.8B, during cam retard the settling time of the LPV controller is quicker than the PI controller in most cases, especially when the engine oil pressure is 414 kPa (60 psi).

The mean 10 to 90% rising time from the ten test runs is displayed in Figs. 5.9A and 5.9B. The rising time performance during cam advance is very similar for each of the controllers as displayed in Fig. 5.9A. However, as shown in Fig. 5.9B, during cam retard it is quite clear that the LPV and PI controllers are faster than the $\mathcal{H}_2$ controller by an unmistakable amount.

5.5 Conclusion

A dynamic gain-scheduling controller was designed by employing an observer-based state feedback design and static multi-objective $\mathcal{H}_2/\mathcal{H}_\infty$ controller synthesis. By examining the frequency response of the LPV controller and comparing it to a previously obtained ro-

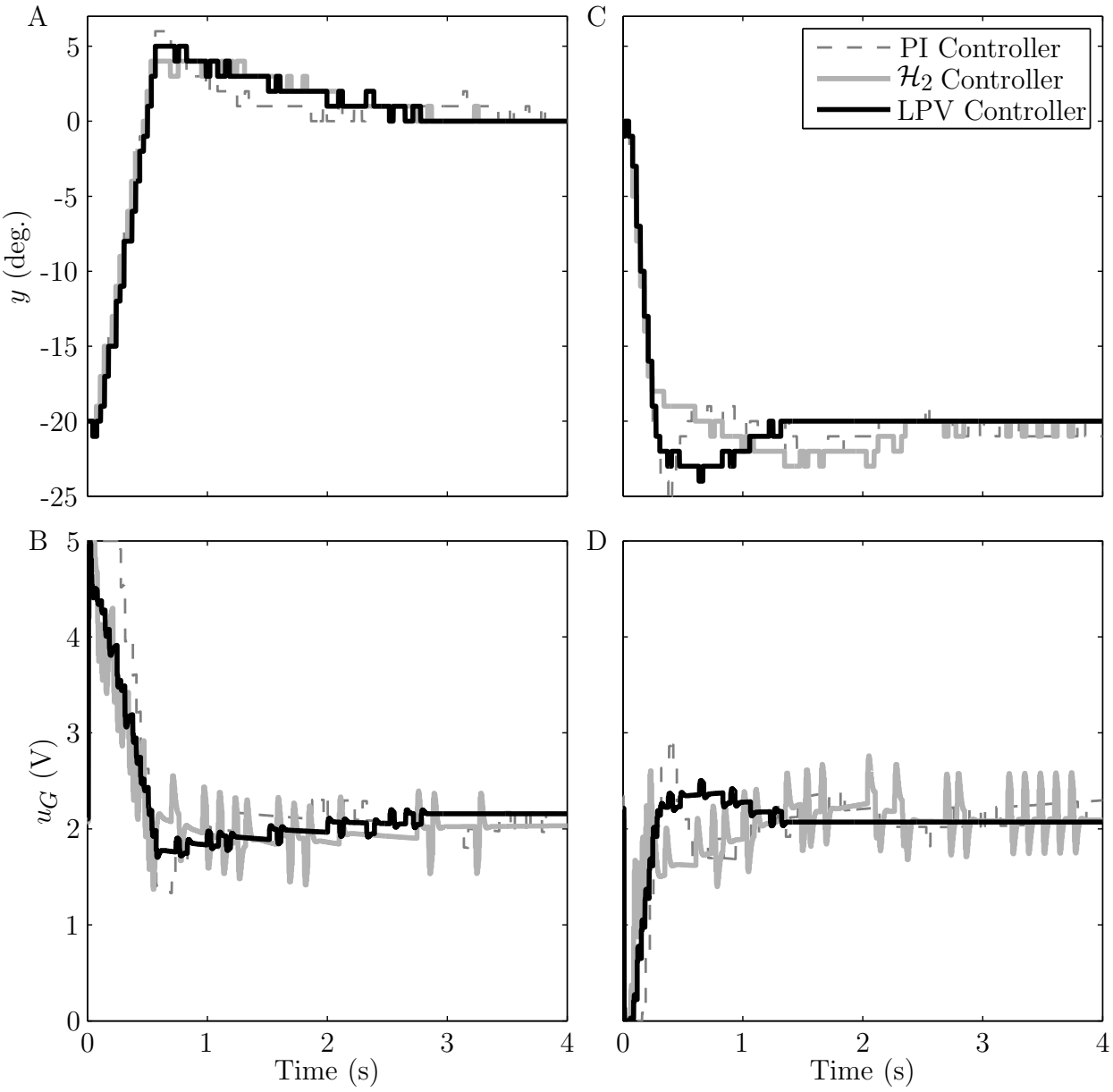

Figure 5.6: Cam advance response at 900rpm with 310kPa oil pressure.

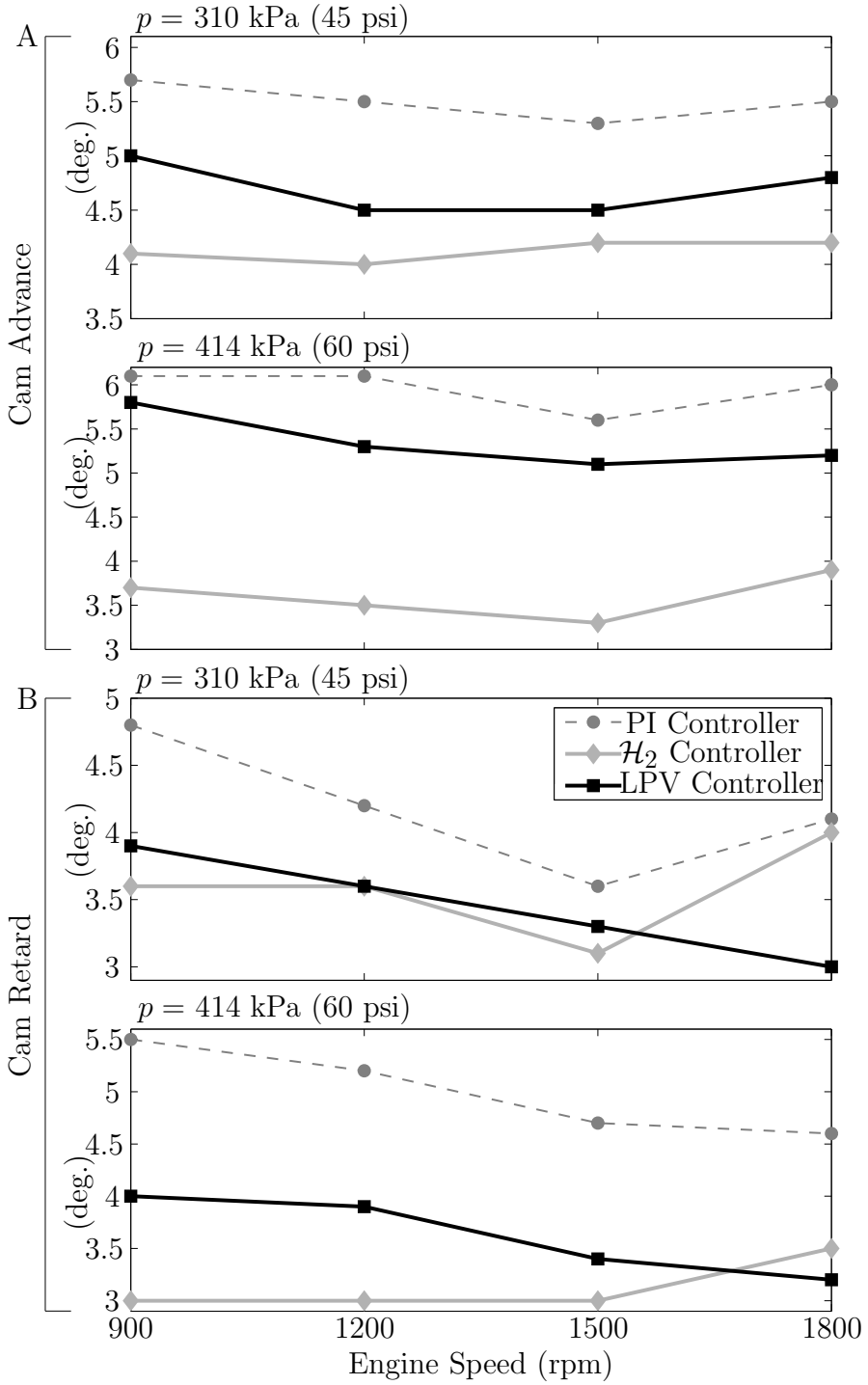

Figure 5.7: Mean overshoot for each controller operated at an oil pressure of 45 and 60 psi and engine speeds of 900, 1200, 1500, and 1800 rpm. Plot A displays the mean overshoot for cam advance and plot B displays the mean overshoot for cam retard.

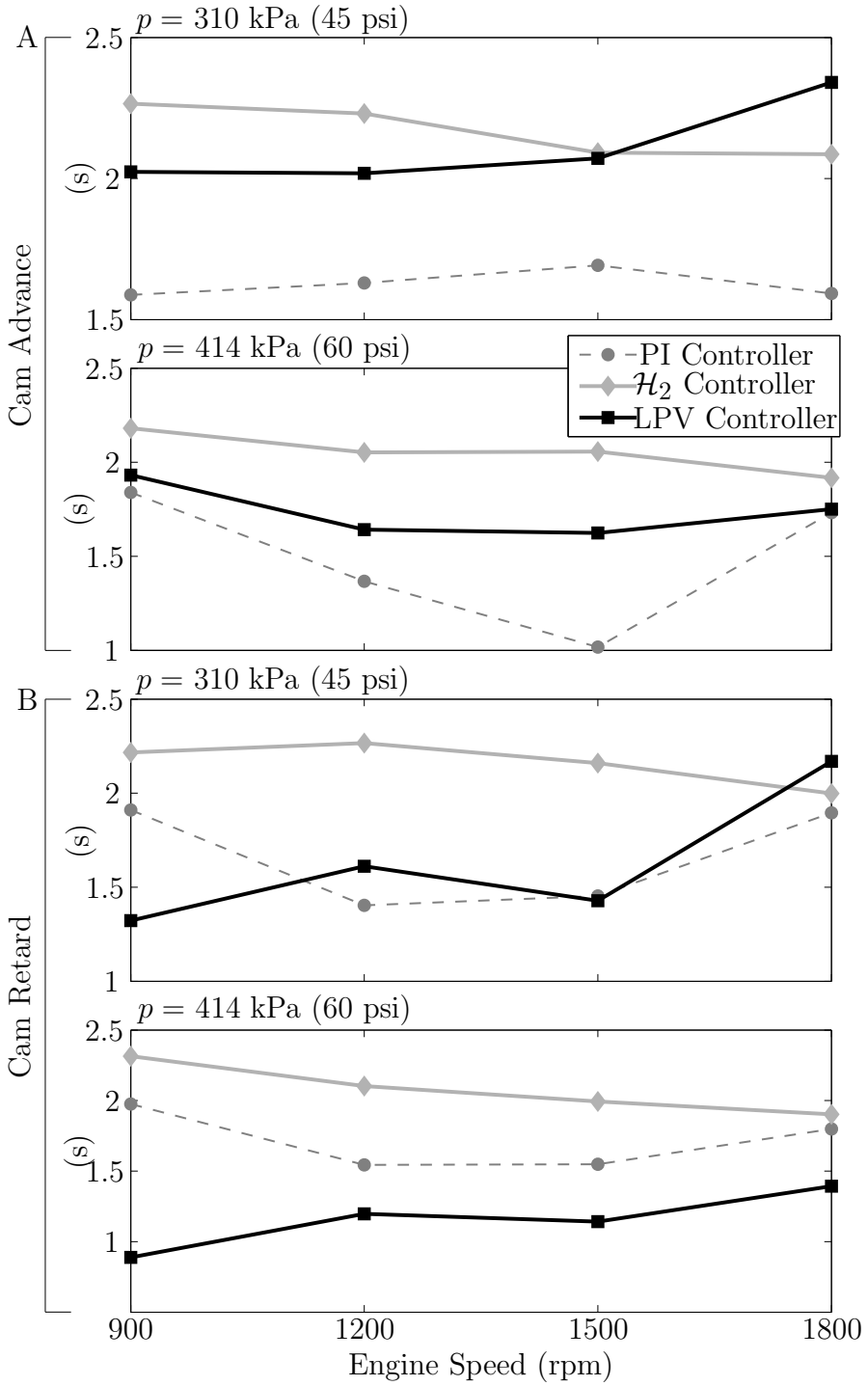

Figure 5.8: Mean 5% settling time for each controller operated at an oil pressure of 45 and 60 psi and engine speeds of 900, 1200, 1500, and 1800 rpm. Plot A displays the mean settling time for cam advance and plot B displays the mean settling time for cam retard.

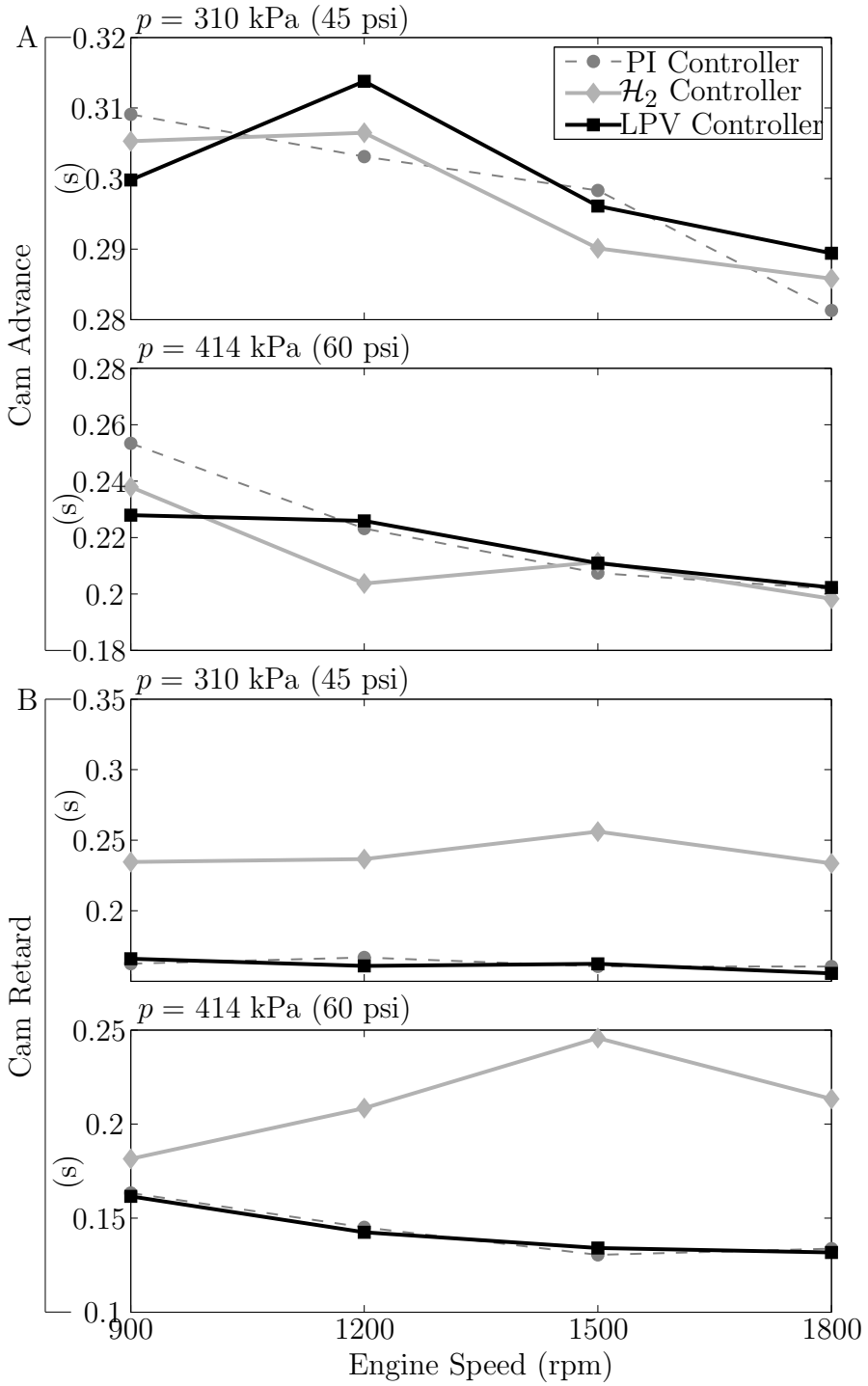

Figure 5.9: Mean 10 to 90% rising time for each controller operated at an oil pressure of 45 and 60 psi and engine speeds of 900, 1200, 1500, and 1800 rpm. Plot A displays the mean rising time for cam advance and plot B displays the mean rising time for cam retard.

bust $\mathcal{H}_2$ OCC controller, the LPV controller was found to reduce the operating bandwidth variation of the closed-loop system by approximately 60%. The frequency response of each system also demonstrated that the LPV controller had lower control effort over the crucial frequency range of 1-20 Hz. This was validated by the bench tests run with each controller, which showed that the LPV controller had much lower control variance than the robust $\mathcal{H}_2$ OCC controller. Also, the LPV controller has lower overshoot than the PI controller at all operating conditions with similar settling and response time characteristics. Additionally, the LPV controller was designed with a systematic approach while the PI controller was obtained through ad hoc testing.

Chapter 6

Dynamic, Output-Feedback, Gain-Scheduling Control of an Electric Variable Valve Timing System

6.1 Introduction

The fuel economy, emissions, and performance of an internal combustion (IC) engine are heavily influenced by the intake and exhaust valve timing. With a conventional valvetrain system, the intake and exhaust valve timing can only be optimized for a single operating condition. That is, the optimized valve timing can either improve fuel economy and reduce emissions at low engine speeds or maximize engine power and torque outputs at high engine speeds. Due to the growing fuel economy demands and emissions regulations, continuously variable valve timing (VVT) systems [37] were developed. The challenging problem of improving fuel economy and reducing emissions at low engine speed while maintaining engine performance at high engine speed can be addressed with the use of VVT systems.

To adjust the intake and exhaust timing, two of the most common cam phasing systems

are a hydraulic vane type cam phaser [37, 20] and an electric cam phaser [45, 63, 27, 50, 51]. The advantage of hydraulic VVT systems is that only minor changes are required to implement them on conventional valvetrain systems, which reduces the design and engineering effort. However, the performance of hydraulic VVT systems is significantly degraded at some engine operating conditions. For instance, during engine cold start before the engine oil is warmed up the hydraulic VVT system cannot be activated and must remain in the default position [27]. Also the response time of the electric VVT is significantly shorter than the hydraulic VVT, which makes it possible to be used for the mode transition control between spark-ignited and homogeneously charge compression ignition combustion [78]. The electric cam phaser studied in [50, 51] uses a planetary gear train driven by an electric motor operated with respect to the current engine speed to phase the camshaft. In [50, 51], an $\mathcal{H}_2$ controller is designed using the output covariance constraint (OCC) control design approach [87, 51]. Promising results were obtained, however, in [51] it is noted that the engine oil viscosity has a significant impact on the performance of the electric cam phaser. Thus in this chapter, the physics based model developed in [50, 51] will be reconsidered with a time-varying friction coefficient to account for the variation of the engine oil viscosity to obtain a linear parameter-varying (LPV) system. The obtained LPV system is then used to develop a gain-scheduled, dynamic, output-feedback controller.

The use of LPV modeling and control in automotive applications has received a great deal of attention. LPV modeling and control techniques have been applied to both diesel engines [65, 55] and gasoline spark-ignition engines [88, 82, 66, 69, 71]. In [65], LPV control techniques are applied to the air path of turbocharged diesel engines to control the transient exhaust gas fraction pumped into the cylinders to reduce nitrous oxide emissions. In [55], an LPV identification technique is applied to a nonlinear turbocharged diesel engine to

obtain an LPV model suitable for control synthesis. In [88], a continuous-time LPV model is developed considering only engine speed as a time-varying parameter. In [82], a large variable time delay is present in the air-fuel ratio control loop for a lean burn spark ignition engine. LPV control methods are used to compensate for the variable time delay. In [66] and [69], event-based gain-scheduling proportional-integral (PI) and proportional-integral-derivative (PID) controllers are developed using the wall-wetting parameters and engine speed as time-varying parameters. In [71], the techniques used in [66] and [69] were augmented to develop an observer-based dynamic LPV controller using the dynamics of the plant for a hydraulic VVT system. In this chapter, a dynamic, output-feedback gain-scheduling controller with a guaranteed ℓ_2 to ℓ_∞ gain is designed for the electric VVT system considered in [50, 51] by applying a controller synthesis technique that builds on the techniques provided in [13].

The conventional application of gain-scheduling control involves the calibration of controller gains in a field test for the best performance as functions of system operational conditions. However, in addition to the fact that this approach can be very expensive and time consuming the system stability and performance are not guaranteed for all time-varying parameters. The purpose of this chapter is to efficiently develop a dynamic, output-feedback gain-scheduling controller with guaranteed stability and performance over all time-varying parameters. The first step to accomplish this is to obtain a discrete-time LPV model of the electrical VVT system since the LPV control technique to be used is based in discrete time. As previously mentioned, the physics based model derived model developed in [50, 51] is considered with a time-varying friction coefficient to account for the variation of the engine oil viscosity. Since the model of the electric VVT system developed in [50, 51] is a continuous time model, the LPV model of the electrical VVT system must then be discretized. Then the discrete-time LPV system is converted to a polytopic system, which is an LPV system with

a polytopic dependency on a scheduling parameter that takes values in the unit-simplex, so that the guaranteed ℓ_2 to ℓ_∞ discrete-time LPV control synthesis can be performed to obtain the gain-scheduled controller matrices of the dynamic, output-feedback controller.

As stated previously, an ℓ_2 to ℓ_∞ gain control design is performed in this chapter. A controller with a guaranteed ℓ_2 to ℓ_∞ gain provides strict bounds on the regulated output while minimizing the control input. Compared to the $\mathcal{H}_\infty$ performance specification, also known as an ℓ_2 to ℓ_2 gain, used in many LPV gain-scheduled controllers which only guarantee that the root-mean-square gain from the exogenous input to the regulated output is bounded, a controller designed with a guaranteed ℓ_2 to ℓ_∞ gain provides hard constraints on the performance outputs for any exogenous input with bounded ℓ_2 energy. Thus controllers with an ℓ_2 to ℓ_∞ gain control design are very useful in applications where hard constraints on responses or actuator signals cannot be ignored, such as space telescope pointing [86] and machine tool control.

6.2 Plant dynamics

The electric VVT system studied in this chapter operates with two main components: an electric motor and a planetary gear set. The planetary gear set consists of an outer ring gear, a planet gear carrier with planet gears attached, and a sun gear. The ring gear acts as the VVT pulley, which is driven directly by the crankshaft through a timing belt at half crankshaft speed. The planet gear carrier is connected to electric motor output shaft. The planet gears engage the ring and sun gears. The camshaft is connected to the sun gear. The two inputs to the planetary gear system are the ring gear acting as the VVT pulley and the planet gear carrier which is driven by the electric motor. The output of the planetary

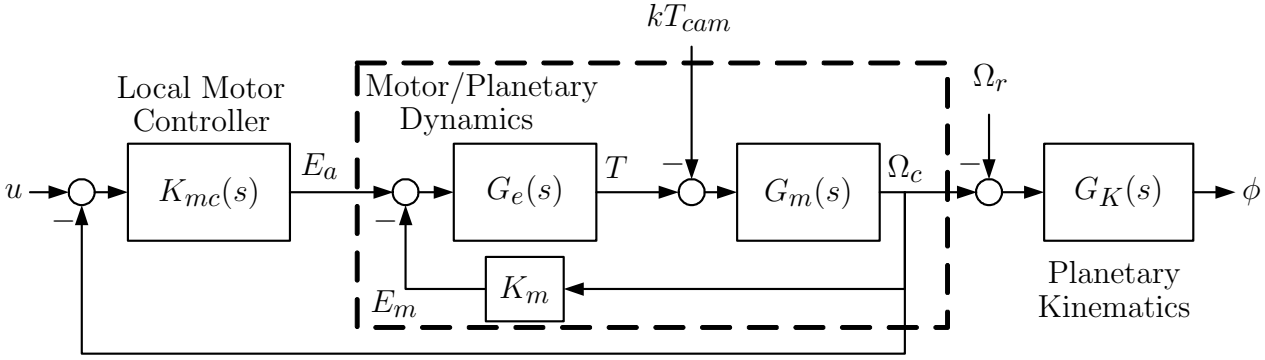

Figure 6.1: The block diagram of the electric motor with the planetary gear system.

gear system is the sun gear which connects directly to the camshaft. The modeling of the electric VVT system was performed in [50, 51]. In the following, an overview of the each of the transfer functions displayed in Fig. 6.1 is provided. The block diagram will be used to develop a state space model to be used for controller synthesis. As shown in Fig. 6.1, the electric VVT system has three main parts that contribute to the system dynamics: the local motor controller, the motor and planetary gear train dynamics, and the planetary gear train kinematics.

6.2.1 Local Motor Controller

The electric motor for the electric VVT system has a local PI controller such that it is operated by providing a desired rotational velocity. The transfer function of the local motor controller is

$$K_{mc}(s) = \frac{k_p s + k_i}{s} \tag{6.1}$$

where k_p and k_i are the proportional and integral gains. With the inputs and outputs displayed in Fig. 6.1, the following state-space equation can be found:

$$\begin{aligned} \dot{x}_{Kmc}(t) &= k_i \left(u(t) - \Omega_c(t)\right) \\ E_a(t) &= x_{Kmc}(t) + k_p \left(u(t) - \Omega_c(t)\right) \end{aligned} \tag{6.2}$$

where the state x_{Kmc} is the integrated error and the output E_a is the motor armature voltage.

6.2.2 Motor and Planetary Gear System Dynamics

The motor and and planetary gear train dynamics contained inside the dashed-line box in Fig. 6.1 are formed by the feedback connection of the transfer functions $G_e(s)$ and $G_m(s)$. The transfer function $G_e(s)$, which represents the input-output relationship from the voltage drop across armature circuit to the torque produced by the motor, is given by

$$G_e(s) = \frac{K_\tau}{L_m s + R_m} \tag{6.3}$$

where the armature resistance and inductance are R_m and L_m, respectively, and K_τ is the motor torque constant. Using the transfer function (6.3), the following state-space equation can be found:

$$\begin{aligned} \dot{x}_e(t) &= -\frac{R_m}{L_m} x_e(t) + \frac{1}{L_m} \left(E_a(t) - E_m(t)\right) \\ T(t) &= K_\tau x_e(t) \end{aligned} \tag{6.4}$$

where the state x_e is the current running through the armature circuit, E_m is the back-EMF voltage, and the output T is the torque produced by the motor.

The transfer function $G_m(s)$, which represents the input-output relationship from the torque acting on the load to the motor speed, is given by

$$G_m(s) = \frac{1}{Js + \beta(t)} \tag{6.5}$$

where J is the lumped inertia of the planetary gear system and the motor shaft and $B(t)$ is the time-varying friction coefficient, to which the oil viscosity is a major contributor. Using the transfer function (6.5), the following state-space equation can be found:

$$\begin{aligned} \dot{x}_m(t) &= -\frac{\beta(t)}{J} x_m(t) + \frac{1}{J}\left(T(t) - kT_{cam}(t)\right) \\ \Omega_c(t) &= x_m(t) \end{aligned} \tag{6.6}$$

where k, given by $k = 1 + 2n_r/n_s$, is the gear ratio from the planetary gear system that disturbance torque form the camshaft T_{cam} acts through and the state x_m is equal to the carrier angular velocity Ω_c.

6.2.3 Planetary Gear System Kinematics

The planetary gear train kinematics is the final part of the electric VVT model. The sun gear of the planetary gear system essentially integrates the difference between the planet carrier rotational velocity, Ω_c, and the ring gear rotational velocity, Ω_r, to obtain the phase for the camshaft. The transfer function G_K is given by

$$G_K(s) = \frac{2(n_r + n_s)}{n_s s} \tag{6.7}$$

where n_r and n_s are the number of teeth on the ring and run gears, respectively. With the transfer function (6.7), the following state-space can be found:

$$\begin{aligned} \dot{x}_K(t) &= \frac{2(n_s + n_r)}{n_s} (\Omega_c - \Omega_r) \\ \phi(t) &= x_K(t) \end{aligned} \tag{6.8}$$

where the state x_K is equal to the phase ϕ of the camshaft.

6.2.4 An LPV System

The state space equations can be gathered together to form the following state space model:

$$\begin{aligned} \dot{x}(t) &= A(\beta(t))x(t) + B_u u(t) + B_d T_{cam}(t) + B_r \Omega_r \\ \phi(t) &= Cx(t) \end{aligned} \tag{6.9}$$

where $x = [x_{K_{mc}}, x_e, x_m, x_K]^T$ and

$$A(\beta(t)) = \begin{bmatrix} 0 & 0 & -k_i & 0 \\ \frac{1}{L_m} & -\frac{R_m}{L_m} & -\frac{k_p + K_m}{L_m} & 0 \\ 0 & \frac{K_\tau}{J} & -\frac{\beta(t)}{J} & 0 \\ 0 & 0 & \frac{2(n_s + n_r)}{n_s} & 0 \end{bmatrix}, B_u = \begin{bmatrix} k_i \\ \frac{k_p}{L_m} \\ 0 \\ 0 \end{bmatrix}, \; B_d = \begin{bmatrix} 0 \\ 0 \\ -\frac{k}{J} \\ 0 \end{bmatrix},$$

$$B_r = \begin{bmatrix} 0 \\ 0 \\ 0 \\ -\frac{2(n_s + n_r)}{n_s} \end{bmatrix}, \; C = \begin{bmatrix} 0 & 0 & 0 & 1 \end{bmatrix}.$$

In order to apply the control synthesis in the next section, a discrete-time LPV system is required. In general, the discretization of the time-varying system (6.9) can be very difficult. However, the oil viscosity rate of variation is very slow compared to the sample rate t_s, such that they occur on different time scales. With this information, we can assume the friction coefficient β is constant during a given time step. As such, the following discrete-time system can be found:

$$\begin{aligned} x_d(k+1) &= A_d(\beta)x_d(k) + B_{u,d}(\beta)u(k) + B_{d,d}(\beta)T_{cam}(k) + B_{r,d}\Omega_r(k) \\ \phi(k) &= C_d x_d(k) \end{aligned} \tag{6.10}$$

where

$$\begin{aligned} A_d(\beta) &= \exp(A(\beta)t_s), \\ B_{u,d}(\beta) &= \left(\int_0^{t_s} \exp(A(\beta)\tau)d\tau\right) B_u, \\ B_{d,d}(\beta) &= \left(\int_0^{t_s} \exp(A(\beta)\tau)d\tau\right) B_d, \\ B_{r,d} &= \left(\int_0^{t_s} \exp(A(\beta)\tau)d\tau\right) B_r, \\ C_d &= C. \end{aligned} \tag{6.11}$$

This computation could be performed with the symbolic toolbox in MATLAB by letting β be a symbolic variable. Then, for each element in the system matrices that still contains the friction coefficient β, the 1^{st}-order Taylor series expansion can be performed as done in [66] to obtain the discrete-time LPV system. However, it was found that with the continuous-time system (6.9), this approach was found to be excessively time consuming. Instead, a much more efficient numerical approach based on the linear least squares technique [31] was used to obtain (6.10).

6.2.4.1 Linear least squares estimation of discrete-time LPV system

For any given fixed friction coefficient β, the discrete-time system can be easily computed to obtain the discrete-time state matrix

$$A_d(\beta) = \begin{bmatrix} a_{11}(\beta) & a_{12}(\beta) & a_{13}(\beta) & 0 \\ a_{21}(\beta) & a_{22}(\beta) & a_{23}(\beta) & 0 \\ a_{31}(\beta) & a_{32}(\beta) & a_{33}(\beta) & 0 \\ a_{41}(\beta) & a_{42}(\beta) & a_{43}(\beta) & 1 \end{bmatrix}, \tag{6.12}$$

and input matrices

$$B_{u,d}(\beta) = \begin{bmatrix} b_{u,1}(\beta) \\ b_{u,2}(\beta) \\ b_{u,3}(\beta) \\ b_{u,4}(\beta) \end{bmatrix}, \; B_{d,d}(\beta) = \begin{bmatrix} b_{d,1}(\beta) \\ b_{d,2}(\beta) \\ b_{d,3}(\beta) \\ b_{d,4}(\beta) \end{bmatrix}. \tag{6.13}$$

After computing each of these discrete-time matrices over a range of β values, it was noted that the parameter variation with respect to β appeared to be affine. With this information, the coefficients of $A_d(\beta)$, $B_{u,d}(\beta)$, and $B_{d,d}(\beta)$ were assumed to have the following form

$$\begin{aligned} a_{ij}(\beta) &= p_{ij}(\beta) + \epsilon, \\ b_{u,i}(\beta) &= p_{u,i}(\beta) + \epsilon, \\ b_{d,i}(\beta) &= p_{d,i}(\beta) + \epsilon, \end{aligned} \tag{6.14}$$

where ϵ is noise due to numerical error and model mismatch and p_{ij}, $p_{u,i}$, and $p_{d,i}$ are affine functions with respect to β such that

$$\begin{aligned} p_{ij}(\beta) &= \theta_{ij,0} + \theta_{ij,1}\beta, \\ p_{u,i}(\beta) &= \theta_{u_i,0} + \theta_{u_i,1}\beta, \\ p_{d,i}(\beta) &= \theta_{d_i,0} + \theta_{d_i,1}\beta. \end{aligned} \tag{6.15}$$

The unknown parameters $\theta_{ij,0}$, $\theta_{ij,1}$, $\theta_{u_i,0}$, $\theta_{u_i,1}$, $\theta_{d_i,0}$, and $\theta_{d_i,1}$ can be collected into the following unknown parameter vectors:

$$\Theta_{ij} = \begin{bmatrix} \theta_{ij,0} \\ \theta_{ij,1} \end{bmatrix}, \quad \Theta_{u,i} = \begin{bmatrix} \theta_{u_i,0} \\ \theta_{u_i,1} \end{bmatrix}, \quad \Theta_{d,i} = \begin{bmatrix} \theta_{d_i,0} \\ \theta_{d_i,1} \end{bmatrix} \tag{6.16}$$

such that (6.15) can be re-written with the following linear regression model:

$$\begin{aligned} p_{ij}(\beta) &= h(\beta)\Theta_{ij} \\ p_{u,i}(\beta) &= h(\beta)\Theta_{u,i} \\ p_{d,i}(\beta) &= h(\beta)\Theta_{d,i} \end{aligned} \tag{6.17}$$

where $h(\beta)$ is given by

$$h(\beta) = \begin{bmatrix} 1 & \beta \end{bmatrix}. \tag{6.18}$$

Thus, given M randomly selected values for the friction coefficient β, we would like to determine the linear least square estimates $\hat{\Theta}_{ij}$, $\hat{\Theta}_{u,i}$, and $\hat{\Theta}_{d,i}$ that minimize the following

residual sums of squares:

$$S(\Theta_{ij}) = \sum_{l=1}^{M} |a_{ij}(\beta_l) - h(\beta_l)\Theta_{ij}|^2, \tag{6.19}$$

$$S(\Theta_{u,i}) = \sum_{l=1}^{M} |b_{u,i}(\beta_l) - h(\beta_l)\Theta_{u,i}|^2, \tag{6.20}$$

$$S(\Theta_{d,i}) = \sum_{l=1}^{M} |b_{d,i}(\beta_l) - h(\beta_l)\Theta_{d,i}|^2, \tag{6.21}$$

where $|\cdot|$ denotes the magnitude operator on a complex number. If we let Y_{ij}, $Y_{u,i}$, and $Y_{d,i}$ be the collection of "measurements" and H be the collection of $h(\beta)$ for all M friction coefficients β such that

$$\begin{aligned} Y_{ij} &= \begin{bmatrix} a_{ij}(\beta_1) \\ \vdots \\ a_{ij}(\beta_M) \end{bmatrix}, \quad Y_{u,i} = \begin{bmatrix} b_{u,i}(\beta_1) \\ \vdots \\ b_{u,i}(\beta_M) \end{bmatrix}, \\ Y_{d,i} &= \begin{bmatrix} b_{d,i}(\beta_1) \\ \vdots \\ b_{d,i}(\beta_M) \end{bmatrix}, \quad \text{and} \quad H = \begin{bmatrix} h(\beta_1) \\ \vdots \\ h(\beta_M) \end{bmatrix}, \end{aligned} \tag{6.22}$$

then the residual sum of squares equations (6.19)-(6.20) can be re-written as

$$S(\Theta_{ij}) = \left(Y_{ij} - H\Theta_{ij}\right)^T \left(Y_{ij} - H\Theta_{ij}\right), \tag{6.23}$$

$$S(\Theta_{u,i}) = \left(Y_{u,i} - H\Theta_{u,i}\right)^T \left(Y_{u,i} - H\Theta_{u,i}\right), \tag{6.24}$$

$$S(\Theta_{d,i}) = \left(Y_{d,i} - H\Theta_{d,i}\right)^T \left(Y_{d,i} - H\Theta_{d,i}\right). \tag{6.25}$$

In [31], it is shown that the estimates that minimize each residual sum of squares are given

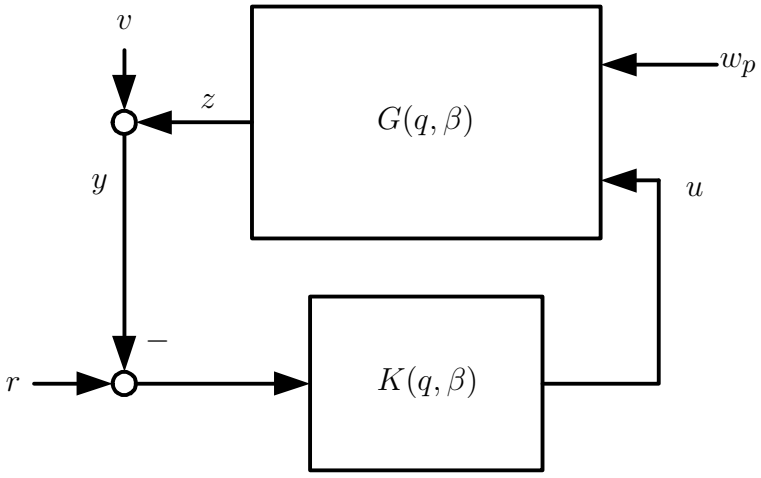

Figure 6.2: Proposed control scheme for the electrical VVT system.

by

$$\begin{aligned}\hat{\Theta}_{ij} &= \left(H^T H\right)^{-1} H^T Y_{ij},\\ \hat{\Theta}_{u,i} &= \left(H^T H\right)^{-1} H^T Y_{u,i},\\ \hat{\Theta}_{d,i} &= \left(H^T H\right)^{-1} H^T Y_{d,i}.\end{aligned} \tag{6.26}$$

By using this method, an approximate of the discrete-time LPV system (6.10) can be efficiently obtained by computing the discrete-time state-space matrices at a finite number of randomly selected friction coefficients β, and then by solving for the linear least square estimates as given by (6.26).

6.3 LPV gain-scheduling controller design

The objective of the control system is to regulate the cam phase to a reference phase using output feedback control against the disturbance signal w_p and the time-varying parameters. In particular, we want to guarantee the stability and performance of the closed-loop system for any finite energy disturbance and engine oil viscosity variations. The proposed control

architecture is illustrated in Fig. 6.2. This scheme has a single component, that being the dynamic, output-feedback, gain-scheduled controller, $K(q, \beta)$.

6.3.1 Guaranteed ℓ_2 to ℓ_∞ gain controller

The plant $G(q, \beta)$ in Fig. 6.2 can be represented as the following open-loop discrete-time polytopic LPV system

$$\begin{aligned} x_p(k+1) &= A_p(\lambda_k)x_p(k) + B_p(\lambda_k)u(k) + D_p(\lambda_k)w_p(k) \\ z_p(k) &= C_p(\lambda_k)x_p(k) \\ y(k) &= C_y(\lambda_k)x_p(k) + v(k) \end{aligned} \tag{6.27}$$

where $x_p(k)$ is the state, $u(k)$ is the control input, $w_p(k)$ is an exogenous ℓ_2 disturbance weighted by the positive definite symmetric matrix W_p, and $z_p(k)$ is the vector of all dynamic variables of interest, and $y(k)$ is the vector of measurements corrupted by the noise $v(k)$ weighted by the positive definite symmetric matrix V. The system matrices belong to a polytope similar to the one introduced in (2.11).

Suppose that we apply to the plant (6.27) a strictly proper, dynamic, output-feedback, stabilizing control law of the form

$$\begin{aligned} x_c(k+1) &= A_c(\lambda_k)x_c(k) + B_c(\lambda_k)y(k), \\ u(k) &= C_c(\lambda_k)x_c(k). \end{aligned} \tag{6.28}$$

Then the resulting closed-loop system is given by

$$\begin{aligned} x(k+1) &= \mathcal{A}(\lambda_k)x(k) + \mathcal{B}(\lambda_k)w(k), \\ z_p(k) &= \mathcal{C}_p(\lambda_k)x(k), \\ z_u(k) &= \mathcal{C}_u(\lambda_k)x(k), \end{aligned} \tag{6.29}$$

where $x = [x_p^T,\ x_c^T]^T$, $w = [w_p^T,\ v^T]^T$, $W = \text{block diag}[W_p, \quad V]$, and

$$\begin{aligned} \mathcal{A}(\lambda_k) &= \begin{bmatrix} A_p(\lambda_k) & B_p(\lambda_k)C_c(\lambda_k) \\ B_c(\lambda_k)C_y(\lambda_k) & A_c(\lambda_k) \end{bmatrix}, \\ \mathcal{B}(\lambda_k) &= \begin{bmatrix} D_p(\lambda_k)W_p^{1/2} & 0 \\ 0 & B_c(\lambda_k)V^{1/2} \end{bmatrix}, \\ \mathcal{C}_p(\lambda_k) &= \begin{bmatrix} C_p(\lambda_k) & 0 \end{bmatrix}, \\ \mathcal{C}_u(\lambda_k) &= \begin{bmatrix} 0 & D_u(\lambda_k)C_c(\lambda_k) \end{bmatrix}. \end{aligned} \tag{6.30}$$

Then, as shown in Chapter 3, a controller that minimizes the (weighted) control energy

$$Z_u(\lambda_k) = \text{trace}\left\{R\mathcal{C}_u(\lambda_k)\bar{\mathcal{P}}(\lambda_k)\mathcal{C}_u(\lambda_k)^T\right\},\ R > 0 \tag{6.31}$$

of the closed loop system, subject to an ℓ_2 to ℓ_∞ gain $\overline{Z}_p$ given by

$$\|z_p\|_\infty^2 \leq \overline{\sigma}\left(\overline{Z}_p\right)\|w\|_2^2. \tag{6.32}$$

where $Z_p(\lambda_k) = \mathcal{C}_p(\lambda_k)\bar{\mathcal{P}}(\lambda_k)\mathcal{C}_p(\lambda_k)^T \leq \overline{Z}_p$, can be efficiently solved for by a convex optimization with the LMI constraints given in Theorem 10.

6.3.2 $\mathcal{H}_\infty$ (ℓ_2 to ℓ_2 gain) Controller

For comparison with the guaranteed ℓ_2 to ℓ_∞ gain controller, an $\mathcal{H}_\infty$ controller is designed as well. The $\mathcal{H}_\infty$ controller differs from the ℓ_2 to ℓ_∞ gain controller in that it has the following property:

$$\|z\|_2 \leq \eta \|w\|_2 \tag{6.33}$$

where $z = [z_p^T,\ z_u^T]^T$. This is also known as the ℓ_2 to ℓ_2 gain, or root-mean-square gain. The main difference is the lack of the maximum singular value constraint. This is the reason why $\mathcal{H}_\infty$ controllers are not suitable when hard constraints cannot be ignored.

The $\mathcal{H}_\infty$ controller designed is also a strictly proper, dynamic, output-feedback controller and has the form given in (6.28). The $\mathcal{H}_\infty$ controller synthesis was carried out to minimize the $\mathcal{H}_\infty$ performance η with LMIs developed based on the work presented in [12] and [13].

6.4 Simulation Results

A simulation study was performed on the electrical VVT system to effectiveness of the guaranteed ℓ_2 to ℓ_∞ gain controller compared to the $\mathcal{H}_\infty$ controller. The parameter values used in this study for the electrical VVT system are displayed in Table 6.1. During the simulation, the engine speed was set to 1500 and the cam phase, ϕ, was stepped from 0° to 10° for 10 seconds and then back to 0°. The ℓ_2 disturbance in Fig. 6.3 was used as the cam load disturbance T_{cam}.

The guaranteed ℓ_2 to ℓ_∞ controller was designed with an ℓ_2 to ℓ_∞ gain given by

$$Z_p = 9.5434 \times 10^{-4}\,\text{rad}^2$$

Table 6.1: Electric VVT System Parameters

t_s	5 μs	K_τ	45 $\frac{\text{Nm}}{\text{A}}$
n_s	30 teeth	K_m	1/90 Vs
n_r	60 teeth	J	0.2 kgm^2
L_m	0.01 H	k_p	1 Vs
R_m	1 Ω	k_i	0.1 V

which is equivalent to a maximum displacement of 1.77° from the desired cam phase. The other control design parameters were chosen to be

$$W_p = 10, \quad V = 0.0012, \quad \text{and} \quad R = 1.$$

The parameters W_p, V, and R were also used to synthesize the $\mathcal{H}_\infty$ controller as well.

During the gain-scheduled controller design, it was assumed that the friction coefficient β varied between 0.5 and 2 , with the smaller friction coefficient corresponding to low oil viscosity (or oil that has been heated up) and the larger friction coefficient corresponding to high oil viscosity (oil that is cold or at room temperature). Since the oil viscosity varies slowly, simulations were performed at the following three friction coefficients: 2, 1, and 0.5, corresponding to the behavior that might occur when engine oil is heated up. The results of each simulation are displayed in Figs. 6.4-6.6.

In Figs. 6.4-6.6, the cam phase obtained when using the guaranteed ℓ_2 to ℓ_∞ gain controller is displayed by the solid black line, whereas the cam phase obtained when using the $\mathcal{H}_\infty$ controller is displayed by the solid grey line. The reference cam phase is displayed by a dashed line and can be seen in the close-up details of Figs. 6.4A-6.6A. The bound representing the maximum allowable displacement is displayed by a dash-dot line. Notice in

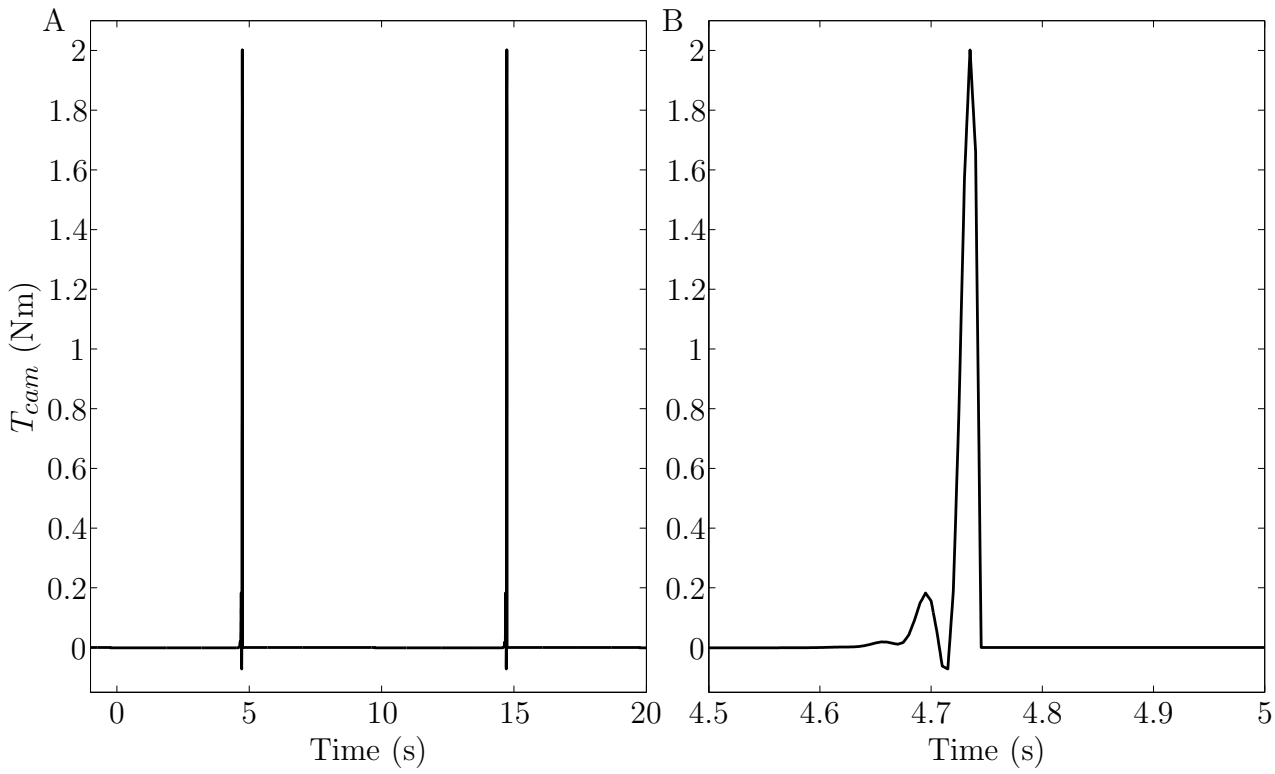

Figure 6.3: Cam load disturbance.

Figs. 6.4A-6.6A that the cam phase stays within the bounds when using the ℓ_2 to ℓ_∞ gain controller. However, for each friction coefficient value, the cam phase violates the bound when using the $\mathcal{H}_\infty$ controller.

The activation voltage of the electrical VVT motor is displayed in Figs. 6.4B-6.6B. A saturation of ± 14 was placed on the motor activation voltage during the simulation. As clearly displayed in Figs. 6.4B-6.6B, the ℓ_2 to ℓ_∞ controller uses large amounts of the activation voltage potential during the cam phase changes compared to the $\mathcal{H}_\infty$ controller, which is why it reaches the reference cam phase about 10 times faster than the $\mathcal{H}_\infty$ controller. Also during the cam load disturbance, as displayed in the details in Figs. 6.4B-6.6B, the ℓ_2 to ℓ_∞ gain controller uses ever so slightly more potential to ensure that the maximum displacement bound is not violated. Notice also, that as the friction coefficient gets smaller, the activation

voltage needed to hold the cam phase at the desired position decreases since the motor does not have to work against the oil as much with lower oil viscosities.

6.5 Conclusion

In this chapter, a discrete-time, LPV system representing the electric VVT system is developed with engine oil viscosity as the time-varying parameter. A gain-scheduled, dynamic, output-feedback controller is then designed such that the closed-loop system will have a guaranteed ℓ_2 to ℓ_∞ gain, which is very closely related to the physical performance constraints. For comparison, an $\mathcal{H}_\infty$ controller is also designed to demonstrate the benefit of guaranteed ℓ_2 to ℓ_∞ gain controllers. Simulation study results demonstrate the effectiveness of the proposed scheme.

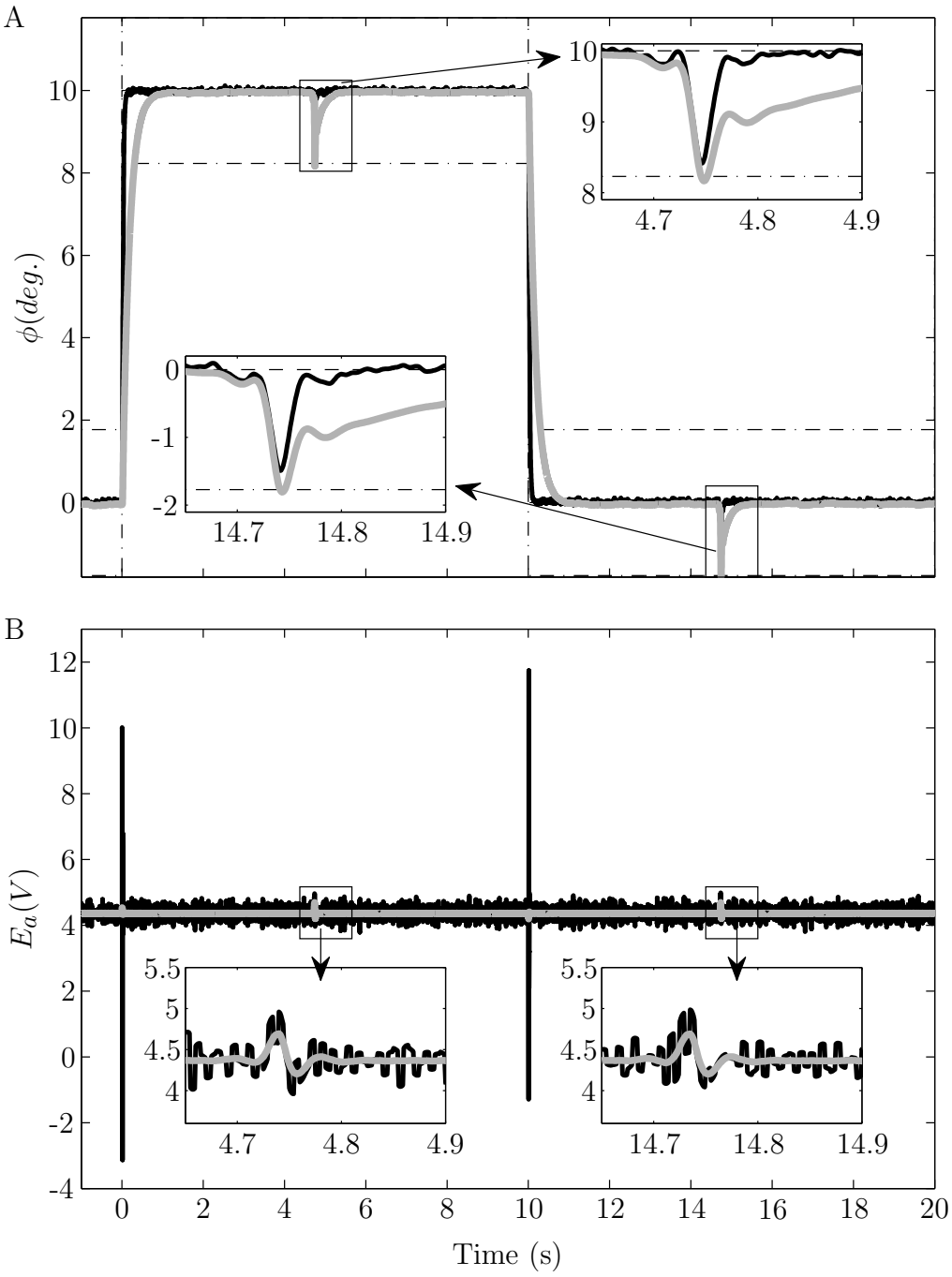

Figure 6.4: Electrical VVT simulation with $\beta = 2$.

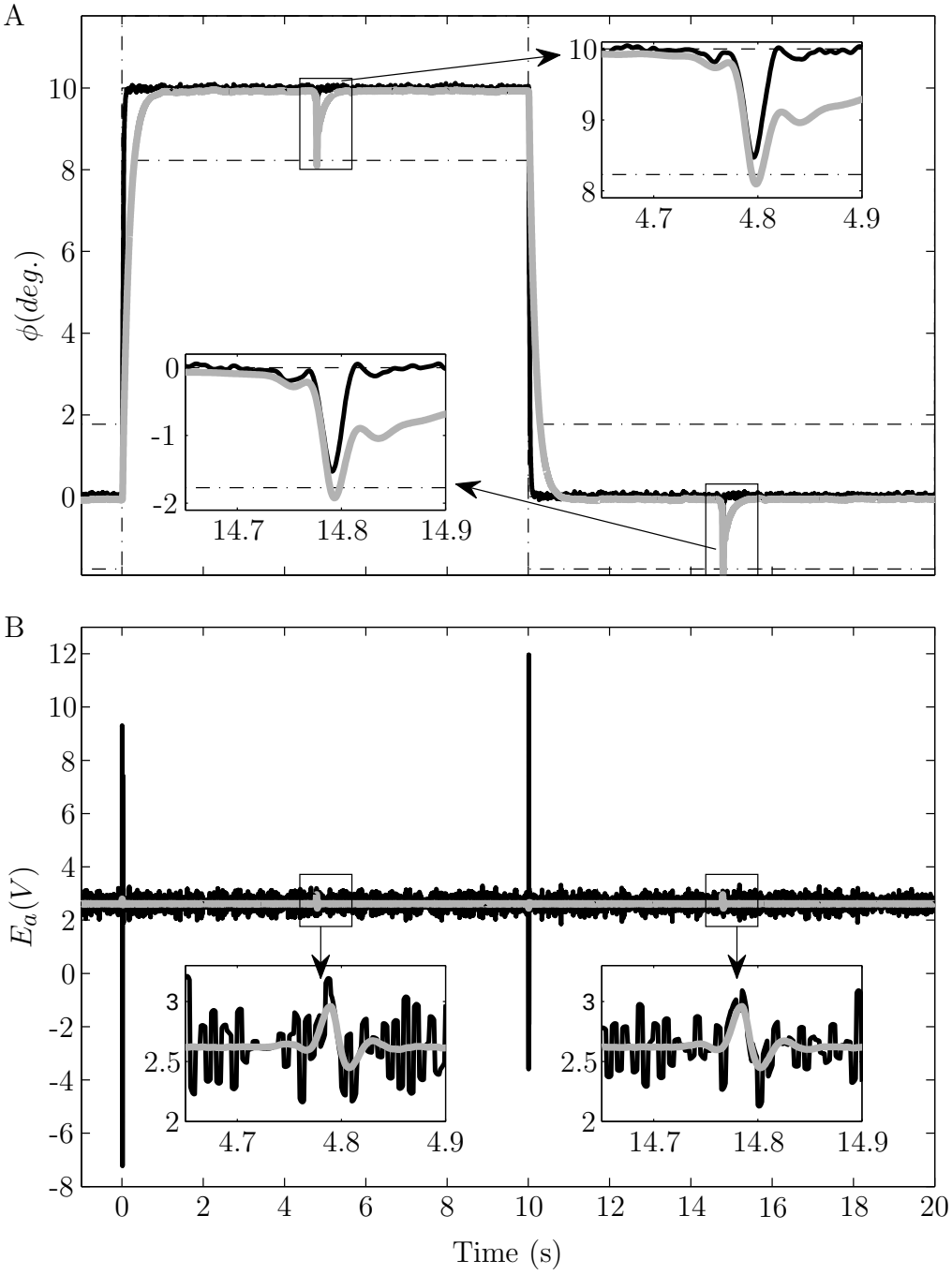

Figure 6.5: Electrical VVT simulation with $\beta = 1$.

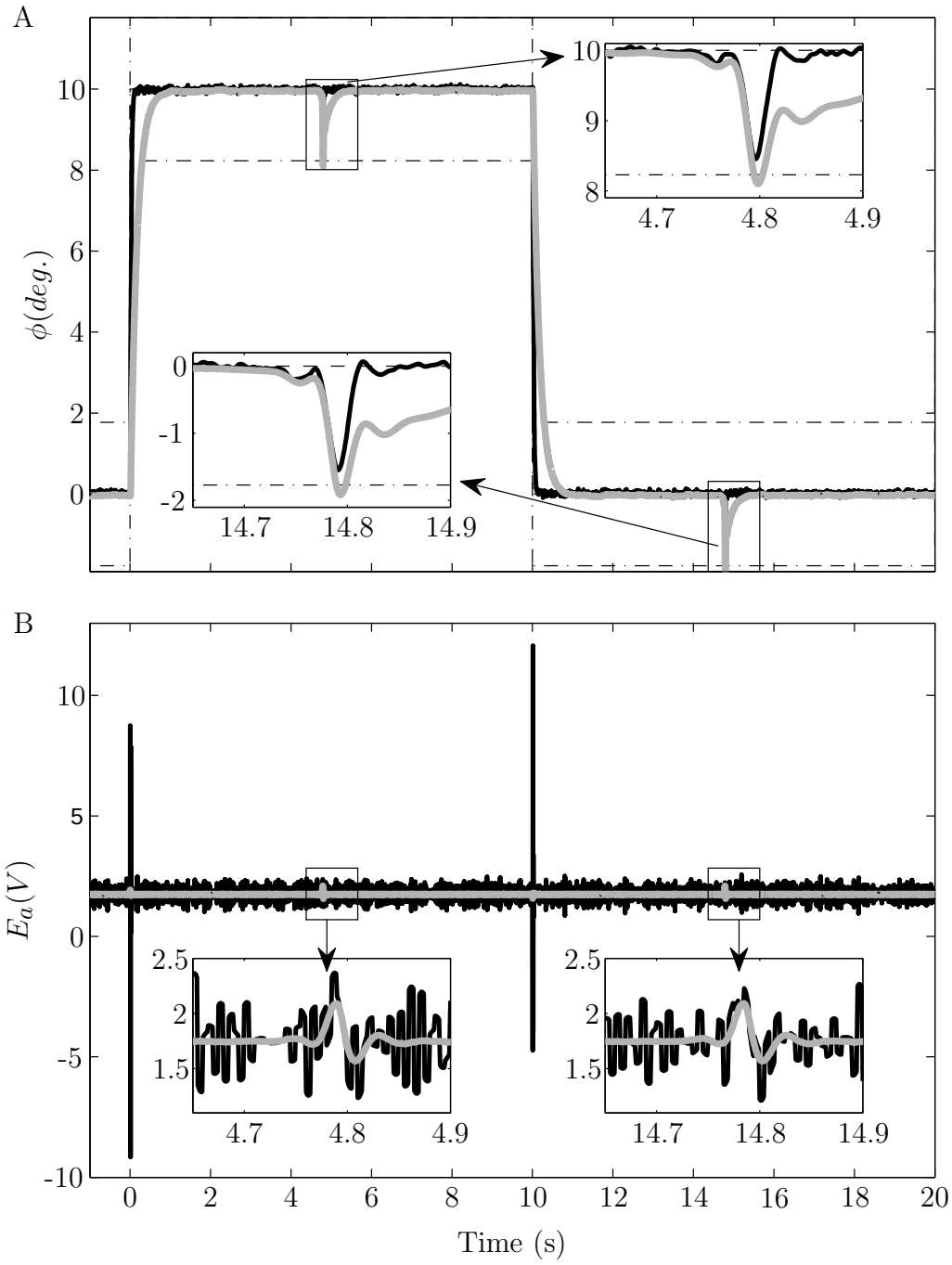

Figure 6.6: Electrical VVT simulation with $\beta = 0.5$.

Chapter 7

Conclusions and Future Research

7.1 Summary

In this dissertation, first the current LPV control theory methods were reviewed. Second, since the current LPV control theory was missing the ability to design LPV controllers with physically meaningful performance design constraints that could guarantee hard bounds, the current theory was extended to allow the use of $\ell_2 - \ell_\infty$ gain performance constraints. Controller synthesis LMIs are provided for the synthesis of state-feedback and dynamic output-feedback controllers with guaranteed $\ell_2 - \ell_\infty$ gain and $\mathcal{H}_\infty$ performance. To demonstrate the effectiveness of the controller synthesis LMIs provided a numerical design example is considered for both the state-feedback and dynamic output-feedback control designs.

Also included in this dissertation is the application of the current and newly developed LPV methods to engine control problems. In Chapter 4, gain-scheduling PI and PID controllers were developed for the air-to-fuel ratio control of port-fuel-injection processes with the wall-wetting parameter and engine speed as the time-varying parameters. Simulation and HIL simulation results demonstrate the successful application of current LPV control theory to obtain a gain-scheduling controller. The HIL simulation results also demonstrate the feasibility of implementing the obtained gain-scheduling controller on a hardware controller that could be used as an engine control module.

In Chapter 5, a dynamic output-feedback gain-scheduling controller was designed for a

hydraulic variable valve timing actuator. This was done by employing an observer-based state feedback design and static multi-objective $\mathcal{H}_2/\mathcal{H}_\infty$ controller synthesis. The LPV controller designed was compared with the robust $\mathcal{H}_2$ OCC controller and an ad-hoc PI controller designed in [52]. The LPV controller was found to have much lower control variance than the robust $\mathcal{H}_2$ OCC controller. Also, while the LPV controller is more complex than the PI controller in both concept and implementation, it has lower overshoot than the PI controller at all operating conditions with similar settling and response time characteristics. Additionally, the LPV controller was designed with a systematic approach while the PI controller was obtained through ad hoc testing.

The guaranteed $\ell_2 - \ell_\infty$ gain controller synthesis techniques provided in Chapter 3 are applied to the control of the electric variable valve timing actuator with engine oil viscosity as the time-varying parameter in Chapter 6. A gain-scheduled, dynamic, output-feedback controller is designed such that the closed-loop system will have a guaranteed ℓ_2 to ℓ_∞ gain. To demonstrate the benefit of guaranteed ℓ_2 to ℓ_∞ gain controllers, an $\mathcal{H}_\infty$ controller is also designed for comparison. The simulation study results demonstrate the effectiveness of the proposed scheme.

7.2 Specific Contributions

The contributions of this research to systematic gain-scheduling control are as follows:

1. The characterization of the ℓ_2 to ℓ_∞ gain performance constraint as an LMI constraint for discrete-time polytopic LPV systems [73].

2. Guaranteed ℓ_2 to ℓ_∞ controller synthesis LMIs for the state-feedback and dynamic output-feedback control of discrete-time polytopic LPV systems. These controllers

can provide hard constraints on system outputs when the exogenous input is modeled as a bounded ℓ_2 disturbance [73].

3. Chapter 4 is the first work to develop an air-to-fuel ratio gain-scheduling controller for the port-fuel-injection process using the wall-wetting parameters and the engine speed as scheduling variables [66, 69, 67, 70, 68].

4. In Chapter 4, a novel approach is developed to express the parameter variation of the continuous-time oxygen sensor dynamics in the event-based discrete-time model with minimal error [66].

5. In Chapter 5, a systematic approach is provided for the design of gain-scheduling controllers when system identification is used to obtain the system model [71].

6. In Chapter 6, an LPV model is developed for the electrical VVT system with engine oil viscosity as the time-varying parameter [72], which large impact on the response time according to [49].

7. In Chapter 6, a method for obtaining an approximate discrete-time LPV system from a continuous-time LPV system based on the linear-least squares estimation method is provided [72].

7.3 Future Research

The following topics deserve future investigation:

1. The guaranteed $\ell_2 - \ell_\infty$ gain control design considered in this research minimized the control effort subject to desired system output constraints. It would also be interesting

to investigate a guaranteed $\ell_2 - \ell_\infty$ gain control design that finds the best achievable performance for a fixed amount of control energy, meaning that the control energy would be constrained and the performance of the system outputs would be optimized as much as possible.

2. A systematic framework for the off-line estimation of the wall-wetting parameters over all operating conditions for the a given intake manifold would be desirable for the practical application of wall-wetting parameters as a scheduling parameter for gain-scheduling control.

   (a) It may also be necessary to develop on-line estimation procedure to validate the wall-wetting parameters stored in the engine control unit in case the wall-wetting parameters change over the life of the engine due to build up of fuel residuals.

3. The hydraulic VVT system studied in Chapter 5 was only capable of being operated at low engine speeds. To demonstrate the benefits of the LPV approach, a wider range of engine operating conditions needs to be considered.

4. A mixed $\ell_2 - \ell_\infty / \mathcal{H}_\infty$ LPV controller design should be performed for the electrical VVT system and that controller should be tested on an engine equipped with an electrical VVT actuator.

APPENDICES

Appendix A

Linear Fractional Transformation

For completeness, we will now give the definition of a linear fractional transformation (LFT). Linear fractional transformations are used to efficiently formulate the interconnection of multi-input multi-output sub-systems with multiple sources, such as uncertainties, noises, disturbances, and varying parameters. As given by [84], the possibly complex coefficient matrix M is partitioned as

$$M = \begin{bmatrix} M_{11} & M_{12} \\ M_{21} & M_{22} \end{bmatrix} \in \mathbb{C}^{(p_1+p_2)\times(q_1+q_2)} \tag{A.1}$$

with $\Delta_\ell \in \mathbb{C}^{q_2 \times p_2}$ and $\Delta_u \in \mathbb{C}^{q_1 \times p_1}$. A lower LFT is given with respect to Δ_ℓ as

$$\mathcal{F}_\ell(M, \Delta_\ell) = M_{11} + M_{12}\Delta_\ell \left(I - M_{22}\Delta_\ell\right)^{-1} M_{21}. \tag{A.2}$$

An upper LFT is given with respect to Δ_u by

$$\mathcal{F}_u(M, \Delta_u) = M_{22} + M_{21}\Delta_u \left(I - M_{11}\Delta_u\right)^{-1} M_{12}. \tag{A.3}$$

From the diagrams in Fig. A.1, the reason behind the terminology of lower and upper LFTs should be clear. The set of equations representing the lower LFT diagram in Fig. A.1a are

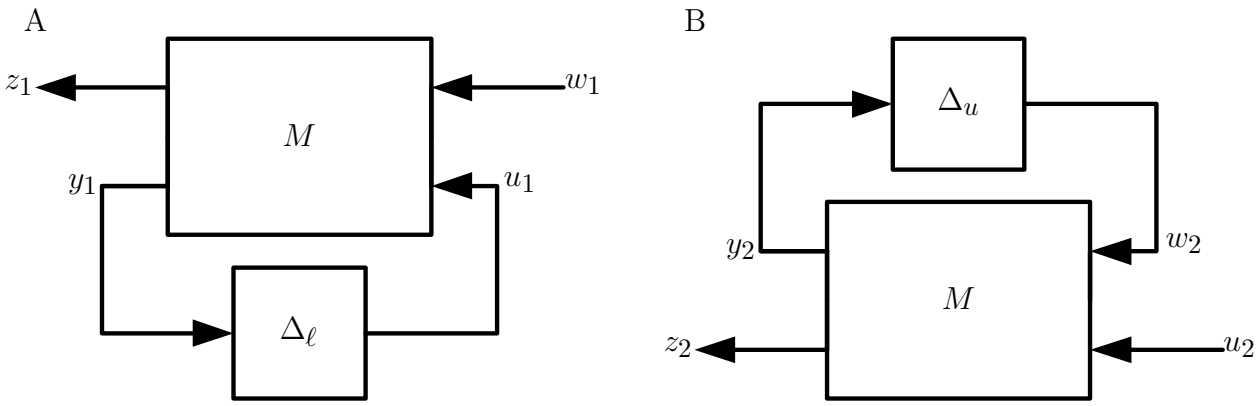

Figure A.1: (a) Diagram of a lower LFT. (b) Diagram of an upper LFT.

given by

$$\begin{bmatrix} z_1 \\ y_1 \end{bmatrix} = \begin{bmatrix} M_{11} & M_{12} \\ M_{21} & M_{22} \end{bmatrix} \begin{bmatrix} w_1 \\ u_1 \end{bmatrix}, \qquad u_1 = \Delta_\ell y_1, \tag{A.4}$$

and the equations representing Fig. A.1b are given by

$$\begin{bmatrix} y_2 \\ z_2 \end{bmatrix} = \begin{bmatrix} M_{11} & M_{12} \\ M_{21} & M_{22} \end{bmatrix} \begin{bmatrix} u_2 \\ w_2 \end{bmatrix}, \qquad u_2 = \Delta_u y_2. \tag{A.5}$$

The partitioning of M depends on the interconnections with the isolated parameter Δ_ℓ or Δ_u and can be determined using the MATLAB function "sysic" [6].

Appendix B

Port Fuel Injection System Matrices

The state-space matrices for the LPV system in (4.23) have been found to be

$$A = \begin{bmatrix} 0.91 & 0 & 0.0369 & 0 & 0 & 0 & 0 & 0 \\ 0.2617 & 0 & 0.1544 & 0 & 0 & 1.4352 & 0 & 0 \\ 0 & 0 & 0.8475 & 0 & 0 & 0 & 0 & 0 \\ 0 & 1.4506 & 0 & 0.2231 & 0.3972 & 0 & 0 & 0 \\ 0 & 2.6311 & 0 & 0 & 0.3114 & 0 & 0 & 0 \\ 0 & 0 & 0 & 0 & 0 & 0.9986 & 0 & 0 \\ 0 & 0 & 0 & 0 & 0 & 0 & 1.9972 & -0.9985 \\ 0 & 0 & 0 & 0 & 0 & 0 & 0.9987 & 0 \end{bmatrix} \in \mathbb{R}^{8\times 8} \tag{B.1}$$

$$B_0 = \begin{bmatrix} -0.09 & 0.0625 & 0 & 0 & 1 & 0 & 0 \\ 0.2617 & 0.2617 & 0 & 0 & 0 & 0 & 0 \\ 0 & -0.2585 & 1.6949 & 1.6949 & 0 & 0 & 0 \\ 0 & 0 & 0 & 0 & 0 & 0.0664 & -0.0027 \\ 0 & 0 & 0 & 0 & 0 & 0.0436 & -0.0073 \\ 0 & 0 & 0 & 0 & 0 & 0 & 0 \\ 0 & 0 & 0 & 0 & 0 & 0 & 0 \\ 0 & 0 & 0 & 0 & 0 & 0 & 0 \end{bmatrix}$$

$$\begin{bmatrix} 0 & 0 & 0 & 0 & 0 & 0 & 0 \\ 0 & 0 & 0 & 0 & 0 & 0 & 0 \\ 0 & 0 & 0 & 0 & 0 & 0 & 0 \\ -0.0214 & -0.0179 & -0.0933 & -0.4891 & -0.0984 & 0.0608 & 0.0975 \\ -0.0186 & -0.0134 & 0 & -0.7266 & 0.1211 & 0.3095 & 0.2231 \\ 0 & 0 & 0 & 0 & 0 & 0 & 0 \\ 0 & 0 & 0 & 0 & 0 & 0 & 0 \\ 0 & 0 & 0 & 0 & 0 & 0 & 0 \end{bmatrix} \in \mathbb{R}^{8\times 14} \tag{B.2}$$

$$B_1 = \begin{bmatrix} 0 & 0 & 0.0043 \\ 0 & 0 & 0.0179 \\ 0 & 0 & -0.0073 \\ 0 & 0 & 0 \\ 0 & 0 & 0 \\ 0.3756 & 0 & 0 \\ 0 & 0.0266 & 0 \\ 0 & 0 & 0 \end{bmatrix} \in \mathbb{R}^{8\times 3}, \tag{B.3}$$

$$B_2 = \begin{bmatrix} 0.0369 \\ 0.1544 \\ 0 \\ 0 \\ 0 \\ 0 \\ 0 \\ 0 \end{bmatrix} \in \mathbb{R}^{8\times 1} \tag{B.4}$$

$$C_0 = \begin{bmatrix} 0 & 0 & 1 & 0\ 0\ 0\ 0\ 0 \\ 0 & 0 & 0 & 0\ 0\ 0\ 0\ 0 \\ 0 & 0 & 0.1525 & 0\ 0\ 0\ 0\ 0 \\ 0 & 0 & -1 & 0\ 0\ 0\ 0\ 0 \\ -1 & 0 & 0.41 & 0\ 0\ 0\ 0\ 0 \\ 0 & 63.6832 & 0 & 0\ 0\ 0\ 0\ 0 \\ 0 & 0 & 0 & 0\ 0\ 0\ 0\ 0 \\ 0 & 0 & 0 & 0\ 0\ 0\ 0\ 0 \\ 0 & 0 & 0 & 0\ 0\ 0\ 0\ 0 \\ 0 & 25.2968 & 0 & 0\ 0\ 0\ 0\ 0 \\ 0 & 0 & 0 & 0\ 1\ 0\ 0\ 0 \\ 0 & 0 & 0 & 0\ 0\ 0\ 0\ 0 \\ 0 & 0 & 0 & 0\ 0\ 0\ 0\ 0 \\ 0 & 0 & 0 & 0\ 0\ 0\ 0\ 0 \end{bmatrix} \in \mathbb{R}^{14\times 8}, \tag{B.5}$$

$$C_1 = \begin{bmatrix} 0 & 0 & 0 & -1 & 0 & 0 & 0.015 & 0.015 \end{bmatrix} \in \mathbb{R}^{1\times 8} \tag{B.6}$$

$$D_{00} = \begin{bmatrix} 0 & 1.6949 & 0 & 0 & 0 & 0 \\ 0 & -1.6949 & 0 & 0 & 0 & 0 \\ 0 & 0.2585 & -1.6949 & -1.6949 & 0 & 0 \\ 0 & -1.6949 & 0 & 0 & 0 & 0 \\ -1 & 0.6949 & 0 & 0 & 0 & 0 \\ 0 & 0 & 0 & 0 & 0 & 0 \\ 0 & 0 & 0 & 0 & 0 & 0 \\ 0 & 0 & 0 & 0 & 0 & 0 \\ 0 & 0 & 0 & 0 & 0 & 0 \\ 0 & 0 & 0 & 0 & 0 & 0 \\ 0 & 0 & 0 & 0 & 0 & 0 \\ 0 & 0 & 0 & 0 & 0 & 0 \\ 0 & 0 & 0 & 0 & 0 & 0 \end{bmatrix} \in \mathbb{R}^{14\times 14}, \tag{B.7}$$

$$\begin{bmatrix} 0 & 0 & 0 & 0 & 0 & 0 & 0 & 0 \\ 0 & 0 & 0 & 0 & 0 & 0 & 0 & 0 \\ 0 & 0 & 0 & 0 & 0 & 0 & 0 & 0 \\ 0 & 0 & 0 & 0 & 0 & 0 & 0 & 0 \\ 0 & 0 & 0 & 0 & 0 & 0 & 0 & 0 \\ 0 & 0 & 0 & 0 & 0 & 0 & 0 & 0 \\ 1 & 0 & 0 & 0 & 0 & 0 & 0 & 0 \\ 0 & 1 & 0 & 0 & 0 & 0 & 0 & 0 \\ 0 & 0 & 1 & 0 & 0 & 0 & 0 & 0 \\ -0.4891 & -0.0984 & 0.0608 & 0.0975 & 1 & 0 & 0 & 0 \\ 0 & 0 & 0 & 0 & 0 & 0 & 0 & 0 \\ 0 & 0 & 0 & 0 & 0 & 1 & 0 & 0 \\ 0 & 0 & 0 & 0 & 0 & 0 & 1 & 0 \\ 0 & 0 & 0 & 0 & 0 & 0 & 0 & 1 \end{bmatrix}$$

$$D_{01} = \begin{bmatrix} 0 & 0 & 0.1161 & 1 \\ 0 & 0 & -0.1161 & 0 \\ 0 & 0 & 0.0073 & 0 \\ 0 & 0 & -0.0476 & 0 \\ 0 & 0 & 0.0476 & 0.41 \\ 0 & 0 & 0 & 0 \\ 0 & 0 & 0 & 0 \\ 0 & 0 & 0 & 0 \\ 0 & 0 & 0 & 0 \\ 0 & 0 & 0 & 0 \\ 0 & 0 & 0 & 0 \\ 0 & 0 & 0 & 0 \\ 0 & 0 & 0 & 0 \end{bmatrix} \in \mathbb{R}^{14\times 3}, \tag{B.8}$$

$$D_{02} = \begin{bmatrix} 1 \\ 0 \\ 0 \\ 0 \\ 0.41 \\ 0 \\ 0 \\ 0 \\ 0 \\ 0 \\ 0 \\ 0 \\ 0 \\ 0 \end{bmatrix} \in \mathbb{R}^{14\times 1} \tag{B.9}$$

$$D_{10} = \begin{bmatrix} 0 & 0 & 0 & 0 & 0 & 0 & 0 & 0 & 0 & 0 & 0 & 0 & 0 & 0 \end{bmatrix} \in \mathbb{R}^{1\times 14}, \tag{B.10}$$

$$D_{10} = \begin{bmatrix} 0 & 0 & 0 \end{bmatrix} \in \mathbb{R}^{1\times 14}, \tag{B.11}$$

$$D_{10} = \begin{bmatrix} 0 \end{bmatrix} \in \mathbb{R}. \tag{B.12}$$

BIBLIOGRAPHY

BIBLIOGRAPHY

[1] P. Apkarian and R. J. Adams. Advanced gain-scheduling techniques for uncertain systems. *IEEE Transactions on Control Systems Technology*, 6(1):21–32, 1998.

[2] P. Apkarian, P. Gahinet, and G. Becker. Self-Scheduled $\mathcal{H}_\infty$ Control of Linear Parameter-Varying Systems: A Design Example. *Automatica*, 31(9):1251–1261, 1995.

[3] Pierre Apkarian and Pascal Gahinet. A convex characterization of gain-scheduled $\mathcal{H}_\infty$ controllers. *IEEE Transactions on Automatic Control*, 40(5):853–864, 1995.

[4] Pierre Apkarian, Paulo C. Pellanda, and Hoang Duong Tuan. Mixed H_2/H_∞ multichannel linear parameter-varying control in discrete time. *Systems & Control Letters*, 41(5):333–346, 2000.

[5] K.J. Astrom and B. Wittenmark. *Computer-controlled systems: theory and design*. Prentice Hall New York, 1996.

[6] G.J. Balas, J.C. Doyle, K. Glover, A. Packard, and R. Smith. μ-analysis and synthesis toolbox. *Users Guide. The MathWorks Inc., South Natick, Massachusetts*, 2001.

[7] A. Balluchi, L. Benvenuti, M. D. di Benedetto, C. Pinello, A. L. Sangiovanni-Vincentelli, and R. PARADES. Automotive engine control and hybrid systems: challenges and opportunities. *Proceedings of the IEEE*, 88(7):888–912, 2000.

[8] NF Benninger and G. Plapp. Requirements and performance of engine management systems under transient conditions. *SAE 910083*, 1991.

[9] Dennis S. Bernstein and Wassin M. Haddad. LQG Control with an H_∞ Performance Bound: A Riccati Equation Approach. *IEEE Transactions on Automatic Control*, 34(3):293–305, 1989.

[10] J. Caigny, J. Camino, R. Oliveira, P. Peres, and J. Swevers. Gain scheduled H_∞-control of discrete-time polytopic time-varying systems. In *Proceedings of 47th IEEE Conference on Decision and Control*, pages 3872–3877, 2008.

[11] J. Caigny, J. Camino, R. Oliveira, P. Peres, and J. Swevers. Gain scheduled H_2-control of discrete-time polytopic time-varying systems. In *Congresso Brasileiro de Automatica*, 2008.

[12] J. Caigny, J. Camino, R. Oliveira, P. Peres, and J. Swevers. Gain scheduled $\mathcal{H}_2$ and $\mathcal{H}_\infty$ control of discrete-time polytopic time-varying systems. *IET Control Theory and Applications*, 4:362–380, 2010.

[13] J. Caigny, J. Camino, R. Oliveira, P. Peres, and J. Swevers. Gain-scheduled dynamic output feedback control for discrete-time lpv systems. *International Journal of Robust and Nonlinear Control*, 22:535–558, 2012.

[14] J. Cassidy Jr and M. Athans. On the design of electronic automotive engine controls using linear quadratic control theory. *IEEE Transactions on Automatic Control*, 25(5):901–912, 1980.

[15] Mahmoud Chilali and Pascal Gahinet. H_∞ Design with Pole Placement Constraints: An LMI Approach. *IEEE Transactions on Automatic Control*, 41(3):358–367, 1996.

[16] SB Choi, JK Hedrick, V. Kelsey-Hayes, and MI Livonia. An observer-based controller design method for improving air/fuel characteristics of spark ignition engines. *IEEE Transactions on Control Systems Technology*, 6(3):325–334, 1998.

[17] M. C. De Oliveira, J. C. Geromel, and J. Bernussou. Extended H_2 and H_∞ norm characterizations and controller parametrizations for discrete-time systems. *International Journal of Control*, 75(9):666–679, 2002.

[18] M.C. de Oliveira, J. Bernussou, and J.C. Geromel. A new discrete-time robust stability condition. *Systems & Control Letters*, 37(4):261–265, 1999.

[19] MC De Oliveira, JC Geromel, and J. Bernussou. An LMI optimization approach to multiobjective controller design for discrete-time systems. In *Proceedings of the 38th IEEE Conference on Decision and Control*, volume 4, pages 3611–3616. IEEE, 1999.

[20] P. H. Dugdale, R. J. Rademacher, B. R. Price, J. W. Subhedar, and R. L. Duguay. Ecotec 2.4L VVT: A Variant of GM's Global 4-Cylinder Engine. *SAE 2005-01-1941*, 2005.

[21] P. Gahinet. Explicit controller formulas for LMI-based H_∞ synthesis. *Automatica*, 32(7):1007–1014, 1996.

[22] P. Gahinet, A. Nemirovski, AJ Laub, and M. Chilali. Matlab LMI control toolbox. *The MathWorks Inc*, 1995.

[23] Pascal Gahinet, Pierre Apkarian, and Mahmoud Chilali. Affine parameter-dependent Lyapunov functions and real parametric uncertainty. *IEEE Transactions on Automatic Control*, 41(3):436–442, 1996.

[24] A.U. Genç, K. Glover, and R. Ford. Nonlinear control of hydraulic actuators in variable cam timing engines. In *MECA International Workshop*, University of Salerno, Italy, September 2001.

[25] Ali Umut Genç. *Linear Parameter-Varying Modelling and Robust Control of Variable Cam Timing Engines*. PhD thesis, University of Cambridge, 2002.

[26] Lino Guzzella and Christopher H. Onder. *Introduction to Modeling and Control of Internal Combustion Engine Systems*. Springer, 2004.

[27] M. Hattori, T. Inoue, Z. Mashiki, A. Takenaka, H. Urushihata, S. Morino, and T. Inohara. Development of variable valve timing system controlled by electric motor. *SAE 2008-01-1358*, 2008.

[28] J.B. Heywood, D.R. Cohn, and L. Bromberg. Optimized fuel management system for direct injection ethanol enhancement of gasoline engines, June 5 2007. US Patent 7,225,787.

[29] T. Ikoma, S. Abe, Y. Sonoda, H. Suzuki, Y. Suzuki, and M. Basaki. Development of V-6 3.5-liter Engine Adopting New Direct Injection System. *SAE 2006-01-1259*, 2016:293, 2006.

[30] Isaac Kaminer, Pramod P. Khargonekar, and Mario A. Rotea. Mixed H_2/H_∞ Control for Discrete-time Systems via Convex Optimization. *Automatica*, 29(1):57–70, 1993.

[31] S. M. Kay. *Fundamentals of Statistical Signal Processing: Estimation Theory*, volume 1. Prentice Hall PTR, Upper Saddle River, New Jersey, 1993.

[32] Pramod P. Khargonekar and Mario A. Rotea. Mixed H_2/H_∞ Control: A Convex Optimization Approach. *IEEE Transactions on Automatic Control*, 36(7):824–837, 1991.

[33] Michal Kočvara and Michael Stingl. PENBMI User's Guide (Version 2.1). 2006.

[34] J. Löfberg. Yalmip : A toolbox for modeling and optimization in MATLAB. In *Proceedings of the CACSD Conference*, Taipei, Taiwan, 2004.

[35] Izumi Masubuchi, Atsumi Ohara, and Nobuhide Suda. LMI-Based Controller Synthesis: A Unified Formulation and Solution. *International Journal of Robust and Nonlinear Control*, 8(8):669–686, 1998.

[36] Larry Mianzo, Huei Peng, and Ibrahim Haskara. Transient Air-Fuel Ratio H_∞ Preview Control of a Drive-By-Wire Internal Combustion Engine. *Proceedings of American Control Conference*, pages 2867–2871, 2001.

[37] Y. Moriya, A. Watanabe, H. Uda, H. Kawamura, M. Yoshiuka, and M. Adachi. A Newly Developed Intelligent Variable Valve Timing System - Continuously Controlled Cam Phasing as Applied to New 3 Liter Inline 6 Engine. *SAE 960579*, 1996.

[38] Kenneth R. Muske and James C. Peyton Jones. A Model-based SI Engine Air Fuel Ratio Controller. *Proceedings of American Control Conference*, pages 3284–3289, 2006.

[39] R. Nagamune and J. Choi. Parameter reduction of estimated model sets for robust control. *Journal of Dynamic Systems, Measurement, and Control*, 132(2), March 2010. DOI: 10.1115/1.4000661.

[40] Ricardo C. L. F. Oliveira and Pedro L. D. Peres. Robust stability analysis and control design for time-varying discrete-time polytopic systems with bounded parameter variation. In *Proceedings of 2008 American Control Conference*, Seattle, WA, June 2011.

[41] Ricardo C.L.F. Oliveira and Pedro L.D. Peres. Time-varying discrete-time linear systems with bounded rates of variation: Stability analysis and control design. *Automatica*, 45(11):2620–2626, 2009.

[42] C.H. Onder. Model-Based Multivariable Speed and Air-To-Fuel Ratio Control of An SI Engine. *SAE 930859*, 1993.

[43] Stephen Pace and Guoming G. Zhu. Sliding Mode Control of a Dual-Fuel System Internal Combustion Engine. In *Proceedings of ASME Dynamic Systems and Control Conference*, Hollywood, CA, October 2009.

[44] Andy Packard. Gain scheduling via linear fractional transformations. *Systems & Control Letters*, 22(1):79–92, 1994.

[45] R. J. Pierik and J. O. Wilson. Engine timing drive with fixed and variable phasing. *US Patent 5327859*, 1994.

[46] J.D. Powell, N.P. Fekete, and C.F. Chang. Observer-Based Air-Fuel Ratio Control. *IEEE Control Systems Magazine*, 18:72–83, 1998.

[47] W.F. Powers, B.K. Powell, and G.P. Lawson. Applications of optimal control and Kalman filtering to automotive systems. *International Journal of Vehicle Design Special Publication SP4*, 1983.

[48] Z. Ren and G Zhu. Pseudo-random binary sequence closed-loop system identification error with integration control. *Proceedings of the Institution of Mechanical Engineers, Part I: Journal of Systems and Control Engineering*, 223(6):877–884, 2009. DOI: 10.1243/09596518JSCE794.

[49] Zhen Ren. *System identification and control design for internal combustion engine variable valve timing systems*. PhD thesis, Michigan State University, 2011.

[50] Zhen Ren and Guoming Zhu. Modeling and control of an electric variable valve timing system for SI and HCCI combustion mode transition. In *Proceedings of 2011 American Control Conference*, San Fransisco, CA, June 2011.

[51] Zhen Ren and Guoming Zhu. Modeling and control of an electric variable valve timing system. *submitted to Journal of Mechatronics*, 2012.

[52] Zhen Ren and Guoming G. Zhu. Integrated System ID and Control Design for an IC Engine Variable Valve Timing System. *ASME Journal of Dynamic Systems, Measurement and Control*, 2010. DOI: 10.1115/1.4003263.

[53] JG Rivard. Closed-Loop Electronic Fuel Injection Control of the Internal-Combustion Engine. *SAE 730005*, 1973.

[54] Mario A. Rotea and Pramod P. Khargonekar. H^2-optimal Control with an H^∞-constraint: The State Feedback Case. *Automatica*, 27(2):307–316, 1991.

[55] J.V. Salcedo and M. Martnez. LPV identification of a turbocharged diesel engine. *Applied Numerical Mathematics*, 58:1553–1571, 2008.

[56] Carsten Scherer, Pascal Gahinet, and Mahmoud Chilali. Multiobjective Output-Feedback Control via LMI Optimization. *IEEE Transactions on Automatic Control*, 42(7):896–911, 1997.

[57] Jeff S. Shamma and Michael Athans. Guaranteed properties of gain scheduled control for linear parameter-varying plants. *Automatica*, 27(3):559–564, 1991.

[58] S. Skogestad and I. Postlethwaite. *Multivariable feedback control: analysis and design (2nd Edition)*. Wiley New York, 2005.

[59] J.F. Sturm. Using SeDuMi 1.02, a MATLAB toolbox for optimization over symmetric cones. *Optimization methods and software*, 11(1):625–653, 1999.

[60] Kenji Suzuki, Tielong Shen, Junichi Kako, and Yasufumi Oguri. Individual A/F Control with Fuel-Gas Ratio Estimation for Multi-cylinder IC Engines. *Proceedings of American Control Conference*, pages 5094–5099, 2007.

[61] L.N. Trefethen and D. Bau. *Numerical linear algebra*. Society for Industrial and Applied Mathematics, 1997.

[62] Raymond C. Turin and Hans P. Geering. Model-Reference Adaptive A/F Ratio Control in an SI Engine Based on Kalman-Filtering Techniques. *Proceedings of American Control Conference*, pages 4082–4090, 1996.

[63] H. Urushihata and H. Iida. Variable valve timing control device of internal combustion engine. *US Patent 7363896 B2*, 2008.

[64] Joe Warren, Scott Schaefer, Anil N. Hirani, and Mathieu Desbrun. Barycentric coordinates for convex sets. *Advances in Computational Mathematics*, 27(3):319–338, 2007.

[65] Xiukun Wei and Luigi del Re. Gain Scheduled $\mathcal{H}_\infty$ Control for Air Path Systems of Diesel Engines Using LPV Techniques. *IEEE Transactions on Control Systems Technology*, 15(3):406–415, 2007.

[66] Andrew White, Jongeun Choi, Ryozo Nagamune, and Guoming Zhu. Gain-scheduling control of port-fuel-injection processes. *IFAC Journal of Control Engineering Practice*, 2010. DOI: 10.1016/j.conengprac.2010.12.007.

[67] Andrew White, Jongeun Choi, Ryozo Nagamune, and Guoming Zhu. Gain-Scheduling Control of Port-Fuel-Injection Processes. In *Proceedings of 2010 American Control Conference*, Baltimore, MD, June 2010.

[68] Andrew White, Jongeun Choi, and Guoming Zhu. Dynamic Gain-Scheduling Controller Design for Port-Fuel-Injection Processes. In *Proceedings of 2011 American Control Conference*, San Fransisco, CA, June 2011.

[69] Andrew White, Guoming Zhu, and Jongeun Choi. Hardware-in-the-Loop Simulation of Robust Gain-Scheduling Control of Port-Fuel-Injection Processes. *IEEE Transaction on Control System Technology*, 2010. DOI: 10.1109/TCST.2010.2095420.

[70] Andrew White, Guoming Zhu, and Jongeun Choi. Hardware-In-the-Loop Simulation of Robust Gain-Scheduling Control of Port-Fuel-Injection Processes. In *Proceedings of 2010 Dynamic Systems and Control Conference*, Baltimore, MD, September 2010.

[71] Andrew White, Guoming Zhu, and Jongeun Choi. Mixed $\mathcal{H}_2/\mathcal{H}_\infty$ observer-based LPV control of a hydraulic engine cam phasing actuator. *IEEE Transaction on Control System Technology*, 2012. DOI: 10.1109/TCST.2011.2177464.

[72] Andrew White, Guoming Zhu, and Jongeun Choi. Dynamic, output-feedback, gain-scheduling control of an electric variable valve timing system. *to be submitted*, 2013.

[73] Andrew White, Guoming Zhu, and Jongeun Choi. Optimal LPV control with hard constraints. *to be submitted*, 2013.

[74] David A. Wilson. Convolution and hankel operator norms for linear systems. *IEEE Transactions on Automatic Control*, 34(1):94–97, 1989.

[75] F. Wu and K. Dong. Gain-scheduling control of LFT systems using parameter-dependent Lyapunov functions. *Automatica*, 42(1):39–50, 2006.

[76] Fen Wu. A generalized LPV system analysis and control synthesis framework. *International Journal of Control*, 74(7):745–759, 2001.

[77] Fen Wu, Xin Hua Yang, Andy Packard, and Greg Becker. Induced l_2-norm control for LPV systems with bounded parameter variation rates. *International Journal of Robust and Nonlinear Control*, 6:2379–2383, 1996.

[78] Xiaojian Yang and Guoming Zhu. SI and HCCI combustion mode transition control of a multi-cylinder HCCI capable SI engine. *IEEE Transaction on Control System Technology*, 2012. DOI: 10.1109/TCST.2012.2201719.

[79] Xiaojian Yang and Guoming G. Zhu. A Mixed Mean-Value and Crank-Based Model of a Dual-Stage Turbocharged SI Engine for Hardware-In-the-Loop Simulation. In *Proceedings of 2010 American Control Conference*, Baltimore, MD, June 2010.

[80] Y. Yildiz, A. Annaswamy, D. Yanakiev, and I. Kolmanovsky. Adaptive Air Fuel Ratio Control for Internal Combustion Engines. *Proceedings of American Control Conference*, pages 2058–2063, 2008.

[81] Jie Yu and Athanasios Sideris. $\mathcal{H}_\infty$ control with parametric Lyapunov functions. *Systems & Control Letters*, 30(1):57–69, 1997.

[82] Feng Zhang, Karolos M. Grigoriadis, Matthew A. Franchek, and Imad H. Makki. Linear Parameter-Varying Lean Burn Air-Fuel Ratio Control for a Spark Ignition Engine. *Journal of Dynamic Systems, Measurement and Control*, 192:404–414, 2007.

[83] Kemin Zhou and John C. Doyle. *Essentials of Robust Control*. Prentice Hall, Upper Saddle River, New Jersey, 1998.

[84] Kemin Zhou, John C. Doyle, and Keith Glover. *Robust and Optimal Control*. Prentice Hall, Upper Saddle River, New Jersey, 1996.

[85] Guoming Zhu. $\mathcal{L}_2$ *and* $\mathcal{L}_\infty$ *Multiobjective Control for Linear Systems*. PhD thesis, Purdue University, 1992.

[86] Guoming Zhu, Karolos M. Grigoriadis, and Robert E. Skelton. Covariance control design for hubble space telescope. *Journal of Guidance, Control, and Dynamics*, 18(2):230–236, 1995.

[87] Guoming Zhu, Mario Rotea, and Robert E. Skelton. A convergent algorithm for the output covariance constraint control problem. *SIAM Journal on Control and Optimization*, 35:341–361, 1997.

[88] Rohit A. Zope, Javad Mohammadpour, Karolos M. Grigoriadis, and Matthew Franchek. Air-fuel ratio control of spark ignition engines with TWC using LPV techniques. *Proceedings of ASME Dynamic Systems and Control Conference*, 2009.